EXPERIMENTAL THERMAL-HYDRAULIC STUDY OF A SUPERCRITICAL CO$_2$ NATURAL CIRCULATION LOOP

BY

JAVAD MAHMOUDI

A Thesis submitted to the Faculty of Graduate Studies of

The University of Manitoba

In partial fulfillment of the Requirements of the degree of

MASTER OF SCIENCE

Department of Mechanical and Manufacturing Engineering

University of Manitoba

Winnipeg

Abstract

An experimental thermal-hydraulic study of a rectangular supercritical CO_2 natural circulation loop with a horizontal heated channel was conducted at different steady-state conditions. Experiments were performed at different pressures of 7.6, 8, 8.5, and 9.5 MPa and different inlet temperatures of 20, 25, and 30˚C, with different inlet and outlet valve openings. This study was aimed to procure a data bank of pressure-drop measurements along the heated channel, characterize the loop parameters in the steady-state conditions, and extend the limited available experimental results on flow oscillations for supercritical natural circulation loops.

Approximately 450 experimental steady-state data-points were generated. Each data-point included measurements of pressure-drop along the heated channel, pressure-drop across the inlet and outlet valves, applied heat on the heated channel (0-120 kW/m^2), system pressure, temperature, and flow rate. Detailed information of the frictional pressure-drop, local head loss coefficients, and steady-state curves of the mass flow rate versus power was derived for steady-state conditions. In addition to the steady-state data-points, several cases with flow oscillations were observed in the loop.

In pressure-drop study, the frictional pressure-drops were derived from the experimental measurements and were compared against the frictional pressure-drops calculated from available friction-factor correlations in the literature. It was also shown that buoyancy induces a secondary flow in the horizontal tube, which increases the frictional pressure-drop. Due to the large averaged buoyancy along the heated channel in the present study, most of the friction-factor correlations underestimated derived frictional pressure-drops from the experiment. However, all the frictional pressure-drop data obtained in this study

fell within 1-1.2 of the Blasius formula. Therefore, among available correlations used for comparison, the Blasius formula is suggested for use in numerical 1-dimensional modeling.

Steady-state curves of the mass flow rate versus power showed that an increase in the system pressure and/or a decrease in the inlet temperature enhance the mass flow rate in the loop. Moreover, it was concluded that the energy balance is an erroneous method for calculating the CO_2 flow rate.

Flow oscillations were observed in several cases in the negative slope part of the flow rate versus power curve when the outlet temperature was considerably higher than the pseudo-critical temperature. However, in the previous experimental studies of supercritical flow instability, the outlet temperature during oscillations was close to the pseudo-critical temperature. The flow oscillations obtained in this study were similar to the second type of density wave oscillations (DWO) in two-phase natural circulation loops. Flow oscillations were observed for the cases with an inlet temperature of 20-25ºC when the system pressure was 7.6-8.5 MPa. No flow oscillations were observed at a system pressure of 9.5 MPa.

Acknowledgment

I would like to express my appreciation and thanks to my advisors, Dr. V. Chatoorgoon and Dr. R.W. Derksen, for their valuable guidance. I would also like to thank my committee members, Dr. H. Soliman, Dr. E. Bibeau, and Dr. S. Sherif for their helpful comments and suggestions. I am also grateful to AECL and the Mechanical Engineering Department for the financial support of this project. Last but not least, I would like to thank my lovely wife, Elaheh and my family for their wonderful support, guidance, and patience.

Table of Contents

List of Tables

List of Figures

NOMENCLATURE

ΔP	Pressure Drop (Pa)
f	Friction Factor
L	Length (m)
D	Diameter (m)
G	Mass Flux (kg/s.m^2)
ρ	Density (kg/m^3)
h	Enthalpy (kJ/kg)
H	Height (m)
g	Gravity (m/s^2)
q	Power (kW)
q"	Heat Flux (W/m^2)
K	Local Pressure Drop Coefficient
k	Thermal Conductivity W/(m·K)
R	Radius (m)
$\dot{q}$	Heat Generation (W/m^3)
ϑ	Kinematic Viscosity (m^2/s)
$\dot{m}$	Mass Flow rate (kg/s)
β	Thermal expansion (1/°K)

Subscripts

fr	Frictional
l	Local
ac	Acceleration
g	Gravitational
ave	Average
i	No. of cell
b	Property for the Bulk Value
w	Property near the wall

CHAPTER 1

INTRODUCTION

The Super-Critical Water-cooled Reactor (SCWR) is one of the six new reactor technologies for Generation IV reactors which were proposed by the Generation IV International Forum (GIF) (U.S. DOE Nuclear Energy Research Advisory Committee and the Generation IV International Forum, 2002). GIF finalized the research plan for SCWR in 2007. Currently, 32 organizations in 13 countries have initiated research and development on feasibility of employing SCWR for generating electricity (DOE Office of Nuclear Energy, 2007). SCWRs are basically Light Water Reactors (LWRs) which operate at pressures above the critical pressure of water (22.1 MPa). LWRs are one type of thermal reactors which use demineralized water instead of heavy water as its coolant and neutron moderator. Two most common LWRs are Boiling Water Reactors (BWRs) (operate at about 7 MPa) and Pressurized Water Reactors (PWRs) (operate at about 16 MPa). BWRs convert the water into steam directly in the reactor and then the steam passes through the turbine, but in PWRs, the generated heat in the reactor is transferred to high pressure water which is not boiling. The energy of this hot water is transferred to a secondary water loop via a steam generator and converts the water into steam in the secondary loop. Another technology that will be employed in SCWRs is the supercritical fossil-fired steam generator which the US has started to use in power generation plants in 1950.

In the design of a SCWR, proven technologies in BWRs, PWRs, and supercritical fossil-fired steam generators are employed. The coolant in a SCWR is pumped through the fuel bundles directly, similar to BWRs. However, since its working pressure (25 MPa) is

above the critical pressure, the coolant does not undergo a two-phase region and therefore acts the same as the coolant in the PWRs or water in a supercritical fossil-fired steam generator. These characteristics bring unique advantages for SCWRs compared to the generation III reactors. First of all, using water at higher pressure, and consequently higher temperature, increases the thermal efficiency of the plant from 33% to about 44% (U.S. DOE Nuclear Energy Research Advisory Committee and the Generation IV International Forum, 2002, DOE Office of Nuclear Energy, 2007, MacDonald et al., 2003, Danielyan, 2003). Moreover, since SCWR operates above the critical pressure, the water remains single-phase throughout the system and therefore the need for the recirculation and jet pumps, pressurizer, steam generators, steam separators, and dryers is eliminated (MacDonald et al., 2003). Figure 1.1 shows the operating conditions for BWRs, PWRs, and SCWRs. Although, Figure 1.1 shows that the outlet temperature of water in a SCWR is about 450ºC, different outlet temperatures are considered in different designs. For example, outlet temperature of a SCWR is 500 ºC in (DOE Office of Nuclear Energy, 2007, MacDonald et al., 2003, Danielyan, 2003) or 550 ºC in (U.S. DOE Nuclear Energy Research Advisory Committee and the Generation IV International Forum, 2002) or Up to 625 ºC in (Khartabil, 2009).

Figure 1.1(a) shows the phase diagram of water with equilibrium boundaries which separate solid (S), liquid (L), and vapor (V) regions of the substance. The equilibrium boundary between the vapor and liquid ends at the critical point in which the distinction between the liquid and vapor phases disappears. Figure 1.1 (b) illustrates the same process on the temperature-entropy (T-s) diagram. The area below the T-s diagram is equivalent to the amount of heat that can be transferred or removed from the fluid during

a process. Considering this concept, Figure 1.1 (b) shows that more heat can be transferred to water in the supercritical pressures (SCWR) compared to the subcritical pressures (BWR, PWR).
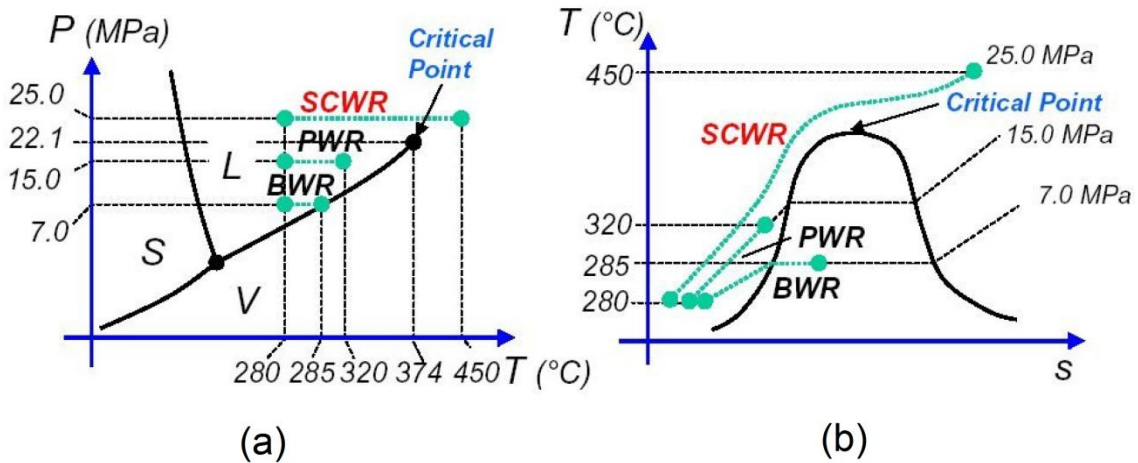
Figure 1.1: SCWRs operating conditions compare to BWRs and PWRs

(a) Phase diagram, (b) Temperature-entropy diagrams (Danielyan, 2003)

All in all, the main mission of employing the SCWRs is generating low-cost electricity. However, there are some challenges which have to be addressed before the commercial deployment of SCWRs. GIF introduced three technology gaps for SCWRs. The first concern is SCWR materials and structures; the second problem is SCWR safety, including power-flow stability during operation; and the last concern is plant design which will come up after addressing the first two issues (U.S. DOE Nuclear Energy Research Advisory Committee and the Generation IV International Forum, 2002). Thermal-hydraulics and safety of the SCWRs is one of the project arrangements between Canada and GIF with regard to research and development of Generation IV reactors.

1.1 Supercritical Fluid

In thermodynamics, the critical point of a substance is defined as the highest temperature and pressure in which both liquid and vapor phases exist at the same time in equilibrium. Any substance above its critical point (critical temperature and critical pressure) is called supercritical fluid. Different fluids have different critical temperature and pressures. For example the thermodynamic critical point of water is 374 ºC and 22.1 MPa, while it is 31.1ºC and 7.39 MPa for CO_2. CO_2, helium, or Freon are surrogate fluids which can be utilized for performing experiments in SCWR's research and development programs since they have considerably lower critical pressures and temperatures. This change leads to a significant time and cost reduction in constructing and operating the experimental facilities (DOE Office of Nuclear Energy, 2007). In the present experimental study, CO_2 was used as the working fluid.

As mentioned before, a distinctive feature of a supercritical fluid compared to a subcritical fluid is that if a fluid at pressures above its critical pressure is heated or cooled homogenously, it is converted from liquid to gas (or vice versa) continuously without appearance of vapor and liquid phases at the same time. In the other words, there is only one single phase during the homogenous heating or cooling of a substance at supercritical pressures. While if a subcritical fluid undergoes the same process at a constant pressure, it experiences a two-phase region in which both liquid and vapor phases co-exist. This difference is shown in Figure 1.2 for subcritical and supercritical water. Figure 1.2 (a) shows the variation of bulk density versus temperature and Figure 1.2 (b) shows the variation of bulk enthalpy versus temperature both at constant pressures.
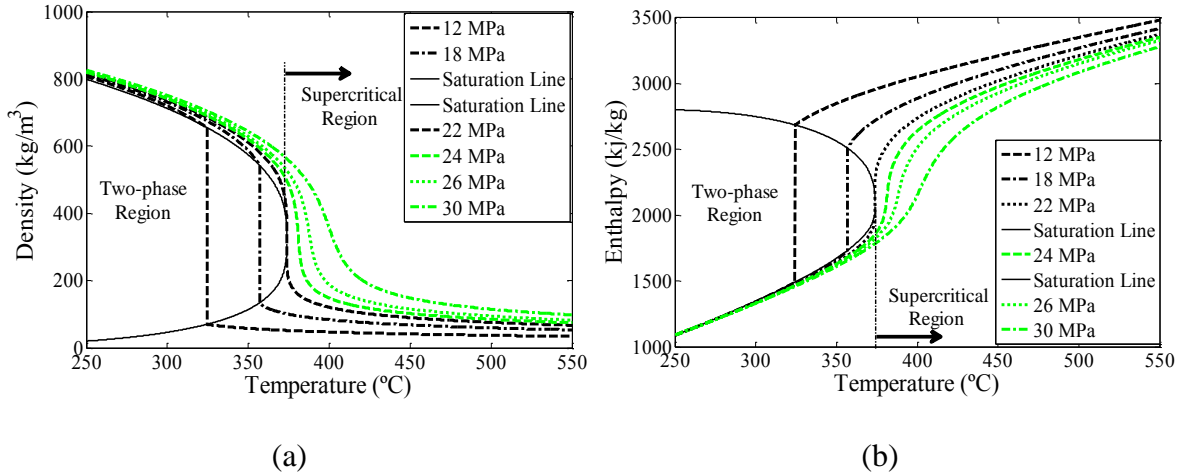
Figure 1.2: (a) variation of bulk density vs. temperature; (a) variation of bulk enthalpy vs. temperature (NIST Refprop- Lemmon et al. 2013)

Variation of thermo-physical properties with temperature at supercritical pressures is strong as shown in Figure 1.3. At pressures close to the critical pressure, the variation of thermo-physical properties is sharper. In the other words, the change in properties with temperature for water at 23 MPa is sharper than water at 25 MPa. The temperature corresponded to the maximum heat capacity (C_p) at each supercritical pressure is called "pseudo-critical temperature". Pseudo -critical temperature increases with an increase in pressure and strong variations of thermo-physical properties occur near pseudo-critical temperatures.
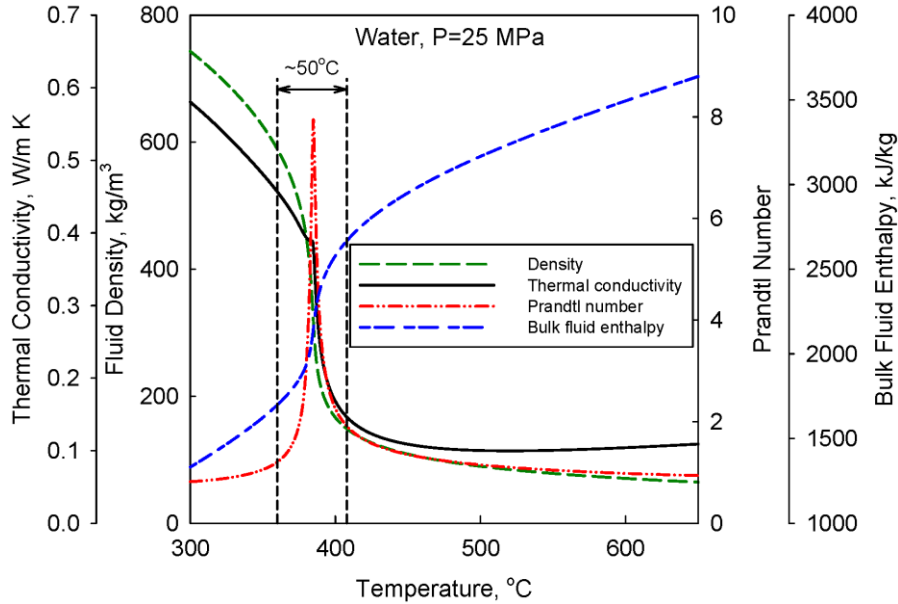
Figure 1.3: Variation of thermo-physical properties with temperature at 25 MPa for water

(Pioro, 2013)

Figure 1.4 shows the variation of heat capacity for subcritical and supercritical water. Enlarged heat capacity region near the pseudo-critical temperature is another distinctive feature of supercritical fluid which brings additional benefits if it is used in a thermal reactor. Figure 1.4 clearly shows the area of C_p for both supercritical and subcritical pressures.

Using a fluid with high heat capacity means that it is possible to use a lower coolant mass flow rate for removing heat from the reactor core. Reduction in the mass flow rate leads to a decrease in pressure-drop and, consequently, a reduction in the size of reactor coolant pump, piping and associated equipment (U.S. DOE Nuclear Energy Research Advisory Committee and the Generation IV International Forum, 2002).
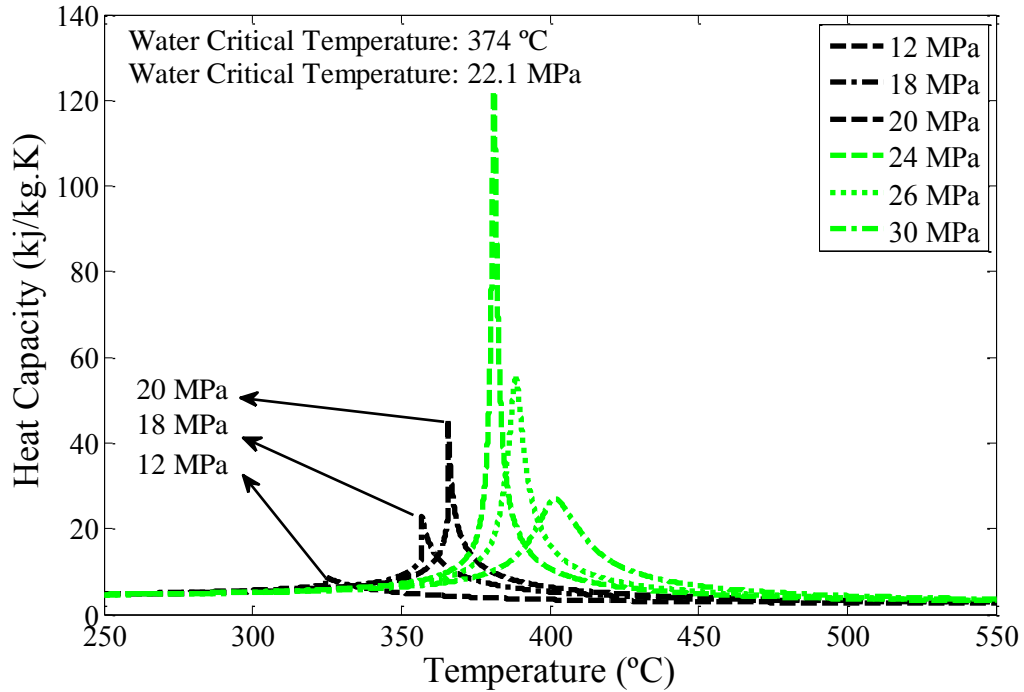
Figure 1.4: Variation of heat capacity with temperature at subcritical and supercritical

pressures (NIST Refprop- Lemmon et al. 2013)

1.2   Supercritical Flow Instability

According to the technology roadmap for the generation IV reactors defined by GIF in 2002, safety is one of the main concerns for employing SCWRs (U.S. DOE Nuclear Energy Research Advisory Committee and the Generation IV International Forum, 2002). Safety of a nuclear reactor is of great importance when the normal cooling is disrupted in the reactor core. Interruption in normal flow conditions may occur during flow oscillations in a fuel bundle. All regimes of flow instabilities have been thoroughly investigated experimentally and numerically in two-phase flows due to its importance in the development stage of BWRs. However, flow instability is not fully understood for supercritical flow.

7

Boure et al. (1973) proposed the widely accepted classification of two-phase flow instabilities. Flow instabilities are of two main types which are static (excursive) and dynamic (oscillatory). In the static instability, the mass flow rate of the coolant drifts spontaneously from its steady-state condition to another steady-state condition (Khabensky & Gerliga, 2012), while in the oscillatory instability, the mass flow rate at the inlet of the heated channel or a fuel bundle starts oscillating. Density Wave Oscillations (DWOs) are one type of dynamic instability which has been most extensively investigated in two-phase flows. DWOs result from multiple regenerative feedbacks between flow rate, pressure-drop and change in the density as a result of the rate of vapor generation in a boiling channel (Stenning & Veziroglo (1965), Boure et al. (1973), Kakac & Bon (2008)).

Supercritical flow may become unstable similar to the two-phase flow. Flow oscillations are highly undesirable as they may lead to mechanical vibrations, problems in system control, and in extreme circumstances, disturb the heat transfer characteristics so that the heat transfer surface may burn-out. Thermal fatigue is another potential cause of damage which a thermal reactor may experience during continual cycling of wall surface temperature in a closed loop. Thermal stresses in the wall and cladding material may cause mechanical breakdown and in the worst case scenario, release radioactive materials (Kakac & Bon (2008)).

In conclusion, flow instability is an undesirable phenomenon that must be avoided in a thermal reactor. Numerous experimental studies have been done on two-phase flow to identify the instability boundaries for different types of instability. However, these margins need to be revealed for supercritical flow.

1.3   Natural Circulation Loops

Natural circulation loops are systems of piping in which flow is driven by density difference between two vertical legs. Flow is heated by a heat source at the bottom and is then cooled down by a heat sink at the top of the loop. Side heating and cooling is another possible configuration for natural circulation loop. Due to the gravity effect, lighter fluid raises and heavier falls down (Greif 1988). Since this transition happens in a closed loop, fluid movement is established in the loop without any need to a pump. Driving force in a natural circulation loop is correlated to the density difference in the two legs multiplied by the height difference of the heat sink and the heat source as shown in Figure 1.5.
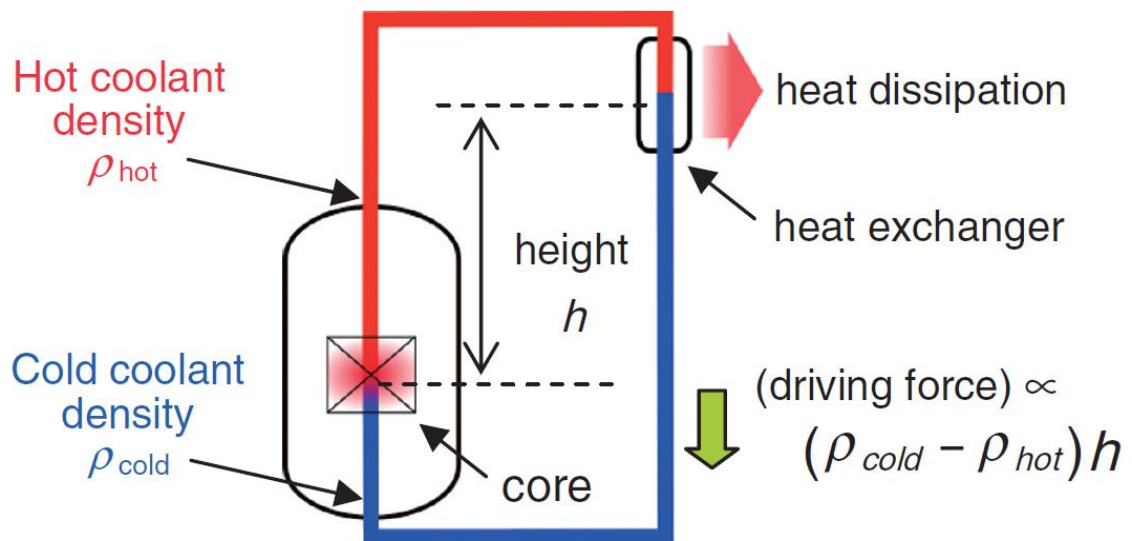
Figure 1.5: Natural Circulation Loop (Doda et al. 2011)

Natural circulation systems have many applications in the industry. They are widely used in solar water heaters. They are also used for cooling heat engines or nuclear reactors.

Natural circulation in BWRs is a proven technology which was employed in the Dodewaard (183 MWth) and Humboldt Bay (165 MWth) nuclear reactors. Economic Simplified Boiling Water Reactor (ESBWR) is the newest design of Generation III+ reactors which is solely operating based on the natural circulation principle to remove the reactor core heat without using a circulation pump. ESBWR was offered by GE-Hitachi Nuclear Energy (GEH) and is under the final stages of approval by the Nuclear Regulatory Commission (NRC).

Natural circulation is a passive safety feature which creates increased design safety, integrity, and reliability, while simultaneously reduces overall cost of a reactor. Passive safety components do not require active controls or (human) operational involvement to avoid accidents in the event of malfunction. For example, in a natural circulation loop flow is ensured as long as there is a heat source and a heat sink in the system. Natural circulation could be employed as a design criterion for the SCWRs similar to ESBWRs. Also, natural circulation could be employed as a back-up in a SCWR to remove reactor core heat in case of losing power to the circulation pump.

1.4   Objective of the study

Natural circulation offers many advantages for new generation reactors, both in terms of increasing passive safety features and simplification of a thermal reactor. Natural circulation can be employed as an independent design or as an additional passive safety component in SCWRs. However, based on extensive knowledge from two-phase flow, natural circulation is prone to flow oscillations due to the delicate counterbalance of the driving head and pressure-drop. Therefore, one important part of research and development on SCWRs is studying flow instability of supercritical flow in natural

circulation loops. For this reason a single channel rectangular natural circulation loop was built at the University of Manitoba (Tummalapalli, (2007)) to investigate the pressure-drop and flow oscillations of supercritical CO_2.

There are several licencing codes that have been used for thermal-hydraulic instability analysis for reactors, such as RELAP5, CATHINA, etc. However, the validity of these codes for supercritical flow needs to be investigated. This is viable by modeling the experimental studies on supercritical flow. Unfortunately, experimental research on flow instability of supercritical flow is at the very first stages of its progress and there are very limited experimental data for flow oscillations.

The pressure-drop of supercritical flow in a fuel bundle or in a heated channel is an important parameter for studying flow instability. There are some empirical correlations for pressure-drop in supercritical flow, but they are uncertain.

Therefore, the objectives of this study are to:

1- Procure a data bank of pressure-drop measurement along the heated channel and assess existent frictional pressure-drop formulae

2- Provide detailed information of the loop parameters in the steady-state conditions. This information will be useful in numerical modeling of the experiments.

3- Extend available experimental knowledge and results on flow oscillations for supercritical natural circulation loops.

CHAPTER 2

LITERATURE REVIEW

2.1 Scope of the Review

In this chapter, previous studies on pressure-drop and determination of the friction-factor for supercritical flow in round tubes, experimental studies on the density wave oscillations in two-phase natural circulation loops, and numerical and experimental studies of supercritical flow instability in natural circulation loops are reviewed.

To design a SCWR, it is important to evaluate both the pressure-drop and heat transfer properties of supercritical water in a fuel bundle. Experimental studies on pressure-drop and determination of the friction-factor were performed mainly in the Soviet Union in the 60's and 70's for supercritical water and CO_2. Based on these studies, a few empirical formulae for friction-factor were proposed for different orientations of heated channels (vertical or horizontal) and flow directions (upward or downward for vertical tubes). Due to the strong variation of thermo-physical properties of supercritical fluids, both near the wall and along the heated channel, and occurrence of the heat transfer deterioration (HTD) phenomenon in some cases (HTD corresponds to a region where the heat transfer coefficient decreases and the wall temperature increases), it is difficult to propose a general formula for friction-factor for supercritical flow. Due to the importance of pressure-drop in studying the flow behavior in a natural circulation loop, a major part of this study is focused on the pressure-drop components and especially frictional pressure-drop determination for supercritical flow.

Flow instability concepts and definitions came from the two-phase flow instability studies. It is of great importance to understand the mechanism of the flow instability in

two-phase natural circulation loops. There is an enormous amount of numerical, analytical, and experimental studies on flow instability in two-phase natural circulation loops. However, only those experimental studies on DWO's in two-phase natural circulation loops are reviewed in this chapter.

The last part of the review is focused on the numerical and experimental studies of flow instability in supercritical natural circulation loops.

2.2   Pressure-Drop

Pioro et al. (2004) conducted a survey on the hydraulic resistance of supercritical fluids flowing in heated channels. They summarized total pressure-drop components as follows:

$$\Delta P = \sum \Delta P_{fr} + \sum \Delta P_l + \sum \Delta P_{ac} + \sum \Delta P_g \tag{2.1}$$

where $\sum \Delta P_{fr}$ is the frictional pressure-drop, $\sum \Delta P_l$ is the local pressure-drop, $\sum \Delta P_{ac}$ is the acceleration pressure-drop, and $\sum \Delta P_g$ is the gravitational pressure-drop.

ΔP_{fr} is defined as follows:

$$\Delta P_{fr} = f \frac{L}{D} \frac{G^2}{2 \rho_{ave}} \tag{2.2}$$

where f is the friction-factor coefficient, L is the length of the tube, D is the inner diameter of the tube, G is the mass flux (flow rate (kg/s) divided by the cross sectional area of the tube (m^2)), and ρ_{ave} is the arithmetic averaged density of the inlet and outlet density. However, when the pseudo-critical region is passed in the heated tube, the integral averaged value of density should be used (Pioro et al., 2004).

ΔP_l is due to the flow obstruction and is defined as follows:

$$\Delta P_l = K \frac{G^2}{2\rho} \qquad (2.3)$$

ΔP_{ac} is due to the acceleration of the flow and is defined as follows:

$$\Delta P_{ac} = G^2 \left(\frac{1}{\rho_{out}} - \frac{1}{\rho_{in}} \right) \qquad (2.4)$$

ΔP_g is due to gravity and is defined as follows:

$$\Delta P_g = \pm g \left(\frac{\rho_{out} + \rho_{in}}{2} \right) L \sin\theta \qquad (2.5)$$

where θ is the heated tube inclination angle to the horizontal plane. The sign "+" is for

upward flow and "–" is for the downward flow.

The friction-factor for a non-isothermal turbulent flow is usually obtained by multiplying

the isothermal turbulent friction-factor (in smooth tubes) by a correction coefficient.

These correction coefficients correlate the thermo-physical properties near the wall with

those of the bulk flow. The isothermal friction-factors used for this purpose are mainly

the formula of Filonenko (1954) for smooth circular tubes and turbulent flows and the

formula of Itaya (1945) for circular tubes and turbulent flows.

The formula of Filonenko is as follows:

$$f_{iso} = \frac{1}{\left(1.82 \log_{10}^{Re_b} - 1.64 \right)^2} \qquad (2.6)$$

which is valid within the range of $4 \times 10^3 \leq Re_b \leq 10^{12}$

The formula of Itaya is as follows:

$$f_{iso} = \frac{0.314}{0.7 - 1.65 \log_{10}^{Re_b} + \left(\log_{10}^{Re_b} \right)^2} \qquad (2.7)$$

which is valid within the range of $3 \times 10^3 \leq Re_b \leq 4 \times 10^6$

Generally, for calculating the frictional pressure-drop, the total pressure-drop is measured across the heated tube with a differential pressure transducer. Using the steady-state measurements (including flow rate, inlet and outlet temperatures, and system pressure), the thermo-physical properties of supercritical fluid are obtained from a property data-base (NIST RefProp package). Then this information is used to specify the components of pressure-drop. Calculated acceleration pressure-drop, local pressure-drop, and gravitational pressure-drop are then deducted from the total pressure-drop to obtain the frictional pressure-drop.

Petkhov & Popov (1963) performed a theoretical study on heat transfer and hydraulic resistance of turbulent flows with variable thermo-physical properties. Popov (1967) utilized that procedure to study the heat transfer and hydraulic resistance of turbulent supercritical CO_2 flow. He proposed the following equations for calculating the friction-factor based on his theoretical work for supercritical CO_2:

$$\frac{f}{f_{iso}} = \left(\frac{\bar{\rho}}{\rho_b}\right)^{0.74} \ where \ \ \bar{\rho} = \frac{\int_{T_b}^{T_w} \rho \, dT}{T_w - T_b} \quad \text{with} \pm 5\% \text{ deviation} \tag{2.8}$$

$$\frac{f}{f_{iso}} = \left(\frac{\rho_w}{\rho_b}\right)^{0.4} \quad\quad\quad \text{with} \pm 10\% \text{ deviation} \tag{2.9}$$

The experimental works on pressure-drop of supercritical flows are presented in Table 2.1. These experiments were done for different supercritical fluids with different orientations of heated tube (vertical or horizontal).

Table 2.1: Experimental studies on supercritical flow pressure-drop

Reference	Flow Parameter				Flow Geometry		Proposed friction-factor formula
	Fluid-Pressure (MPa)	Inlet Temperature (°C) - inlet Enthalpy (kJ/kg)	q (kW/m²)	G (kg/m²s)	Tube Material-Diameter (mm) - Length (m)	Orientation	
Tarasova & Leont'ev (1968)	Water-22.6-26.5	variable	580-2320	2000; 5000	SS-D=3.34 mm-L=0.134; D=8.03 - L=0.602	Vertical	$\frac{f}{f_{iso}} = \left(\frac{\mu_w}{\mu_b}\right)^{0.22}$ With ±5% deviation; f_{iso}= Filonenko (1954) eq.
Yamashita et al. (2003)	HCFC22-5.5	Not specified; 225-395	0-60	700	Inconel 600 smooth- D=4.4 - L=2;	Vertical up-flow	$\frac{f}{f_{iso}} = \left(\frac{\mu_w}{\mu_b}\right)^{0.72}$ With ±15% deviation; f_{iso}= Itaya (1945) formula For normal HT
Ishigai et al. (1981)	Water-24.5	Not specified; 220, 800	150, 1370	500, 1000, 1500	Polished SS tube D=3.9 -L=0.625;	Vertical up-flow & down-flow	$\frac{f}{f_{iso}} = \left(\frac{\mu_b}{\mu_w}\right)^{-0.25}\left(\frac{\rho_b}{\rho_w}\right)^{-0.18}$ With ±15% deviation; f_{iso}= Itaya (1945) eq. For normal HT
Kondrat'ev (Pioro et al. 2004)	Water-22.6, 24.5, 29.4		120, 1200	$30\times10^3<Re<10^5$	Polished SS tube D=10.47 -L=0.521	horizontal	$f = 0.188Re^{-0.22}$ With ±10% deviation; Exception when $T_b \approx T_{pc}$

Table 2.1: Experimental studies on supercritical flow pressure-drop (continued)

Reference	Flow Parameter				Flow Geometry		Proposed friction-factor formula
	Fluid-Pressure (MPa)	Inlet Temperature (ºC) - inlet Enthalpy (kJ/kg)	q (kW/m^2)	G (kg/m^{2}s)	Tube Material-Diameter (mm) - Length (m)	Orientation	
Razumovskiy (1984)(1990)	Water-23.5	Not specified; 1400-1800	657-3385	2000-Re<350×10^3	Polished SS tube D=6.28 -L=0.6	Vertical up-flow	$\frac{f}{f_{iso}} = \left(\frac{\mu_w}{\mu_b}\frac{\rho_w}{\rho_b}\right)^n$ $n = 0.15 \ for$ $h_b \leq 1500 \ kJ/kg$ $or \ 2250 \ kJ/kg \leq h_b$ With ±15% deviation; $n = 0.18 \ for$ $1400 \ \leq h_b \leq 2200 \ kJ/kg$ With ±20% deviation f_{iso}= Filonenko (1945) eq.
Kurganov & Kaptil'ny (1992) (Turbulence Measurement)	CO$_2$-9	Not specified; 500-740	170-440	800-2100	Polished SS tube D=22.7 -L=2.951	Vertical up-flow & down-flow	Suggested Popov (1967) formula with ±20% deviation; $\frac{f}{f_{iso}} = \left(\frac{\rho_w}{\rho_b}\right)^{0.4}$ f$_{iso}$= Filonenko (1954) eq. For both normal and DHT

Table 2.1: Experimental studies on supercritical flow pressure-drop (continued)

Reference	Flow Parameter				Flow Geometry		Proposed friction-factor formula
	Fluid-Pressure (MPa)	Inlet Temperature (ºC) - inlet Enthalpy (kJ/kg)	q (kW/m^2)	G (kg/m^{2}s)	Tube Material-Diameter (mm) - Length (m)	Orientation	
Petukhov et. al. (1980)	CO_2 7.5-7.8; 8; 9	18-20; Not specified	870-1480	3294-4130	Polished SS tube D=8 -L=1.8	horizontal	In agreement with Popov (1967) formula For both normal and DHT
Petukhov et. al. (1983)	CO_2 7.7; 8.9	Not specified; 520-720	384-1053	1000-4100	Polished SS tube D=8 -L=1.67	Horizontal, up-flow, & down-flow	Suggested Popov (1967) formula with ±15% deviation; For both normal and DHT
Kuraeva & Protopopov (1974)	CO_2 8; 10	19-88; Not specified	Up to 2500	1140-7400	Polished SS tube D=4.1 -L=0.208	Horizontal	Proposed Tarasova & Leont'ev (1968) formula with ±20% deviation for Gr/Re^2<5.10^{-4}; and $$\frac{f}{f_{iso}} = \left(\frac{\mu_w}{\mu_b}\right)^{0.22} \times 2.15 \times \left(\frac{Gr}{Re^2}\right)^{0.1}$$ for 5.10^{-4}<Gr/Re^2<3.10^{-1}

Tarasova & Leont'ev (1968) performed an experimental study on pressure-drop of supercritical water in vertical channels, using short length smooth heated tubes. During each series of experiments, pressure, inlet mass flux and the amount of power on the tubes were held constant while the inlet temperature was increased. Using this method, they were able to observe the effect of the variation of thermo-physical properties on the friction-factor. They showed that there is a reduction in the friction-factor compared to isothermal friction-factor in the pseudo-critical region. However, they did not take into account the acceleration and gravitational pressure-drops in their calculations. Their results are within ±5% of their proposed formula for friction-factor.

Kondrat'ev (1969) studied the pressure-drop for horizontal flow of supercritical water. He observed a reduction in the friction-factor in the pseudo-critical region similar to the results of Tarasova & Leont'ev (1968). He concluded that a reason for this reduction could be the reduced kinematic viscosity in the pseudo-critical region. His formula predicted the friction-factor with ±10%, when the bulk fluid temperature was not close to the pseudo-critical temperature.

Kuraeva & Protopopov (1974) performed pressure-drop measurements for turbulent flow of CO_2 in a horizontal channel. However, the wall temperature was not measured during their experiments and they used theoretical methods for calculating the wall temperature. Finally, they obtained friction-factor results within ±20% of the formula of Tarasova & Leont'ev (1968).

Petukhov et al. (1980 and 1983) performed an improved experimental study for investigating the pressure-drop of turbulent supercritical CO_2 flowing horizontally and vertically (up-flow and down-flow) both in normal and deteriorated heat transfer regimes.

They used the "two pressure-drops" technique for measuring the pressure-drop along the heated and unheated sections. The scheme of this technique is shown in Figure 2.1. In this technique, the entrance length pressure-drop is not included in the pressure-drop measurements. Using this method, they were able to obtain the friction-factor formula for supercritical CO_2 when flowing through a heated and an isothermal section. They concluded that the formula of Filonenko (1954) could be used for isothermal flow of supercritical CO_2 within $\pm 4.5\%$ even in pseudo-critical region. They also showed that the one-dimensional flow model (based on mass averaged flow parameters) is not accurate for calculating the acceleration pressure-drop especially in the deteriorated heat transfer region.
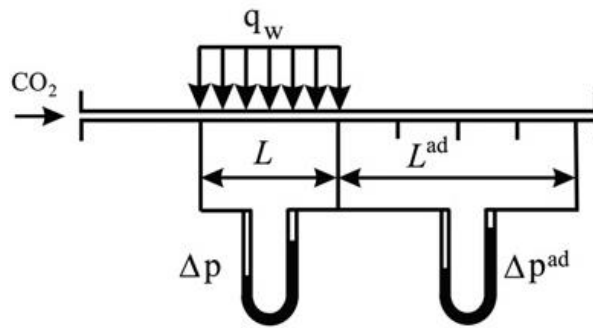
Figure 2.1: The scheme of hydraulic measurements in the "two pressure-drops"

technique (Kurganov et al., 2012)

Petukhov et al. (1980) also concluded that their experimental results fall within $\pm 15\%$ of Equation (2.9) which was proposed by Popov (1967).

Ishigai et al. (1981) used their experimental results on pressure-drop for upward and downward supercritical water flow and proposed a friction-factor formula which is shown in Table 2.1. They accounted for the acceleration pressure-drop in their data

reduction. They also confirmed a reduction in friction-factor for the pseudo-critical region compared to the isothermal formulae for turbulent flow.

Razumovskiy et al. (1984) conducted pressure-drop measurements by using the "two pressure-drops" technique (introduced by Petukhov et al., 1980) for upward flow of supercritical water. They claimed that the proposed formulae for CO_2 in supercritical conditions are not suitable for water, since the thermo-physical properties of these fluids are different. They also showed that the acceleration pressure-drop is significant in deteriorated heat transfer regions. They divided the supercritical water into three different regions based on bulk enthalpy values and proposed a formula for friction-factor for the cases where $h_b \leq 1500\,\text{kJ/kg}$ or $2250\,\text{kJ/kg} \leq h_b$. Later, Razumovskiy et al. (1990) completed their study by proposing another formula for the transition region (pseudo-critical region) from liquid to gaseous state when $1400 \leq h_b \leq 2200\,\text{kJ/kg}$ (see Table 2.1).

Kurganov & Kaptil'ny (1992) performed experimental turbulent measurements of velocity and enthalpy fields using supercritical CO_2 in a heated tube. They used micro-thermocouples and pitot tube for this purpose. Integral equations of mass, momentum and energy were used with experimental measurements in order to determine the friction-factor. Finally, they concluded that the Filonenko equation can be used with ±12% deviation for supercritical CO_2 in isothermal conditions. Moreover, they confirmed the formula of Popov (1967) (Equation 2.9) with an uncertainty of ±20% for upward and downward flows.

Yamashita et al. (2003) carried out a study on the hydraulic resistance of supercritical R22 flowing upward in a circular tube. They used a one-dimensional flow model to

calculate the friction-factor along a two meters tube in the normal heat transfer region. They proposed a formula for this region with a ±12% uncertainty band. They also observed a reduction in the friction-factor in the pseudo-critical region which was attributed to the reduction of kinematic viscosity of the fluid near the tube wall due to the high wall temperature.

Kurganov and Maslakova (2010) adopted a method for calculating the heat transfer coefficient for supercritical water in the normal heat transfer region and proposed a new formula for friction-factor as follows:

$$\frac{f}{f_{iso}} = \left(\frac{\rho_w}{\rho_b}\right)^{N_\rho} \left(\frac{\mu_w}{\mu_b}\right)^{N_\mu} \tag{2.10}$$

$$N_\rho = 0.38 + 0.06 \tanh(H_b), \; N_\mu = 0.2 + 70/Re_b^{0.66}, \text{ and} \tag{2.11}$$

$$H_b = [(h_b - h_{m0}) + (h_b - h_{m1})]/\left((h_{m1} - h_{m0})\right) \tag{2.12}$$

where $h_{m0} = 1500 \; kJ/kg$ and $h_{m1} = 2900 \; kJ/kg$ for water; and $h_{m0} = 500 \; kJ/kg$, $h_{m1} = 780 \; kJ/kg$ for CO_2.

Kurganov et al. (2013) reviewed the methodological basis proposed by Petukhov et al. (1980) for studying the pressure-drop of supercritical flow in a round tube in heating and isothermal conditions for both normal and deteriorated heat transfer regimes. Results of previous experimental measurements of velocity and temperature fields in heated tube (reported by Kurganov & Kaptil'ny, 1992) were presented. Using a one-dimensional flow model (Equations 2.1 to 2.5) in calculating the friction-factor, sources of error in one-dimensional modeling were pointed out. They concluded that the flow inertia in the supercritical region could be many times larger than the corresponding "one-dimensional" data calculated based on mass averaged flow parameters (Equations 2.1 to 2.5). This affects the friction-factor determination in supercritical conditions.

Fang et al. (2012) performed a statistical study on experimental pressure-drop data for supercritical R410A and R404A, and CO_2, when they were cooled in small diameter tubes and 18 pressure-drop data for R22 heating which was reported by Yamashita et al. (2003). Although they mentioned that the friction-factor in isothermal conditions is lower than its value in supercritical cooling and is higher than its value in supercritical heating, they proposed a general friction-factor formula based on their data reduction for both heating and cooling conditions.

2.3　Density Wave Oscillations in Two-phase Natural Circulation Loops

Density wave oscillation is the most investigated type of flow instability in two-phase boiling systems. Stenning (1964) and Stenning and Veziroglo (1965) performed fundamental experimental studies towards understanding the mechanism of self-sustained DWOs. Their explanation on the mechanism of DWO's was widely accepted later. It was confirmed by Yadigaroglu and Bergles (1972), Boure et al. (1973), Belblidia and Bratianu (1979), Rizwan-Uddin (1994), Kakac and Bon (2008), and other researchers that DWOs occur due to multiple regenerative feedbacks between the flow rate, vapour generation rate, and pressure-drop. A simple explanation for this mechanism is given by Rizwan-Uddin (1994) and is shown in Figure 2.2. Considering a heated channel with two local restrictions at the inlet and the outlet, fluid enters the heated channel in single-phase (high density or liquid state) condition and by applying heat, it undergoes phase change and finally leaves the channel in two-phase (low density or gaseous state) condition. If we consider the location where the flow starts boiling as the boiling boundary, then the heated channel can be divided into two parts with different densities. Pressure-drop across the heated channel is assumed to be constant as the boundary condition.

Inlet	Single Phase region (High Density)		Two-Phase region (Low Density)	

Inlet Restriction · Boiling Boundary · Outlet Restriction
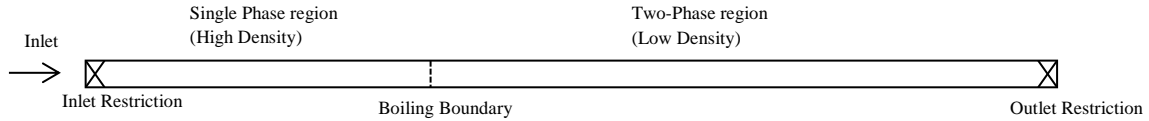
Figure 2.2: Mechanism of DWO

Now applying a positive perturbation in velocity at the channel inlet, the positive perturbation in velocity causes an increase in the density in the two-phase region and causes the outlet restriction pressure-drop to increase when it reaches the channel exit. So to keep the pressure-drop constant across the channel (as the boundary conditions), an instantaneous negative perturbation in pressure-drop is induced to the inlet restriction which leads to a negative perturbation in the inlet velocity. The negative velocity perturbation causes a density wave with lower density to travel toward the channel exit and thus the pressure-drop at the channel exit decreases as the fluid with lower density reaches the exit, resulting in an increase in the inlet velocity and starting the cycle again.

Kakac and Bon (2008) and Boure et al. (1973) conducted complete reviews on boiling two-phase flow instability and Boure et al. (1973) proposed a widely accepted classification for two-phase flow instabilities based on the distinction between the static and dynamic instabilities. This classification of flow instabilities in two-phase flow is shown in Table 2.2.

It is evident from Table 2.2 that although DWOs were introduced and observed as self-sustained (limit-cyclic) oscillations in experimental studies, they are recognized as one type of two-phase flow instabilities. In the other words, limit cyclic oscillations are still known as flow instabilities, even though they do not show diverging flow oscillations.

Table 2.2: Classification of flow instabilities (Boure et al., 1973)

Class	Type	Mechanism/Cause	Characteristic
Static Instabilities			
Static Instabilities	Flow excursion or Ledinegg instability	If the system is operated in the negative slope region of the pressure-drop versus flow rate curve.	Flow undergoes sudden large amplitude excursion to new stable operating condition
	Boiling Crisis	Ineffective removal of heat from heated surface	Wall temperature excursion and flow oscillation
Fundamental relaxation instability	Flow pattern transition instability	Bubbly flow has less void but higher pressure-drop than that of annular flow	Cyclic flow pattern transitions and flow rate variations
Compound relaxation	Bumping, geysering or chugging	Periodic adjustment of metastable condition, usually due to lack of nucleation sites	Periodic process of superheat and violent evaporation with possible expulsion and refilling
Dynamic Instabilities			
Fundamental (or pure) dynamic instabilities	Acoustic oscillations	Resonance of pressure waves	High frequencies(10-100 Hz) related to time required for pressure wave propagation in system
	Density wave oscillations	Delay and feedback effects in relationship between flow rate, density, and pressure-drop	Low frequencies (1Hz) related to transit time of a continuity wave
Compound dynamic instabilities	Thermal oscillation	Interaction of variable heat transfer coefficient with flow dynamics	Occurs in film boiling
	Parallel channel instability	Interaction among small number of parallel channels	Various modes of flow redistribution
Compound dynamic instability as secondary phenomenon	Pressure-drop oscillations	Flow excursion initiates dynamic interaction between channel and compressible volume	Very low frequency periodic process (0.1 Hz)

2.3.1 Density Wave Oscillations in Two-phase Natural circulation Loops

Numerous experimental, numerical, and analytical studies were done on two-phase flow instability in natural circulation loops. However, only the experimental studies of flow instability in two-phase natural circulation loops are reviewed in this section.

Jain et al. (1966) performed the most detailed experimental study on self-sustained flow oscillations in a natural circulation loop for several risers and test section geometries, over a wide range of pressure from 200 to 1500 psia. Later on, Fukuda and Kobori (1979) conducted experimental and numerical studies on forced and natural circulation loops. They detected two types of density wave oscillations in their experimental loop which were named: Type I and Type II.

Type I instability occurs at very low steam quality (x≈0) conditions at the outlet, mainly in vertical up-flow heated channels, where the pressure-drop perturbations and the flow rate disturbances are predominantly caused by gravity (Khabenski and Gerliga, 2012). On the other hand, type II instability occurs at relatively high power when steam quality at the outlet of heated channel is close to one. This type of instability is due to interaction between inlet mass flow rate, void formation and pressure-drop and is characterized by regularity of mode, cycle, and amplitude of flow fluctuations (Khabenski and Gerliga, 2012). Fukuda and Kobori (1979) showed regions of flow instability on a mass flow rate versus power diagram for their experimental studies. Two parallel heated channels oriented vertically were used in their experimental loop. Figure 2.3 shows unstable regions for type I and type II instabilities for both forced (curve A) and natural circulation (Curve B) cases. Fukuda and Kobori (1979) showed that in a natural circulation loop, by increasing the power from zero, mass flow rate increases and Type I DWO may occur.

26

However, further increase in power causes a stable flow in the loop (near the peak) and by applying more heat, the type II instability appears in the negative slope portion of flow rate versus power curve.
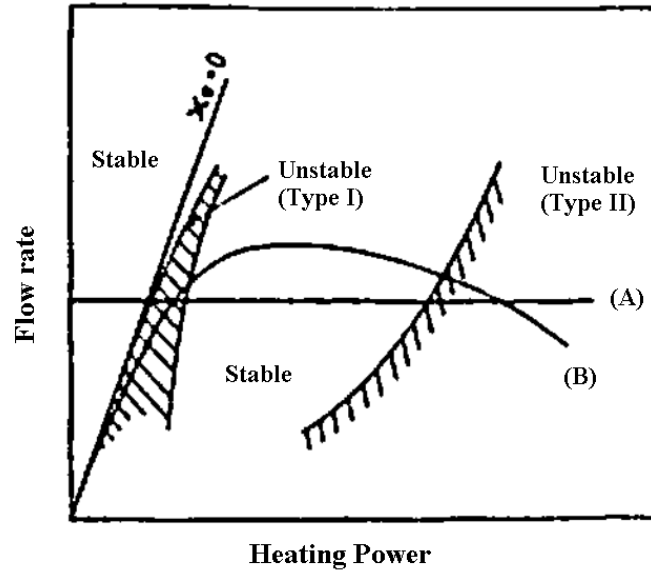
Figure 2.3: Regions of Type I and Type II instabilities for a (A): forced and (B) natural circulation loop, (Fukuda and Kobori, 1979)

This behavior in flow regimes was also confirmed by Kyung and Lee (1994). As shown in Figure 2.4, they observed three distinctive circulation modes while increasing heat flux at constant pressure and inlet temperature conditions in their experimental facilities using Freon-113. Periodic circulation in the positive slope part of the inlet mass flow rate (or velocity) versus power; followed by continuous circulation and another periodic circulation (B) in the negative slope part of mass flow rate (or velocity) versus power curve. The heated channel in this experiment was oriented vertically and Freon-113 was flowing upward in the channel.
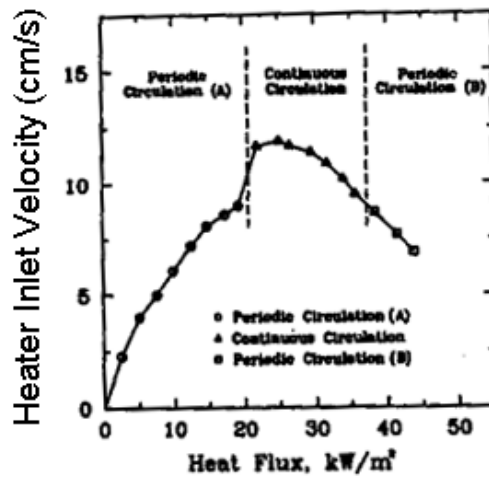
Typical variation of heater inlet velocity
(H=15 cm, Kin=602, Kout=41, Tsub= 20C)

Figure 2.4: Typical variation of heated inlet velocity, and flow regimes

(Kyung and Lee, 1994)

Figure 2.5 shows the transition from periodic oscillation (A) to continuous circulation (non-oscillatory) and the transition from continuous circulation to the self-sustained periodic oscillation (B) during an increase in the heat flux.
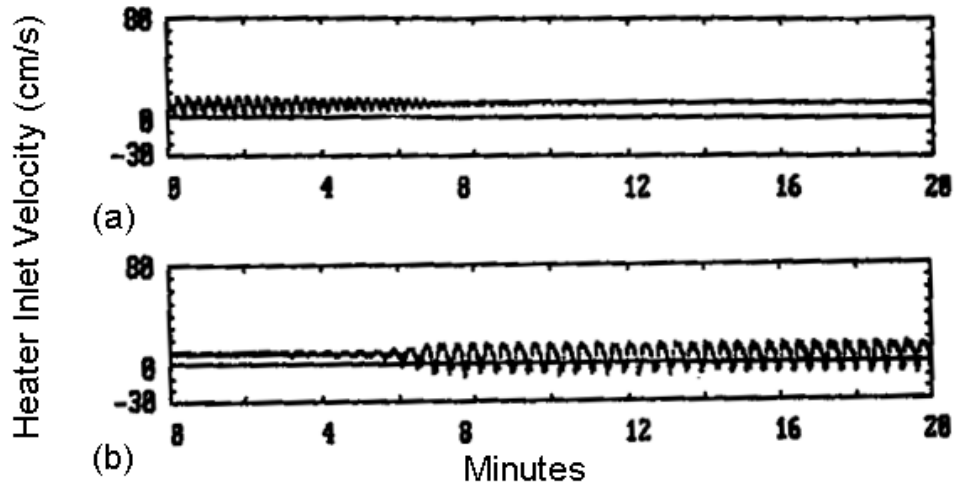
Figure 2.5: Flow pattern transition with variation of heat flux (Kyung and Lee,1994)

Kumar et al. (2012) conducted both numerical and experimental research on two-phase flow natural circulation loop instability in a vertical heated channel. They observed both the type I and type II instability and a stable two-phase operation zone at various pressures and inlet sub-cooling. Figure 2.6 shows the system behaviour during the transition from type I zone instability to continuous stable flow. This figure clearly shows the evolution of cyclic oscillation during the power increase.
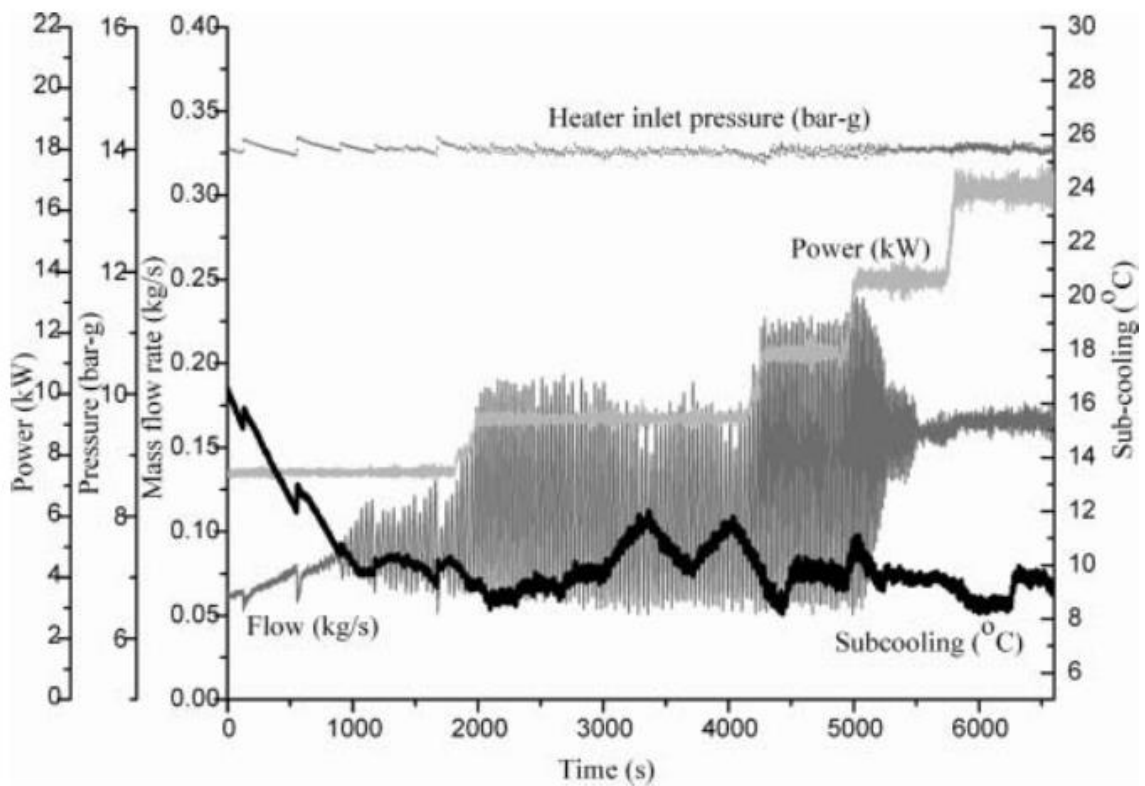
Figure 2.6: Typical transition from Type I instability zone

(Kumar et al., 2012)

Following the stable circulation of the flow, the second type of DWOs was observed in their experiment at a higher heat flux as shown in Figure 2.7.
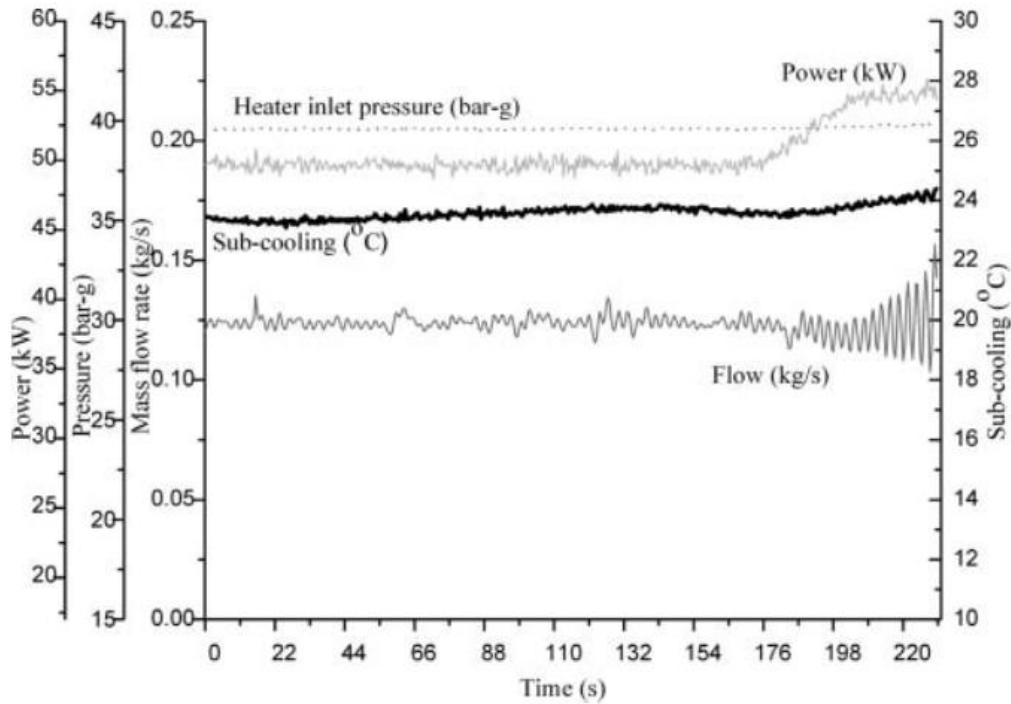
Figure 2.7: Type II density wave oscillations initiation

(Kumar et al., 2012)

Flashing induced density wave oscillation is another type of instability that may occur in natural circulation loops when the vertical heated channel is accompanying a long vertical unheated riser or chimney (the riser is used to increase the length of the hot-leg in a natural circulation loop to enhance the mass flow rate). Flashing is a sudden increase of vapor generation due to the reduction in the hydrostatic head. During this process, the hot liquid leaving the heater experiences a decrease in the static pressure when it flows upward in the chimney. Meanwhile, the saturation temperature decreases and part of liquid is converted to steam. In the early start-up phase of a natural circulation loop, this phenomenon can induce self-sustained flow oscillations. Wissler et al. (1956) were the first to report that flashing causes instability at low pressures. As an example for this type

of instability, Dimmick et al. (1990) designed and constructed an electrically heated natural circulation loop to simulate the behavior of SLOWPOK heating reactor and to use the experimental data to validate four different numerical codes. They performed experiments in both single-phase and two-phase flow. Experimental results of steady-state and transient tests were compared with the numerical codes and agreement was achieved. Also, the SPORTS code (Chatoorgoon (1986)) was able to predict flashing induced density wave oscillations similar to their transient test. Most recently, this phenomenon was investigated by Manera (2003) and Furuya (2006). Furuya (2006) showed that by increasing the pressure from 0.1 MPa to 0.5 MPa, the flashing effect diminishes.

2.4   Density Wave Oscillations in Supercritical Natural Circulation Loops

In this section numerical, analytical and experimental studies on flow instability for supercritical natural circulation loops are reviewed.

Harden and Boggs (1964) and Cornelius and Parker (1964) carried out an experimental and analytical studies of closed natural circulation loops with Freon-114 as the working fluid. Both of these experiments were done at pressures close to the critical pressure of Freon-114. High-frequency thermo-acoustic wave oscillations and low-frequency flow oscillations were reported in these works. Cornelius and Parker (1964) did not observe any flow oscillations when they used a pump in their system (using a pump increases the mass flow rate in the system). The first comprehensive analytical study of various supercritical flow instability modes was reported by Zuber (1966). He concluded that both excursive (static) and oscillatory (dynamic) instabilities may occur in supercritical flow, similar to two-phase boiling systems. The effect of various parameters on flow

oscillations in a single heated channel was studied. However, his analytical approach was adopted for heated channels and not natural circulation loops. Daney et al. (1979) and Fukuda et al. (1992) reported density wave oscillations along coiled heated channels (not natural circulation) using Helium as the working fluid. By introducing SCWR as a new design for thermal rectors, research on flow stability of supercritical flow in natural circulation loops, regained attention.

Chatoorgoon (2001) conducted an analytical and numerical study of flow stability in a single-channel natural circulation loop. His numerical analysis showed an instability mode which he purported it is different from the two-phase flow instabilities. Results of his one-dimensional non-linear numerical stability code (SPORTS code developed by Chatoorgoon, 1986) were compared with an analytical model of supercritical flow instability. In his analytical approach, he postulated that instability boundary could be approximated by the criteria:

$$\frac{\partial(flow)}{\partial(Q)} = 0 \tag{2.13}$$

This condition corresponds to the maximum mass flow rate in the mass flow rate versus power curve. Based on this approximation, non-dimensional parameters governing flow instability of supercritical single-channel natural circulation loop were developed. Later on, Chatoorgoon et al. (2005a) and Chatoorgoon et al. (2005b) examined the validity of those non-dimensional parameters using the SPORTS code with different supercritical fluids including H_2O, CO_2, and H_2. In their numerical study, different vertically-oriented rectangular loops with constant areas were modeled. In all models, the heat source was located at the center of the lower horizontal pipe as a heated length and the heat sink was located on the top segment. This model is shown in Figure 2.8. Variable parameters in

their study were: inlet and outlet K factor, inlet temperature and pressure, length of the heated source and the height of the loop.
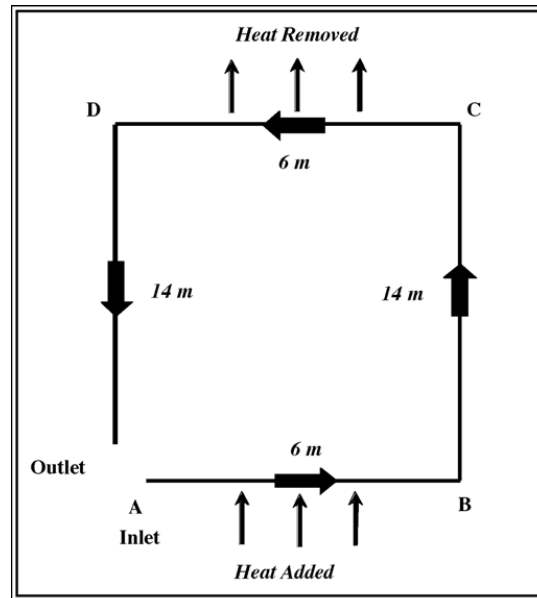
Figure 2.8: Schematic of the loop for height of 14 meter for vertical legs

(Chatoorgoon et al., 2005b)

With constant and equal boundary conditions for inlet and outlet pressures and a constant inlet temperature, equations of mass, momentum and energy were solved using the SPORTS code. For the instability study, a perturbation was introduced to the inlet flow rate and time-trace of the inlet flow variation was monitored. For a stable system, the perturbation diminished with time, but for an unstable case, the perturbation grew. Based on Chatoorgoon et al. (2005a) and Chatoorgoon et al. (2005b), the instability boundary was defined as the power where the oscillations neither decayed nor grew in a transient run. Figure 2.9 shows that the system was stable at the power of 1550 kW and was unstable at 1650 kW. In this case, 1600 kW was considered as the instability boundary.
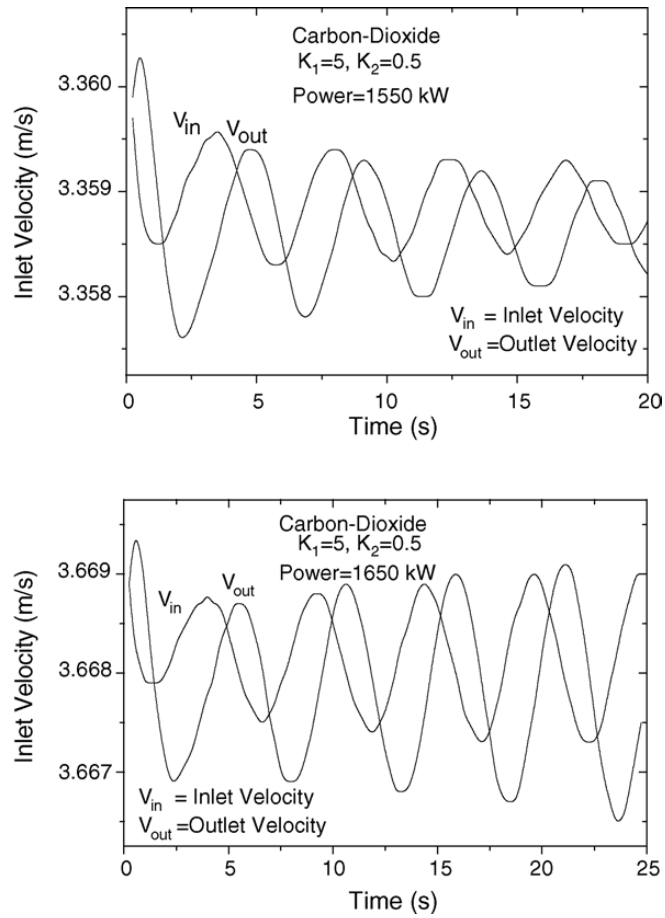
Figure 2.9: Transition of stability for supercritical CO_2 loop

(Chatoorgoon et al., 2005b)

At the end, they concluded that the flow instability boundary is somewhere within 95-100% of the maximum flow rate in the mass flow rate versus power curve (Figure 2.10). This trend was found to be similar for different geometries with different boundary conditions and working fluids discussed in their study.
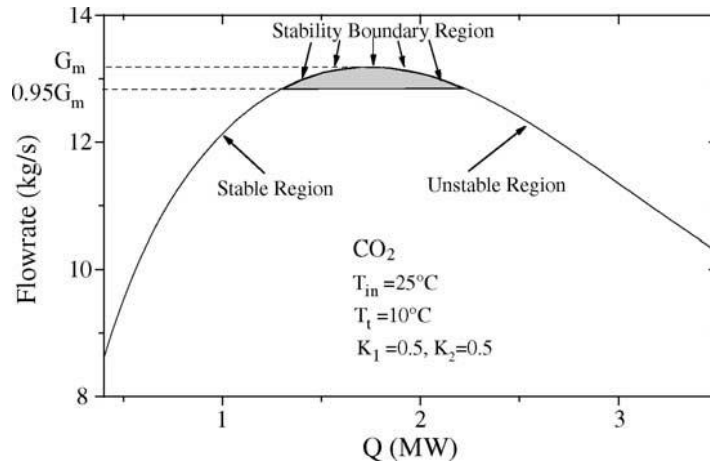
Figure 2.10. Steady-state profile showing stable, unstable and stability boundary regions

for CO_2. (Chatoorgoon et al., 2005b)

Chatoorgoon and Upadhye (2005) conducted a linear stability analysis for the supercritical flow instability in natural convection loops. The reason for this study was to verify the validity of SPORTS code in prediction of instability. This study was done based on classical control theory by linearization of the one-dimensional non-linear conservation equations of mass, momentum and energy, accompanied by the boundary conditions. Finally, they obtained 95% agreement between linear and nonlinear predictions for instability boundary.

Experimental and numerical studies of supercritical CO_2 flow instability in a single channel natural circulation was performed by Lomperski et al. (2004). In their experiment, a two-meter heated channel was located in the lower horizontal tier and a heat sink was located at the top tier. They performed their experiments with power in the range of 0-15 kW, in a wide range of operating pressures and inlet temperatures to the heated channel. They used an orifice for introducing a pressure-drop in the hot-leg of the loop in a few tests. Moreover, they used an energy balance across the heated channel for

calculating the mass flow rate in the loop. Although their numerical model predicted flow instability in the loop, they did not observe any flow instability in their experimental tests.

Jain and Corradini (2005) made an attempt to obtain experimental results for the instability of supercritical CO_2. Although they were not successful in obtaining instability in the experiment, they developed a linear code for stability analysis of three different geometries for natural circulation loops with water or CO_2 as the working fluids.

They found that the instability boundary is different for different combinations of geometries and working fluids. Moreover, their numerical approach predicted flow oscillations in the negative slope part of the mass flow rate versus power curve. They concluded that the flow instability boundary is not strictly related to the peak region of the mass flow rate versus power curve.

Jain and Rizwan-uddin (2008) carried out a 1-dimensional numerical study for investigating flow instability in natural circulation loops with CO_2 as the working fluid. They compared the steady-state curve of mass flow rate versus power with other numerical studies reported by Chatoorgoon et al. (2005b) and obtained close agreement with the steady-state solution. However, their results for instability boundary deviated substantially from results reported by Chatoorgoon et al. (2005b). This disagreement was attributed to the large time steps used in Chatoorgoon et al. (2005b). The study of Jain and Rizwan-uddin showed the instability boundary in the positive slope portion of mass flow rate versus power curve, far from the maximum mass flow rate.

Swapnalee et al. (2012), performed steady-state experiments with supercritical CO_2 and water to validate the generalized correlation they proposed for estimating the steady-state

flow in supercritical natural circulation loops. The model was validated by limited experimental water data. Also, a numerical analysis was performed to predict the static instability boundary for both CO_2 and water. The static instability boundary was found only for supercritical water and not for CO_2. Moreover, no static instability was reported experimentally.

Sharma et al. (2012) performed numerical and experimental studies on a supercritical natural circulation loop in the steady-state conditions. They reproduced the experimental measurement of flow rate with their numerical code (NOLSTA) and obtained $\pm15\%$ deviation in numerical results compared to experimental data. Also, Sharma et al. (2013) reported experimental results of instability for a supercritical CO_2 natural circulation loop with horizontal heated channel and horizontal cooler. In addition to the horizontal heating and horizontal cooling configuration, they tried vertical heating and cooling, but they did not observe flow oscillation in those cases. They performed their experiments at pressures 8.1-9.1 MPa with constant water flow rates in the secondary side for cooling (10-15 lpm and 34 lpm) while they were increasing power on the heated channel. They did not have a flow-meter in their loop and therefore they were using an energy balance across the heated channel for calculating mass flow rate. For flow oscillations cases the heater inlet temperature was between 27 ºC -31ºC (close to critical temperature) and the outlet temperature was oscillating between 29-45 ºC. They modified the NOLSTA code for including the wall heat capacitance effect and they showed that wall thickness stabilizes the system. They also mentioned that in all the cases of flow oscillations, the volumetric expansion coefficient of CO_2 was very high. Figure 2.11 shows a sample of flow oscillations they observed in their experiment
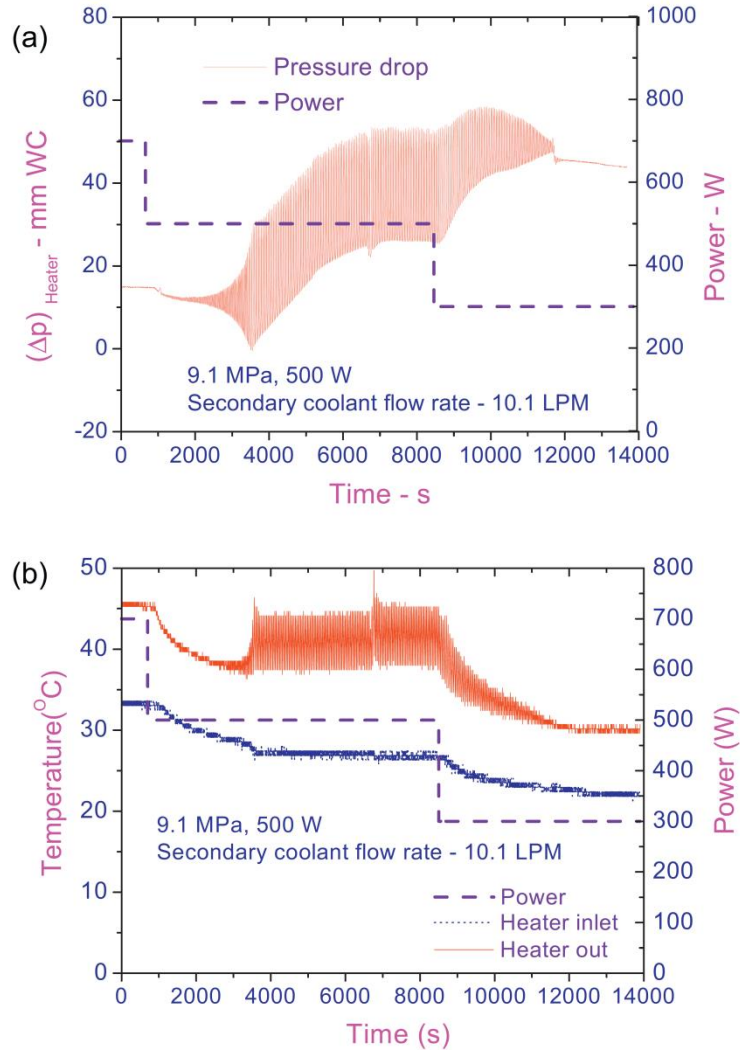
Figure 2.11 Typical unstable behavior at 500 W for horizontal heating and horizontal

cooling (a) pressure-drop across the heated channel

(b) inlet and outlet temperature (Sharma et al., 2013)

Debrah et al. (2013) conducted a numerical analysis for flow instability in natural circulation loops by taking into account the effect of the tube wall thickness. They then adopted the non-dimensional parameters of Ambrosini and Sharabi (2008) for heated channels, for natural circulation loops.

Chen et al. (2013) reported flow instability in their supercritical water natural circulation loop. The oscillations were observed when the outlet temperature of water in the heated channel was close to the pseudo-critical temperature. The heated section in their study was placed vertically and an annular heat exchanger was placed horizontally at the top tier. In their experiments, power was increased gradually, and power, inlet and outlet temperatures, and wall temperature were recorded. Mass flow rate in their study was calculated using an energy balance. Experiments were performed using three different test-sections with different diameters and they claimed observing both static and oscillatory types of instability. In their study, static instability was characterized by a sharp reduction in the mass flow rate when the outlet temperature of the heated channel was close to or higher than the pseudo-critical temperature. A sample of unstable cases is shown in Figure 2.12.
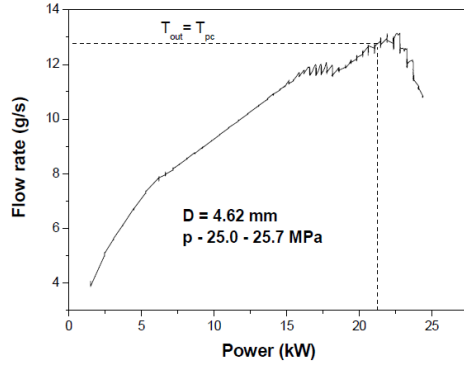
(a) D = 4.62 mm
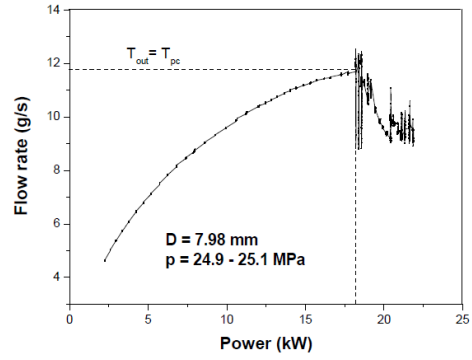
(b) D = 7.98 mm
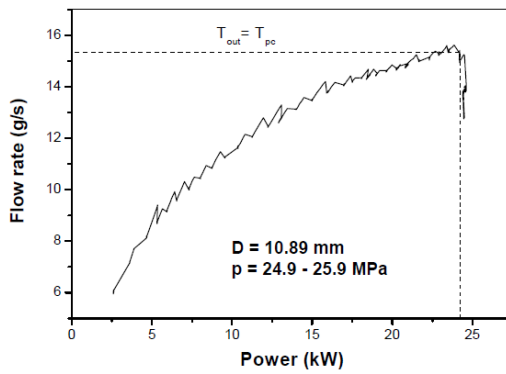
(c) D = 10.89 mm
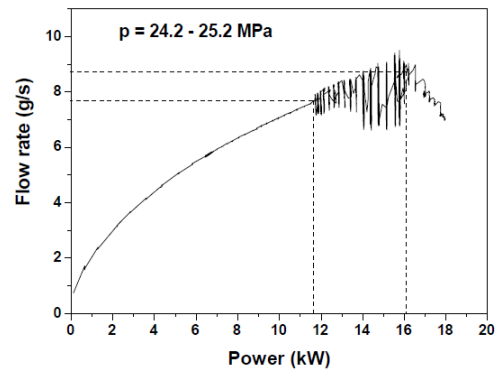
(d) D = 4.62 mm

Figure 2.12: Variation of flow rate with power (Chen et al., 2013)

They also recognized local fluctuations of the heated wall temperature as the dynamic instability which is not a correct criterion for characterizing dynamic instability. These oscillations of wall surface temperature was observed for a tube with the diameter of 4.62 mm when the outlet temperature of water was lower than the pseudo-critical temperature, while the heated wall surface temperature was higher than the pseudo-critical temperature. (Figure 2.13)
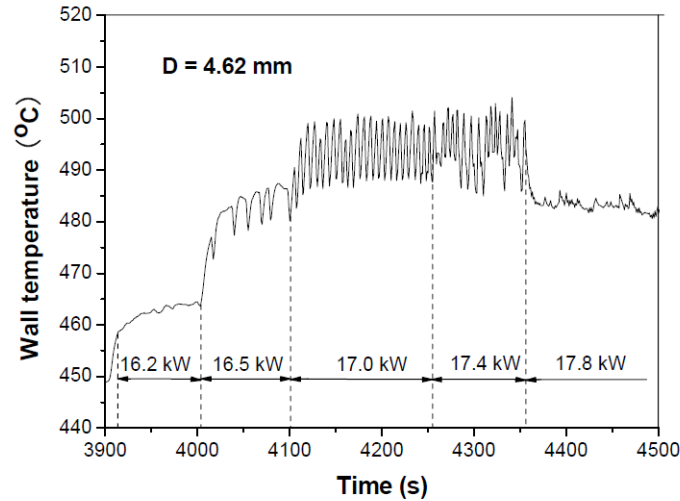
Figure 2.13: Wall temperature in the power range of 16.2-17.8 kW (Chen et al., 2013)

Although, Chen et al. (2013) showed new experimental data for flow oscillations in their supercritical natural circulation loop, they did not provide sufficient detailed information of their experimental work, which is useful for numerical modeling and validation of numerical codes. Two main sources of inaccuracy in their experiment for calculating mass flow rate are: strong variation of the enthalpy with temperature in the pseudo-critical region, along with the fact that a thermocouple measures the temperature of a point in the flow and is not necessarily representative of the measured bulk temperature. Moreover, their study did not provide experimental measurement of pressure-drop along the heated channel and the heat exchanger that are important in studying both steady-state and instability modes of a natural circulation loop.

Lv et al. (2013) performed an experimental study for a supercritical water loop with a single vertical heated channel. Their study showed flow oscillations in the positive slope part of mass flow rate versus power curve. The oscillations vanished by increasing the

power level and they did not reach to the maximum flow rate (peak mass flow rate versus power curve) in their tests. Instabilities appeared when the outlet temperature of water in the heated zone was close to the critical temperature (374.2ºC), and always began with an increase in the mass flow rate. During flow oscillations, system parameters such as the mass flow rate, the outlet temperature of water in the heated zone and system pressure fluctuated periodically, and the periodicities changed with the heating power. Their results of flow instability are shown in Figure 2.14.
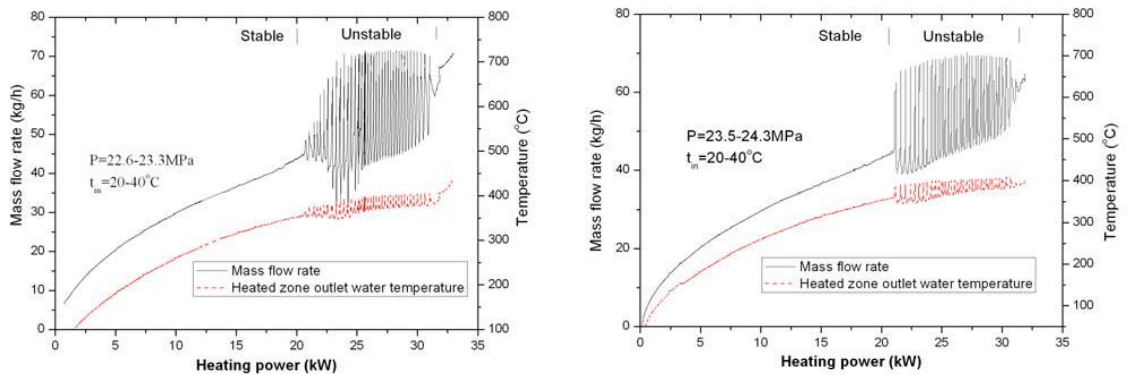
Pressure: 22.6~23.3MPa   Pressure: 23.5~24.3MPa

Figure 2.14: General trends of supercritical water natural circulation instabilities

(Lv et al., 2013)

The results presented by Lv et al. (2013) are very similar to the first type of DWO (Type I) (which occurs mostly in vertical two-phase boiling natural circulation loops with relatively low coolant velocities (Khabensky & Gerliga (2012)) instability in two-phase natural circulation loops. Type I instability in boiling systems occurs in the positive slope part of the mass flow rate versus power curve, when outlet temperature is close to the saturation temperature, and in results reported by Lv et al. (2013), the outlet temperature was close to the pseudo-critical temperature.

In both the studies of Chen et al. (2013) and of Lv et al. (2013), system pressure was not kept constant during the tests and this makes it more difficult to model the tests using licensed codes. It is noteworthy that both of these studies were done in the loops with vertical heated channel when water was flowing upward.

2.5 Summary

From this literature review it can be found that very limited experimental data is available for instability in supercritical natural circulation loops. Moreover, in many experiments, steady-state parameters of the loop were not addressed thoroughly to be used in the numerical modeling and validation of licensing numerical codes. It should be noted that, in all of the experiments reviewed in Chapter 2, flow oscillations were observed when the outlet temperature was close to the pseudo-critical temperature and no flow oscillations are reported at relatively high outlet temperatures (above pseudo-critical temperature).

.

CHAPTER 3

EXPERIMENTAL FACILITIES AND TEST PROCEDURES

3.1   Introduction

This chapter is devoted to the explanation of the experimental set-up, components, instruments and the test procedure. The initial test section consisted of an inlet header, three parallel heated channels (circular tubes), and an outlet header which was designed and fabricated by Stern Laboratories (2007). Tummalapalli (2007) performed design, product selection, piping, and assembling of the rest of the experimental set-up. The experimental facilities were originally designed for supercritical water as the working fluid; however, throughout the designing process, selections of some components were changed to make the loop appropriate for supercritical CO_2 (considerably lower working temperature and pressure condition) instead of supercritical water. Tummalapalli (2007) performed only pressure testing of the loop at 10 MPa and no experimental results were generated.

For this study, the available experimental set-up was modified for single channel application by removing inlet/outlet headers and adding a turbine flow-meter for accurate measurement of volumetric flow rate of CO_2. Moreover, the heated channel was designed and assembled for multiple measurements of pressure-drop along the heated channel. Minor improvements and troubleshooting in the differential pressure transducer measuring range, power supply, and secondary side water supply (for cooling) were done during the first stage of exploratory experimental tests. A new Data Acquisition System (DAS) for measuring signals was installed by a summer student in 2011.

3.2 Experimental set-up and components

The experimental set-up is a rectangular loop with a horizontal length of 725.8 cm and a height of 101.6 cm, oriented vertically with the test section at the middle of the horizontal lower tier and a heat exchanger at the middle of the horizontal upper tier (see Figure 3.1, and Appendix D). An accumulator (SB 600-10 A 1/002 S1–345 C) is connected to the cold side of the loop, with the aim of adjusting the pressure in the loop during experiments. Two pneumatic ball valves are located upstream and downstream of the heated channel to introduce pressure-drops in the system. An evacuation pump is attached to the right hand side vertical leg of the loop for removing air from the loop. Then the loop is filled with CO_2 grade 4.5 (99.995% purity) using a booster pump. Direct current electricity is passed through the Inconel tube in the test section for generating heat. A heating tape is wrapped around the right vertical leg to decrease the density of CO_2 in that leg and to initiate flow movement in the loop. Supercritical CO_2 flows counter clock-wise in the loop. There is also a large settling chamber in the lower part of the loop which was not used in any of the experiments in the present study. The settling chamber can be part of the loop by closing or opening the manual ball valves (BV-1, BV-2, BV-3, and BV4). Figure 3.1 shows a schematic of the experimental facilities used in the present study.

In addition to the mechanical components explained above, Figure 3.1 shows the measured data during tests. An absolute pressure transducer is connected to the loop, below the accumulator, to measure the system pressure. Two resistance temperature detectors (RTDs) are installed at the inlet and outlet of the heated channel for measuring the flow temperature. It should be noted that there is no mixing chamber at the outlet of
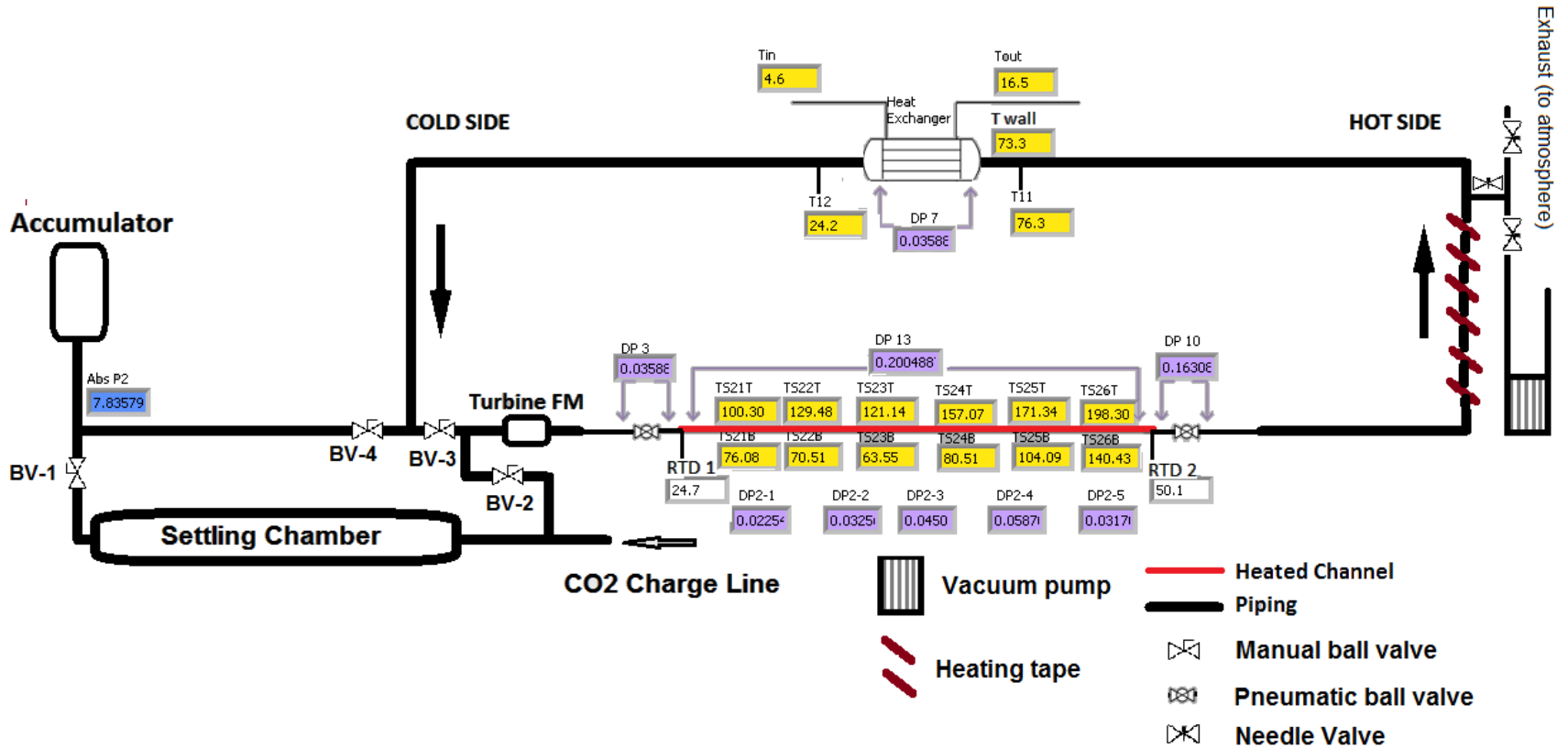
Figure 3.1: Schematic of the supercritical natural circulation loop

the heated channel and therefore, RTD2 is not representative of the mass flow averaged temperature. RTD2 is not used in any calculation in this study. There are also four 1/8" K-type thermocouples for measuring the temperature at the inlet and outlet of the heat exchanger in the CO_2 side and in the water side (Cooling loop). There are also twelve 1/16" K-type thermocouples attached to the bottom and top of the heated channel surface at six locations along the channel for measuring the wall surface temperature. Nine differential pressure transmitters are located at different parts of the loop to measure the pressure-drop. Pressure-drop across the inlet and outlet pneumatic valves, total and the segmental pressure-drops along the heated channel, and pressure-drop across the heat exchanger in the CO_2 side are measured. Voltage-drop across the heated channel and amperage from the rectifier are measured for calculating the applied heat on the channel. The most crucial measured parameter in this experiment is the volumetric flow rate of CO_2 in the loop which is done by using a turbine flow-meter. Also a paddlewheel flow meter is used to measure the water flow rate in the secondary side (cooling loop).

3.3 Components

3.3.1 Heated Channel

The heated channel is a 259 cm long Inconel 625 polished circular tube (OD: 0.75", ID: 0.51") which is heated by DC current through two conductors which are welded to the flanges (1" Class 2500, WN XXS) on either side of the heated channel. Inconel 625 has good electrical and thermal conducting properties which provide uniform heat flux on the heated tube. Two pieces of 1/8" coupling are welded to 1" (SCH. XXS) for measuring

47

Heated channel (OD: 19.05, ID:12.95, Length: 2590)

All dimensions in mm

Conductor

Conductor
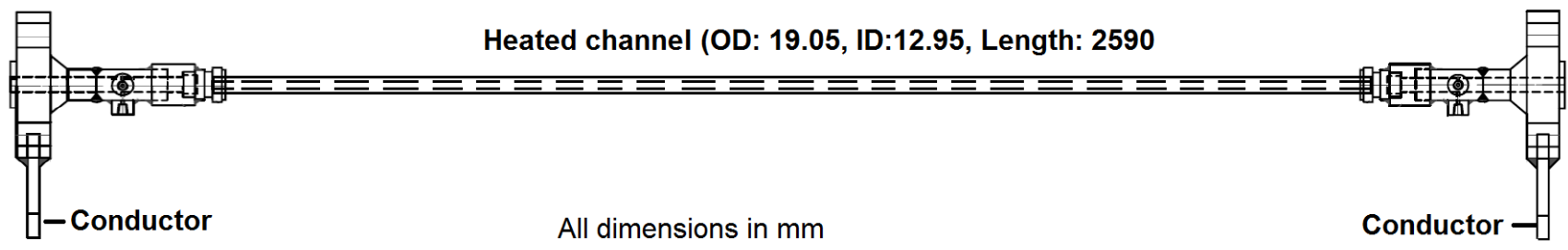
(a) Front view of the heated channel

Dielectric Fitting   DP Cell

Tee Union   1/8" Tubing
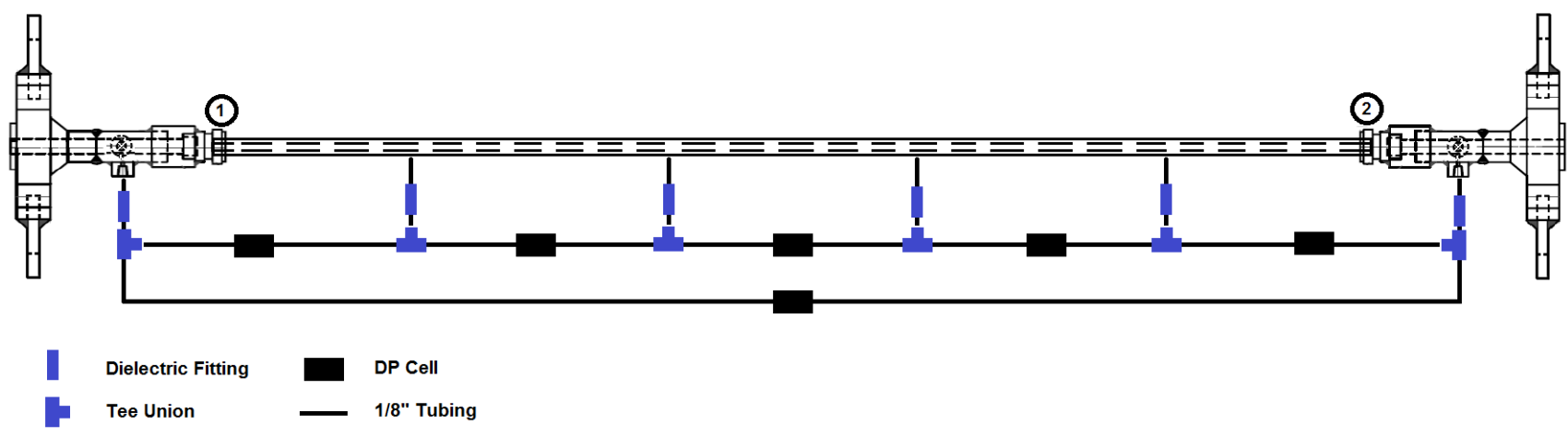
(b) Top View of the heated channel with DP transducers arrangement

Figure 3.2: Front and top view of the heated section

48

the flow temperature and pressure-drop. In this study, the heated channel was tapped for additional segmental pressure-drop measurements along the heated section and the entire differential pressure transmitter were installed at the same height as the pressure taps and the heated channel. Also, there were two small area changes at the inlet and outlet of the heated channel when it's connected to the flanges (locations 1 & 2 on Figure 3.2 (b)).

3.3.2   Piping

The loop piping is 1 1/4" SCH. XXH stainless steel 316L pipes (OD: 42.16 mm and ID: 22.61mm), 90º elbows and tees. Stainless steel flanges (1.1/4" and 1" WN, Class 2500 B16 XXH SA182 F316/316L) are used to join the various components (test section, heat exchanger, inlet/outlet pneumatic valves, turbine flow meter) of the loop. Flexitalic gaskets are used between the stainless steel flanges to make the facility pressure tight and leak proof.

3.3.3   Heat Exchanger

Cooling is accomplished by a miniature 1-1 shell and tube heat exchanger (Exergy LLC, Part No. 01259). This heat exchanger consists of 127 stainless steel tubes (3.2mm OD, 0.32mm thick). The amount of heat removed from the heat exchanger is set manually by changing the control valve located on the secondary side. Supercritical CO_2 and water are flowing in the opposite directions in the heat exchanger.

3.3.4   Power Supply

A rectifier (EMHP 20-1500) provides 20 Volts with 1500 Amps and totally 30 kW power in this experiment. However, the maximum power is limited by the resistance of the heated channel. In all experiments performed in this study maximum attained power (heat

supplied to the channel) was about 14 kW. To prevent from electrical shock due to high amperage, the test section is electrically isolated from the rest of the loop by using glass filled teflon® glass gaskets between the stainless steel flanges and insulating sleeves to the flange bolts.

3.3.5 Accumulator

A bladder accumulator (10.0 Lts, Hydac®) accompanied by a single stage pressure regulator (PR-57 series, GO Regulator®), connected to a nitrogen gas bottle and to the accumulator, are used to control the pressure in the loop. The accumulator consists of a fluid section (supercritical CO_2) and a gas section (N_2), which are separated by the gas-proof bladder. The fluid section is located in the lower part of the accumulator connected to the loop and the gas section is located in the upper part of the accumulator and is connected to the high pressure N_2 bottle (Praxair® industrial N2 with 2200 psi pressure).

3.3.6 Ball valves

Four manual and two pneumatic ball valves are installed in the loop for controlling the flow in the loop. Manual ball valves (BV-1, BV-2, BV-3, and BV-4: H27 series Habonim®) are shown in Figure 3.1. By closing BV-1 and BV-4, the settling chamber is removed from the rest of the loop. In all of the experiments reported in this study, the settling chamber was excluded from the loop by closing BV-1 and BV-4. In addition to the manual valves, two electro-pneumatic valves of the size ¾" are installed at the inlet and outlet of the channel with the purpose of introducing a pressure-drop in the loop. Each of these electro-pneumatic valve assemblies consists of a valve (Jarecki®), an actuator

(Habonim®), and a position controlling transducer (Flowserve®), providing the operator to control valves positions throughout the tests using the DAS.

3.3.7 Evacuation pump

A vacuum pump (R5-PB0003 A, Busch®) capable of achieving 29.8 inHg vacuum is installed for evacuation of the loop and elimination of air which is done before pressuring the loop. The vacuum pump is connected to the vertical right riser by using stainless steel tubing, needle valves, and compression fittings.

3.3.8 CO2 supply and booster pump

Grade 4.5 carbon dioxide (99.995% purity) cylinders supplied by Praxair® are used to fill the loop to the required pressure after the evacuation process. The cylinders are supplied at 850 psi (5.8 MPa, while critical pressure for CO2 is 7.4 MPa) and hence, they cannot be used directly to pressurize the loop to the desired supercritical pressures. To attain the required carbon dioxide pressure in the loop, a Maxpro® gas booster (DLE30-1) was installed by Tummalapalli (2007). The gas booster raises the pressure of the carbon dioxide from the cylinder pressure up to 1450 psi inside the experimental facility.

3.4 Instrumentation

Several instruments were used in this study to measure and control different variables. These variables include pressure, flow temperature, mass flow rate, amperage and voltage drop, inlet/outlet valve position, and heated wall surface temperature. Table 3.1 lists the specification and measured variable of each instrument used in this experiment.

Table 3.1: Specifications and measured variable of instruments

Instrument	Specification	Measured variable
Absolute Pressure Transducer-Abs P2	GP:50 Industrial pressure transducer Model: 311-C-RO-3-CJ, Range: 0-1500 psi	System absolute pressure Located bellow the accumulator
RTD1- RTD2	OMEGA Engineering Model: P-M-A-1/8-6-1/8-P-3, Ungrounded RTD1 Range: 0-60 ºC RTD2 Range: 0-150 ºC	RTD1: Flow temperature at the Inlet to the heated channel RTD2: Flow temperature at the outlet from the heated channel (both of them include read-out)
CO_2 flow rate-FM1	OMEGA Engineering Model: FTB-1421 Range: 0.6-3 GPM	Mass flow rate at the inlet to the heated channel (cold side) (include a read-out)
Water flow rate-FM2	Seametrics Model: SPX-050, 1/2" Low Flow Meter Range: 0.1-10 GPM	Mass flow rate of cooling water in the secondary side (include a read-out)
Thermocouple-T11	OMEGA Engineering Model: K-type, 1/8" sheath diameter	Flow temperature of CO_2 at the inlet to the heat exchanger (hot stream-inlet)
Thermocouple-T12	OMEGA Engineering Model: K-type, 1/8" sheath diameter	Flow temperature of CO_2 at the outlet from the heat exchanger (hot stream-outlet)
Thermocouple-Tin	OMEGA Engineering Model: K-type, 1/8" sheath diameter	Flow temperature of water at the inlet to the heat exchanger (cold stream-inlet)
Thermocouple-Tout	OMEGA Engineering Model: K-type, 1/8" sheath diameter	Flow temperature of water at the outlet from the heat exchanger (cold stream-outlet)
Thermocouple-TS21B,TS21T, TS22B,TS22T, TS23B,TS23T, TS24B,TS24T, TS25B,TS25T, TS26B,TS26T	OMEGA Engineering Model: K-type, 1/16" sheath diameter, Ungrounded	Heated wall surface temperature (B: bottom, T: top, 21-26 are 6 section along the heated channel)
Differential Pressure Transducer-DP 2-1, DP 2-2, DP 2-3, DP 2-4, DP 2-5, DP 7,	Valydine Engineering Corporation Model: DP 303 Range: 0-0.3 psi	DP 2-1 to DP2-5 are pressure-drop along the heated channel and DP7 is pressure-drop across the heat exchanger for CO_2
Differential Pressure Transducer-DP 13	Valydine Engineering Corporation Model: DP 303 Range: 0-0.5 psi	Total pressure-drop along the heated channel

Table 3.1: Specifications and measured variable of instruments (Continued)

Differential Pressure Transducer- DP 3, DP 10	Valydine Engineering Corporation Model: DP 360 Range: 0-8 psi	Pressure-drop across inlet pneumatic valve (DP3) and pressure-drop across outlet pneumatic valve (DP10)
Isolated DC voltmeter- TR2	Wilkerson Instrument Co. Model: SR2101 Range: 0-20 volts	Voltage drop across the heated channel
Amperage*	Rectifier Model: EMHP 20-1500 Range: 0-1500 ohm	Amperage is calculated from voltage drop (mv) across a shunt resistor located in the back of rectifier (I=measured voltage drop*15)

*A linear correlation for calculating amperage was developed based on voltage drop across the heated channel and calculated amperage (I= (voltage drop)*43.806+1.856). This correlation was used for calculating power.

3.5   Modifications in the Experimental Facilities

Throughout many exploratory tests in the first phase of this study, some major and minor modifications were made in the experimental facilities which are explained below.

1- Increase in the power supply

At the beginning of experiments, the maximum attainable power was about 8 kW which was limited by the breaker maximum amperage limit (600 Amps). By adding another breaker to the circuit, the maximum available power was increased to 14 kW and higher temperatures of CO_2 were achieved at the outlet of heated channel.

2- Increase in the secondary side water flow rate

By increasing the maximum amperage of the power supply, the cooling capacity of the loop needed to be increased. Tap water was used in the secondary side for cooling. The maximum flow rate for cooling was 18 lpm before modifications and it reached 28 lpm after modifications. A new paddlewheel flow meter with a higher

measuring range was selected and installed. It should be noted that the inlet temperature of water to the heat exchanger varies in summer (about 12-13 ℃) and winter (about 4-5 ℃). This variation in the inlet temperature, affects the cooling capacity of the system.

3- Segmented Pressure taps along the heated section

To make measurements of pressure-drop more accurate along the heated channel at subcritical and supercritical temperatures, extra pressure taps were installed along the heated channel. For this purpose, SS-200-R-4BT bore through reducers were welded to the side of heated channel by a certified welder for high pressure facilities. Dielectric fittings (SS-4-DE-6), T- unions (SS-200-3), needle valves (SS-ORS2), and seamless 1/8" tubing (SS-T2-S-028-20) (all from Swagelok) were used for assembling and installing DP 303 cells.

4- Remove inlet and outlet headers

The experimental facility was originally designed and constructed for three parallel channels (Figure 3.3 (a)). In that design, an inlet header for separating and an outlet header for collecting flow in three heated channels were devised. In addition to the headers, two pneumatic valves (1¼" size), one upstream of the inlet header and one downstream of the outlet header on the main line had been installed.

However, the focus of this study was pressure-drop and flow instability of a single channel natural circulation loop. Moreover, large temperature gradients for CO_2 were observed frequently in the outlet header between the middle and end sections (temperature was not homogeneous in the outlet header) and also, the transient time

for the loop to reach a steady-state conditions was long. Hence, it was decided to remove both inlet and outlet headers, and a large size pneumatic valve (1¼" size) upstream of the inlet header (Figure 3.3 (b)). This change will make the numerical modeling of the loop easier and closer to the reality. The other advantage obtained from removing the inlet/outlet headers was providing some space for installing the turbine flow-meter. Prior to this point, mass flow rate of CO_2 was calculated based on energy balance. In Chapter 4, the uncertainty of this method will be discussed.
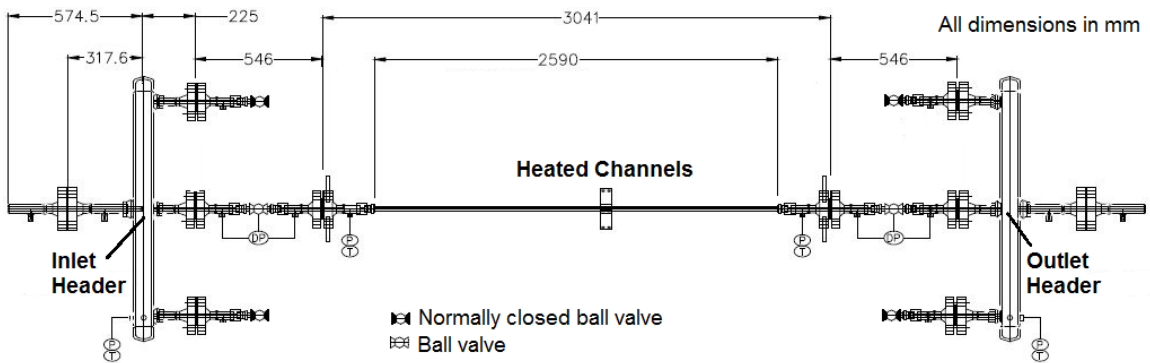
(a) before removing headers
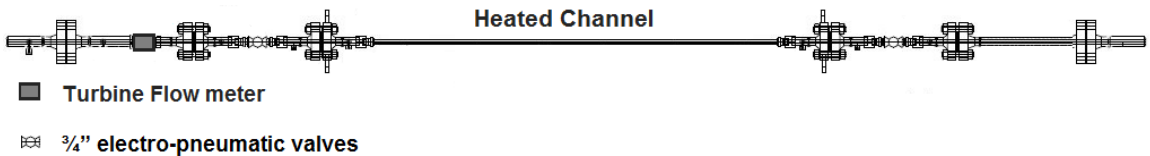
(b) after removing headers

Figure 3.3: Top view of the heated section

5- Adding the Turbine Flow-meter

Before removing the headers, an attempt was made to obtain flow rate measurements of CO_2 by using an ultrasonic flow meter. A significant amount of time was spent on installing and testing two ultrasonic flow meters (UTXDR-407 (2 MHz) and GC868 -

Clamp-On Gas Ultrasonic Flow Meter) which operate based on the sound speed of the medium, but none of them worked for this application due to low sound speed of supercritical CO_2. Finally, it was concluded that due to the very low sound speed of supercritical CO_2 (150 m/s) and large thickness of the piping (9.7 mm), flow rate measurement was impossible for these conditions with the examined ultrasonic meters.

After a comprehensive search on venturi, coriolis, and turbine flow meters, an FTB-1421 turbine flow meter from OMEGA Engineering was selected for this application. The required modifications in the loop were made to install the flow meter in the cold side and upstream of the heated channel in the horizontal tier.

3.6   Steps to Prepare the Supercritical Loop for Experiment

In the set-up preparation of the loop, which could take a week, the following steps were taken:

- Calibration

Calibration of some instruments used in the tests was based on provided calibration certificates by companies. For example, the turbine flow meter in the primary side was supplied with a 5-Point NIST traceable calibration certificate for water. Figure 3.4 shows the effect of viscosity of fluid on the calibration of a turbine flow meter. In this figure, the x-axis shows the volumetric flow rate (Q) and the y-axis shows the meter factor. For fluids with low viscosities (close to 1 centistokes) the meter factor remains constant, especially for the linear part of this plot ($Q > 10^{-4}$ m^3/s). Since the kinematic viscosity of supercritical CO_2 (0.07 centistokes) is about fourteen times smaller than the kinematic viscosity of water (1 centistokes), the accuracy of the turbine flow meter is not greatly affect using supercritical CO_2. However, for the available flow-meter, the meter over

predicts the flow rate at the bottom range of the meter for fluid with specific gravity close to 0.7 and lower.

The calibration of the DP cells was done regularly before pressurizing the loop. DP cells calibration was performed using a T-140-200"WC pressure calibrator with a Martel hand pump. The calibration was performed by adjusting the ZERO and the SPAN on the demodulator for zero and maximum differential pressure on the DP cells. After this step, all fittings were tightened and the loop was ready for leakage test.
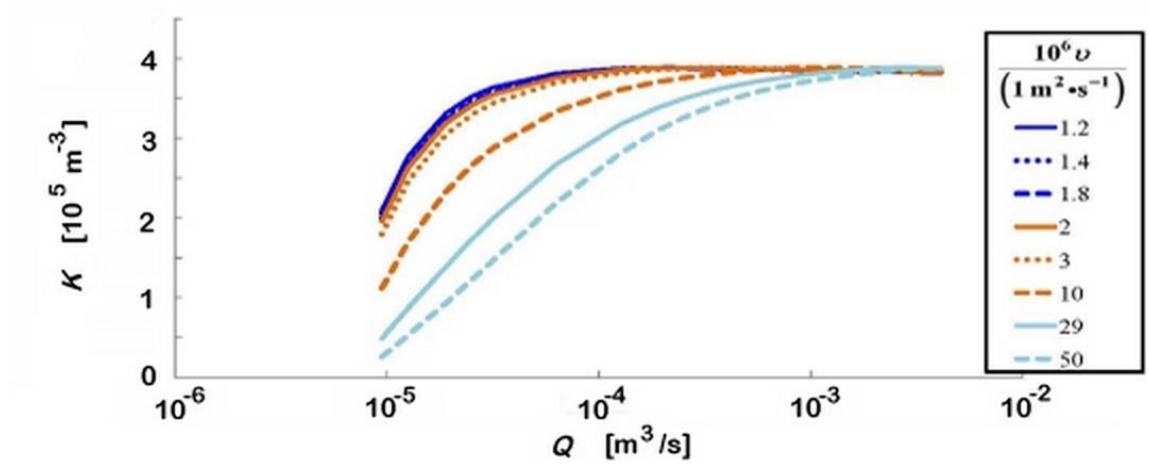
Figure 3.4: Effect of the fluid viscosity on the calibration of turbine flow meter,

(NIST, 2012)

- Leakage test

After calibrating the DP cells and connecting all the fittings, the loop was pressurized up to 400-500 psi by CO_2. The loop kept under this pressure for one day to see whether the pressure remained constant or decreased because of the leakage. In the event that a pressure-drop was observed in the system, soapy water was used for the leak testing. Leakage test for flanges was done by using water and a transparent tape which was wrapped around the gap between the two flanges.

- Evacuation

After the leakage test, the loop was depressurized and a vacuum pressure gage was installed on the loop. The vacuum pump had to be on for about 20-24 hrs. However, it had to be turned off to cool down after 6-7 hours of continues operation and then be turned on again.

- Pressurizing

Pressurizing the loop was the next step in this preparation process. For this purpose, a needle valve which was located below the vacuum gauge was closed and the vacuum gauge was replaced with a 0-1500 psi pressure gauge. Then the valves connecting the CO_2 cylinder to the loop were opened and the pressure increased in the loop. After the loop and cylinder reached the same pressure, the booster pump was turned on to increase the pressure in the loop to 6-7 MPa. Two to three CO_2 cylinders were used both to do the leakage test and to fill out the loop to the desired pressure. Extra caution had to be taken when using the booster pump because the connecting hose and the high pressure part of the booster got hot during continuous operation of the booster pump and the high pressure O-rings and plastic gaskets might have failed. It is recommended to turn off and turn the booster pump on in the intervals of 15 minutes on and 15 minutes off.

Pressure spikes from the booster affected the calibration of the DP cells and turbine flow meter. Therefore, a procedure was planned to decrease this effect by directing the flow to the settling chamber by shutting off BV-2, BV-3 and partially closing BV-1 and BV-4. It's recommended to open the valve in the secondary side and cools down the loop during pressurizing the loop. When desired pressure was achieved, the loop remained for a day to stabilize. In the next day, the calibrations of the DP cells were checked to see if they

show zero value when there was no flow in the loop. If the offset in this case was more that 3% of the full range of the DP cells, the calibration was gone and they had to be recalibrated again and above steps had to be repeated. It worth noting that, a small leakage from one side of a DP cell causes an offset in the output signal of that DP cell. If the offset for zero flow (Δp=0) is more than 3% of the full scale range of the DP cell, recalibration of the DP cell is required. Also, a differential pressure more than 5 times of the diaphragm measuring range deforms the diaphragm permanently and destroy it.

3.7   Test Procedure

The test procedure for the first stage of this study was designed to measure the pressure-drop along the heated channel in the steady-state conditions. In the second stage, measurements were used to address the steady-state conditions (power, inlet/outlet K factors, and flow rate) which led to the flow oscillation in the loop. The following steps were taken in performing the tests:

1- All the signals were recorded by computer in the steady-state conditions at room temperature.

2- The heating tape was turned on.

3- After 15-20 minutes the manual valve in the secondary side (cooling system) was opened for about 1 lpm flow rate of water.

4- The rectifier was turned on and the breakers were turned on as well.

5- A small amount of power (0.1-0.2 kW) was applied to the heated channel.

6- Power was increased to 1.1 kW over 15-20 minutes.

7- Cooling water was adjusted in the secondary side until the desired inlet temperature was reached at the inlet to the heated channel.

8- The pressure regulator on the accumulator was adjusted to the desired working pressure in the loop.

9- The transit time of the loop was about 1 minute and after making any changes, therefore, it took a few minutes for the loop to stabilize.

10- After the flow was established in the loop, inlet/outlet pneumatic valves were closed partially to the desired angle.

11- After a while the heating tape was turned off

12- When the parameters were stable, data recording was performed for steady-state conditions for about 5 minutes.

13- Power was increased to the next level by 0.6 kW (nominal) increments.

14- Cooling water was adjusted to keep the inlet temperature of CO_2 constant.

15- By increasing the power, a portion of the high density CO_2 was converted to low density CO_2 and caused a pressure increase in the loop. This increase in pressure had to be compensated by the accumulator to assure constant pressure throughout the tests.

This process was continued to reach one of the limiting parameters which confine the increase of power on the heated channel. These parameters were wall surface temperature at TS25B (150ºC, which was increased to 220 C later), cooling water flow rate (28 lpm) and maximum voltage from the rectifier (20 Volts). Each steady-state data point explained above took 25-30 minutes on average and for a set of experimental steady-state data which varied from 12-20 steady-state data points, 6-9 hours continuous data taking was needed.

3.8   Independent Variable and Test Matrices

As mentioned before, in a natural circulation loop, flow rate is dependent to the power on the heated channel, pressure-drop along the heated channel and inlet and outlet valves, inlet temperature, and system pressure. Test matrices were developed based on these independent variables. A sample of the performed tests is shown in Table 3.2.

Table 3.2: Test matrix of performed experiments

Status	Test ID.	Date	System Pressure (MPa)	Inlet Temperature (C)	Valve Position		Power range (kW)	No. of Points
					Inlet	Outlet		
✓	PD-1-040913-x	April 9th, 13	7.6	25-26	Fully open	Fully open	1.2-11.9	19
✓	PD-2-041013-x	April 10th, 13	7.6	25-26	Fully open	35° closed	1.2-11.3	18
✓	PD-3-041113-x	April 11th, 13	7.6	25-26	Fully open	40° closed	1.2-9.5	16
✓	PD-4-041213-x	April 12th, 13	7.6	25-26	Fully open	30° closed	1.2-11.9	19
✓	PD-5-041713-x	April 17th, 13	7.6	25-26	30° closed	Fully open	1.2-11.3	18
✓	PD-6-041813-x	April 18th, 13	7.6	25-26	40° closed	Fully open	1.6-11.9	18
✓	PD-7-042413-x	April 24th, 13	8.5	25-26	Fully open	Fully open	1.2-11.3	17
✓	PD-8-050113-x	May 1st, 13	8.5	25-26	Fully open	30° closed	1.2-12.4	20
✓	PD-9-050213-x	May 2nd, 13	7.6	25-26	45° closed	Fully open	2.9-10.7	13
✓	PD-10-050313-x	May 3rd, 13	9.5	25-26	Fully open	Fully open	1.2-12.5	19
✓	PD-11-051013-x	May 10th, 13	7.6	20-21	Fully open	Fully open	1.2-10.7	17
✓	PD-12-051313-x	May 13th, 13	7.6	20-21	Fully open	30° closed	1.2-9.5	15
✓	PD-13-052213-x	May 22nd, 13	9.5	20-21	Fully open	Fully open	1.3-8.75	14
✓	PD-14-052313-x	May 23rd, 13	7.6	20-21	Fully open	40° closed	1.8-8.1	12
✓	PD-15-052413-x	May 24th, 13	8.5	20-21	Fully open	Fully open	1.25-8.3	13
✓	PD-16-052713-x	May 27th, 13	9.5	20-21	Fully open	31° closed	1.2-7.7	12
✓	PD-17-052713-x	May 27th, 13	8.5	20-21	Fully open	40° closed	1.7-7.1	10
✓	PD-18-052913-x	May 29th, 13	7.6	20-21	45° closed	Fully open	1.6-6.3	9
✓	PD-19-053013-x	May 30th, 13	8.5	20-21	45° closed	Fully open	2.65-6.5	8
✓	PD-20-060613-x	June 6th, 13	8.5	29-30	Fully open	Fully open	1.1-10.7	17

Table 3.2. Test matrix of performed experiments (continued)

Status	Test ID.	Date	System Pressure (MPa)	Inlet Temperature (C)	Valve Position		Power range (kW)	No. of Points
					Inlet	Outlet		
✓	PD-21-060713-x	June 7th, 13	8.5	29-30	Fully open	35° closed	1.1-7.7	12
✓	PD-22-061013-x	June 10th, 13	7.6	29-30	Fully open	40° closed	1.1-6.5	10
✓	PD-23-061213-x	June 12th, 13	7.6	29-30	Fully open	Fully open	1.1-8.9	14
✓	PD-24-061313-x	June 13th, 13	7.6	29-30	Fully open	30° closed	1.1-7.1	11
✓	PD-25-061413-x	June 14th, 13	8.5	25-26	Fully open	40° closed	1.2-7.7	12
✓	PD-26-061813-x	June 18th, 13	9.5	33-34	Fully open	Fully open	1.2-7.1	11
✓	PD-27-062813-x	June 28th, 13	8.5	25-26	Fully open	40° closed	1.2-5.9	9
✓	PD-28-030513-x	March 5th, 13	8	25-26	Fully open	Fully open	1.1-10.8	17
✓	PD-29-030613-x	March 6th, 13	8	25-26	Fully open	36° closed	1.1-9.5	16
✓	PD-30-030713-x	March 7th, 13	8	25-26	Fully open	40° closed	1-8.2	12
✓	PD-31-030813-x	March 8th, 13	8	25-26	Fully open	46° closed	1.1-7.2	11
✓	PD-32-031513-x	March 15th,13	8	25-26	Fully open	Fully open	1.1-10.7	17
								456

Experiments were performed at four different pressures of 7.6, 8, 8.5, and 9.5 MPa, and three different inlet temperatures of 20, 25, and 30 ºC, with different inlet and outlet valves positions. Totally, 456 steady-state experimental data points were collected which includes measurement of pressure-drop along the heated channel, pressure-drop across inlet and outlet valves, applied heat on the heated channel (0-120 kW/m2), system pressure, inlet temperature, and CO_2 flow rate.

The test ID was planned which consists of 4 parts. PD X-XXXXXX-X which stands for Pressure-Drop-Test No.-MMDDYY-Nominal Power, respectively. The first three parts show the type of measurement, test number and the date which the experiment was performed. The last part shows the nominal power on the heated channel for each steady-

state condition. Some of the above experiments led to flow oscillations in the loop, which will be discussed in Chapter 5.

CHAPTER 4

DATA REDUCTION METHODOLOGY

4.1 Introduction

In this chapter, first, the methodology for deriving information from the measured data is explained. Then, the measured pressure-drop data across the heated channel is compared with the summation of the calculated pressure-drop from available friction-factor formulae and the estimated acceleration pressure-drop. Finally, steady-state conditions preceding flow oscillations in the loop are addressed. This information is required for validating available numerical thermal-hydraulic codes.

A MATLAB code was developed for reduction of the experimental data. The NIST Refprop program was linked to MATLAB to obtain thermo-physical properties of CO_2. Moreover, a simplified geometry of the loop including the piping length, diameter and area changes is shown in appendix A for modeling purposes. In the following section, the data reduction procedure is shown accompanied by figures for clarification.

4.2 Steady-State Parameters

4.2.1 Mass Flow rate

Volumetric flow rate was measured using the turbine flow meter located in the cold side of the loop. The mass flow rate was computed from the measured volumetric flow rate using the inlet density. The inlet density was obtained from Refprop with measured inlet temperature and system pressure. Based on the certificate of calibration provided by OMEGA Engineering, the nominal meter-factor for the flow-meter is 4359.887 pulse/liter.

4.2.2 Power on the Heated Channel

The power dissipated in the heated section is calculated for each steady-state condition by multiplying the measured voltage drop across the heated channel by the measured amperage from the rectifier. A sample of the results of mass flow rate and power calculations are shown in Figure 4.1 for PD-11-051013-x. As shown in Figure 4.1, mass flow rate increases with increasing power in the buoyancy dominant region and decreases in the pressure-drop dominant region.
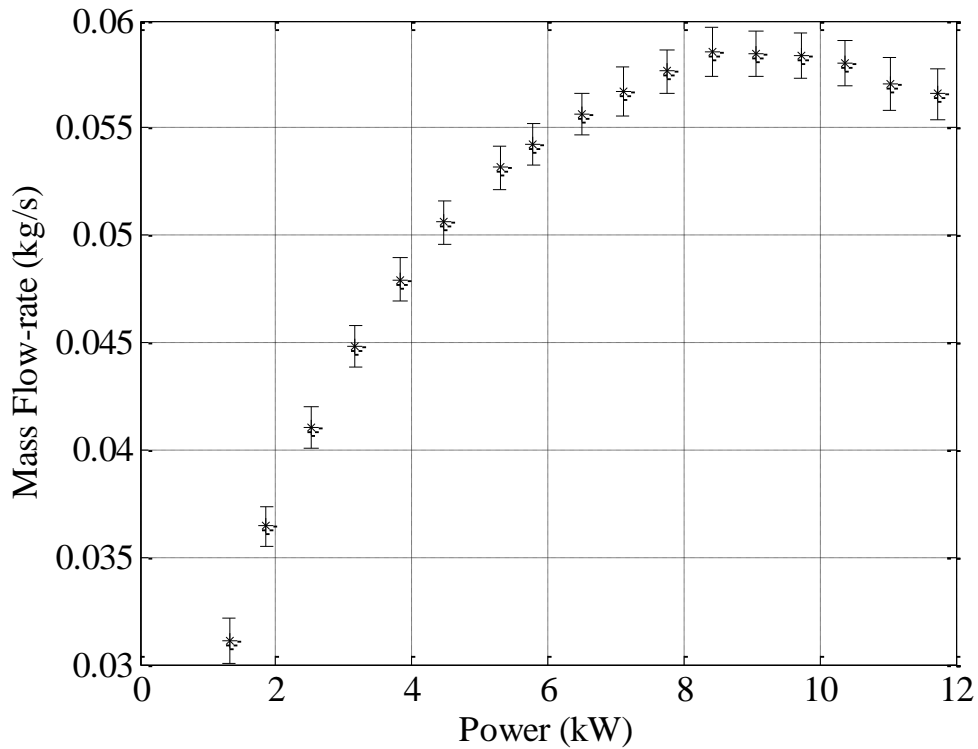
Figure 4.1. Mass flow rate vs. power for PD-11-051013-x

4.2.3 Inlet and Outlet Valves Local Pressure-drop Coefficient (K_{in}, K_{out})

Inlet and outlet local pressure drop coefficients (K factors) were calculated based on Equation (2.3). The measured pressure-drops across the inlet and outlet obstructions

include a pneumatic ball valve and a portion of piping upstream and downstream of the valve. Therefore, to estimate the value of local pressure loss coefficient for the pneumatic valves only, the pressure-drop for both wide open (zero K factor) and partially closed conditions were measured. Based on the measured pressure-drop for the wide open valve, an equivalent K factor was calculated. The same procedure was followed to compute the K factor for a partially closed valve and by subtracting the K factor from the partially closed condition from the wide open valve conditions, the K factor for the ball valve was estimated. Computed K factors were in agreement with the data provided in the Handbook of Hydraulic Resistance by Idelchik (1993) for ball valves.

4.2.4 Thermo-physical Properties of CO_2 along the Heated Channel

The measured inlet temperature and system pressure and the calculated mass flow rate and power on the heated channel, along with the NIST RefProp package were used for calculating the bulk thermo-physical properties of CO_2 along the heated section. It was assumed that the heat flux is uniformly distributed and changes linearly with the length of the heated channel. In the other words, the enthalpy of the flow changes linearly from h_{in} at the inlet to h_{out} at the outlet (h_{out} is calculated based on the energy balance with a known inlet enthalpy, power and mass flow rate from $q=m(h_2-h_1)$. Total pressure-drop along the heated channel was negligible compared to the system pressure (0.002 MPa of pressure-drop compare to the system pressure of 7.6 to 9.5 MPa). Therefore, it was assumed that the pressure is constant along the heated channel and equals to the system pressure. The computed thermo-physical properties were used to calculate the velocity and the Reynolds number along the heated channel. Re number was calculated using

Equation (4.1). The total length of the heated channel was divided into 1114 cells and the subscript i represents the cell number.

$$Re_i = \frac{\rho_i u_i d_{tube}}{\mu_i} = \frac{G d_{tube}}{\mu_i}$$

(4.1)

Figure 4.2 shows the variation of bulk temperature and dynamic viscosity of CO_2 along the heated channel for PD-11-051013-10.75 (10.75 is the nominal power (kW) on the heated channel).
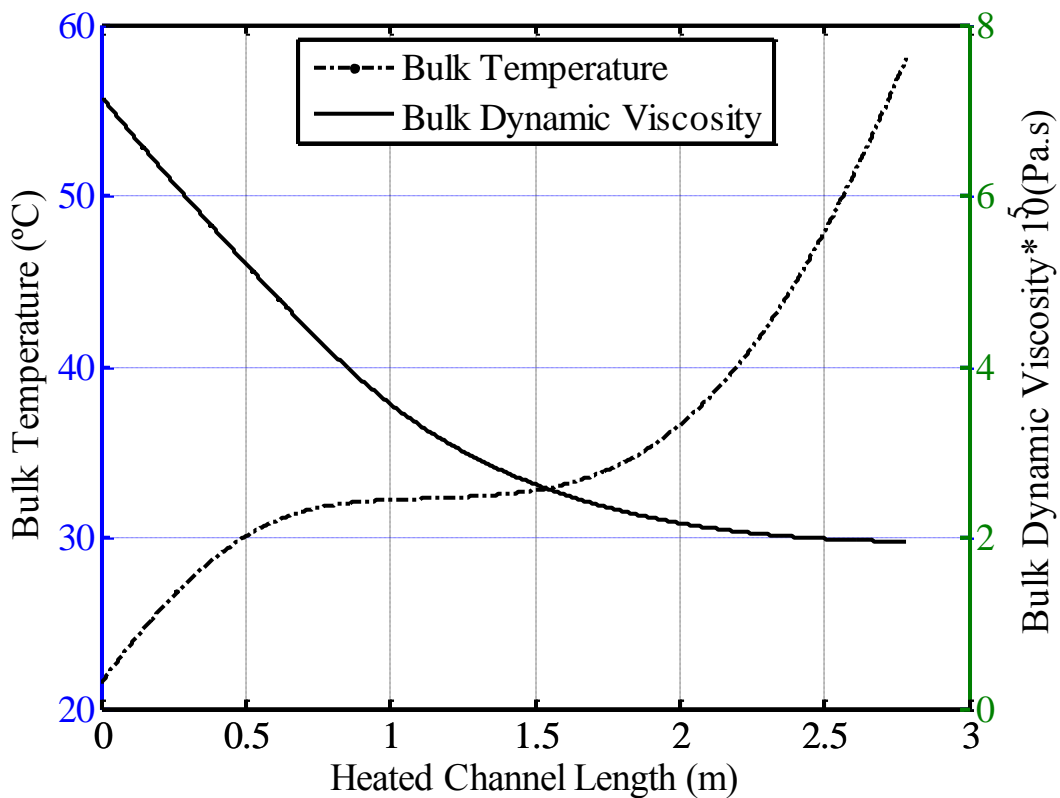
Figure 4.2. Variation of Bulk temperature and dynamic viscosity along the heated channel for PD-11-051013-10.75

Figure 4.3 shows the variation of bulk velocity for the same experiment. It shows that the velocity of CO_2 at the inlet is close to 0.5 m/s and reaches ~ 2.4 m/s at the outlet of the

heated channel. The reason for this increase in the velocity is the reduction of density along the channel.
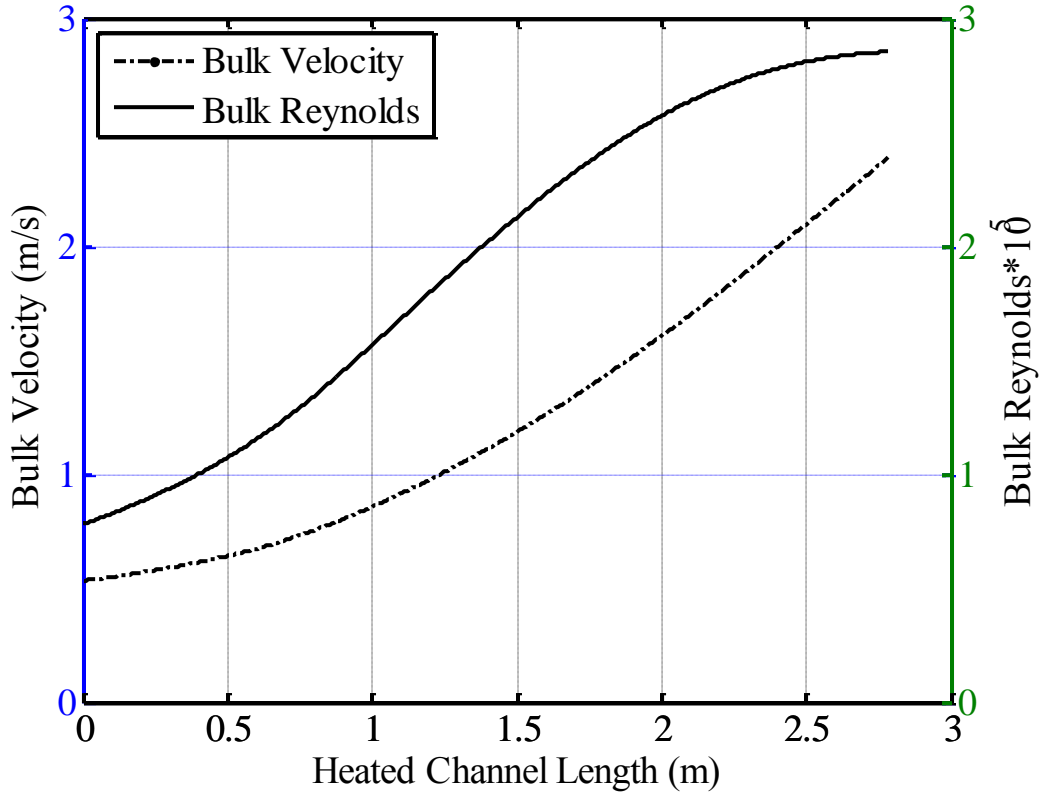
Figure 4.3. Variation of bulk velocity and Reynolds number along the heated channel for PD-11-051013-10.75

4.2.5 Wall Surface Temperature

For each steady-state test, the top and the bottom surface temperatures of the heated channel were measured at six locations along the heated channel. Two Piecewise Cubic Hermite Interpolating Polynomial (PCHIP) were fitted on the temperature data points; one for the top surface temperatures and one for the bottom surface temperatures. Since the thickness of the tube (0.12") is not small compared to the outside diameter of the heated channel (0.75"), the inner surface temperature needs to be computed to find a

better estimation of thermo-physical properties near the heated wall. Hence, the one-dimensional cylindrical heat conduction equation in the radial direction (neglecting axial and angular conduction) was solved numerically along the heated channel with two boundary conditions of surface temperature and the adiabatic boundary at the outer surface of the channel (the heated channel is insulated with 1" fiberglass pipe insulation).

$$\frac{1}{r}\frac{\partial}{\partial r}\left(kr\frac{\partial T}{\partial r}\right) + \dot{q} = 0 \quad B.C. \ T = T_s \ \& \ \frac{\partial T}{\partial r} = 0 \ @ \ r = R_o \tag{4.2}$$

As mentioned before, the heated channel was divided into 1114 cells, each with a length of 2.5 mm. For each cell, the temperatures at the top and the bottom of the outer surface were known from the PCHIPs. Using the surface temperature with known heat generation ($\dot{q}$) in the channel, the temperatures at the top and the bottom of the inner surface were calculated from Equation (4.3) for each cell.

$$T_{s-inner} = \frac{\dot{q}}{4k}\left(R_{outer}^2 - R_{inner}^2\right) + \frac{\dot{q}R_{outer}^2}{4k}\ln\left(\frac{R_{inner}}{R_{outer}}\right) + T_{s-outer} \tag{4.3}$$

where, R_o and R_i are the outer and the inner radiuses of the heated channel and k is the thermal conductivity of the wall .

It was found that the temperature difference between the inner and the outer surfaces was less than 10 ℃ for both the top and the bottom of the channel. It should be noted that in the calculations, the thermal conductivity of the wall, varies with temperature.
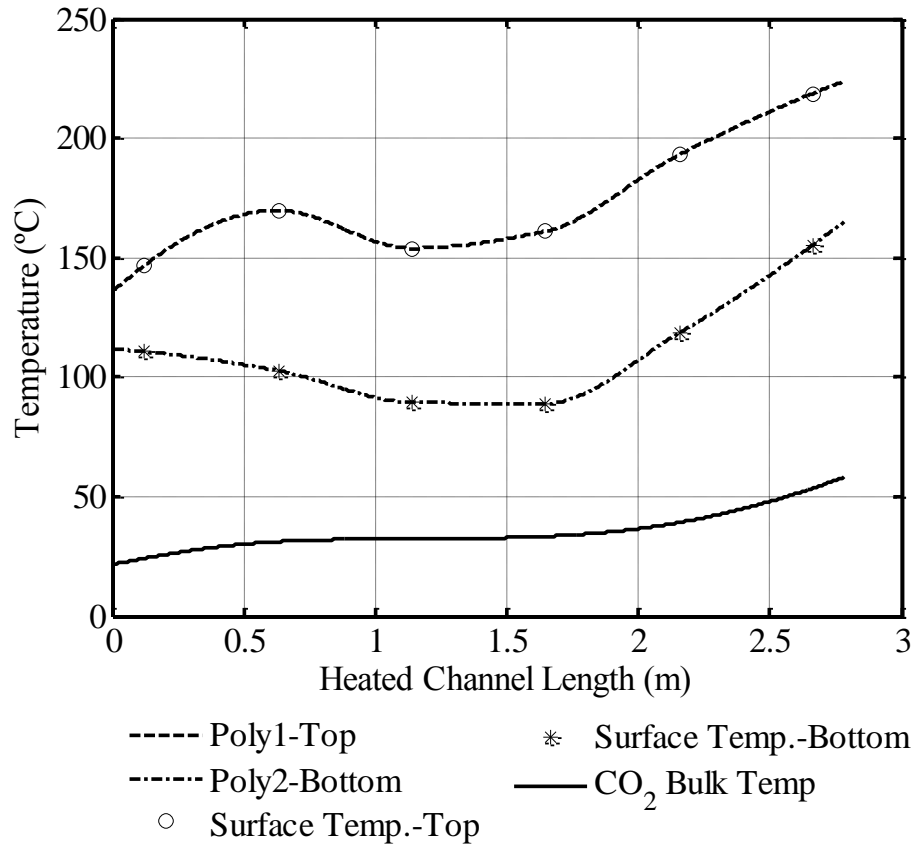
Figure 4.4. Bulk and wall outer surface temperature for PD-11-051013-10.75

The temperature gradient from the top to the bottom of the tube was less than 60-70°C for this case and arithmetic average of the top and the bottom temperatures was considered as the wall surface temperature for all steady-state tests. Using wall surface temperature and system pressure, all near-wall thermo-physical properties of CO_2 can be obtained from Refprop package. Figure 4.5 shows the variation of density and viscosity near the wall along the heated channel.
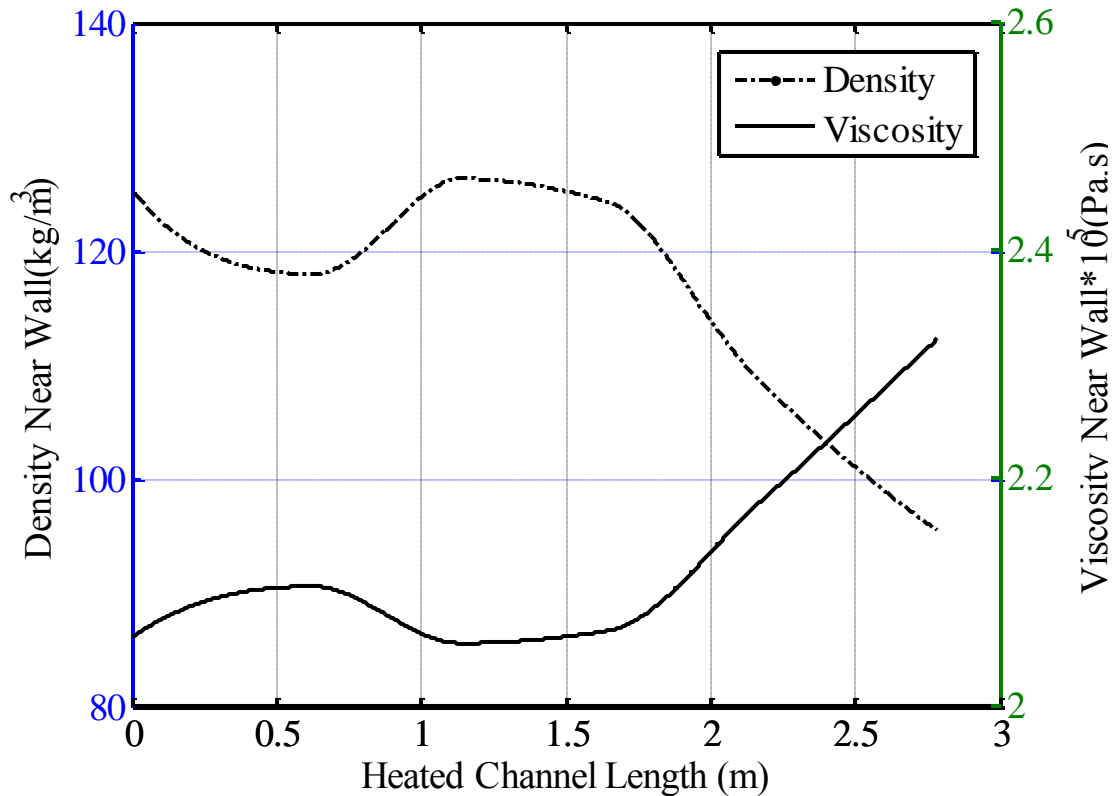
Figure 4.5. Density and dynamic viscosity near the wall along the heated channel for
PD-11-051013-10.75

Using the near-wall properties along with the bulk properties of the flow, makes it possible to model existent friction-factor formulae and compute the frictional pressure-drops from them and compare them to the experimental measurements.

The heat loss from the heated channel to the ambient was calculated based on available empirical formulae for the Rayleigh number and the averaged Nusselt number in free convection around a horizontal circular pipe (Equations 4.4 and 4.5). The dissipated heat to the insulation by conduction is equal to the amount of heat which is transferred from the outer surface of the insulation to the environment. Two equations of heat conduction in the insulation, and convective heat transfer to the environment were solved

simultaneously to find the outer surface temperature of insulation, and the heat loss, using the marching method.

$$Ra_D = \frac{g\beta(T_s - T_\infty)D^3}{\vartheta\alpha}$$

(4.4)

$$\overline{Nu}_D = \left\{0.60 + \frac{0.387Ra_D^{1/6}}{[1 + (0.559/Pr)^{9/16}]^{8/27}}\right\}^2$$

(4.5)

4.2.6 Pressure-Drop Components

Each measured pressure-drop data across the heated channel included the acceleration pressure-drop, frictional pressure-drop, and two local pressure-drops due to area changes at the inlet and outlet of the heated channel. Due to the horizontal orientation of the heated tube, there is no gravitational pressure-drop. Therefore Equation (2.1) is re-written as follow:

$$\Delta P_{measured} = \Delta P_{fr} + \Delta P_l + \Delta P_{ac}$$

(4.6)

There is an area contraction at the inlet from 0.6" to 0.51"; and there is an area enlargement at the outlet from 0.51" to 0.6". Local pressure-drop coefficients for these area changes are calculated according to the Idelchik (1993) and shown in Appendix A. Local pressure-drops and acceleration pressure-drop were deduced from the total measured pressure-drop and the frictional pressure-drop was obtained. Therefore, we have:

$$\Delta P_{frictional} = \Delta P_{Measured} - (\Delta P_l + \Delta P_{ac})$$

(4.7)

The acceleration pressure-drop was calculated using Equation (4.8) from the mass flux and inlet and outlet densities, as follows:

$$\Delta P_{ac} = G^2 \left(\frac{1}{\rho_{out}} - \frac{1}{\rho_{in}} \right)$$

(4.8)

One important part of this study is to see the performance of available friction formulae for the supercritical region. The Reynolds number and the bulk and near wall properties were used at each node to calculate the friction-factor and frictional pressure-drop along the heated channel for each cell (local values of frictional pressure-drop) using Equation (4.9) as follows:

$$\Delta P_{fr,i} = f \frac{l_i}{D} \frac{G^2}{2\rho_i}$$

(4.9)

where i is the number of the cell. The integral of the local frictional pressure-drop represents the total frictional pressure-drop along the channel for steady-state conditions. This value was compared to the $\Delta P_{Frictional}$ (Equation 4.7) and the comparison is shown in Figure 4.6 and is explained thoroughly in Section 5.2.
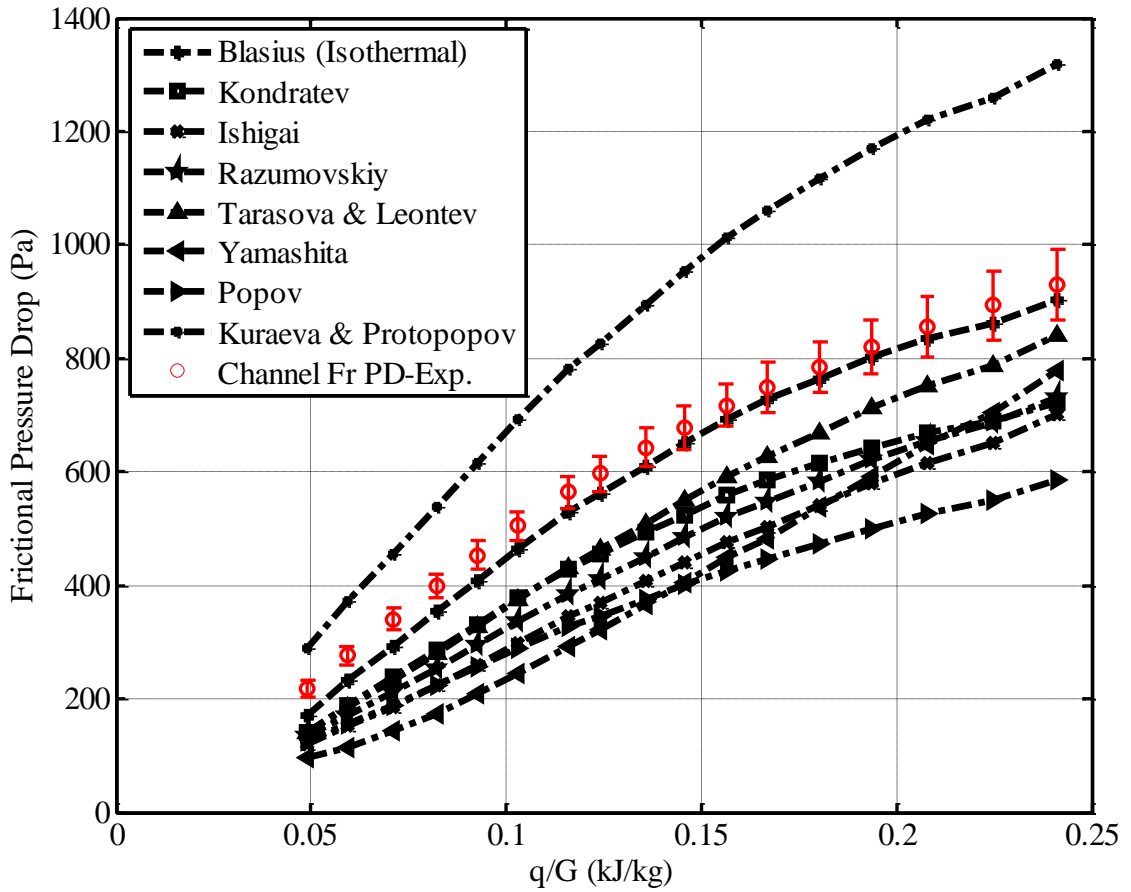
Figure 4.6. Comparison of frictional pressure-drop between experiment and available

friction formulae PD-11-051013-x (This plot includes all 17 data points)

4.2.7 Local Pressure-Drop Coefficient for Area Changes

Cross-section area is not uniform along the loop. The area changes insert local pressure-drops in the system. For numerical modeling of the loop, equivalent local pressure-drop coefficients are needed to be determined. The result of local K factors for area changes is calculated according to the Idelchik (1993) and summarized in the Appendix A.

4.2.8 Local Pressure-drop Coefficient for the Heat Exchanger

The heat exchanger has a complex geometry with an unknown local pressure-drop coefficient. An attempt was made to find the equivalent local loss coefficient for the heat exchanger at the inlet and outlet of the heat exchanger. The detailed of the applied method and the heat exchanger geometry are explained in Appendix B.

4.3   Flow Oscillations

4.3.1   Experimental Observations during Flow Oscillations

Flow oscillations were observed several times in different tests. The main signal representative of flow oscillations was the turbine flow meter. However, other signals also behaved accordingly during oscillations of flow rate. For example, the outlet temperature of the heated channel oscillated out of phase with the inlet mass flow rate. Due to the presence of high frequency fluctuations in some of the signals such as the flow-meter and the DP cells, a second order Butterworth low pass filter was applied to extract the buried signal. The cut-off frequency was determined based on the Fast Fourier Transform (FFT) of the auto-correlated signal (which was derived from the original signal). In the following, an example for this procedure for the test PD-14-052313-x is explained.

After increasing power from 7.40 ± 0.06 kW to 8.40 ± 0.08 kW, flow oscillations were observed. These oscillations were recorded for 100 minutes and period of oscillations was about 41 seconds. Figure 4.7 shows the output signal of DP 2-1 during flow oscillations. The auto-correlation function of the DP 2-1 signal is shown in Figure 4.8.
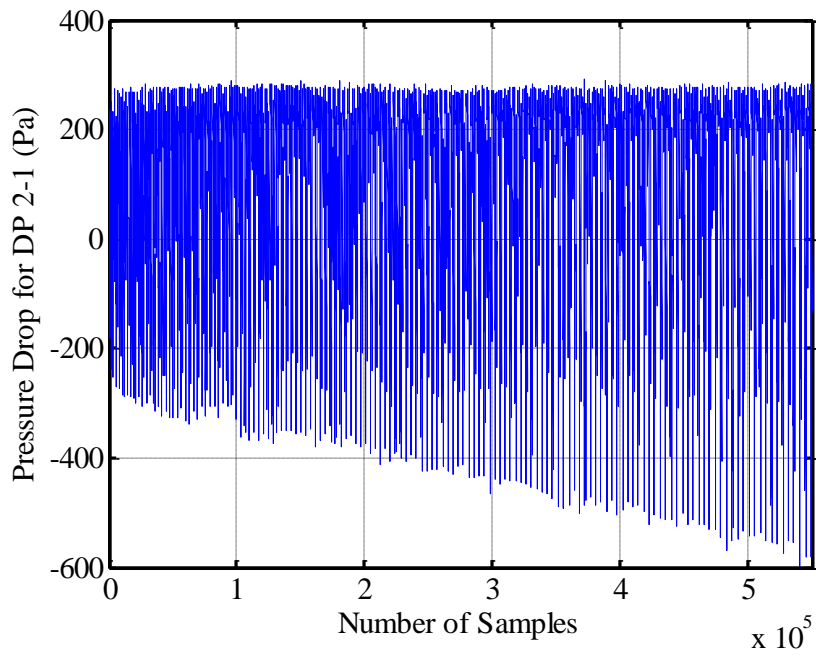
Figure 4.7: Recorded signal during flow oscillations for DP 2-1for PD-14-052313-x
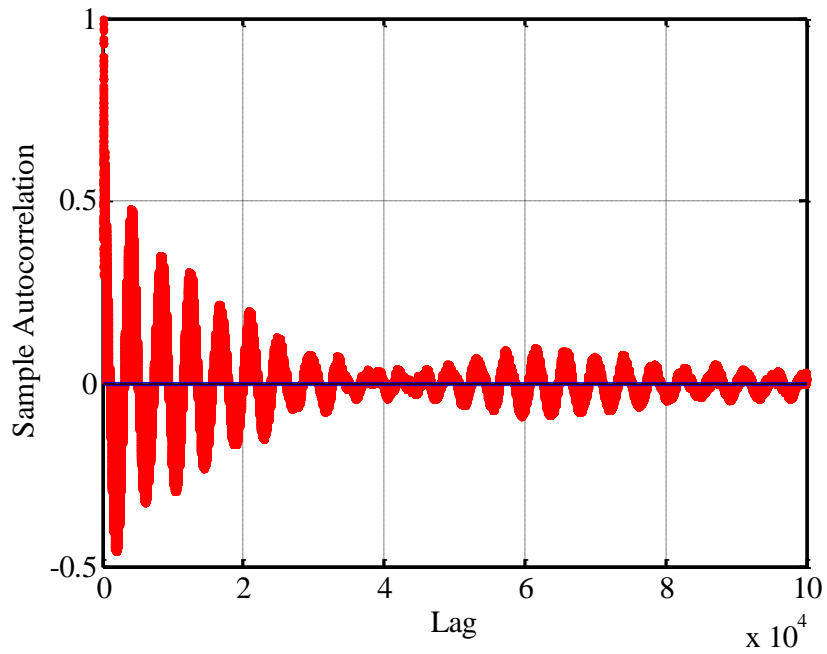
Figure 4.8: Auto-correlation of recorded signal during flow oscillations for DP 2-1for

PD-14-052313-x

Figure 4.9 shows that the dominant frequency of the signal is 0.02441 Hz. Therefore, the period of oscillation for this dominant frequency is 40.9 seconds which is equal to the period of oscillation of the outlet temperature.
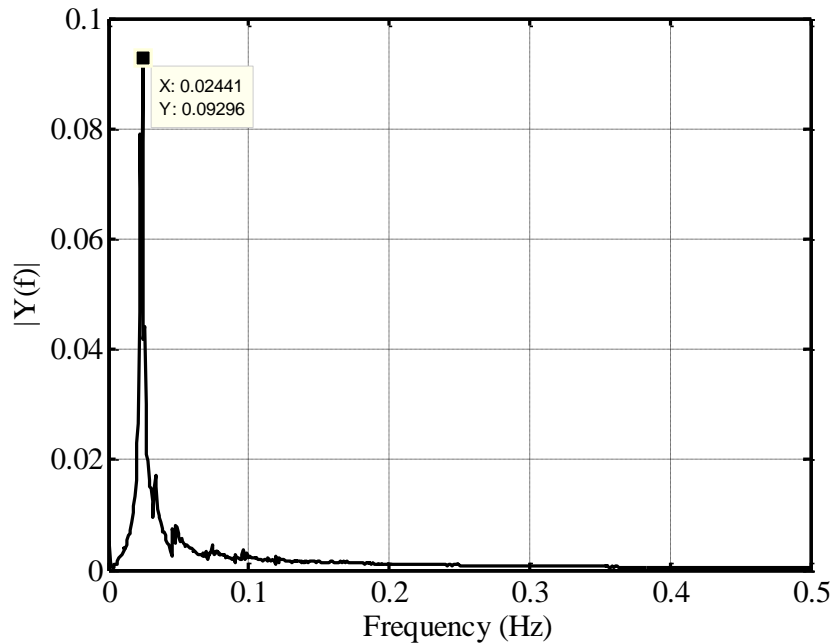
Figure 4.9: Dominant frequency of the signal from FFT

The computed dominant frequency was used to set the cut-off frequency for the Butterworth Low pass filter to 0.03 Hz. Figure 4.10 shows recorded signal of DP 2-1 before and after applying low pass filtering. A similar procedure was employed to extract the buried signals in other test.
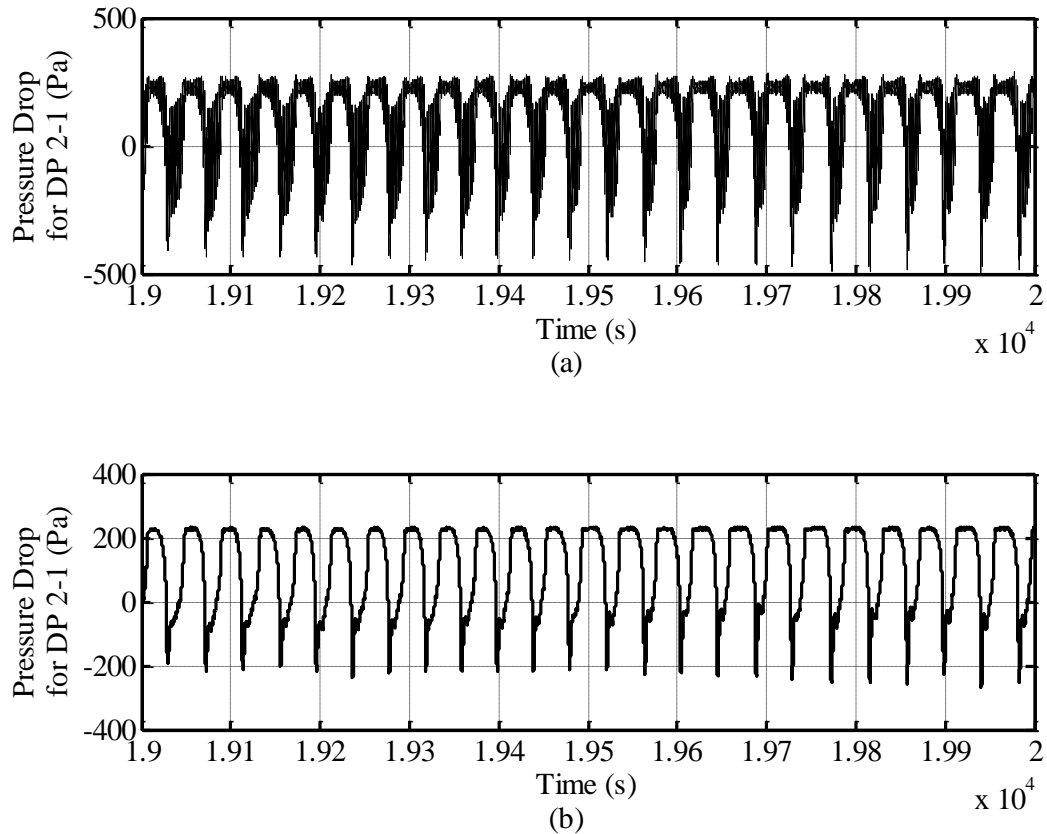
Figure 4.10: (a) Recorded signal for DP 2-1

(b) Extracted signal after applying low pass filter

4.3.2   Flow Oscillations and Mass Flow rate versus Power Curve

All previous studies regarding flow oscillations showed the onset of flow oscillations somewhere on the mass flow rate versus power curve; therefore, the same method was used in this study. In Chapter 5, the detailed steady-state conditions preceding flow oscillations are addressed for each case and the behavior of the loop during flow oscillations is explained. As an example, flow oscillations emerged in the test PD-14-052313-x when power was increased from 7.4 ± 0.06 kW (solid circle in Figure 4.11) to 8.4 ± 0.08 kW. It should be noted that since mass flow rate decreases with power increase

in the negative slope portion of the curve, the mass flow-rate at the onset of instability is smaller than the solid circle in Figure 4.11.
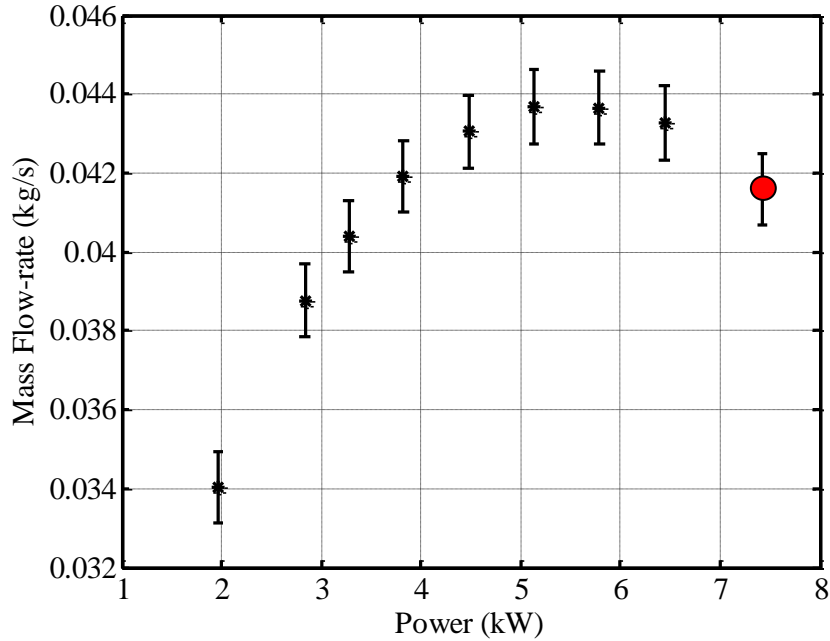
Figure 4.11: Steady-state flow rate versus Power

(Inlet temperature ~21°C, System pressure: 7.6 Mpa, $K_{inlet-valve}= 0$, $K_{outlet-valve}= 19.9$

4.4   Uncertainty Analysis

4.4.1   Uncertainty analysis

An uncertainty analysis was conducted for all steady-state experiments to specify the intervals of uncertainty for each parameter. The propagation of uncertainties for calculated parameters were calculated based on the numerical method outlined by Moffat (1988). In the uncertainty analysis, random errors (calculated based on 20 to 1 odds or 95% confidence), uncertainty of the measuring instruments, and the accuracy of the

calibrating device (for the differential pressure transducers) were considered. Uncertainty analysis results are provided in the appendix C for each steady-state data point.

Based on the uncertainty analysis, it was found that the uncertainty intervals for mass flow rate and power on the heated channel are about ±0.001 kg/s and ±0.10 kW (at high heat flux), respectively. Uncertainty of measured absolute pressure was found to be ±0.02 MPa. A large temperature difference between RTD2 (outlet temperature from the heated channel) and T11 (inlet temperature to the heat exchanger) was observed in some tests. The tip of RTD2 was located at the center of the outlet of the heated tube and does not measure the bulk temperature of CO_2 at the outlet. The uncertainty of inlet temperature (RTD1) was ±0.4ºC and the uncertainty of outlet temperature based on energy balance reached ±5ºC (at outlet temperatures above 100˚C).

4.4.2   Repeatability

To perform the repeatability test, two tests (PD-25-061413-x) which included 10 steady-state data-points were done (PD-25-062813-x). Both of these tests were performed with an approximately 40º degree closed outlet valve and a wide open inlet valve at 8.5 MPa with 25-26ºC inlet temperature. The results for mass flow rate were within less than 0.001 kg/s difference. One reason for this difference is that the outlet pneumatic valve position was not exactly the same for the two experiments. Figure 4.12 shows the comparison of flow rate for these two tests.
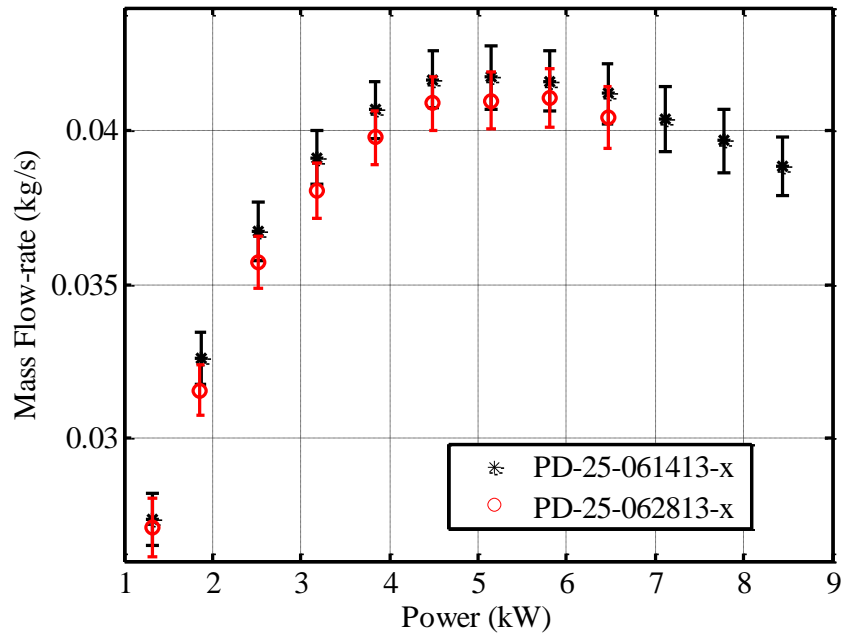
Figure 4.12: Repeatability of the experiment

CHAPTER 5

RESULTS AND DISCUSSION

5.1 Introduction

The present experimental work includes 32 "data sets" with different operating conditions (inlet temperature, system pressure, and inlet/ outlet valves openings). For each "data set", the inlet temperature to the heated channel, system pressure, and valves positions were kept constant and the power was increased as a step function. Power was increased for each data set until one of the limiting parameters (maximum power coming from the rectifier, cooling capacity of the secondary side, or the heated wall surface temperature at TS25B) was reached. Each "data set" consisted of several steady-states "data points" that were obtained within 7-8 hours of continuous operation of the loop. Totally 456 steady-state data points were collected and analysed (two data sets were repeated for the purpose of repeatability). For each steady-state data point, the pressure-drop along the heated channel, flow rate, power, flow temperature, and the heated wall temperature were recorded. In this chapter, the analysed results of the pressure-drop, steady-state parameters of the loop, and flow oscillations results are discussed. Also, the propagation of uncertainties was calculated based on the numerical method outlined by Moffat (1988) and is shown in Appendix C, as an absolute value of each measured and calculated parameter.

5.2 Pressure-drop Along the Heated Channel

The methodology for calculating the pressure-drop components for the heated channel was discussed in Chapter 4. Figure 5.1 shows the variation of pressure-drop components along the heated channel for PD-1-090413-x. Noting that, by increasing the power, the

outlet density decreases and the acceleration pressure-drop increases along the heated channel. The calculated acceleration pressure-drop was deduced from the measured channel pressure-drop to obtain the frictional pressure-drop. In Figure 5.1, the x-axis shows the ratio of the heat flux to the mass flux (q"/G). This parameter was used by Razumovskiy (1976), Petukhov et al. (1980), and Kurganov and Kaptil'ny (1992) to present the pressure-drop. Figure 5.1 shows that at large values of q/G, the acceleration pressure-drop is significant, while at lower q/G, frictional pressure-drop is larger.
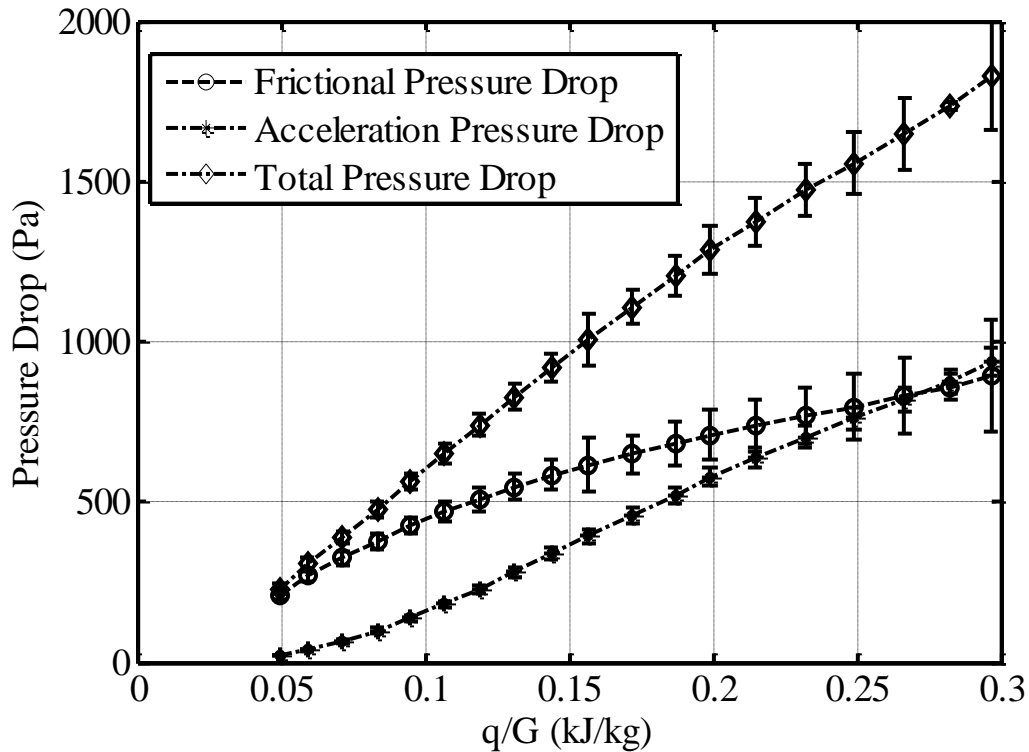
Figure 5.1: : Variation of pressure-drop components across the horizontal heated channel for: PD-1-090413-x

The procedure for deriving the frictional pressure-drop based on the proposed formulae in the literature was explained in Chapter 4. Table 5.1 shows the formulae which were used

to compare their estimation with the frictional pressure-drop obtained from present tests. The results of this comparison are shown in Figure 5.2 for PD-1-090413-x.

Table 5.1: Friction-factor formulae used for comparison

Name	Formula
Blasius	$f = 0.184 Re^{-0.2}$
Kondrat'ev	$f = 0.188 Re^{-0.22}$
Ishigai	$\dfrac{f}{f_{iso}} = \left(\dfrac{\mu_b}{\mu_w}\right)^{-0.25} \left(\dfrac{\rho_b}{\rho_w}\right)^{-0.18}$
Razumovskiy	$\dfrac{f}{f_{iso}} = \left(\dfrac{\mu_w}{\mu_b}\dfrac{\rho_w}{\rho_b}\right)^{n}$
Tarasova & Leontev	$\dfrac{f}{f_{iso}} = \left(\dfrac{\mu_w}{\mu_b}\right)^{0.22}$
Yamashita	$\dfrac{f}{f_{iso}} = \left(\dfrac{\mu_w}{\mu_b}\right)^{0.72}$
Popov	$\dfrac{f}{f_{iso}} = \left(\dfrac{\rho_w}{\rho_b}\right)^{0.4}$
Kuraeva & Protopopov	$\dfrac{f}{f_{iso}} = \left(\dfrac{\mu_w}{\mu_b}\right)^{0.22} \times 2.15 \times \left(\dfrac{Gr}{Re^2}\right)^{0.1}$

* subscripts b and w corresponds to the bulk and near wall properties

Figure 5.2 shows that the frictional pressure-drop for this data set is slightly higher than the pressure-drop calculated based on available friction-factor formulae for the supercritical flow, except for the data of Kuraeva and Protopopov (1974). Although Kuraeva and Protopopov were the only ones to include the effect of buoyancy (Gr/Re2) in their proposed correlation, their prediction of frictional pressure-drop is significantly higher than the obtained results in this study. Figure 5.2 also suggests that the trend of the Yamashita (2003) formulae is different from both the other correlations and the current experimental results.
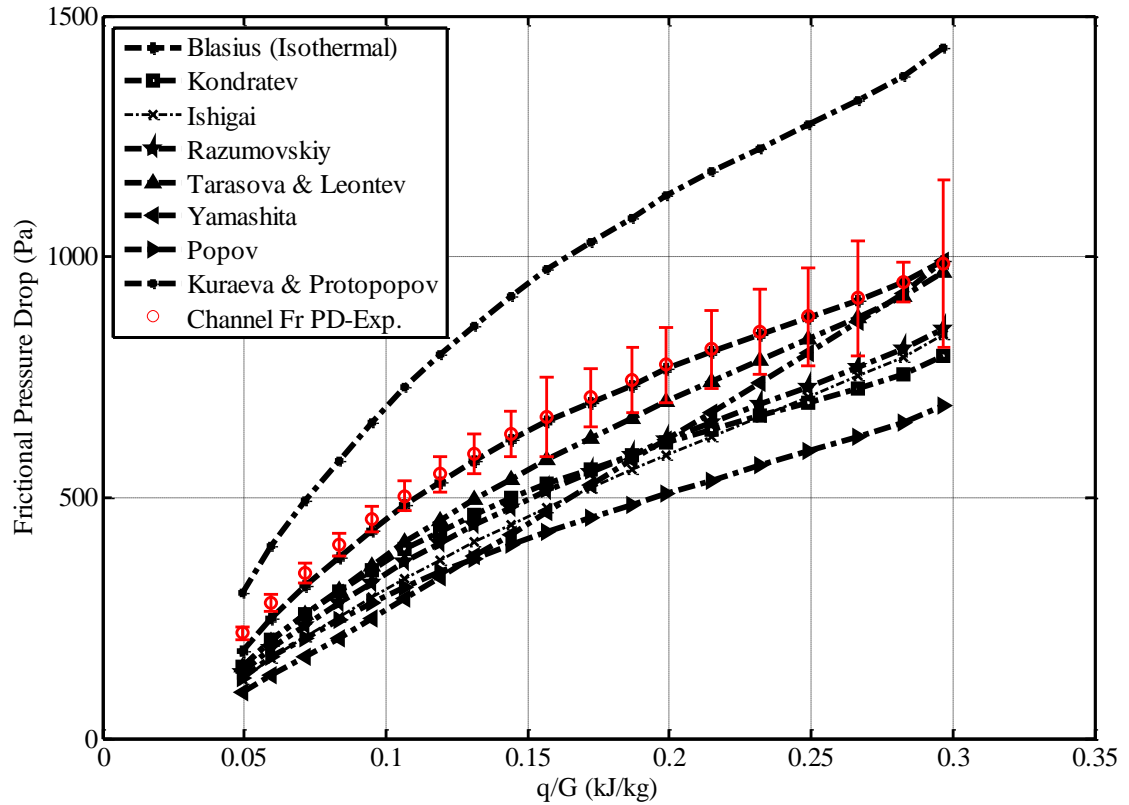
Figure 5.2: Comparison of the frictional pressure-drop between available correlations and the present study for PD-1-090413-x

The root mean square error (RMSE) of the available correlations from the current experimental data is shown in Table 5.2. From Table 5.2, the Blasius formula and Tarasova and Leontev show the least RMSE compared to other formulae for data set PD-1-090413-x.

Table 5.2: RMSE of available formulae

compared to the experimental results

	RMSE (Pa)
Blasius	17.8
Kondratev	143.1
Ishigai	166.0
Razumovskiy	138.7
Tarasova & Leontev	77.2
Yamashita	160.2
Popov	230.9
Kuraeva & Protopopov	307.7

It should be noted that in the present study, the total measured pressure-drop (DP13, L/D≈215) was used in calculations of pressure-drop. The measured segmental pressure-drops are given in the Appendix C for future studies.

5.2.1 Effect of Buoyancy on the Pressure-drop

Buoyancy is an important parameter which affects both the pressure-drop and heat transfer. There are three criteria which were proposed to quantify the buoyancy effect in experimental studies. Jackson and Hall (1979b) proposed a criterion to evaluate the buoyancy effects in horizontal flows. They suggested that for $Gr/Re_b^2 \leq 10^{-3}$, the effect of buoyancy could be ignored, where Gr/Re_b^2 is the ratio of buoyancy forces to the inertia forces. The Grashof number is determined using Equation (5.1).

$$Gr = \frac{gD^3 \left(1 - \frac{\rho_w}{\rho_b}\right)}{\vartheta_b^2} \qquad (5.1)$$

Jackson and Hall (1975) also proposed another criterion to account for the effect of buoyancy near the critical region for vertical flow. They suggested that if $\overline{Gr}/Re_b^{2.7} \leq 10^{-5}$ the effect of buoyancy could be neglected.

The third criterion was proposed by Petukhov et al. (1974) and recommended the use of Gr_q/Gr_{th} to account for the buoyancy effects for supercritical horizontal flow. This criterion is mainly used for heat transfer studies in supercritical conditions. Petukhov et al. suggested that if $Gr_q/Gr_{th}<1$ the effect of bouncy is negligible.

The buoyancy effect in the horizontal supercritical flow causes stratification of the flow, where, the low density fluid occupies the upper part of the channel and the high density fluid flows near the lower surface. Large temperature difference between the top and bottom surface temperature of the heated wall which is shown in Figure 4.4 is a sign of stratified flow in the horizontal tube. Free-convection due to the buoyancy in the horizontal pipe induces a secondary flow with transverse circulation which increases the frictional pressure-drop.

Gr/Re^2 was reported in a few experimental pressure-drop studies. Ishigai et al. (1981) reported that their data fell into $Gr/Re^2<0.013$-0.035, while for the Razimuvsky et al. (1984) experimental data Gr/Re^2 was less than 0.003. Kuraeva & Protopopov (1974) were the only ones to include the buoyancy effect in their calculation for approximating the frictional pressure-drop; however, their proposed correlation over-estimated the present frictional pressure-drop data significantly (Figure 5.2). In the present study the averaged Gr/Re^2 along the heated channel was between 0.1-0.8, which is significantly

higher than the previous studies by Ishigai et al. (1981) and Razimuvsky et al. (1984). Also, it was found from the present study that the frictional pressure-drop is dependent to the averaged value of Gr/Re^2. The "data sets" with lower mass flow rates have larger values of Gr/Re^2 and consequently, larger frictional pressure-drops compare to thier calculated frictional pressure drop base on the Blasius formula.

In the following, the influence of buoyancy on the frictional pressure-drop is discussed for two cases with the least and greatest effects of buoyancy. Figure 5.3 shows the averaged value of Gr/Re^2 for two data sets with the same inlet temperatures and system pressures but different mass flow rates. Figure 5.3 clearly shows that the buoyancy is dominant at low values of q/G (when bulk temperature is below the pseudo-critical temperature). By increasing the power, the bulk flow temperature crosses the pseudo-critical temperature and the ratio of density near the wall to the bulk density decreases and the buoyancy effect reduces.
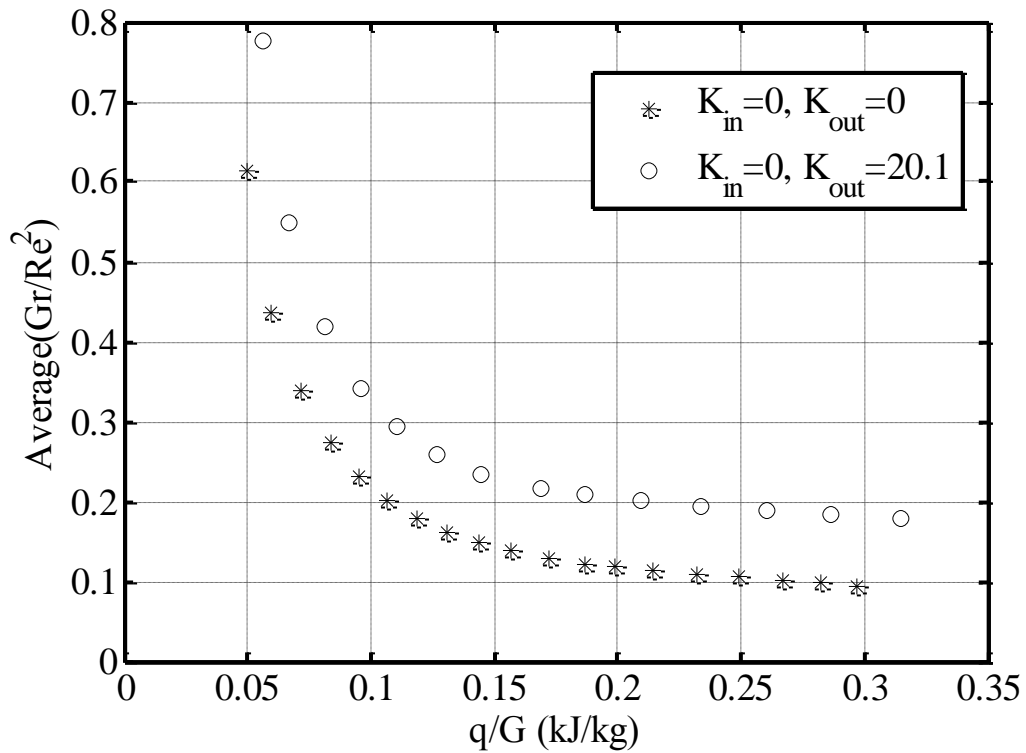
Figure 5.3: Comparison of the averaged Gr/Re^2 along the channel for PD-1-090413-x

$(K_{in}=K_{out}=0)$ and PD-3-110413-x $(K_{in}=0, K_{out}=20.1)$

Figures 5.4 and 5.5 show the calculated pressure-drop for the two cases shown in Figure 5.3. Figure 5.4 corresponds to the case with lower buoyancy effects, shows that the frictional pressure-drop is slightly higher than the Blasius formula for low q/G. Figure 5.5 with relatively higher buoyancy effect shows larger deviation of the results from the Blasius formula.

Similar trends for frictional pressure-drop at high buoyancy effects were also observed for other experiments at 8.5 Mpa, at low mass flow rates. Buoyancy was not affected considerably with system pressure.
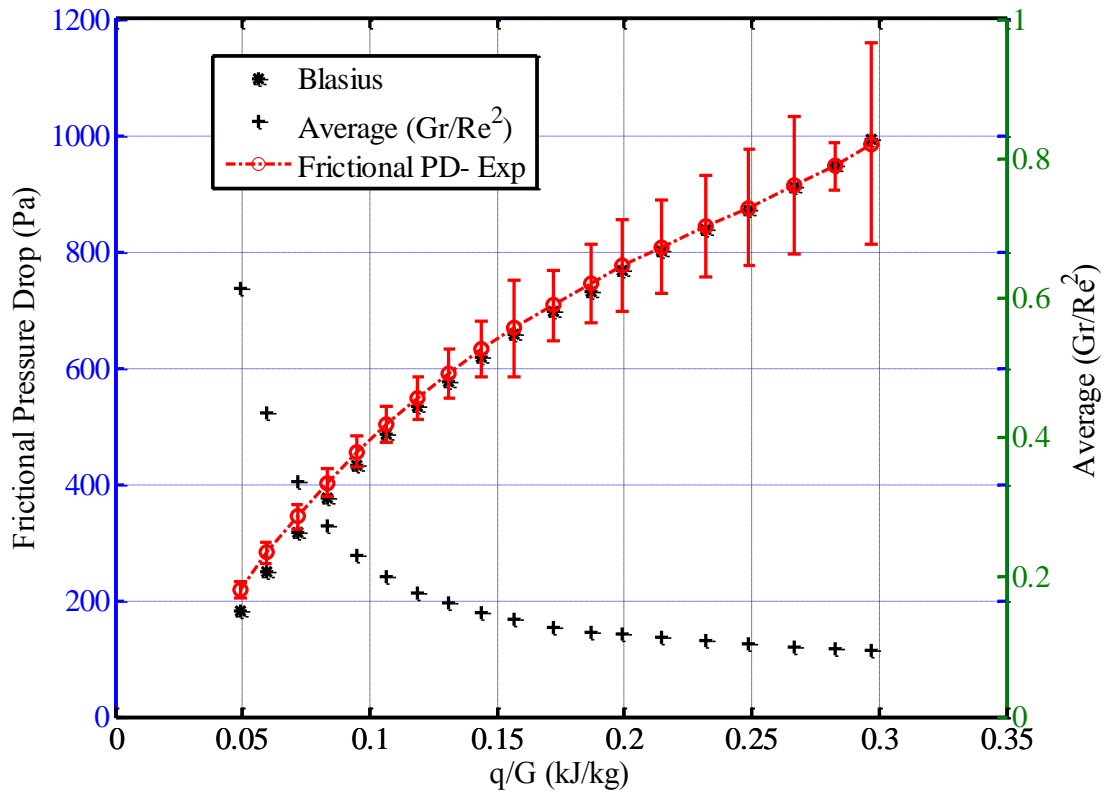
Figure 5.4: Comparison of frictional pressure-drop, Experiment versus Blasius formula

for PD-1-090413-x (K_{in}=0,K_{out}=0)
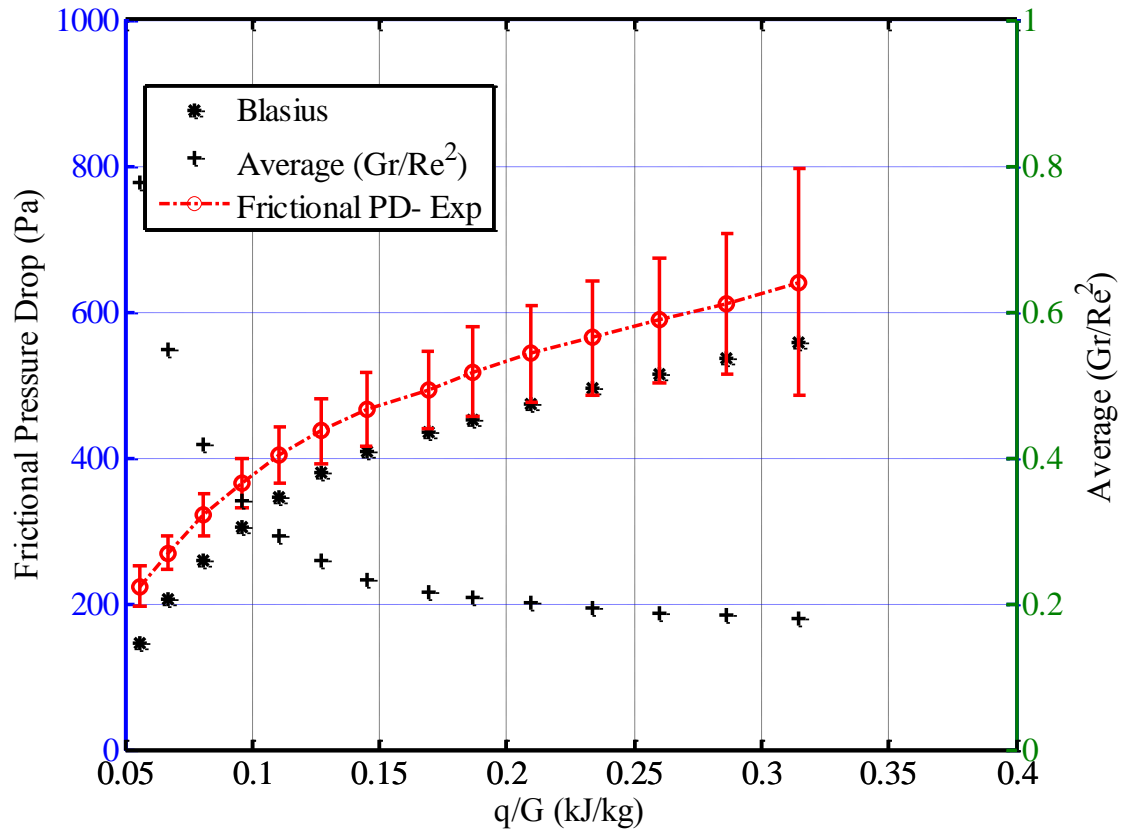
Figure 5.5: Comparison of frictional pressure-drop, Experiment versus Blasius Formula

for PD-3-110413-x (K_{in}=0, K_{out}=20.1)

The ratios of the frictional pressure-drop from the above experiments to the Blasius

prediction of frictional pressure-drop were calculated and are shown in Tables 5.3 and 5.4

for PD-3-090413-x and PD-3-110413-x, respectively.

Table 5.3: Comparison of frictional pressure-drop from experiment with Blasius formula for PD-1-090413-x

Test ID	Frictional Pressure Drop.(Pa)-Experiment	Blasius	Ratio (Frictional Pressure-drop/Blasius)
PD-1-040913-1.2	218.3	180.8	1.21
PD-1-040913-1.7	282.1	250.1	1.13
PD-1-040913-2.3	344.0	315.7	1.09
PD-1-040913-2.9	401.8	375.4	1.07
PD-1-040913-3.5	456.3	432.6	1.05
PD-1-040913-4.1	503.2	485.6	1.04
PD-1-040913-4.7	548.4	532.9	1.03
PD-1-040913-5.3	591.0	576.8	1.02
PD-1-040913-5.9	632.1	619.5	1.02
PD-1-040913-6.5	667.9	658.9	1.01
PD-1-040913-7.1	707.4	696.8	1.02
PD-1-040913-7.7	745.1	732.0	1.02
PD-1-040913-8.3	776.1	767.4	1.01
PD-1-040913-8.9	808.1	801.9	1.01
PD-1-040913-9.5	844.5	837.2	1.01
PD-1-040913-10.1	875.9	872.3	1.00
PD-1-040913-10.7	914.4	910.1	1.00
PD-1-040913-11.3	946.6	947.0	1.00
PD-1-040913-11.9	985.8	992.4	0.99

Table 5.4: Comparison of frictional pressure-drop from experiment with Blasius formula for PD-3-110413-x

Test ID	Frictional Pressure Drop.(Pa)-Experiment	Blasius	Ratio (Frictional Pressure-drop/Blasius)
PD-3-041113-1.2	223	146.9	1.52
PD-3-041113-1.7	269.6	205	1.32
PD-3-041113-2.3	321.1	258.5	1.24
PD-3-041113-2.9	364.9	304.3	1.20
PD-3-041113-3.5	403	345.3	1.17
PD-3-041113-4.1	436.7	379.7	1.15
PD-3-041113-4.7	466.5	409.5	1.14
PD-3-041113-5.4	493.4	434.5	1.14
PD-3-041113-5.9	517.9	452.4	1.14
PD-3-041113-6.5	542.3	472.5	1.15
PD-3-041113-7.1	564.5	494.3	1.14
PD-3-041113-7.7	588.1	514.5	1.14
PD-3-041113-8.3	610.7	536.3	1.14
PD-3-041113-8.9	640.9	557.3	1.15

According to the Tables 5.3 and 5.4, the computed frictional pressure-drops falls within 1-1.2% of the Blasuis formula prediction for both cases with the least and the most effects of buoyancy seen in this experimental study.

It is worth noting that the calculated pressure-drop in the present study is for a natural circulation loop and not a forced convection one. A discrepancy of about 20% for turbulent flow and 70% in laminar flow between the frictional pressure-drops calculated in forced and natural convection were reported by Vijayan and Austregesilo (1994). Vijayan et al. (1991) also reported a 30% over-prediction of frictional and local pressure loss in natural circulation loops compared to the force convection loops. Zirvin (1981) has also reported the same behaviour for frictional pressure-drop in natural convection

loops. All the studies mentioned, pointed out that available friction-factor formulae for isothermal fully developed flow are not valid for natural circulation loops since the secondary flow is present in a natural circulation loop and the assumption of fully developed flow could be violated in a natural circulation loop.

 5.2.2   Reasons for Discrepancy of Present Results for Pressure-drop

The reasons for the discrepancy between the frictional pressure-drops from tests and available formulae for pressure-drop could be explained as follow:

1- In all of the experimental studies reviewed for pressure-drop in Chapter 2, the tube was divided into an unheated and a heated zone with the unheated part upstream of the heated section (length of unheated zone was approximately 50-60 times of the inner diameter). This configuration assures a hydro-dynamically fully developed flow at the entrance to the heated part where pressure-drop measurement is performed. This way, the pressure-drop in the entrance region is eliminated from the pressure-drop measurement.

    In the present study, the channel was not divided into unheated and heated zones and, therefore, the entrance region pressure-drop was included in the measurement of the pressure-drop. However, it is noteworthy that the configuration in the present study including the effect of entrance region in the measurements is closer to reality.

2- The influence of buoyancy in the natural circulation loop which is used in the present study affected the frictional pressure-drop calculation as discussed in Section 5.2.1.

3- Another reason for discrepancy which is less significant is the uncertainties associated with calculation of the local pressure-drops due to area changes at the inlet and outlet of the heated channel. These pressure-drops were deduced from the total measured pressure-drop and acceleration pressure-drop to obtain the frictional pressure-drop.

5.3 Steady-State Parameters of the Loop

5.3.1 A Simplified Model

In a natural circulation loop, the mass flow rate is a dependant variable and is a function of both the driving head (density difference in two vertical legs) and the frictional and local pressure-drops in the loop (acceleration pressure-drop is zero for a closed loop). To show this dependency, a simplified constant area natural circulation loop with a height of L=1 m and equivalent local pressure losses coefficient for the cold side ($K_{ef\text{-}in}$) and hot side ($K_{ef\text{-}out}$), with a point heat source at the lower tier and a point heat sink at the top tier is assumed. This configuration is shown in Figure 5.6.
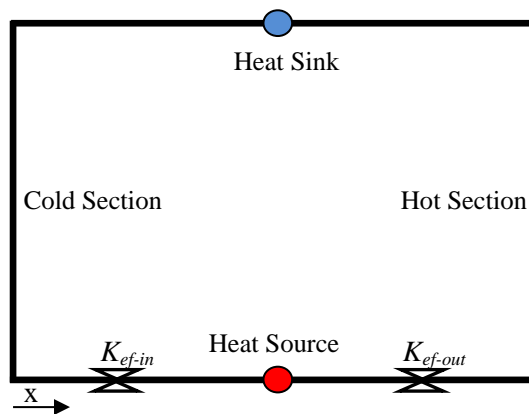
Figure 5.6 Schematic of a natural circulation loop

From the one dimensional conservation of momentum, the counter balance of the driving head and pressure-drops in the steady-state conditions is written as,

$$gH(\rho_{cold} - \rho_{hot}) = K_{ef-in} \frac{G^2}{2\rho_{cold}} + K_{ef-out} \frac{G^2}{2\rho_{hot}} \tag{5.2}$$

where $K_{ef} = K + fl/d$.

Re-writing Equation (5.2) and multiplying it by the cross-section area of the piping, we have:

$$\dot{m} = GA_{cross-section} = A_{cross-section} \sqrt{\frac{gH(\rho_{cold} - \rho_{hot})}{\left(\frac{K_{ef-in}}{2\rho_{cold}} + \frac{K_{ef-out}}{2\rho_{hot}}\right)}} \tag{5.3}$$

$$\dot{m} = \frac{Q}{h_2 - h_1} \tag{5.4}$$

In Equation (5.3), K_{ef-in}, K_{ef-out}, ρ_{cold}, and H are constant for a constant inlet temperature and pressure and the only variable is the outlet density which changes with the increase of power. Outlet density is calculated from outlet enthalpy which was calculated from the energy balance (Equation 5.4) across the heat source by iteration to satisfy both Equations (5.3) and (5.4) across the heat source. The result of this analysis is shown in Figures 5.7 for supercritical CO_2. This figure shows the variation of mass flow rate and outlet temperature versus power.
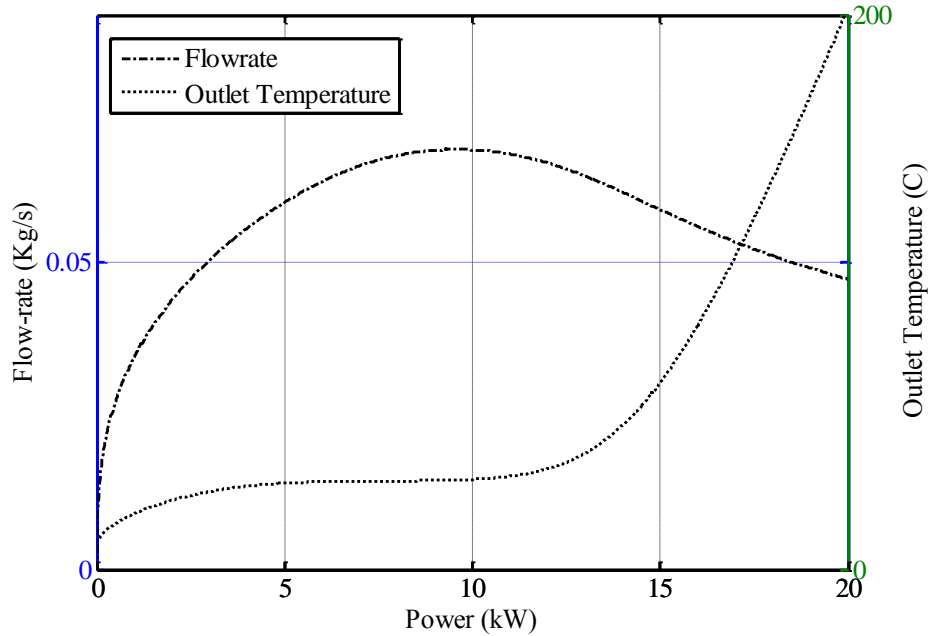
Figure 5.7: Variation of mass flow rate and outlet temperature with power
(P_{system}= 7.6 MPa, T_{in}=10ºC, K_{in}=10, K_{out}=10 and piping ID =0.0129 mm)

Before the peak of mass flow rate, reduction of the outlet density increases the driving head and hence the mass flow rate increases. Further increase in power after the peak, increases the pressure-drop in the hot side of the loop and imposes a lower mass flow rate to keep the counterbalance of the driving head and pressure-drops in the loop. This trend was reported in experimental studies of Jain et al. (1966), Fukuda and Kobori (1979), and Kyoung and Lee (1994) in two-phase natural circulation and was observed in the experimental study of Lomperski et al. (2004) in a supercritical natural circulation loop. The temperature of the fluid in the hot side of the loop, that is shown by the outlet temperature in Figure 5.7 is flat for a portion of the curve due to the nonlinear variation of heat capacity of supercritical fluid in the pseudo-critical region. It should be noted that the peak of the mass flow rate corresponds to a temperatures slightly above the pseudo-critical temperature of the fluid at that pressure.

Figure 5.8 shows the variation of the driving head and pressure-drops in the cold and the hot sides of the loop. Pressure-drop in the cold side is only a function of the variation of mass flow rate (density is constant at the inlet, imposed by the boundary conditions), but the pressure-drop in the hot side is a function of both mass flow rate and the variant outlet density.
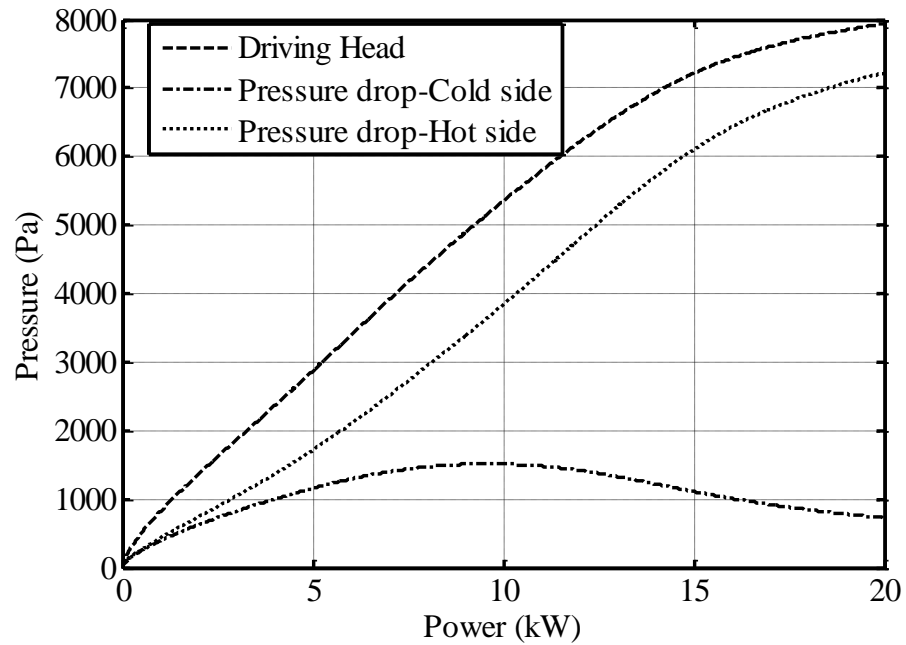
Figure 5.8: Variation of the driving head and pressure-drops with power

(P_{system}= 7.6 MPa, T_{in}=10°C, K_{in}=10, K_{out}=10 and piping ID =0.0129 mm)

5.3.2   Experimental Results of Mass Flow rate

The same trend as explained in Section 5.3.1 was observed for both mass flow rate and outlet temperature in the experiments and are plotted and explained in separate figures. Figure 5.9 shows the variation of mass flow rate and the transit time of the loop with power.
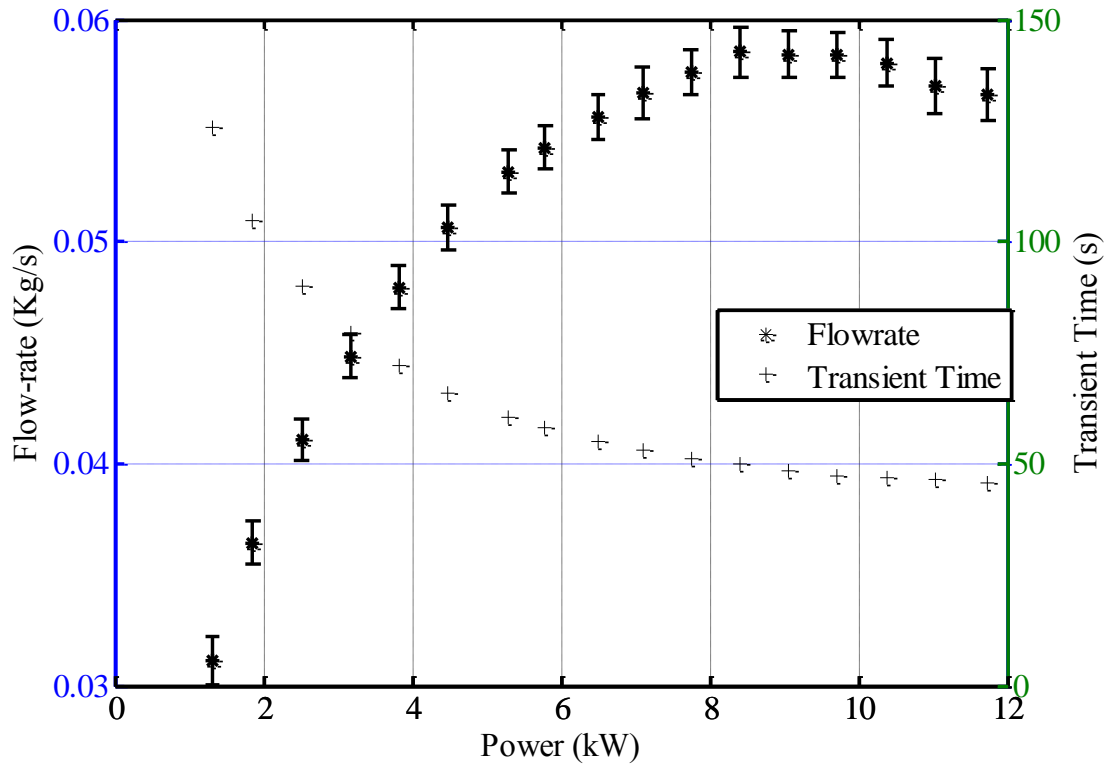
Figure 5.9: Variation of the mass flow rate and transit time with power (P_{system}= 7.6 MPa,

T_{in}=21-22ºC, K_{in}=0, K_{out}=0)

The peak of the mass flow rate was achieved in many experiments in the present study.

The transit time of the loop decreases with an increase in the mass flow rate and varies

from ~ 120 to 48 seconds at high powers.

The outlet temperature of the CO_2 from the heated channel was measured at two locations

in the hot side. The RTD2 was located right at the exit of the heated channel and T11 was

placed at the entrance to the heat exchanger. The measurement of RTD2 was inaccurate

since it was performed at one location in the cross section area and therefore this

temperature is not a representative of the bulk temperature. Also, there was an

uncertainty in measurement of T11 since there was a heat loss to the environment from

the piping in the hot side of the loop. Therefore, the outlet temperature was calculated based on the calculated outlet enthalpy from Equation (5.4).

The results of the three outlet temperatures discussed above are plotted in Figure 5.10 for the same data set.
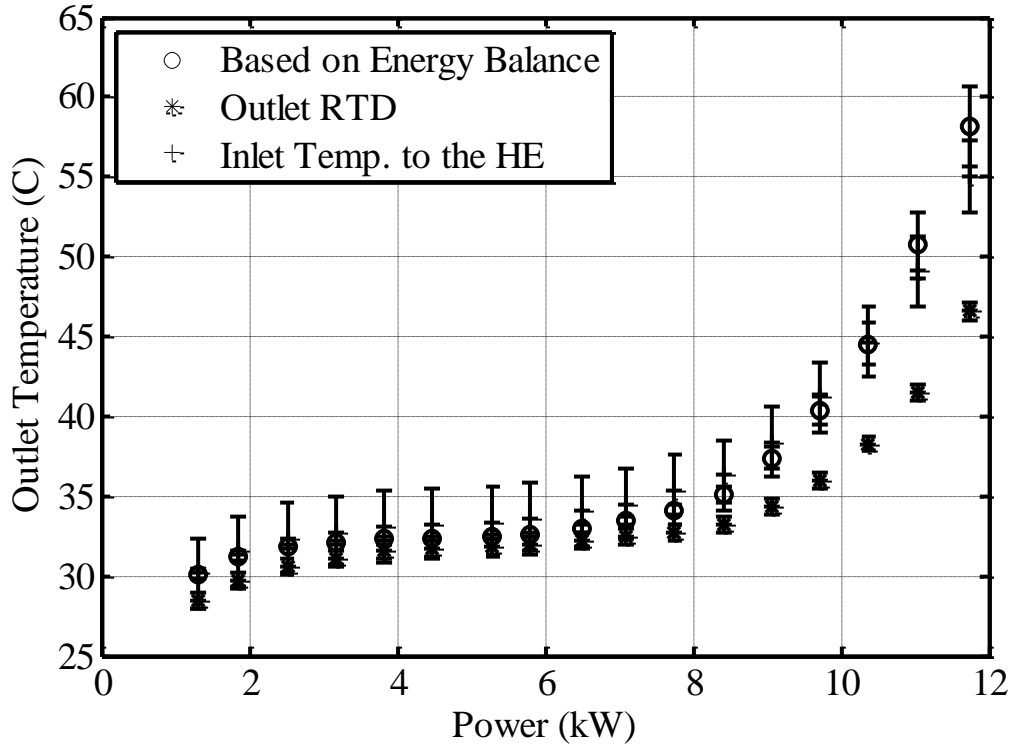
Figure 5.10: Comparison of measured and calculated outlet temperature

(P_{system}= 7.6 MPa, T_{in}=20-21°C, K_{in}=0, K_{out}=0)

It is evident from Figure 5.10 that in the pseudo-critical region, two measurements (RTD2 and T11) and the calculated outlet temperature are close to each other (flat portion of the plot), however by increasing the power and passing through the pseudo-critical region, the measured values deviate from the calculated outlet temperature. RTD2 at the outlet of the heated channel, under-predicts the outlet bulk temperature and T11 shows

lower values compared to the calculated outlet temperature, which means there is a heat loss in the hot side of the loop.

As mentioned in Chapter 2, calculating the mass flow rate of CO_2 based on energy balance is not an accurate method. To show that, the mass flow rates obtained using the energy balance and the flow meter are shown in Figure 5.11 for the same data set. Using the energy balance, the mass flow rate was calculated based on the inlet (RTD1) and outlet (T11) temperatures.
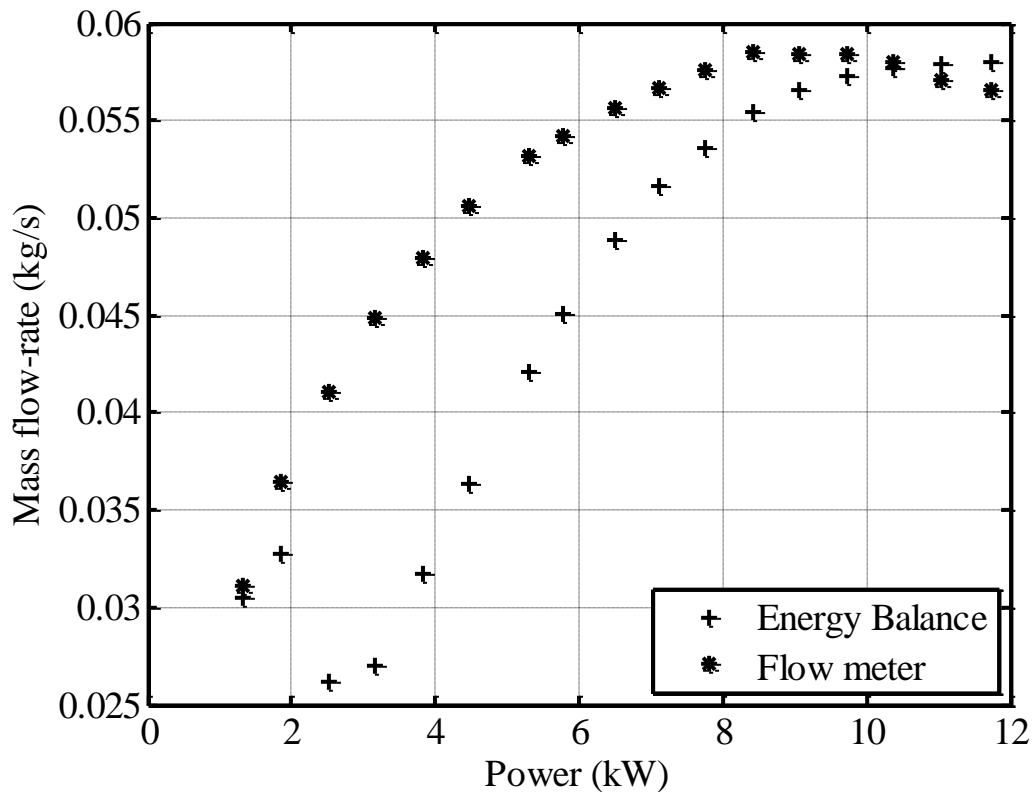
Figure 5.11: Calculated mass flow rate against measured mass flow rate (P_{system}= 7.6 MPa, T_{in}=20-21°C, K_{in}=0, K_{out}=0)

Although Figure 5.10 shows that T11 is in agreement with the calculated outlet temperature, Figure 5.11 shows large deviation of calculated flow rate compared to the

measured value. The reason for this discrepancy is the strong variation of outlet enthalpy with temperature in the pseudo-critical region. Figure 5.11 clearly shows that the inaccuracy associated with using the energy balance for mass flow rate is large.

In addition to the correctness of the outlet bulk temperature, the uncertainty in using the energy balance method for calculating the mass flow rate is another concern which leads to highly inaccurate results. To show this uncertainty, assume that there is a thermo-meter which measures the outlet bulk temperature with an uncertainty of ±0.5ºC. The uncertainty associated with energy balance even if the correct bulk outlet temperature is used, is shown in Figure 5.12. In the positive slope part of this plot (corresponding to the pseudo-critical region) the uncertainty of calculated flow rate is significantly large. However, after crossing the pseudo-critical region, enthalpy changes monotonically and the uncertainty of calculations decreases. Figure 5.12 was obtained at system pressure of 7.6 MPa. However, at higher pressures, the variation of enthalpy with temperature is milder and, therefore, the uncertainty associated with the energy balance is smaller. Increasing the inlet temperature close to the pseudo-critical temperature increases this uncertainty. The above discussion shows that using energy balance method for calculating the CO_2 mass flow rate in the experiment is erroneous.
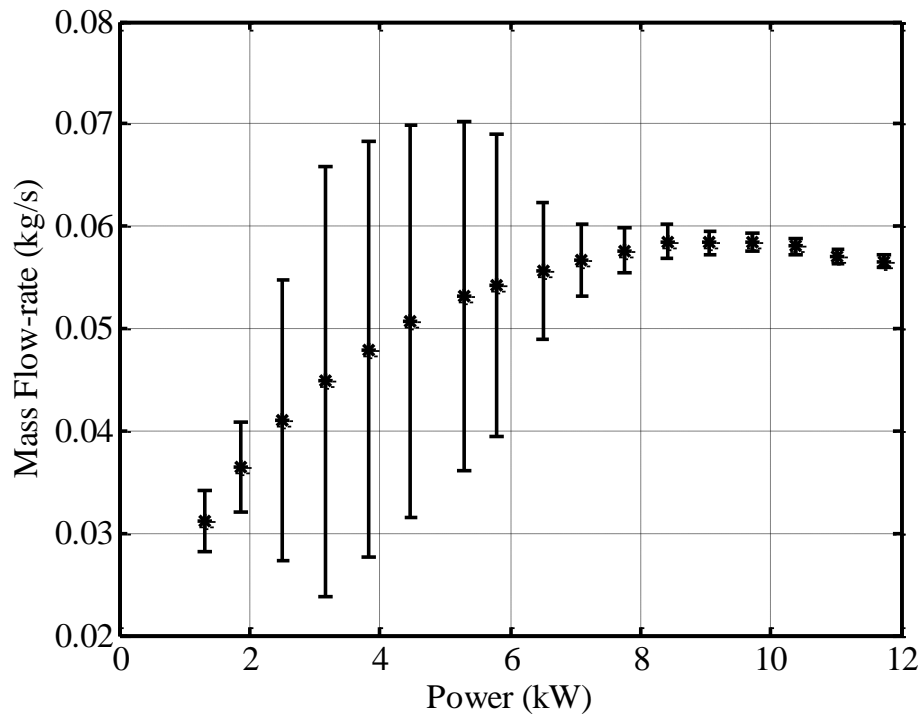
Figure 5.12: Variation of the mass flow rate with power based on correct outlet bulk

temperature (P_{system}= 7.6 MPa, T_{in}=20-21ºC, K_{in}=0, K_{out}=0)

5.3.3   Effect of Loop Pressure on the Mass Flow rate

One of the independent variables in this experiment was the system pressure. Variations

of the measured mass flow rate by power at different pressures are shown in Figure 5.13.

In all of the data sets plotted in Figure 5.13, the inlet temperature was constant at 25-26ºC

and both the inlet and the outlet valves were wide open ($K_{in}=K_{out}=0$).
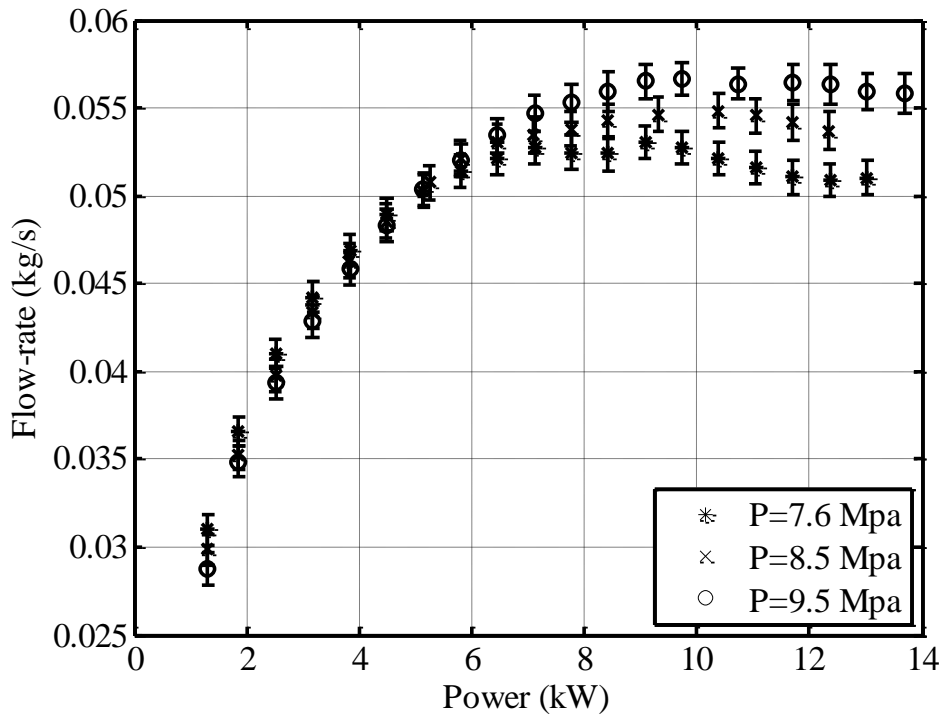
Figure 5.13: Variation of the mass flow rate with power at different system pressures

$(T_{in}=25\text{-}26\ °C,\ K_{in}=0,\ K_{out}=0)$

As shown in Figure 5.13, the peak of mass flow rate was obtained for the data sets plotted. This plot shows that it is possible to achieve a higher flow rate with increasing the system pressure. Based on measured values for flow rate, power and inlet conditions, the outlet temperature is calculated from the energy balance and is plotted in Figure 5.14. This figure shows that the outlet temperature increases strongly after the pseudo-critical region due to decreased heat capacity.
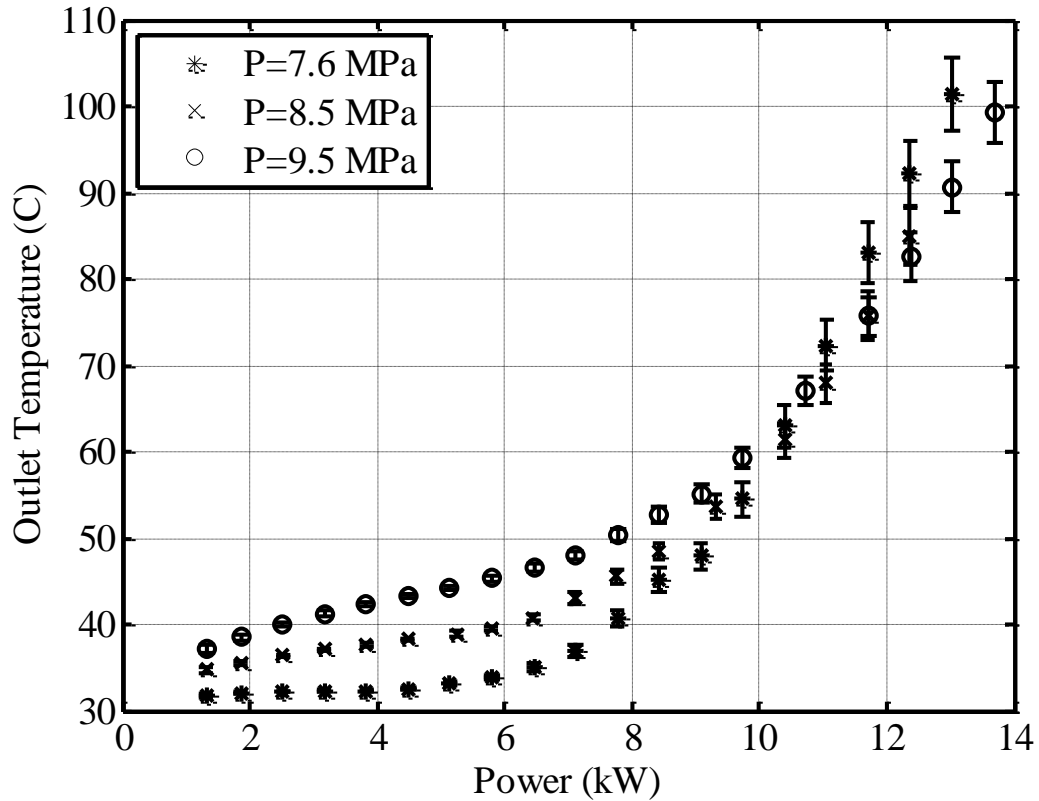
Figure 5.14: Calculated outlet temperature versus power at different system pressures

(T_{in}=25-26ºC, K_{in}=0, K_{out}=0)

The flat part of each curve in Figure 5.14 represents the pseudo-critical temperature at that pressure which corresponds to the peak value of heat capacity.

5.3.4   Effect of Inlet Temperature on the Mass Flow rate

The influence of inlet temperature on the mass flow rate and outlet temperature is shown in figures 5.15 and 5.16. Two data sets at a constant system pressure and wide open inlet and outlet valves but different inlet temperatures are plotted for this purpose. Figure 5.15 shows that the mass flow rate is generally higher at lower inlet temperatures. A lower inlet temperature enhances the driving head in the loop and causes the peak of mass flow

rate to happen at a higher power. This trend is shown in Figure 5.15. The calculated outlet bulk temperatures for these data sets are shown in Figure 5.16. Since both tests were performed at a constant pressure, both curves of outlet temperature show similar values in the flat portion. It should be noted that at high inlet and outlet temperatures, the value of density is low and, therefore, the pressure-drop is higher in the system. This trend was also observed at other system pressures (8.5 and 9.5 MPa).
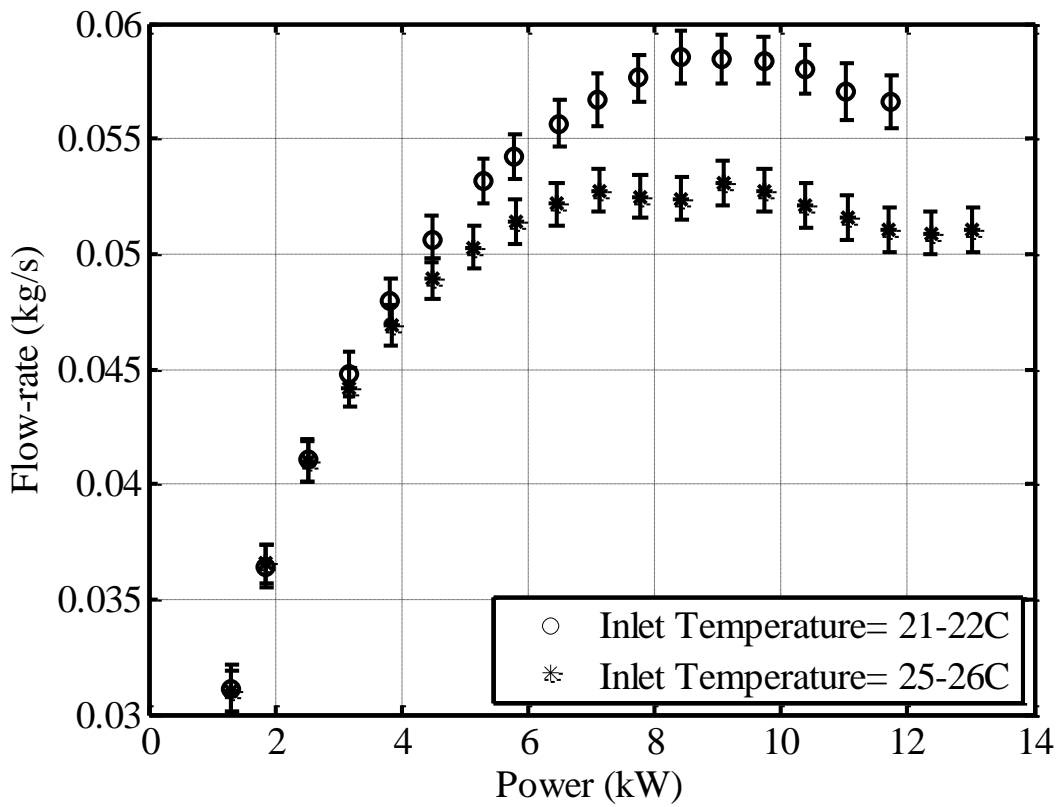
Figure 5.15: Variation of the mass flow rate with power at different inlet temperatures

(System Pressure=7.6 MPa, K_{in}=0, K_{out}=0)
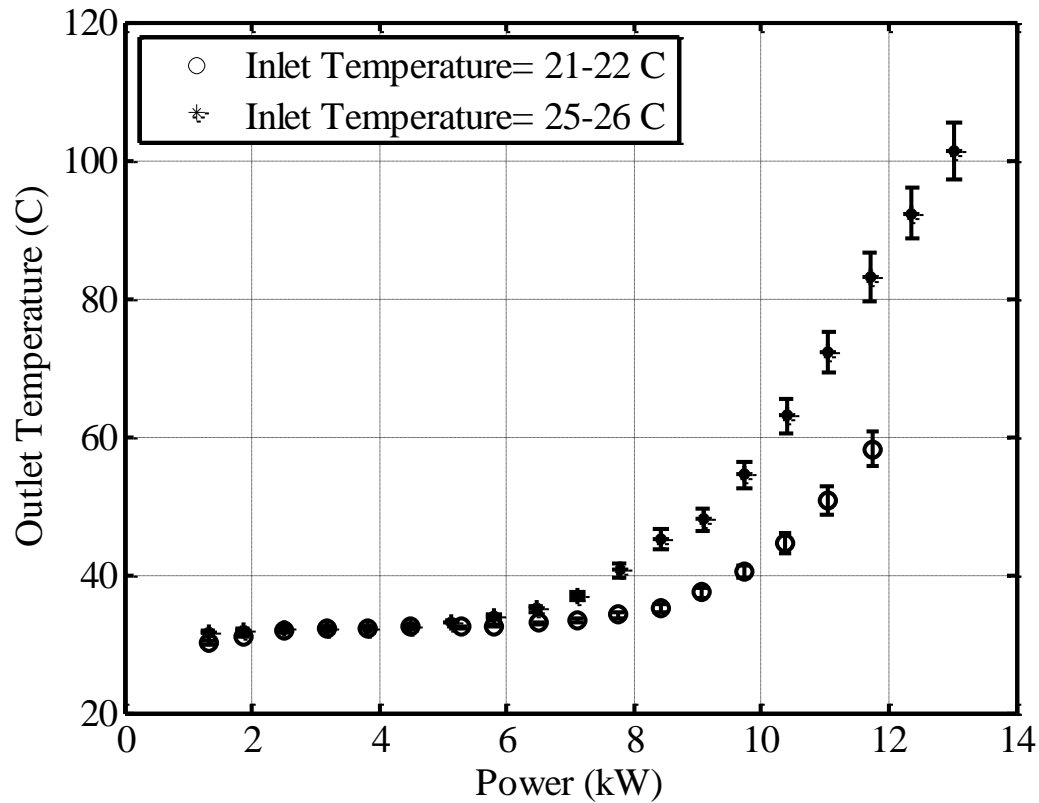
Figure 5.16: Calculated outlet temperature with power at different inlet temperatures

(System Pressure=7.6 MPa, K_{in}=0, K_{out}=0)

5.3.5   Effect of Outlet Valve Throttling on the Mass Flow rate

Partial closing the inlet and/or the outlet valves changes the inlet and outlet K factors in the cold and hot side of the loop. It's obvious that increasing the inlet or outlet K factors increases the pressure-drop in the loop and, therefore, the mass flow rate decreases. Figure 5.17 shows the effect of outlet valve throttling on the mass flow rate when the inlet temperature and the system pressure were constant and the inlet valve was wide open.
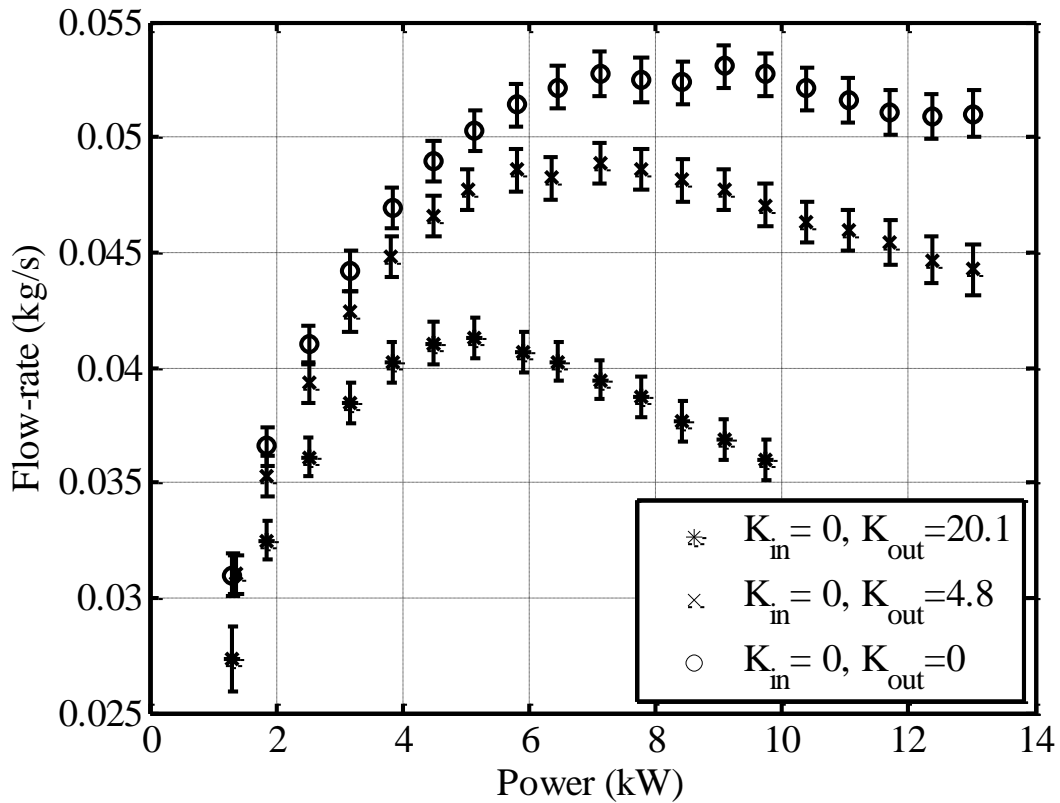
Figure 5.17: Variation of the mass flow rate with power for different outlet K factors

(System Pressure=7.6 MPa, T_{in}=25-26ºC, K_{in}=0)

Figure 5.18 shows the calculated outlet temperature for the same experiments. Since these experiments were performed at the same pressure, flat portions of the curves show the same pseudo-critical temperature. However, after the pseudo-critical region, the outlet temperatures deviates and higher outlet temperatures were observed for the cases with lower mass flow rates at each power.
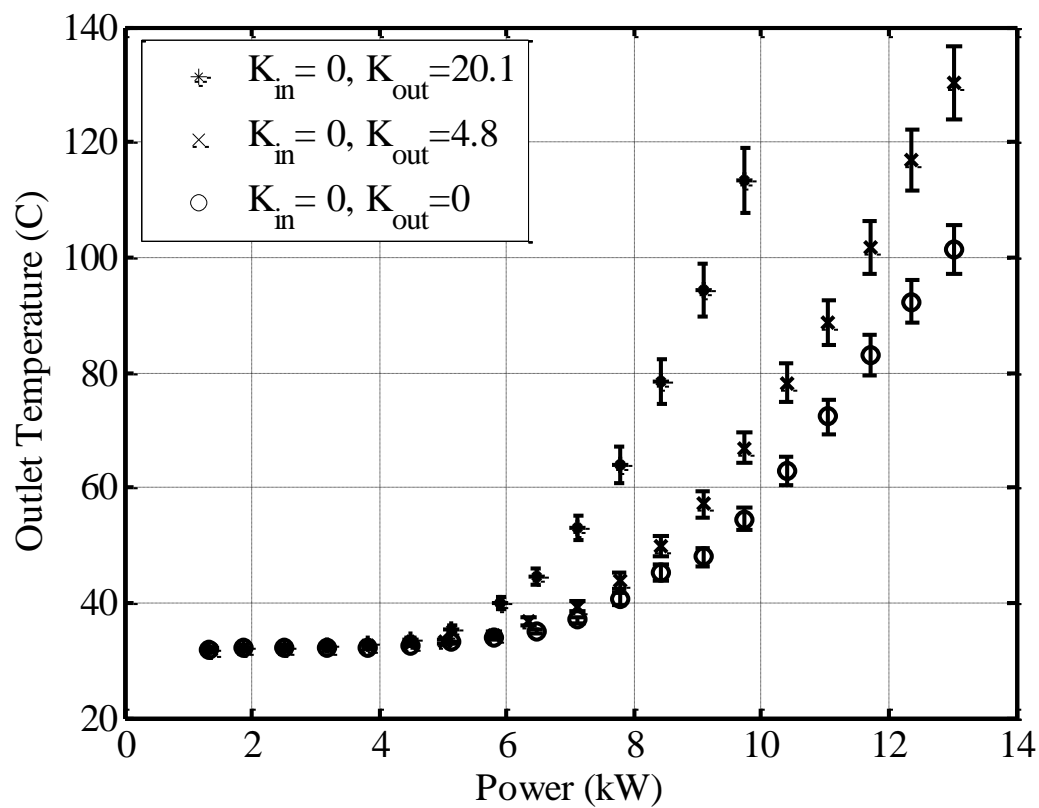
Figure 5.18: Calculated outlet temperature with power for different outlet K factors

(System Pressure=7.6 MPa, T_{in}=25-26ºC, K_{in}=0)

Variations of mass flow rate for different outlet K factors at 8.5 MPa are shown in Figure 5.19. This figure shows the same trend as explained for the case at 7.6 MPa. Moreover, variation of outlet temperature for the same experiments is plotted on Figure 5.20.
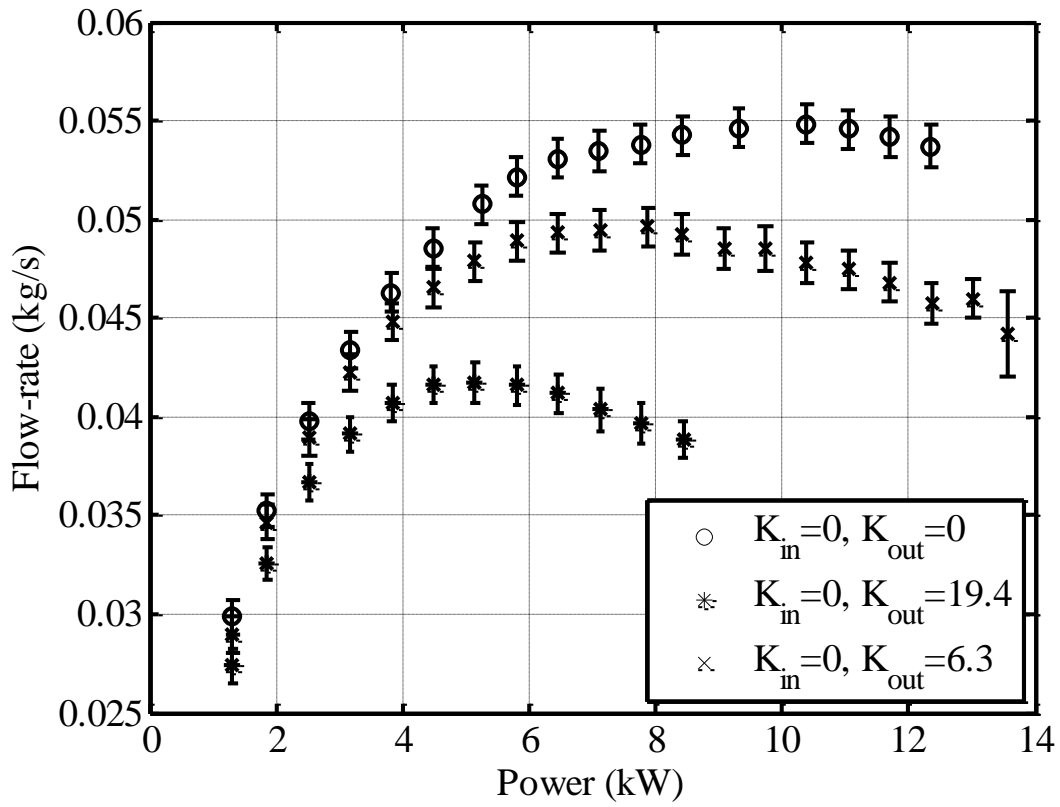
Figure 5.19: Variation of the mass flow rate with power for different outlet K factors

(System Pressure=8.5 MPa, T_{in}=25-26ºC, K_{out}=0)

Figure 5.20: Calculated outlet temperature with power for different outlet K factors

(System Pressure=8.5 MPa, T_{in}=25-26°C, K_{out}=0)

5.3.6   Effect of the Inlet or Outlet Valve Throttling on Mass Flow rate

In this section, two data sets are compared in which the inlet K factor of one data-set is the same as the outlet K factor of the other data-set. This example demonstrates the effect of inlet or outlet K factor on the mass flow rate in the natural circulation loop. Figure 5.21 shows the variation of the flow rate with power for these two cases. This figure shows that the outlet K factor affects the mass flow rate more significantly than the inlet K factor. Corresponding calculated outlet bulk temperatures for Figure 5.21 is shown in Figure 5.22.
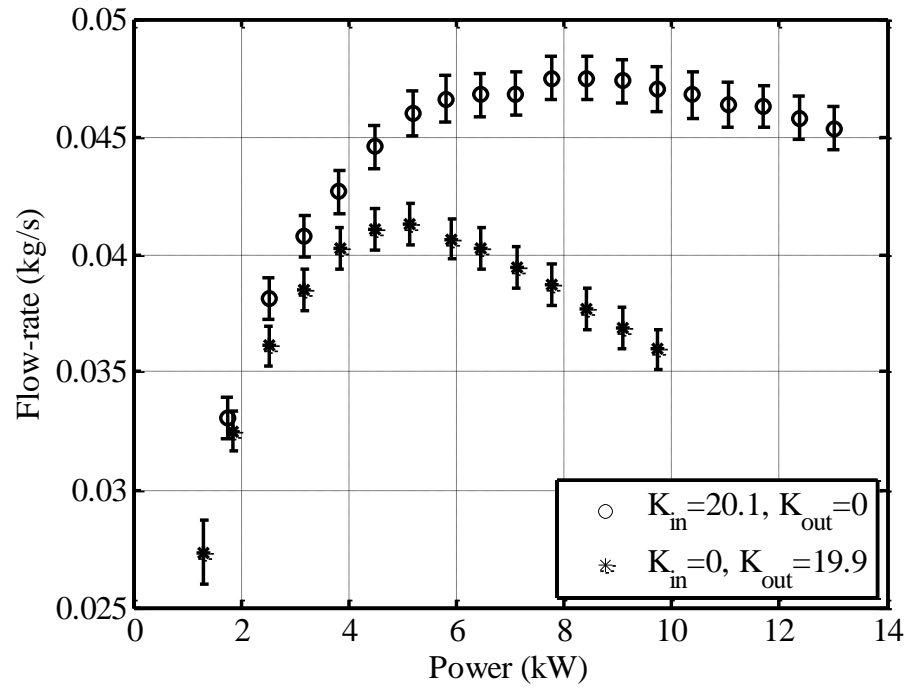
Figure 5.21: Variation of flow rate with power by changing inlet or outlet K factors

(System Pressure=7.6 MPa, T_{in}=25-26 ºC)
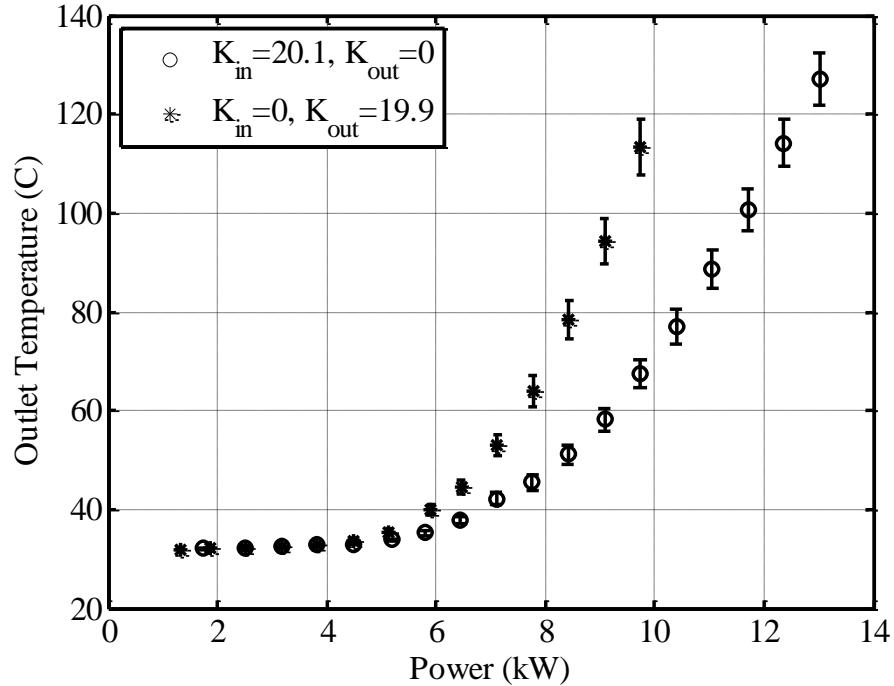
Figure 5.22: Variation of calculated outlet temperature with power for similar inlet/outlet K factors (System Pressure=7.6 MPa, T_{in}=25-26 ℃)

5.3.7 Inlet and Outlet K factors Validation

Inlet and outlet local pressure loss coefficients (K factors) for the pneumatic valves were calculated based on the procedure outlined in Chapter 4. Calculated K factors for this experimental study were in agreement with the data provided by Idelchik (1993) for the cylindrical ball valves with different angles of closing (Table 5.5). Since the Re is higher than 10^4, the K factor is only a function of the geometry of the valve. For two data sets of 30° and 40° closed valves, the data are shown in Table 5.6 and are compared to the results of Idelchik (1993). It should be noted that the K factors for all of the data sets are calculated and reported in the Appendix C. At larger closing angles (45-55 degree), a discrepancy was observed in the provided K factor from Idelchik (1993) and the calculated K factor from the experiments. This is due to the sharp increase of local

pressure loss coefficient at large angles (see the variation of K factor for angles 40º, 50º, and 55º in Table 5.5) and the possible inaccuracy in the adjusted angle of partially closed pneumatic valves in the experiments.

Table 5.5: Local K factor for cylindrical ball valve Idelchik (1993)

$\delta°$	5	10	20	30	40	50	55	67
Local K factor	0.05	0.31	1.84	6.15	20.7	95.3	275	∞

Table 5.6: K factor Results for two data sets

(a) PD-5-041713-x		(b) PD-6-041813-x	
Inlet valve ~30º closed		Inlet valve ~40º closed	
Re	K factor	Re	K factor
38451.5	6.9	43449.8	20.7
46574.9	6.2	50053.6	20.2
53512.3	5.8	54139.7	20.1
56818.7	6.1	57280.7	20.1
60060.9	6.1	59226.9	20.1
62839.2	6.1	61099.2	19.9
64602.0	6.1	62353.2	19.9
65661.0	6.1	62193.0	20.5
66798.3	6.1	63239.2	20.3
67405.7	6.1	63250.0	20.4
67856.9	6.2	63030.1	20.5
67745.3	6.2	62712.7	20.5
67560.8	6.2	62510.6	20.6
67237.3	6.3	62149.3	20.7
66648.2	6.3	61761.2	20.6
66365.7	6.2	62541.0	19.8
65717.8	6.3	61807.8	20.0
64422.8	6.4	60605.4	20.3

For case (a) in Table 5.6, the calculated K factor is 6.2±0.3 (discarding K=6.9) and for the case (b) the K factor is within 20.3±0.5. An uncertainty of ±0.5 in K factor could be considered for these cases.

All in all, the agreement between the calculated K factor and provided K factor in Table 5.5, confirms the correctness of the measured flow rate for these cases.

5.3.8   Flow rate measurement at high inlet temperature (29 ℃ -30℃)

In the experiments performed at high inlet temperatures (29 ℃ -30 ℃) which are close to the critical temperature, it was observed that the outlet temperature calculated based on the energy balance from the measured flow rate, power, and inlet temperature was lower than both the measured temperature of RTD2 (at the outlet of heated channel) and T11 (inlet to the heat exchanger for CO_2), while, the calculated outlet temperature must be higher than both RTD2 and T11 as shown in Figure 5.10. This inconsistency is due to the over-prediction of the volumetric flow rate by the turbine flow-meter at the bottom range of the turbine flow-meter measurement, when the density of the fluid is low (SG < 0.7). The values of the density for CO_2 at temperature of 29-30 ℃, and system pressures of 7.6 and 8.5 MPa are 680 and 730 kg/m3, respectively, which have specific gravities close to 0.7. In this experimental study, the steady-state data for the conditions with an inlet temperature of 29-30℃ are not included in data reduction for pressure-drop; however, they are reported in Appendix C for further study.

5.4   Flow Oscillations

The main purpose of studying flow stability in two-phase or supercritical flow is the evaluation of the stability boundary (the conditions which lead to the flow oscillations).

This task could be done numerically using nonlinear analysis by increasing power and monitoring inlet flow rate to see whether the flow oscillations diverge or converge. However, the task of identifying instability is much more difficult in experimental studies since experimental measurements contain a certain level of noise which may be mistaken with the flow-oscillations. Khabensky and Gerliga (2012) summarized the criteria which have been mostly used in two-phase flow studies for the onset of flow oscillations.

Most of the experimental studies in two-phase flow consider visual observation of the flow as the criterion for detecting flow oscillations (Kyung and Lee (1994), Fukuda and Kobori (1979), Stenning (1964)). For example, Yadigaroglu and Bergles (1972) defined the threshold of instability as the point where disturbance leads to the first observation of self-sustained periodic oscillations with distinguished frequency and amplitude. Saha et al. (1976) defined the onset of instability for a vertical heated channel using Freon-113 as the power where the amplitude of oscillations increases rapidly. This criterion corresponds to the conditions where the amplitude of self-sustained oscillations is between 5-10% of the mean flow rate.

Jain et al. (1966) plotted the normalized standard deviation of fluctuations with respect to the mean flow for self-sustained oscillations versus the heat flux, for two-phase natural circulation loops with different geometries. However, they did not define a certain limit for the normalized standard deviation for the inception of flow oscillations. Wu et al. (2000) reported unstable working conditions in a two-phase water natural circulation loop, where the mass flow rate oscillated in a self-sustained cyclic mode and the ratio of the peak to peak amplitude of oscillations to the mean flow rate was more than 5%.

There is no defined criterion for the threshold of flow instability based on the available experimental knowledge for the supercritical flow natural circulation loops. Lv et al., (2013) reported the oscillation of flow based on experimental observations. Since their experimental facilities were not equipped with a flow meter for recording flow oscillations, they considered outlet temperature oscillations as an indication of flow oscillation.

In the present study, when the ratio of the amplitude of oscillation to the mean flow is more than 5%, the flow was considered unstable.

5.4.1 Flow Oscillations Results

A significant amount of time was spent on performing exploratory tests to locate the unstable working conditions for the present natural circulation loop. To achieve this purpose, some modifications were made on the experimental set-up as discussed in Chapter 3.

Flow oscillations in this study were initiated following a perturbation in the mass flow rate. Any change in any of the independent variables disturbs the velocity of CO_2 flowing into the heated channel. Most of the cases where flow oscillations were obtained occurred after increasing the heat flux on the heated channel, and oscillations of the flow were observed when the outlet temperature was much higher than the pseudo-critical temperature. In the present study, flow oscillations were observed in the negative slope part of the flow rate versus power curve when the outlet temperature was above the pseudo-critical temperature. However, in the other experimental studies in supercritical natural circulation loops, the temperature oscillations were observed when the outlet

temperature was below but close to the pseudo-critical temperature. During flow oscillations, pressure-drop, wall surface temperature, and system pressure oscillated in-phase or out of phase with the flow rate.

To present the flow oscillations, the results of mass flow rate are plotted versus time during a stepwise power increase for a data set. The flow oscillations and the effect of oscillations on the other measured parameters are discussed in the following for four cases of flow oscillations.

Case 1:

Figure 5.23 shows the variation of mass flow rate with the increase of power. The trend of the increase and then decrease of mass flow rate versus power is similar to the steady-state plots which were explained in Section 5.3. The test depicted in Figure 5.23 was performed at 8.00±0.02 MPa with an inlet temperature of 25 ºC -26ºC when the outlet K factors for the pneumatic inlet and outlet valves were 0 and 20, respectively.

Flow instability emerged when the inlet velocity was disturbed at 9.63 kW. Diverging flow oscillations in this case led to the diverging oscillations of the heated wall surface temperature as well, which reached 220ºC at the location of TS25B and the power was killed automatically (abrupt drop in power to zero in Figures 5.23 and 5.24). 220ºC was the temperature limit for the heated channel for safe operation of the loop.
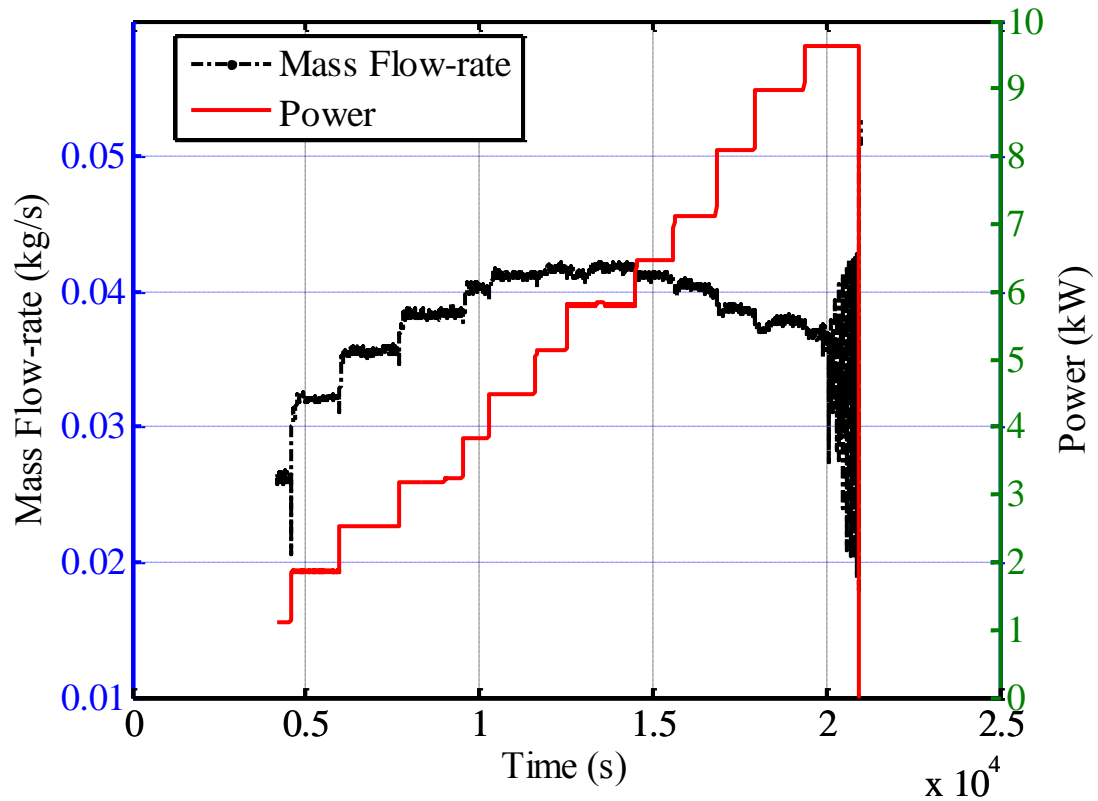
Figure 5.23: Evolution of flow rate leading to the flow instability during power increase

(Case 1: P_{system}=8 MPa, T_{in}=25-26˚C, K_{in}=0, K_{out}=20)

Figure 5.24 shows inlet and outlet temperatures during a power increase for the same data set shown in Figure 5.23. The outlet temperature from the heated channel oscillated out of phase with the inlet flow rate while the inlet temperature and heat flux on the heated channel were constant.

Flow instability started when the outlet temperature was about 85ºC (pseudo-critical temperature of CO_2 at 8 Mpa is ~34.6ºC). However, the reading of outlet temperature was clipped for temperatures above 100ºC due to the adjusted range of RTD2 transmitter. The peak to peak amplitude of the outlet temperature oscillations was 25ºC. The period of

oscillation in this case was ~ 62-64s which is close to the transit time of the loop (~ 62s) for the steady-state conditions just before oscillations emerge.
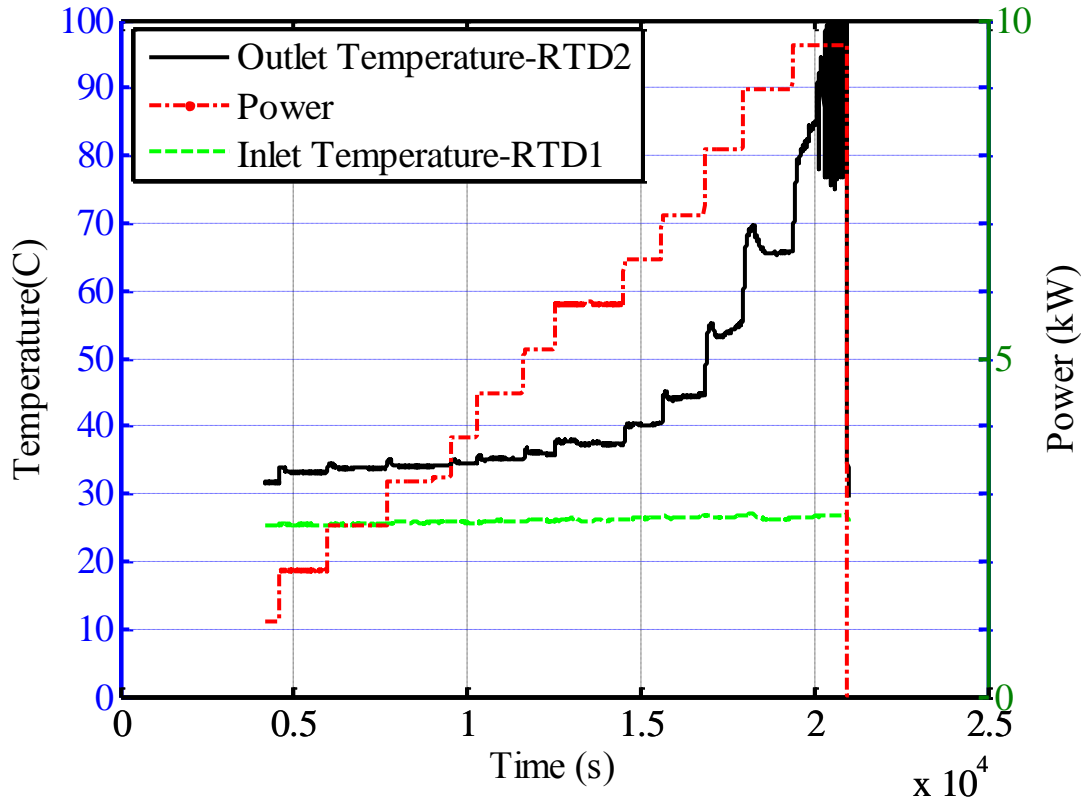
Figure 5.24: Variation of outlet temperature with power increase with constant inlet temperature for Case 1 (Case 1: P_{system}=8 MPa, T_{in}=25-26°C, K_{in}=0, K_{out}=20)

Figure 5.25 shows the flow oscillations with more detailed information of different signals for a shorter period of time.
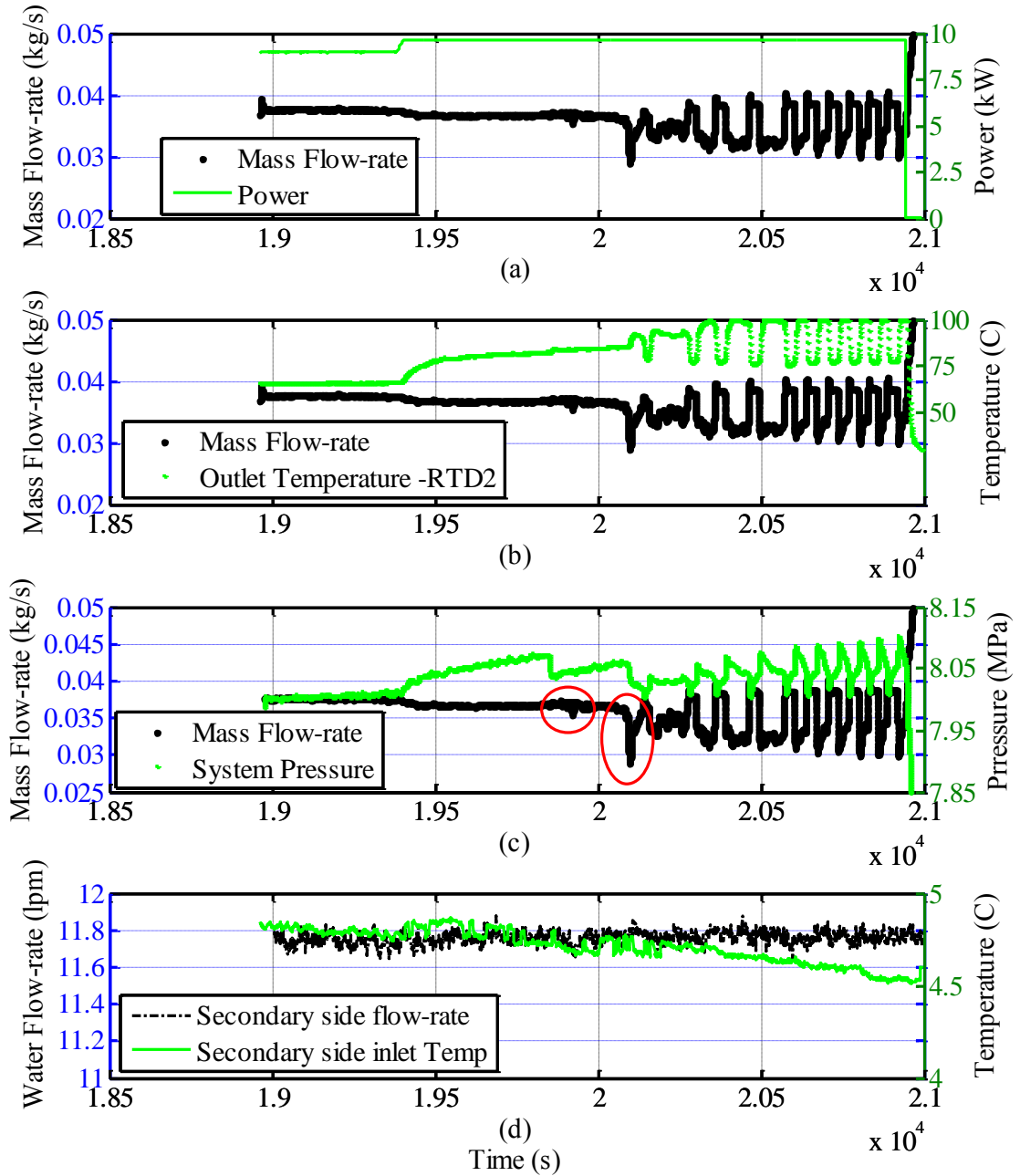
Figure 5.25: Detailed instability results for Case 1 (Case 1: P_{system}=8 MPa, T_{in}=25-26˚C, K_{in}=0, K_{out}=20)

Figure 5.25 (a) shows the time trace of heat flux and flow rate during flow oscillations. A second order Butterworth low pass filter with the cut-off frequency of 0.02 Hz was used for filtering the high frequency noises in the turbine flow-meter signal. Figure 5.25 (b)

shows the oscillations of the outlet temperature and flow rate over time. It is evident from this plot that the outlet temperature oscillates out of phase with flow rate, while the inlet temperature of CO_2 is constant (Figure (5.24)).

When the fluid temperature is increased in a closed loop (constant volume), system pressure increases due to the expansion of the fluid. This trend was recorded during oscillations of the flow for the system pressure. Similar to the outlet temperature curve, system pressure oscillated out of phase with the inlet flow rate (Figure 5.25 (c)). The maximum peak to peak amplitude of oscillations of the system pressure for this case was approximately 0.1 MPa (100 kPa) for the last cycle just before the power shutdown. The circled regions in Figure 5.25 (c) show the disturbances applied to the flow by perturbing the system pressure. Figure 5.25 (d) shows the water flow rate and temperature at the inlet of the heat exchanger in the secondary side. As shown in this plot both the inlet temperature and flow rate in the secondary side were constant during flow oscillations.

The effect of flow oscillation was also observed on the heated wall surface temperature. Figure 5.26 shows the oscillations of outer wall surface temperature at the bottom and at the top of the tube for sections 1 and 6 on the heated channel. Before flow oscillations, a decrease in the wall surface temperature shows an enhancement in heat transfer at the inlet of the heated channel. Moreover, the temperature difference between the top and the bottom thermocouple at section 1 decreased. The enhancement in heat transfer at the inlet to the heated channel (sub-critical region in the heated pipe) was observed frequently in other experiments with flow oscillations. Moreover, it is evident from this plot that wall surface temperatures at the near the inlet and exit of the channel oscillated out of phase with each other.
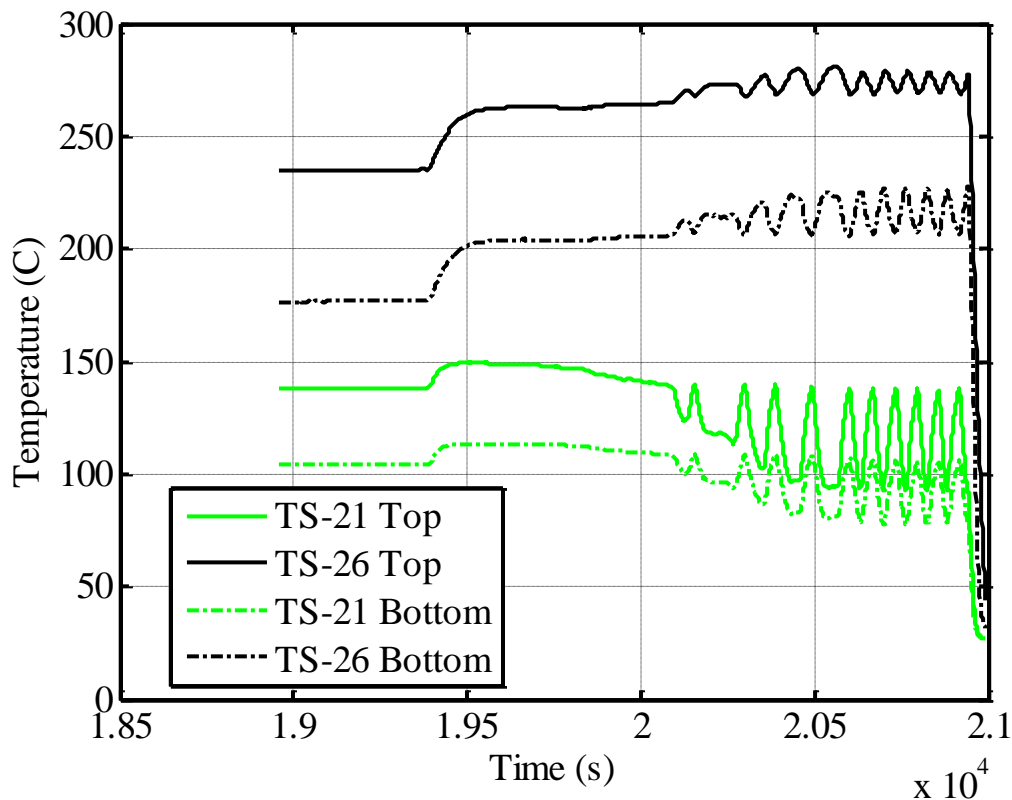
Figure 5.26: Outer wall surface temperature during flow oscillations (Case 1: P_{system}=8

MPa, T_{in}=25-26˚C, K_{in}=0, K_{out}=20)

Case 2:

In addition to the above flow instability case at high outlet temperatures (80-90 ºC), some

flow oscillations were observed at relatively lower outlet temperatures (50-60 ºC), which

are still higher than the pseudo-critical temperature. A sample of flow oscillation for such

a case is shown in Figure 5.27. This data set was taken at 7.6 MPa, with a constant inlet

temperature of 20-21 ºC. The inlet pneumatic valve for this experiment was wide open

and the outlet K factor was 19.9. In this case, the inlet velocity to the heated channel was

disturbed by increasing the power and flow oscillations emerged when the power was

increased from 7.4 kW to 8.4 kW. Self-sustained flow oscillations persisted for approximately 100 minutes at this power and by increasing power, flow oscillations with larger amplitude were observed.
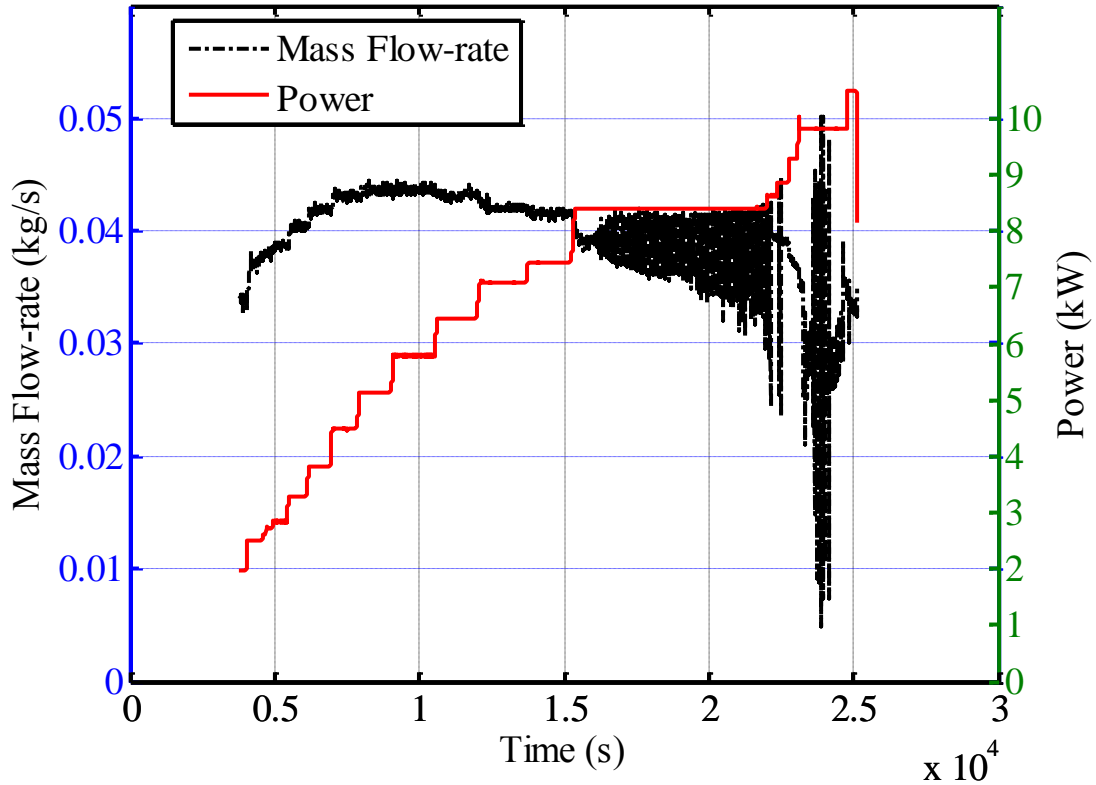
Figure 5.27: Evolution of flow rate with power increase leading to flow oscillations

(Case 2: P_{system}=7.6 MPa, T_{in}=21-22°C, K_{in}=0, K_{out}=19.9)

It should be noted that increasing power in the negative slope part of the flow rate versus power curve, cause a lower mass flow rate in the system. Therefore, by changing the power, mass flow rate changes and a new steady-state condition is achieved. Figure 5.28 shows the recordings of inlet and outlet temperatures for Case 2 (with approximately 10ºC peak to peak amplitude of oscillations) when the inlet temperature and power were constant. Larger amplitude of oscillations (peak to peak) of about 40 ºC was observed at

higher powers in this experiment. Flow oscillations recorded by the outlet RTD were not noisy since the RTD junction is covered with a 1/8" sheath which acts similar to a low-pass filter. Also, this effect reduces the amplitude of the observed temperature oscillations and increases the time response of the RTD at the location of measurement. The amplitude of oscillations at 8.4 kW is more than 5% of the mean flow-rat (Figure 5.27), which was defined previously as the experimental criterion for flow instability in the present study. The oscillations are shown with more details for about 16 minutes (seconds 19,000-20,000) in Figure 5.29.
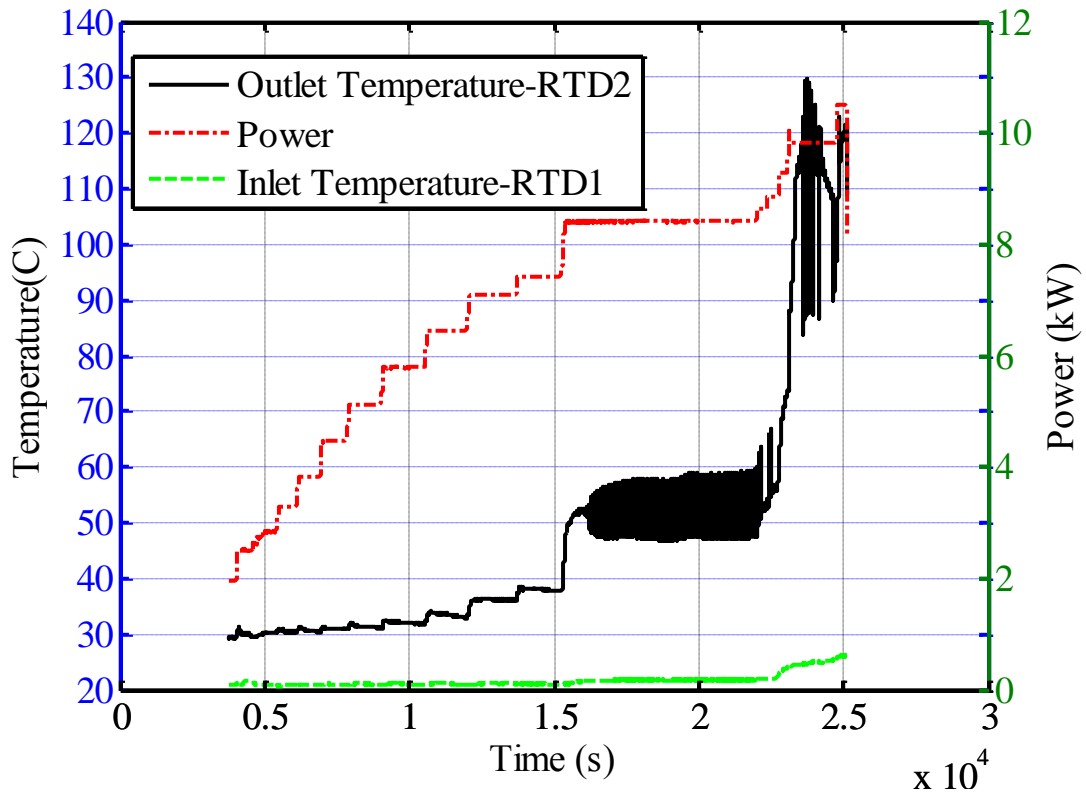
Figure 5.28: Variation of outlet temperature with power increase and constant inlet temperature (Case 2: P_{system}=7.6 MPa, T_{in}=21-22˚C, K_{in}=0, K_{out}=19.9)
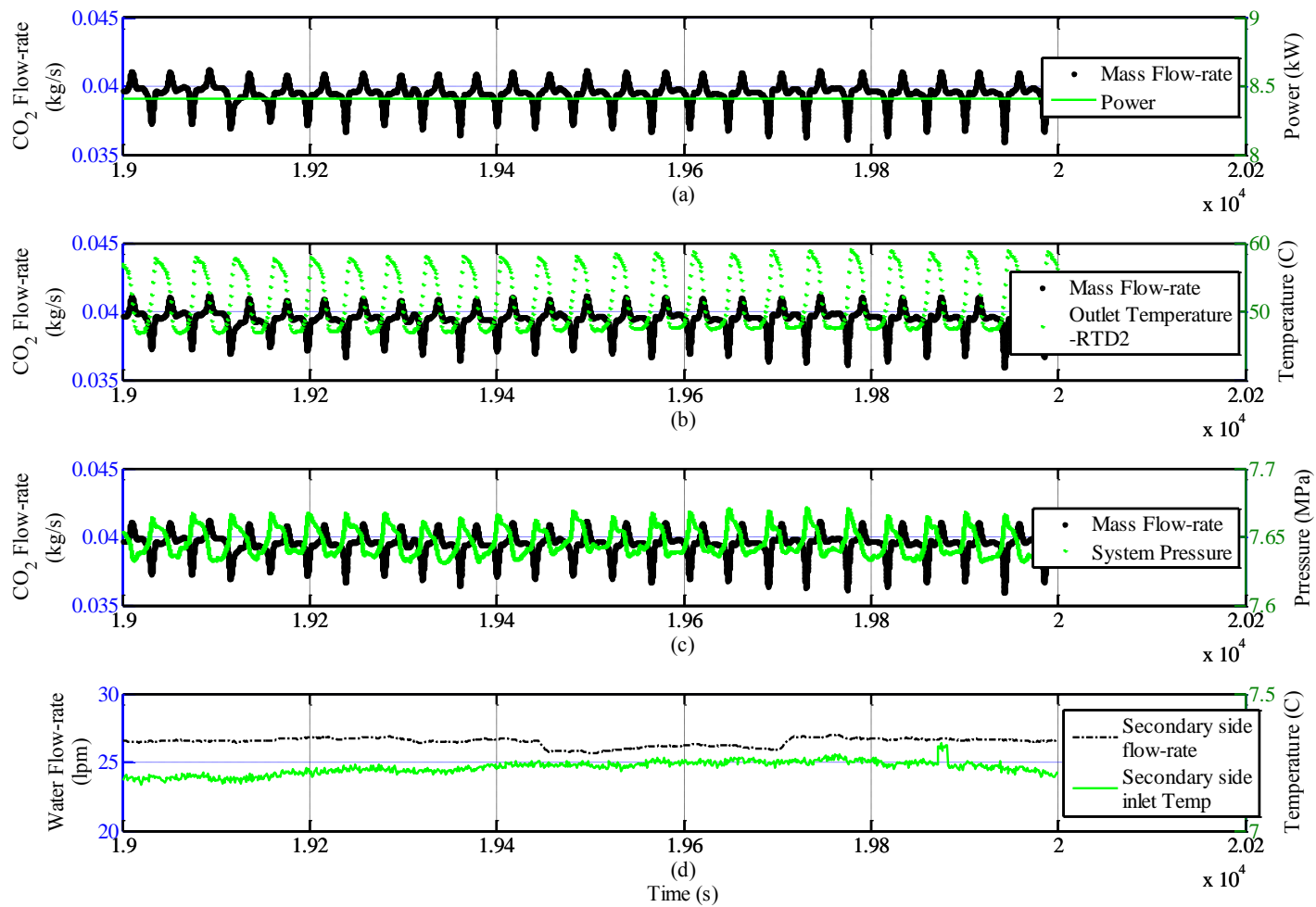
Figure 5.29: Detailed of signals between second 19000-20000 during Flow oscillations (Case 2: P_{system}=7.6 MPa, T_{in}=21-22°C, K_{in}=0, K_{out}=19.9)

Similar to Figure 5.25 (a-d), outlet temperature and system pressure oscillated out of phase with flow oscillations. Also it is evident that during flow oscillations the power, flow rate and the inlet temperature of the cooling flow (water) remained constant.

The above results show that oscillations of outlet temperature, when it is above the pseudo-critical temperature, could be interpreted as an indication of flow instability.

It should be noted that differential pressure transducers showed flow oscillations in the test, however, since in the present experimental study flow oscillations were recorded by the turbine flow-meter directly, the behaviour of the differential pressure transducers are not included here as a sign of instability. Figure 4.10 is a sample of the behaviour of DP2-1 (first differential pressure transducer on the heated channel) during flow oscillations for the data set outlined in Figures 5.27-5.29.

Case 3:

As mentioned before, different independent parameters could be used for disturbing the inlet flow rate. In some experiments, a combination of power change and outlet valve throttling were used for this purpose. As shown in Figure 5.30, at first, the outlet valve was throttled for disturbing the flow rate, however, no flow oscillation was observed and proceeding with increasing power led to flow oscillations. This experiment started at the system pressure of 7.6 MPa and the inlet temperature of 20-21ºC with the inlet K factor of ~52±2.5 and the outlet K factor of 0. However, after throttling the outlet valve, the K factor for the outlet valve increased to ~6 and the system pressure and the inlet temperature increased to 7.96 MPa and 24-25ºC, respectively. Flow oscillations were observed for these conditions when power was increased from 8.70 to 9.53 kW.

Abrupt reduction of flow rate in Figure 5.30 is due to throttling the outlet valve which increases the pressure-drop in the system and induces a lower flow rate in the loop.
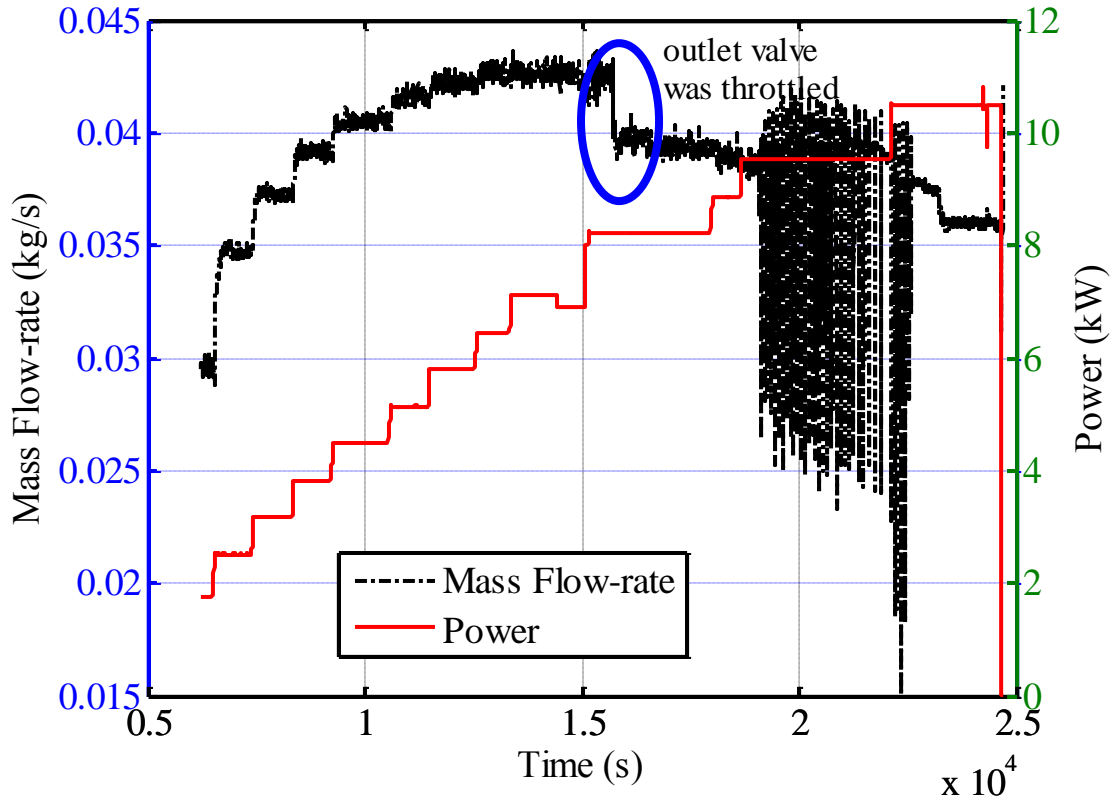
Figure 5.30: Evolution of flow rate with power increase leading to the flow oscillations (Conditions led to flow oscillations for Case 3: P_{system}=7.96 MPa, T_{in}=23-24˚C, K_{in}=52, K_{out}=6)

The ratio of the amplitude of flow rate oscillation to the mean flow was more than 15% in this case and the period of oscillations was about 90 seconds. Figure 5.31 shows the variations of inlet and outlet temperatures during this experiment. The peak to peak amplitude of the outlet temperature oscillations reached 30 ℃ for this case.

The flow oscillations obtained in this experiment were similar to the first case of flow oscillations (Figure 5.23). In both of these experiments the flow rate oscillated between

0.03-0.04 kg/s when the outlet temperature was about 85 ºC at 9.6 and 9.5 kW (see Figure 5.24 and 5.31). However, the inlet and outlet K factors were different in these tests.
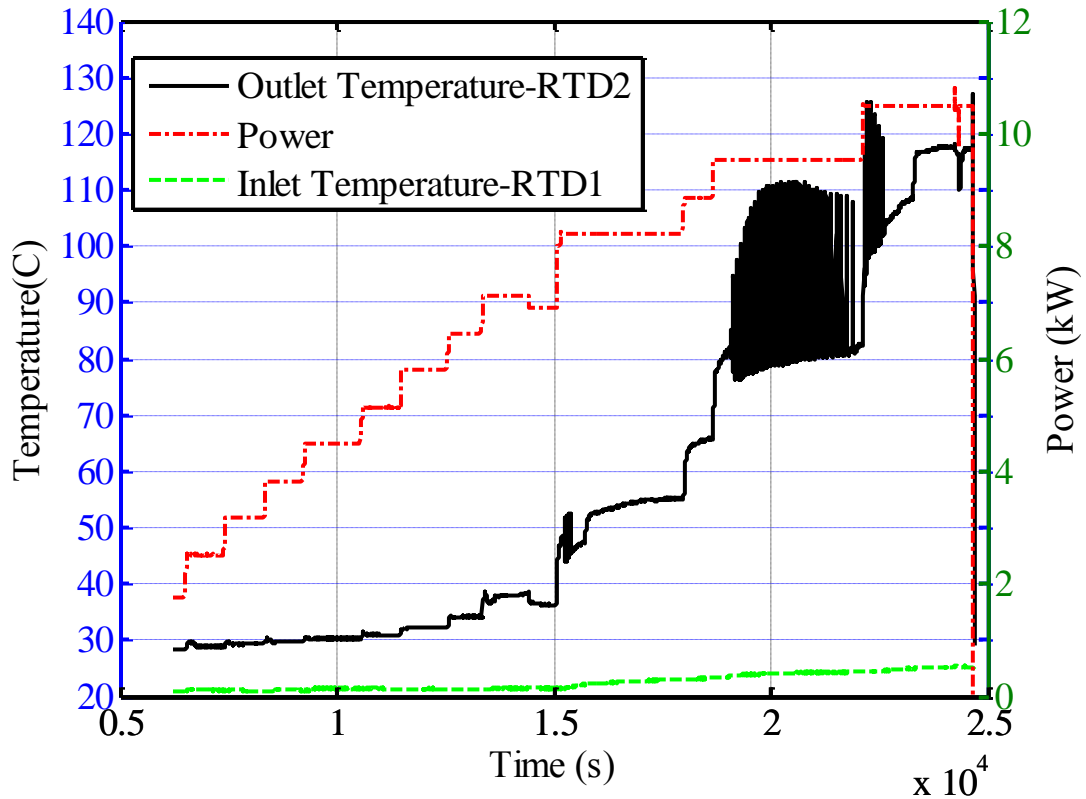
Figure 5.31: Variation of outlet temperature with power increase with constant inlet temperature (Conditions led to flow oscillations for Case 3: P_{system}=7.96 MPa, T_{in}=23-24˚C, K_{in}=52, K_{out}=6)

The more detailed information of experimental parameters is shown in Figure 5.32.
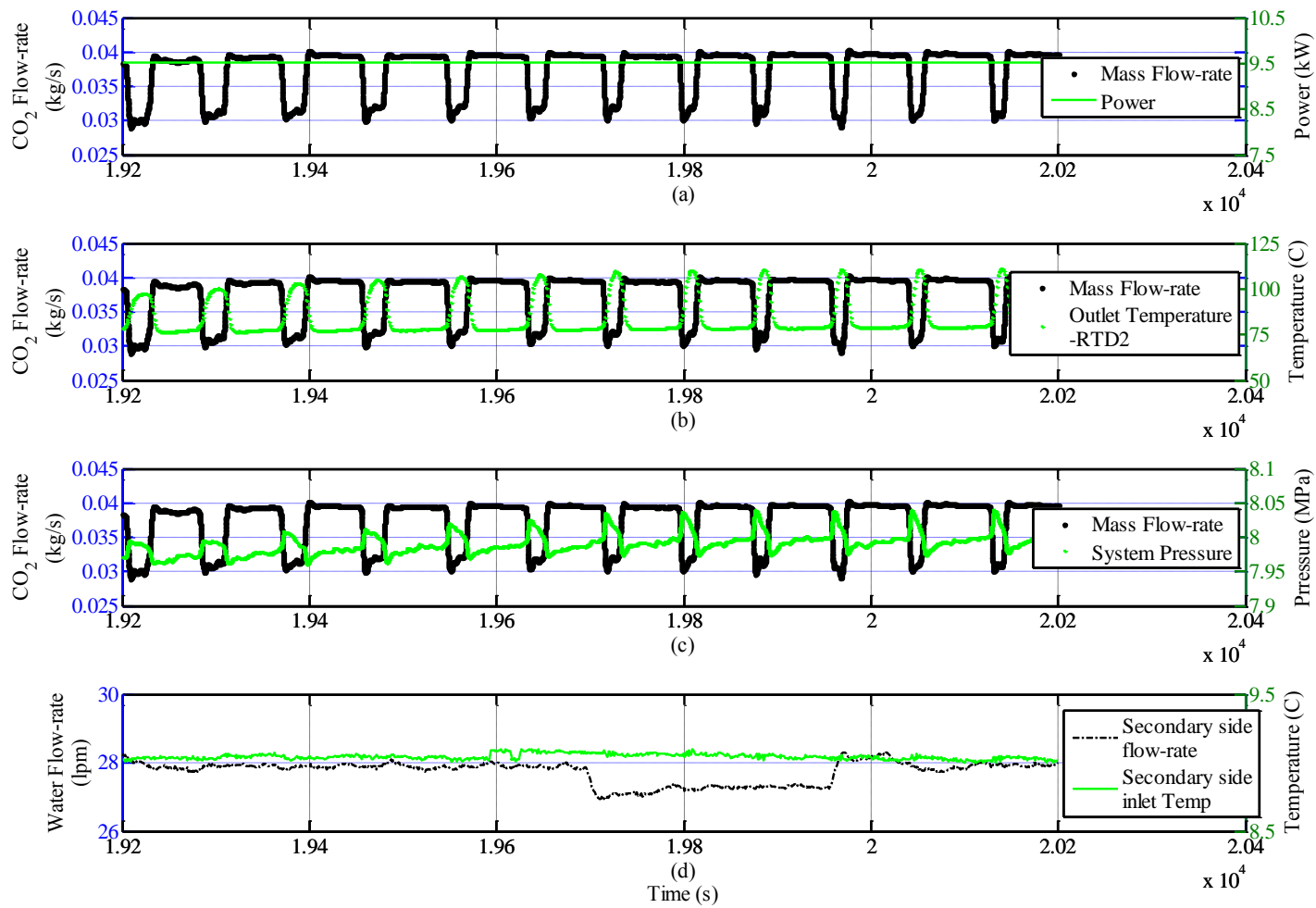
Figure 5.32: Detailed of recorded signal during 19200-20200 s for case 3 (P_{system}=7.96 MPa, T_{in}=23-24˚C, K_{in}=52, K_{out}=6)

The details of the loop at the onset of flow oscillations are shown in Table 5.7. Also, the criterion proposed by Chatoorgoon, (2001) for the instability boundary was examined for the cases 1 and 2. He found that the flow instability boundary is somewhere between 95-100% of the maximum flow-rate in a flow-rate versus power curve for the natural circulation loops. For Case 3, the outlet valve was throttled during the test to make the system unstable. Therefore, the peak of mass flow-rate was not obtained for the valve openings led to flow oscillations.

Table 5.7: The details of the loop parameters at the onset of flow oscillations

Case No.	$\dot{m}_{max}$ (Kg/s) (± 0.001)	$\dot{m}_{ins}$ (Kg/s) (± 0.001)	Q (kW)	P (Mpa)	T_{in} (°C)	K_{in}	K_{out}	$\dfrac{\dot{m}_{ins}}{\dot{m}_{max}} \times 100$ (%)
1	0.042	0.037	9.63	8.03	26.5	0	20	88±5
2	0.0435	0.039	8.41	7.64	21.5	0	19.9	89±5
3	----	0.38	9.53	7.96	23.4	52	6	----

Considering an uncertainty of ±0.001 kg/s for the measurement of flow-meter which was usual in this experimental study (Appendix C) the uncertainty of ±5% (considering maximum value of the error) in the ratio of the mass flow rate at the onset of flow oscillations to the peak mass flow rate was obtained.

5.4.2   Flow Oscillations in Presence of the Inlet and Outlet Headers

Case 4:

Based on the flow oscillation results discussed in Case 1 to Case 3, the outlet temperature oscillations above the pseudo-critical temperature is an indication of flow oscillations. Based on this observation, a few flow oscillations cases were obtained in the presence of the inlet and outlet headers shown in Figure 3.3 (a). Figure 5.34 is a sample of these oscillations at the system pressure of 8 MPa and the inlet temperature of ~22ºC. In this test, the outlet valve was 40° closed, which corresponds to the outlet K factor of 20, while the inlet valve was fully open.

Flow oscillations emerged during a power increase from 9.1 to 9.8 kW. Due to the presence of a large volume header at the outlet, the temperature distribution in the header was not uniform and, although the temperature at the middle of the outlet header was close to 65ºC, the thermocouple located at one end of the header showed a temperature of 35-36 ºC. The outlet temperature was clipped because of the low adjusted range of the outlet RTD transmitter; however, the readout showed an outlet temperature of 70 ºC during flow oscillations.
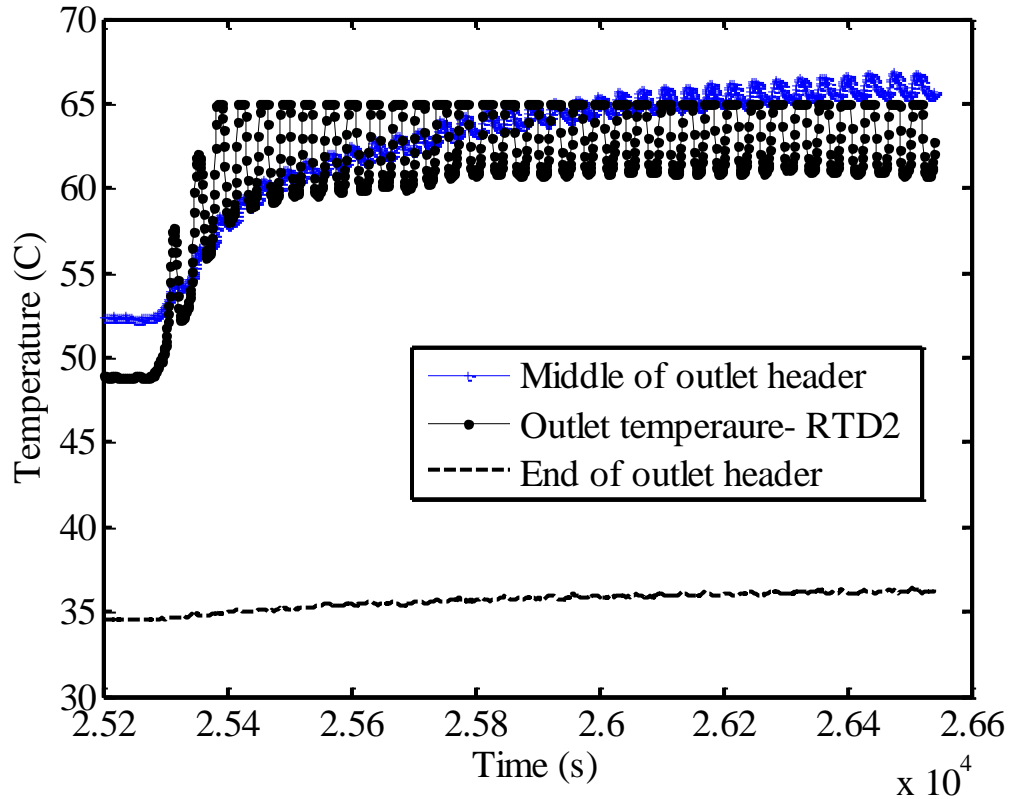
Figure 5.33: Outlet temperature oscillations in presence of inlet and outlet headers

(case 4)

In addition to the flow oscillation cases explained above, the high frequency (~10 Hz) thermo-acoustic pressure wave oscillations were observed frequently in the tests. This phenomenon was captured by the differential pressure transducers only and no sign of this type of dynamic instability was seen in the measured flow rate or the outlet temperature. Fundamentally, thermo-acoustic wave oscillations occur in turbulent flow when the fluid temperature adjacent to the wall reaches the pseudo-critical temperature but the core flow temperature is still sub-critical. These oscillations pose no threat to the cooling of the heated channel, however, when the amplitude of these oscillations was increased, noticeable vibration of the experimental set-up was detected. Stewart et al.

(1973) has reported a comprehensive study on thermo-acoustic wave oscillations in forced convection heat transfer to supercritical pressure water.

5.4.3   Summary

The flow oscillations observed in the present experimental study were similar to the second type of flow oscillations reported in previous studies for two-phase natural circulation loops, as discussed in Chapter 2. In all the cases with flow oscillations, the mass flow rate was close to 0.04 kg/s, when the outlet valve was partially closed. It is worth noting that, no flow oscillations were observed at higher mass flow rates even when the outlet temperature was considerably higher than the pseudo-critical temperature.

CHAPTER 6

SUMMARY, CONCLUSIONS, AND RECOMMENDATIONS

6.1   Summary

An experimental study was performed to determine the thermal-hydraulic behaviour of the supercritical CO_2 in a rectangular natural circulation loop. The experimental set-up consisted of a horizontal electrically heated Inconel-625 tube (L: 2.59 m, OD: 19.05 mm, ID: 12.95 mm) in the lower tier and a water cooled 1-1 shell and tube heat exchanger in the upper tier of the rectangular loop. Experiments were performed at different pressures of 7.6, 8, 8.5, and 9.5 MPa and three different inlet temperatures of 20, 25, and 30ºC, with different inlet and outlet valve openings. Approximately, 450 experimental steady-state data-points were generated. The data include measurements of the pressure-drop along the heated channel, pressure-drop across the inlet and outlet pneumatic valves, applied heat on the heated channel (0-120 kW/m^2), system pressure, temperature of the flow and the heated wall outer surface, and volumetric flow rate. Steady-state curves of mass flow rate versus power, outlet temperature versus power, and detailed information of frictional pressure drop for the heated tube and local head loss coefficients for the pneumatic valves were produced at different steady-state conditions.

The frictional pressure-drop component of the measured total pressure-drop, calculated based on the experimental data, was compared with the existing friction-factor formulae for supercritical flow. Moreover, the influence of buoyancy on the frictional pressure-drop was discussed. The K factors for the pneumatic inlet and outlet valves were derived from the experimental measurements and verified by comparing them against the data of Idelchik (1993).

The mass flow rate, power, and pressure-drop along the heated channel were measured and inlet/outlet K factors were calculated to produce detailed information of the loop in the steady-state conditions, for numerical simulation purposes (Appendix C). The influences of system pressure, inlet temperature, and inlet and outlet vale throttling on the mass flow rate were discussed. Moreover, the uncertainty associated with using the energy balance method for calculating the CO_2 mass flow rate was discussed thoroughly.

Flow instability analysis with the aim of extending available knowledge on flow oscillations in a supercritical natural circulation loops was conducted and the regions of unstable flow were detected in the flow rate versus power curves. The criterion of 5% for the ratio of flow rate oscillations amplitude to the mean flow rate was proposed as the onset of flow instability. Results of flow oscillations (density wave oscillations) were compared to other experimental studies and the detailed information of the loop proceeding to the flow oscillations and the behaviour of the loop during flow oscillations were discussed.

6.2 Conclusions

The conclusions of this experimental study are categorized in three parts: Pressure-drop along the horizontal heated channel for supercritical flow, steady-state parameters of supercritical natural circulation loop, and flow oscillations.

6.2.1 Pressure-drop

1- Available friction-factor formulae used for approximating the frictional pressure-drop underestimated the frictional pressure-drop obtained from this experimental study (except for Kuraeva & Protopopov (1974) and Blasius (1913)).

2- It was shown in this study that for the cases with lower mass flow rate, where the buoyancy effect is larger, the calculated frictional pressure-drop is slightly larger than the Blasius prediction.

3- Frictional pressure-drop data fell within 1-1.20 of the Blasius formula. Therefore, among available formulae used for comparison, the Blasius formula is suggested for use in numerical 1-dimensional modeling of this experimental study.

6.2.2 Steady-state conditions

1- An increase in the system pressure when inlet temperature and valve positions are constant will increase the mass flow-rate in the regions of near the peak and negative slope part of the flow-rate versus power curve. Also, a decrease in the inlet temperature increases the mass flow rate in the loop.

2- If throttling the inlet or outlet valves with the same degree, the outlet valve is dominant in increasing the pressure-drop and decreasing the mass flow rate in the system.

3- It was shown that the energy balance is an inaccurate method for calculating the CO_2 flow rate in the positive slope part of the mass flow rate versus power curve, which corresponds to the pseudo-critical region with strong variation of enthalpy.

6.2.3 Flow oscillations

1- All cases with flow oscillations were observed in the negative slope part of the flow rate versus power curve, which is similar to the second type of density wave oscillations in two-phase natural circulation loops. Moreover, the ratio of the flow-rate at the onset of oscillations was about 88±3% of the maximum flow-rate for two tests.

2- Oscillations of the outlet temperature and loop pressure were out of phase with the oscillations of flow rate.

3- Flow oscillations were observed for the cases with an inlet temperature of 20-25ºC when the system pressure was 7.6-8.5 MPa. No flow oscillations were observed at 9.5 MPa in the experiments performed based on the test matrix.

6.3   Recommendations

6.3.1   Pressure-drop

1- Using a pump in the system provides higher mass flow rates and increases the range of validity of experimental data. Moreover, by using a pump, the flow rate will not be a function of power anymore.

2- The pressure-drop study could be extended by using different tube diameters and roughness. Using a tube with a smaller diameter decreases the influence of buoyancy on the frictional pressure-drop.

3- Including an unheated zone upstream of the heated channel to assure a hydro-dynamically fully developed flow at the entrance to the heated zone.

4- 3-dimensional modeling of the experiment using numerical methods. By validating the measured pressure-drop, it is possible to derive the local frictional pressure-drop along the heated channel.

5- Turbulence measurement of velocity and temperature fields for supercritical flow in the heated channel is the most accurate method for approximating the frictional pressure-drop. However, this requires a new design for the experimental set-up.

6.3.2   Steady-state conditions

1- Further increase in the power supply and the secondary side cooling capacity to obtain more data points in the negative slope part of the mass flow rate versus power curve.

2- Inserting a mixing chamber downstream of the heated channel for direct measurement of outlet temperature lowers the uncertainty of calculations. However, using a mixing chamber adds more pressure-drop to the system and decreases the mass flow rate in the loop.

3- Devising a new flow-meter which is reliable when the inlet temperature is close to the critical temperature (20-30ºC). It is also possible to increase the lengths of the two vertical legs to improve the driving head in the loop. In this case, a Coriolis flow-meter which is the most accurate measuring device can be used.

4- Numerical 3-D modeling of the experiment in the steady-state conditions and comparing with the experimental data which is provided in this study.

6.3.3   Flow oscillations

1- Increasing the range of power and the cooling capacity, are also useful for flow instability study. These changes bring the possibility of increasing the power and monitoring the flow behaviour way down in the negative slope part of the flow rate versus power curve.

2- Numerical 3-dimensional modeling of the whole loop for instability using CFD.

3- Numerical study of the effect of the loop piping thickness on the flow instability. Piping acts like a capacitor in absorbing the heat of the flow.

4- Stability analysis of the supercritical loop using heated channel with different inner diameters and orientations.

References

Ambrosini, W., Sharabi, M., 2008, Dimensionless parameters in stability analysis of heated channels with fluids at supercritical pressures, Nuclear Engineering and Design 238, 1917–1929.

Belblidia, L.A., Bratianu, C., 1979, Density-wave oscillations, Annals of Nuclear Energy Volume 6, Issues 7–8, , Pages 425–444.

Boure, J.A., Bergles, A.E., Tong, L.S., 1973, Review of two-phase flow instability, Nucl. Eng. Des. (25), 165–192.

Chatoorgoon, V., Voodi, A. and Fraser, D., 2005, The Stability Boundary for supercritical Flow in Natural Convection Loops Part I. H2O studies, Nucl. Eng. Des. Vol. 235, 2570–2580.

Chatoorgoon, V., Voodi, A. and Upadhye, P., 2005, The Stability Boundary for Supercritical Flow in Natural Convection Loops Part II. CO2 and H2, Nucl. Eng. Des. Vol. 235, 2005, 2581–2593.

Chatoorgoon, V., 2001, Stability of Supercritical Fluid Flow in a Single-Channel Natural-Convection Loop, International Journal of Heat and Mass Transfer, 44, pp.1963-1972.

Chatoorgoon, V., 1986, SPORTS - A simple non-linear thermalhydraulic stability code ,Nuclear Engineering and Design, Volume 93, Issue 1, Pages 51–67.

Chatoorgoon, V., Upadhye, P., 2005, Analytical studies of supercritical flow instability in natural circulation loop, NURETH-11, Paper 165, Avignon, France.

Chen, Y., Zhao, M., Yang, C., Bi, K., Du, K., 2013, Experiment of heat transfer of supercritical water in natural circulation with different diameters of heated tubes, ISSCWR6-13097, ISSCWER-6, Shenzhen, Guangdong, China.

Cornelius, A.J., Parker, J.D., 1965, Heat transfer instabilities near the critical point, In: Proceedings of the 1965 Heat Transfer and Fluid Mechanics Institute. Stanford University Press, pp. 317– 329.

Daney, D.E., Ludtke, P.R. and Jone, M.C., 1979, An experimental study of thermally-induced flow oscillations in supercritical Helium, J. of Heat Transfer 101, pp.9-14.

Danielyan, D., 2003, Supercritical-Water-Cooled Reactor System - as one of the most promising type of Generation IV Nuclear Reactor Systems.

Debrah, S.K., Ambrosini, W., Chen, Y., 2013, Discussion on the stability of natural circulation loops with supercritical pressure fluids, Annals of Nuclear Energy 54, 47–57.

Dimmick, G.R., Bindner, P.E., Chatoorgoon, V., Schenk, J.R., Sollychin, R., 1990, Thermal-hydraulics R&D for slowpoke heating reactors, Nuclear Engineering and Design, Volume 122, Issues 1–3, Pages 425–434.

Doda, N. et al, 2011, Development of Core Hot Spot Evaluation Method for Natural Circulation Decay Heat Removal in Sodium Cooled Fast Reactor, Proceedings of the 14th International Topical Meeting on Nuclear Reactor Thermalhydraulics (NURETH-14) , Toronto, Canada, NURETH14-170, 13p.

DOE Office of Nuclear Energy, 2007, Generation IV Nuclear Energy Systems Ten-Years Program Plan, Fiscal Year 2007.

Fang, X., Xu, Y., Su, X., Shi, R., 2012, Pressure-drop and friction-factor correlations of supercritical flow, Nuclear Engineering and Design Volume 242, Pages 323–330.

Filonenko, G.K., 1954, Hydraulic resistance of the pipelines, Therm. Eng. (4), 40–44 (in Russian).

Fukuda, K., Hasegawa, S., Kondoh, T., Nozaki, F., and Nagayoshi, T., 1992, Instability of supercritical helium flow, Journal of Heat Transfer: Japanese Research, Vol.21, no: 2, pp.177-186.

Fukuda, K., Kobori, T., 1979, Classification of two-phase flow instability by density wave oscillation model, Journal of nuclear science and technology 16(2) 95-108.

Furuya, M., 2006, Experimental and Analytical Modeling of Natural Circulation and Forced Circulation BWRs – Thermal-Hydraulic, Core-Wide, and Regional Stability Phenomena, PhD thesis.

Greif , R., 1988, Natural Circulation Loops`, J. Heat Transfer 110(4b), 1243-1258.

Harden D.G., Boggs, J.H., 1964, Transient flow characteristics of a natural-circulation loop operated in the critical region, In: Proceedings of the 1964 Heat Transfer and Fluid Mechanics Institute. Stanford University Press, pp. 38–50.

Harden D.G., Boggs, J.H., 1964, Transient flow characteristics of a natural-circulation loop operated in the critical region, In: Proceedings of the 1964 Heat Transfer and Fluid Mechanics Institute. Stanford University Press, pp. 38–50.

Idelchik, I. E. , 1993, Handbook of hydraulic resistance, 2nd edn. Hemisphere, Washington.

Ishigai, S., Kadji, M., Nakamoto, M., 1981, Heat transfer and pressure-drop under water flow at supercritical pressure, JSME J. Ser. B 47 (424) 2333–2349.

Jackson J.D., Hall W.B., 1979, Influences of Buoyancy on Heat Transfer to Fluids Flowing in Vertical Tubes under Turbulent Conditions, in: Turbulent Forced Convection in Channels and Bundles, Hemisphere Publishing Corporation, pp. 613e640.

Jackson, J. D., Hall, W. B., Fewster, J., Watson, A., and Watts, M. J., 1975, Heat Transfer to Supercritical Pressure Fluids, UKAEA, AERER 8158, Design Report 34.

Jain, K.C., 1966, Self-sustained hydrodynamic oscillations in a natural circulation two-phase flow boiling loop, Nuclear Engineering and design 4, 233-252.

Jain, P.K., Rizwan-uddin, 2008, Numerical analysis of supercritical flow instabilities in a natural circulation loop, Nuclear Engineering and Design 238, 1947–1957.

Jain, R., and Corradini, M. L., 2005, A linear stability analysis for natural-circulation loops under supercritical conditions, Thermal Hydraulics, Vol.155, pp.312-323.

Kakac, S., Bon, B., 2008, Review of two-phase flow dynamic instabilities in tube boiling systems`, International Journal of Heat and Mass Transfer 51, 399–433.

Khabensky, V.B., Gerliga, V.A., 2012, Coolant Flow Instabilities in Power Equipment, Book, CRC Press, ISBN 9781466567047.

Khartabil, H., 2009, SCWR: Overview, GIF Symposium – Paris (France) – 9-10 September.

Kondrat'ev, N.S., 1969, Heat transfer and hydraulic resistance with supercritical water flowing in tubes, Therm. Eng. 16 (8), 73–77.

Kumar, P. P., Khardekar, A., Iyer, K. N., 2012, Experimental and Numerical Investigation on a Two-Phase Natural Circulation Test Facility, Heat Transfer Engineering, 33(9):775–785.

Kuraeva, I.V., Protopopov, V.S., 1974, Mean friction coefficients for turbulent flow of a liquid at a supercritical pressure in horizontal circular tubes, High Temp. 12 (1), 194–196.

Kurganov, V. A., Maslakova, I. V., 2010, An integral method of calculation of stabilized heat transfer in tubes in single-phase near-critical region, High Temperature 48: 541-554.

Kurganov, V.A., Kaptil'ny, A.G., 1992, Velocity and enthalpy fields and eddy diffusivities in a heated supercritical fluid flow, Exp. Therm. Fluid Sci. (ETF) 5 (4), 465–478.

Kurganov, V.A., Zeigarnik, Yu.A., Maslakova, I.V., 2013, Heat transfer and hydraulic resistance of supercritical-pressure coolants. Part II: Experimental data on hydraulic

resistance and averaged turbulent flow structure of supercritical pressure fluids during heating in round tubes under normal and deteriorated heat transfer conditions, International Journal of Heat and Mass Transfer 58, 152–167.

Kyung, I. S., Lee, S.Y., 1994, Experimental observations on flow characteristics in an open two-phase natural circulation loop, Nuclear Engineering and Design, Volume 150, Issue 1, 2, 163–176.

Lemmon, E.W., Huber, M.L., McLinden, M.O., 2013, NIST Standard Reference Database 23: Reference Fluid Thermodynamic and Transport Properties-REFPROP, Version 7, National Institute of Standards and Technology, Standard Reference Data Program, Gaithersburg.

Lomperski, S., Cho, D. H., Jain, R., Corradini, M. L., 2004, Stability of a Natural Circulation Loop with a Fluid Heated Through the Thermodynamic Pseudocritical Point, Proceedings of International Congress on Advances in Nuclear Power Plants, Pittsburgh, USA, June 13-17, pp.1736-1741.

LV, F., Huang, Y.P., Wang, Y.L., Yan, X., 2013, Experimental Observation of Supercritical Water Natural Circulation Instabilities, The 15th International Topical Meeting on Nuclear Reactor Thermalhydraulics, NURETH-15 NURETH15-193, Pisa, Italy,.

MacDonald, Ph., Buongiorno, J., Davis, C., Witt, R., 2003, Feasibility Study of Supercritical Light Water Cooled Reactors for Electric Power Production.

Manera, A., 2007, Experimental and analytical investigations on flashing-induced instabilities in natural circulation two-phase systems - applications to the startup of Boiling Water Reactors, PhD thesis.

Petukhov, B.S., Kurganov, V.A., Ankudinov, V.B., 1983, Heat transfer and flow resistance in the turbulent pipe flow of a fluid with near-critical state parameters, High Temp. 21 (1), 81–89.

Petukhov, B.S., Kurganov, V.A., Ankudinov, V.B., Grigor'ev, V.S., 1980., Experimental investigation of drag and heat transfer in a turbulent flow of fluid at supercritical pressure, High Temp. 18 (1), 90–99.

Petukhov, B. S., Polyakof, A. F., Kuleshov, V. A., and Sheckter, Y. L., 1974, Turbulent Flow and Heat Transfer in Horizontal Tubes With Substantial Influence of Thermo-gravitational Forces, Proc. of Fifth Int. Heat Transfer Conference, Tokyo.

Petukhov, B.S., Popov, V. N., 1963, theoretical calculation of heat exchange and frictional resistance in turbulent flow in tubes of an incompressible fluid with variable physical properties, High Temp. 1 (1), 69–83.

Pioro, I. L., Duffey, R. B., Dumouchel, T. J., 2004, Hydraulic resistance of fluids flowing in channels at supercritical pressures (survey), Nuclear Engineering and Design 231, 187–197.

Pioro, I., 2013, Nuclear Power as a Basis for Future Electricity Production in the World: Generation III and IV Reactors, Current Research in Nuclear Reactor Technology in Brazil and Worldwide, Prof. Amir Mesquita (Ed.), ISBN: 978-953-51-0967-9, InTech, DOI: 10.5772/51916.

Popov, V.N., 1967, Theoretical calculation of heat transfer and friction resistance for supercritical carbon dioxide, Heat and mass transfer, Vol 1, 41-48.

Razumovskiy, V.G., Ornatskiy, A.P., Maevskiy, E.M., 1984, Hydraulic resistance and heat transfer of smooth channels with turbulent flow of water of supercritical pressure. Therm. Eng. 31 (2), 109–113..

Razumovskiy, V.G., Ornatskiy, A.P., Mayevskiy, Y.M., 1990, Local heat transfer and hydraulic behavior in turbulent channel flow of water at supercritical pressure, Heat Transfer-Sov. Res., 22 (1), pp. 91–102.

Rizwan-Uddin, 1994, On density-wave oscillations in two-phase flows, International Journal of Multiphase Flow Volume 20, Issue 4, Pages 721–737.

Saha, P., Ishii, M., Zuber, N., 1976, An experimental investigation of the thermally induced two-phase flow oscillations two-phase systems, Trans ASME, J. Heat Transfer 616–622.

Sharma, M., Vijayana, P.K., Pilkhwala, D.S., Asako,Y., 2013, Steady-state and stability characteristics of natural circulation loops, operating with carbon dioxide at supercritical pressures for open and closed loop boundary conditions, Nuclear Engineering and Design 265, 737– 754.

Sharma, M., Pilkhwal, D. S., Vijayan, P. K., Saha, D., Sinha, R. K., 2012, Steady-State Behavior of Natural Circulation Loops Operating With Supercritical Fluids for Open and Closed Loop Boundary Conditions, Heat Transfer Engineering Volume 33, Issue 9, 809-820.

Stenning, A.H., 1964, Instabilities in the flow of a boiling liquid, J. Basic Eng. Trans. ASME Ser. D (86), 213–228.

Stenning, A.H., Veziroglo, T.N., 1965, Flow oscillation modes in forced convection boiling, in: Proceedings of the Heat Transfer and Fluid Mechanics Institute, Stanford Univ. Press, 301–316.

Stenning, A.H., Veziroglo, T.N., 1965, Instabilities in the flow of a boiling liquid, NASA CR-164, University of Miami,.

Stewart E., Stewart P., Watson A., 1973, Thermo-acoustic oscillations in forced convection heat transfer to supercritical pressure water, International Journal of Heat and Mass Transfer, Volume 16, Issue 2, 257–270.

Swapnalee, B.T., Vijayan, P.K., Sharma, M., Pilkhwal, D.S., 2012. Steady-state flow and static instability of supercritical natural circulation loops, Nuclear Engineering and Design 245, 99–112.

Tarasova, N.V., Leont'ev, A.I., 1968, Hydraulic resistance during flow of water in heated pipes at supercritical pressures. High Temp. 6 (4), 721–722.

Tummalapalli, S. K. V. B., 2007, Supercritical Flow Experimental Facility, MSc Thesis, University of Manitoba.

U.S. DOE Nuclear Energy Research Advisory Committee and the Generation IV International Forum, 2002, A Technology Roadmap for Generation IV Nuclear Energy Systems.

Vijayan, P.K. and Austregesilo, H., 1994, Scaling laws for single-phase natural circulation loops, Nuclear Engineering and Design, 152, 331-347,

Vijayan, P.K., Mehta, S.K., Date, A.W., 1991, On the steady-state performance of natural circulation loops", International Journal of Heat and Mass Transfer, v 34, n 9, 2219-2230.

Wissler, E., Isbin, H.S., Amudson, N.R., 1956, Oscillatory Behavior of A Two- Phase Natural-Circulation Loop. AIChE Journal, 2:157–162.

Wu, S. R., Jia, H. J., Jiang, S. Y., Zhang, Y. J., 2000, Investigation on two-phase flow stability in a natural circulation system, Kerntechnik, 65(5-6), 222-226.

Xiong, T., Yan, X., Xiao, Z.J., Li, Y.L., Huang, Y.P., Yu, J.C., 2012, Experimental study on flow instability in parallel channels with supercritical water, Annals of Nuclear Energy 48, pp.60-67.

Yadigaroglu, G., Bergles, A.E., 1972, Fundamental and higher mode density-wave oscillations in two-phase flows, J. Heat Transfer, Trans. ASME 94, 189–195.

Yamashita, T., Mori, H., Yoshida, S., Ohno, M., 2003, Heat transfer and pressure-drop of a Supercritical pressure fluid flowing in a tube of small diameter", Memoirs of the Faculty of Engineering, Kyushu University, v 63, n 4, 227-244.

Zvirin, Y., 1986, The onset of motion in a toroidal thermo-syphon, Journal of Engineering Mathematics, v 20, n 1, p 3-20.

Zuber, N., 1966. An analysis of thermally induced flowoscillations in the near-critical and super-critical thermodynamic region. Rept. NASA-CR-80609. Research and Development Center, General Electric Company, Schenectady, New York, USA.

APPENDIX A

LOOP DIMENSIONS

Figure A.1 shows the detailed dimensions of the loop prepared for the numerical one-dimensional or three-dimensional simulation. The detail of the heat exchanger section is provided in Appendix B.
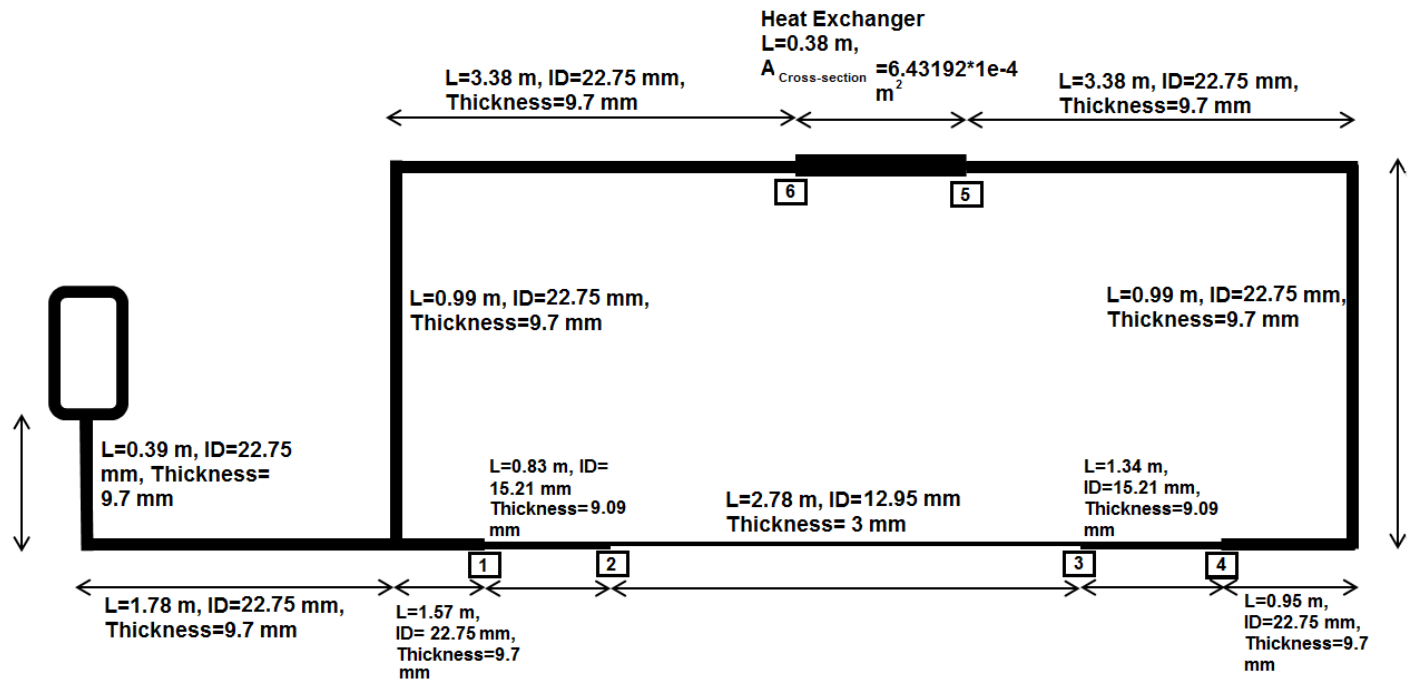
Figure A.1: Dimensions of the natural circulation loop

In addition to the detailed dimension of the loop the locations wherein there is a change in the area of the loop is specified by numbers 1-6 in Figure A-1. As mentioned before, area change, introduces local pressure-drop and therefore local pressure loss coefficient needs to be evaluated. Local K factor for this experiment is calculated using Idelchik (1993).

Section 1: This is a converging area change in the cold side of the loop. This area change happens in a 1" Class 2500 flange which was machined to match the area of the pipe at one side and a flange on the other side. This design was instead of abrupt area contraction to keep the pressure-drop as low as possible in the loop.
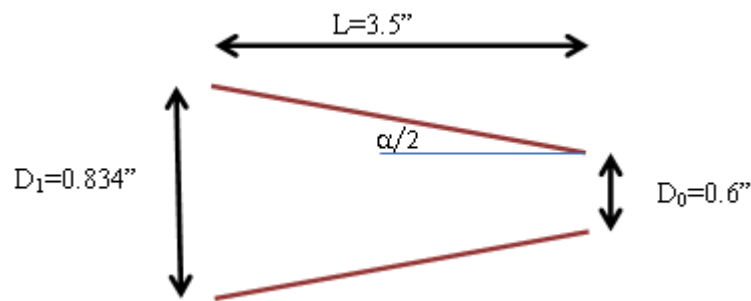
Figure A.2: Converging pipe dimension at section 1

$$\frac{D_1}{D_0} = 1.39$$

$$\alpha = 3.8°$$

Using plots on page 316 of Idelchik, the $K_1=0.07$.

Section 2 & 3: These are an area enlargement and an area contraction occurs at the inlet and outlet of the heated channel. According to Vijayan and Mehta (1991), calculated

values for local pressure-drops for sections 2 and 3 which are located in the heated channel are multiplied to 1.3 as the correction factor.

Section 2
abrupt area contraction (Inlet)

Section 3
Abrupt area enlargement (Outlet)

$$K_2 = 0.5\left(1 - \frac{A_0}{A_2}\right) = 0.51 - \left(\frac{D_0}{D_2}\right)^2$$
$$= 0.138 \times 1.3 = 0.18$$

$$K_3 = \left(1 - \frac{A_0}{A_2}\right)^2 = \left(1 - \left(\frac{D_0}{D_2}\right)^2\right)^2$$
$$= 0.077 \times 1.3 = 0.1$$
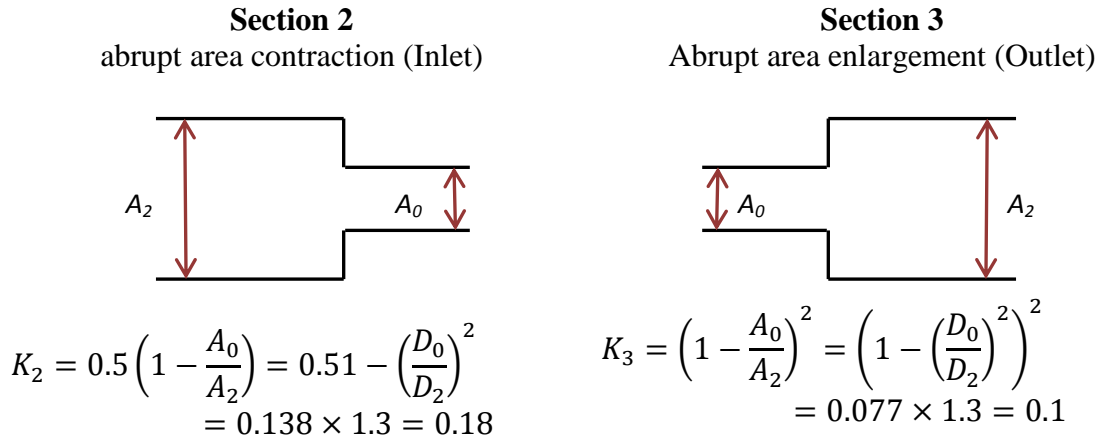
Figure A.3: Abrupt area change at sections 2 and 3

Section 4: The area change in section 4 which is located in the hot side of the loop is similar to the section 3 which is a sudden area enlargement and the equation for section 3 was used for calculating K_4. The calculated K factor for section 4 is 0.3.

Section 5 & 6: Detailed procedure of calculation of K5 and K6 is provided in Appendix B.

Elbows: K factor for the rough elbows with sharp edges along with considering the effect of Re number when the Re >10000 is calculated to be 2.16.

Table A.1 summarizes the local K factors in the loop for numerical modeling

Table A.1: Calculated local K factors

Name	K factor
K_1	0.07
K_2	0.18
K_3	0.01
K_4	0.3
K_5	2
K_6	2.7
Elbows	2.16

APPENDIX B

HEAT EXCHANGER GEOMETRY AND LOCAL PRESSURE LOSSES
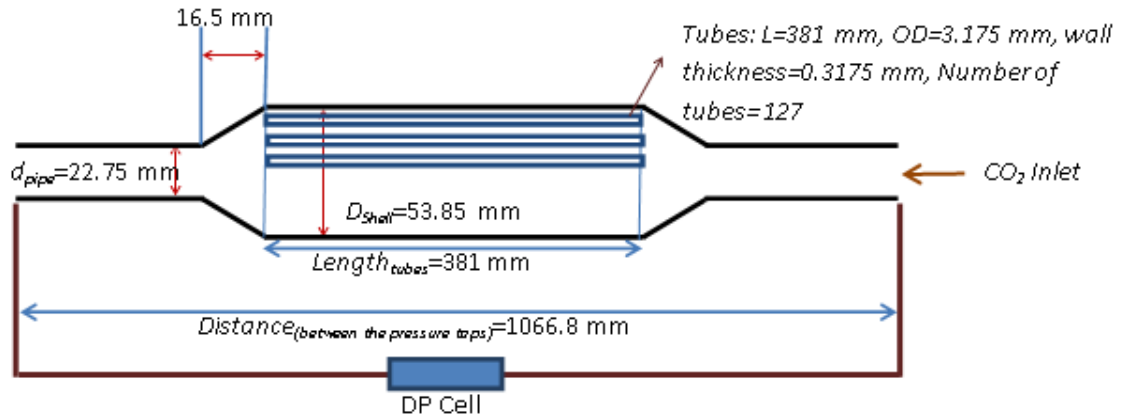
Figure B.1: Heat exchanger configuration and dimensions

Note: This schematic is symmetrical.

Figure B.1 shows the configuration of the heat exchanger. CO_2 is flowing in the tube side of the heat exchanger through 127 small tubes (OD of 3.175 x 0.3175 wall thickness). The diameter of piping widens from 22.75 mm (pipe inner diameter) to 53.85 mm (shell inner diameter) with a distance of 16.5 mm.

Local Pressure loss at the inlet and outlet of the Heat exchanger:

Total measured pressure-drop across the heat exchanger with its components is

$$\Delta P_{measured} = \Delta P_{Piping-inlet} + \Delta P_{Piping-outlet} + \Delta P_{small\ tube} + \Delta P_{ac} \\ + \Delta P_{eq-inlet\ K} + \Delta P_{eq-outlet\ K} \tag{B.1}$$

$\Delta P_{Piping-inlet}$= Frictional pressure-drop along the piping at the inlet portion of the heat exchanger.

$\Delta P_{\text{Piping−outlet}}$= Frictional pressure-drop along the piping at the out portion of the heat exchanger.

$\Delta P_{\text{small tube}}$= Frictional pressure-drop along the small tubes in the heat exchanger (calculated locally and summation of pressure-drop at each node is representative of total frictional pressure-drop along the heat exchanger tubes)

ΔP_{ac}= Acceleration pressure-drop (pressure is built along the heat exchanger)

By assuming fully developed flow, frictional pressure-drop along the piping at the inlet and outlet, and frictional pressure-drop along the heat exchange tubes can be calculated based on local physical properties of the flow.

$\Delta P_{\text{eq−inlet K}}$ and $\Delta P_{\text{eq−outlet K}}$, in Equation (B.1) are representative of local pressure loss due to area change and obstruction at the inlet and outlet of the heat exchanger which are unknowns and could be calculated by

$$\Delta P_{eq-inlet\ K} = K_{eq.inlet}\ \frac{G_{Piping}^2}{2\rho_{inlet}} \tag{B.2}$$

And

$$\Delta P_{eq-outlet\ K} = K_{eq.outlet}\ \frac{G_{Piping}^2}{2\rho_{outlet}} \tag{B.3}$$

There is only one equation with two unknowns. To find inlet and outlet equivalent K factors its assumed that there is a sudden area enlargement at the inlet and a sudden area contraction at the outlet. With this assumption it's possible to approximate the local pressure losses in terms of each other.

<table>
<tr><td>For sudden area enlargement (A: cross-section area)</td><td>For sudden area contraction (A: cross-section area)</td></tr>
</table>
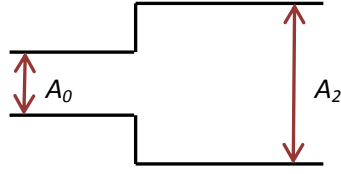
For sudden area enlargement (A: cross-section area)   For sudden area contraction (A: cross-section area)

$$K_{\text{enlargement}} = \left(1 - \frac{A_0}{A_2}\right)^2$$
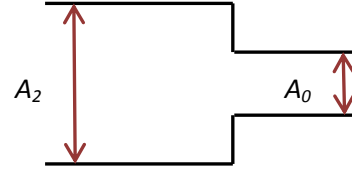
$$K_{\text{contraction}} = 0.5\left(1 - \frac{A_0}{A_2}\right)$$

Figure B.2: Local pressure loss due to area change

Now,

$$\frac{K_{\text{enlargement}}}{K_{\text{contraction}}} = 2 \times \left(1 - \frac{A_0}{A_2}\right)$$

For our case

A0= Area of the piping

$$A_0 = \frac{\pi}{4}(0.02275)^2 = 4.06286 \times 10^{-4}$$

And A2= cross section area of the heat exchanger (tube side)

$$A_0 = \frac{\pi}{4}(0.00254)^2 \times 127 = 6.43192 \times 10^{-4}$$

Therefore

$$\frac{K_{\text{enlargement}}}{K_{\text{contraction}}} = 2 \times \left(1 - \frac{4.06286}{6.43192}\right) = 0.7366 \tag{B.4}$$

Using Equations (B.1)-(B.4), it is possible to find both equivalent inlet and outlet K factor based on local Re number at the inlet and outlet. Calculated pressure loss

coefficient based on above approach is tabulated in Table B.1 based on Re number for inlet and outlet piping.

Table B.1: Local K factor for the inlet and outlet of the heat exchanger

Re (inlet)	Eq. Inlet K factor	Re (outlet)	Eq. outlet K factor
27291.1	3.4	23794.5	4.7
33272.1	2.8	28204.9	3.8
40080.4	2.5	32653.1	3.4
45158.4	2.3	35687.9	3.2
50259.4	2.2	38410.8	3.0
55461.7	2.1	40844.2	2.9
59221.6	2.1	42447.7	2.8
63506.2	2.0	44137.9	2.8
67314.1	2.0	45396.5	2.7
70767.0	1.9	46459.8	2.6
73296.1	1.9	46750.4	2.6
76562.8	1.8	47689.6	2.5
78789.2	1.8	47786.0	2.4
81251.1	1.7	48217.2	2.3
83106.0	1.7	48179.0	2.3

Calculated K factors for inlet to the heat exchanger vary between1.7-3.4 and for the outlet it's between 2.3-4.7. Since the variation of K factor is small, an average value could be used as the local pressure loss at the inlet and outlet of the heat exchanger.

It should be noted that fully developed flow conditions is an unrealistic assumption which was made for simplicity of calculations in this case. However, following explained approach, the equivalent K factors could be calculated including the effect of these uncertainties. Based on the processed data for five data sets, considering $K_{in-HE}=2$ and $K_{out-HE}=2.7$ leads to less than 20% error in calculating heat exchanger total pressure-drop for 75% of the experimental data.

APPENDIX C

RAW AND PROCESSED DATA FROM THE EXPERIMENTAL STUDY

April 9th, 2013- System Pressure: 7.6 MPa, Inlet Temperature: 25-26 ℃, Inlet valve: wide open, Outlet valve: wide open

Table C.1: Averaged values of measured signals during experiment for each data point (PD-1-040913)

Test ID	Inlet Temperature (RTD1) (C)	Pressure (MPa)	Power (kW)	Outlet Temp (RTD2)(C)	T11 (C)	T12(C)	CO_2 volumetric Flow rate $(m^3/s) \times 10^6$	HE-Inlet water Temp.(C)	HE-Outlet water Temp.(C)	Water Flow rate (lpm)
PD-1-040913-1.2	24.8 ± 0.4	7.62 ± 0.02	1.32 ± 0.03	30.9 ± 0.5	32.6 ± 2.2	24.9 ± 2.2	40.5 ± 1.1	11.0 ± 2.2	29.1 ± 2.2	0.9
PD-1-040913-1.7	25.1 ± 0.4	7.59 ± 0.02	1.86 ± 0.03	31.5 ± 0.5	33.2 ± 2.2	24.9 ± 2.2	48.0 ± 1.0	10.6 ± 2.2	28.3 ± 2.2	1.5
PD-1-040913-2.3	25.0 ± 0.4	7.60 ± 0.02	2.52 ± 0.04	32.0 ± 0.5	33.6 ± 2.2	25.1 ± 2.2	53.7 ± 1.0	10.3 ± 2.2	26.9 ± 2.2	2.3
PD-1-040913-2.9	25.2 ± 0.4	7.59 ± 0.02	3.17 ± 0.04	32.2 ± 0.5	33.7 ± 2.2	25.3 ± 2.2	58.2 ± 1.1	10.2 ± 2.2	25.4 ± 2.2	3.3
PD-1-040913-3.5	25.3 ± 0.4	7.59 ± 0.02	3.83 ± 0.04	32.3 ± 0.5	33.8 ± 2.2	25.0 ± 2.2	61.8 ± 1.1	8.6 ± 2.2	24.2 ± 2.2	3.9
PD-1-040913-4.1	25.5 ± 0.4	7.59 ± 0.02	4.49 ± 0.05	32.5 ± 0.5	34.1 ± 2.2	24.6 ± 2.2	64.7 ± 1.1	7.4 ± 2.2	22.9 ± 2.2	4.7
PD-1-040913-4.7	25.8 ± 0.4	7.61 ± 0.02	5.14 ± 0.05	32.8 ± 0.5	34.6 ± 2.2	24.4 ± 2.2	66.8 ± 1.1	6.5 ± 2.2	21.8 ± 2.2	5.5
PD-1-040913-5.3	25.8 ± 0.4	7.61 ± 0.02	5.80 ± 0.05	33.1 ± 0.5	35.2 ± 2.2	24.8 ± 2.2	68.3 ± 1.1	5.7 ± 2.2	20.1 ± 2.2	6.6
PD-1-040913-5.9	25.8 ± 0.4	7.59 ± 0.02	6.46 ± 0.06	33.4 ± 0.5	36.2 ± 2.2	25.0 ± 2.2	69.4 ± 1.1	5.0 ± 2.2	20.3 ± 2.2	6.9
PD-1-040913-6.5	25.7 ± 0.4	7.60 ± 0.02	7.11 ± 0.06	34.3 ± 0.5	37.7 ± 2.2	24.9 ± 2.2	70.1 ± 1.1	4.8 ± 2.2	19.7 ± 2.2	8
PD-1-040913-7.1	26.2 ± 0.4	7.61 ± 0.02	7.77 ± 0.06	36.1 ± 0.5	40.6 ± 2.2	25.1 ± 2.2	70.4 ± 1.1	4.7 ± 2.2	19.6 ± 2.2	8.6
PD-1-040913-7.7	26.3 ± 0.4	7.62 ± 0.02	8.43 ± 0.06	38.4 ± 0.5	43.9 ± 2.2	25.0 ± 2.2	70.3 ± 1.1	4.5 ± 2.2	18.6 ± 2.2	9.9
PD-1-040913-8.3	25.6 ± 0.4	7.60 ± 0.02	9.08 ± 0.07	39.8 ± 0.5	46.3 ± 2.2	24.3 ± 2.2	70.3 ± 1.1	4.2 ± 2.2	17.5 ± 2.2	11.4
PD-1-040913-8.9	25.7 ± 0.4	7.62 ± 0.02	9.74 ± 0.07	43.7 ± 0.5	51.1 ± 2.2	24.5 ± 2.2	70.0 ± 1.1	4.0 ± 2.2	17.4 ± 2.2	12
PD-1-040913-9.5	25.9 ± 0.4	7.61 ± 0.02	10.39 ± 0.07	49.0 ± 0.5	57.6 ± 2.2	24.7 ± 2.2	69.4 ± 1.1	3.9 ± 2.2	17.6 ± 2.2	12.5
PD-1-040913-10.1	26.0 ± 0.4	7.62 ± 0.02	11.05 ± 0.07	55.1 ± 0.6	63.7 ± 2.3	24.8 ± 2.2	68.9 ± 1.1	3.9 ± 2.2	17.2 ± 2.2	13.5
PD-1-040913-10.7	26.2 ± 0.4	7.62 ± 0.02	11.71 ± 0.08	64.1 ± 0.6	72.1 ± 2.3	25.0 ± 2.2	68.4 ± 1.2	3.8 ± 2.2	17.0 ± 2.2	14.2
PD-1-040913-11.3	26.0 ± 0.4	7.62 ± 0.01	12.37 ± 0.08	71.2 ± 0.6	79.7 ± 2.3	24.7 ± 2.2	67.9 ± 1.1	3.6 ± 2.2	16.5 ± 2.2	15.5
PD-1-040913-11.9	25.9 ± 0.4	7.61 ± 0.02	13.02 ± 0.08	80.5 ± 0.7	86.7 ± 2.5	25.3 ± 2.2	68.0 ± 1.2	3.6 ± 2.2	16.5 ± 2.2	16

Table C.2: Averaged values of measured pressure-drops during experiment for each data point (PD-1-040913)

Test ID	DP2-1 (Pa)	DP2-2 (Pa)	DP2-3 (Pa)	DP2-4 (Pa)	DP2-5 (Pa)	DP3 (Pa)	DP13 (Pa)	DP10 (Pa)
PD-1-040913-1.2	107.5 ± 11.1	29.41 ± 11.11	67.49 ± 11.10	38.3 ± 11.2	34.9 ± 10.8	146.2 ± 11.1	250.4 ± 13.5	132.2 ± 132.3
PD-1-040913-1.7	135.6 ± 11.8	38.89 ± 11.66	94.80 ± 11.55	58.6 ± 11.8	44.3 ± 11.2	167.6 ± 11.8	337.6 ± 17.8	174.7 ± 116.9
PD-1-040913-2.3	161.0 ± 12.5	48.51 ± 12.18	123.60 ± 11.96	81.5 ± 12.5	56.0 ± 11.6	186.2 ± 12.5	430.9 ± 20.0	226.9 ± 123.3
PD-1-040913-2.9	182.3 ± 13.2	58.74 ± 13.07	153.58 ± 12.85	106.7 ± 13.5	70.0 ± 12.3	199.6 ± 13.2	527.1 ± 23.0	287.4 ± 134.4
PD-1-040913-3.5	200.1 ± 14.2	68.70 ± 14.14	182.28 ± 13.81	132.1 ± 14.7	89.4 ± 13.2	213.9 ± 14.2	624.5 ± 25.2	355.7 ± 129.4
PD-1-040913-4.1	215.5 ± 15.2	79.56 ± 14.93	210.83 ± 14.42	159.1 ± 15.7	106.5 ± 13.7	224.0 ± 15.2	719.4 ± 28.6	423.6 ± 135.0
PD-1-040913-4.7	229.4 ± 16.9	91.25 ± 16.47	239.19 ± 15.64	187.0 ± 17.7	126.2 ± 14.7	233.8 ± 16.9	816.9 ± 35.1	480.2 ± 137.6
PD-1-040913-5.3	241.3 ± 18.0	102.67 ± 17.56	266.82 ± 16.55	216.2 ± 19.0	146.8 ± 15.6	239.7 ± 18.0	914.2 ± 39.0	533.0 ± 129.0
PD-1-040913-5.9	251.2 ± 19.4	115.31 ± 18.41	295.03 ± 17.80	248.1 ± 20.1	168.5 ± 16.8	243.0 ± 19.4	1015.3 ± 43.5	581.7 ± 145.0
PD-1-040913-6.5	260.4 ± 36.2	127.40 ± 48.07	321.07 ± 51.93	279.9 ± 20.9	188.6 ± 33.7	253.2 ± 36.2	1111.2 ± 80.5	629.6 ± 128.7
PD-1-040913-7.1	269.0 ± 21.3	142.31 ± 20.30	351.43 ± 19.46	315.9 ± 21.6	210.7 ± 18.1	247.7 ± 21.3	1219.6 ± 55.6	683.7 ± 141.7
PD-1-040913-7.7	276.4 ± 23.5	155.53 ± 22.43	379.46 ± 21.64	350.4 ± 23.1	232.9 ± 20.0	248.5 ± 23.5	1321.7 ± 63.1	732.4 ± 131.7
PD-1-040913-8.3	282.5 ± 25.3	165.49 ± 23.59	403.72 ± 22.60	382.8 ± 24.4	253.1 ± 20.9	251.4 ± 25.3	1411.7 ± 72.6	769.8 ± 133.6
PD-1-040913-8.9	287.5 ± 26.2	178.60 ± 24.97	431.54 ± 23.77	417.5 ± 25.3	271.7 ± 21.9	252.1 ± 26.2	1508.2 ± 74.6	810.0 ± 131.5
PD-1-040913-9.5	292.8 ± 27.4	192.89 ± 26.60	463.25 ± 25.54	453.9 ± 26.6	289.8 ± 23.3	248.3 ± 27.4	1610.6 ± 81.1	850.8 ± 134.0
PD-1-040913-10.1	297.2 ± 28.9	205.52 ± 28.78	493.45 ± 27.63	487.9 ± 28.4	304.4 ± 24.8	246.3 ± 28.9	1703.3 ± 94.3	883.4 ± 145.9
PD-1-040913-10.7	305.8 ± 36.4	218.41 ± 64.24	527.40 ± 38.21	524.3 ± 34.7	316.6 ± 26.8	259.7 ± 36.4	1803.3 ± 112.5	916.3 ± 147.1
PD-1-040913-11.3	311.0 ± 10.3	229.85 ± 10.35	559.91 ± 10.35	557.9 ± 10.3	327.5 ± 10.3	264.4 ± 10.3	1893.6 ± 10.3	949.1 ± 151.8
PD-1-040913-11.9	324.8 ± 63.9	242.11 ± 104.86	594.28 ± 46.86	594.9 ± 43.8	339.0 ± 33.8	293.6 ± 63.9	1997.0 ± 166.7	1000.0 ± 97.2

Table C.3: Averaged values of measured wall surface temperature during experiment for each data point (PD-1-040913)

Test ID	TS21T (C)	TS21B (C)	TS22T (C)	TS22B (C)	TS23T (C)	TS23B (C)	TS24T (C)	TS24B (C)	TS25T (C)	TS25B (C)	TS26T (C)	TS26B (C)
PD-1-040913-1.2	35.4	33.8	39.6	34.6	38.1	35.2	39.9	34.9	42.6	35.9	43.4	36.4
PD-1-040913-1.7	37.9	35.7	43.9	36.5	41.9	37.0	43.2	36.4	46.3	37.7	47.4	38.5
PD-1-040913-2.3	41.5	37.8	49.4	39.0	46.4	39.5	47.5	38.6	51.6	40.1	53.6	41.5
PD-1-040913-2.9	46.0	40.5	55.3	41.9	51.2	42.1	52.4	40.7	57.5	42.8	60.5	44.6
PD-1-040913-3.5	51.2	43.5	61.3	45.1	56.6	44.9	58.0	43.0	64.2	45.6	68.3	48.1
PD-1-040913-4.1	57.4	47.2	67.4	48.7	62.8	48.0	64.5	45.5	71.8	48.9	77.6	52.5
PD-1-040913-4.7	64.5	51.7	74.1	52.8	69.6	51.3	71.9	48.5	80.8	52.8	88.6	58.2
PD-1-040913-5.3	71.8	56.5	81.7	56.9	76.6	54.6	79.6	51.4	90.0	56.8	100.1	64.5
PD-1-040913-5.9	79.6	61.9	90.2	61.4	84.0	58.0	87.8	54.5	100.3	61.4	112.8	72.1
PD-1-040913-6.5	87.4	67.6	99.0	66.1	91.3	61.6	96.9	58.1	111.5	67.3	126.3	81.2
PD-1-040913-7.1	96.4	74.5	109.7	71.4	100.8	65.7	107.4	63.0	125.0	75.3	142.4	93.3
PD-1-040913-7.7	105.0	81.1	120.5	76.9	110.0	69.9	118.3	68.1	138.3	83.6	157.8	105.1
PD-1-040913-8.3	112.7	86.7	130.1	81.4	118.1	73.6	127.2	72.1	149.0	90.0	170.0	114.6
PD-1-040913-8.9	122.0	93.8	142.4	87.1	128.4	78.4	139.6	79.1	164.2	101.3	187.5	130.3
PD-1-040913-9.5	131.9	101.4	155.4	93.6	139.1	84.0	153.0	87.7	181.0	114.6	206.4	148.1
PD-1-040913-10.1	141.9	108.9	168.6	100.4	150.2	90.0	166.6	97.3	197.7	128.6	225.2	165.9
PD-1-040913-10.7	151.8	116.6	179.5	106.3	160.8	97.2	181.9	109.5	216.6	145.1	245.7	186.1
PD-1-040913-11.3	160.7	123.7	191.6	113.0	171.6	103.7	195.3	120.1	232.6	158.8	263.0	203.2
PD-1-040913-11.9	166.8	129.4	197.5	116.9	181.7	111.1	209.1	132.2	249.2	173.2	280.5	221.1

Table C.4: Steady-state parameters of the loop (processed data) (PD-1-040913)

Test ID	Power (kW)	Flow rate (kg/s)	Inlet K	Outlet K	Outlet Temp. Calculated (C)	T11(C)	Total Ch. PD (Pa)	Acc. PD.(Pa)	Fr. PD.(Pa)
PD-1-040913-1.2	1.32 ± 0.03	0.031 ± 0.001	0	0	31.8 ± 0.1	32.6 ± 2.2	239.3 ± 13.5	21.0 ± 2.1	218.3 ± 13.7
PD-1-040913-1.7	1.86 ± 0.03	0.037 ± 0.001	0	0	32.0 ± 0.1	33.2 ± 2.2	321.4 ± 17.8	39.4 ± 3.3	282.1 ± 18.1
PD-1-040913-2.3	2.52 ± 0.04	0.041 ± 0.001	0	0	32.2 ± 0.1	33.6 ± 2.2	409.8 ± 20.0	65.8 ± 4.8	344.0 ± 20.6
PD-1-040913-2.9	3.17 ± 0.04	0.044 ± 0.001	0	0	32.3 ± 0.1	33.7 ± 2.2	501.4 ± 23.0	99.6 ± 6.6	401.8 ± 24.0
PD-1-040913-3.5	3.83 ± 0.04	0.047 ± 0.001	0	0	32.3 ± 0.1	33.8 ± 2.2	594.2 ± 25.2	137.9 ± 8.4	456.3 ± 26.6
PD-1-040913-4.1	4.49 ± 0.05	0.049 ± 0.001	0	0	32.6 ± 0.1	34.1 ± 2.2	684.8 ± 28.6	181.6 ± 10.5	503.2 ± 30.5
PD-1-040913-4.7	5.14 ± 0.05	0.050 ± 0.001	0	0	33.2 ± 0.2	34.6 ± 2.2	778.4 ± 35.1	229.9 ± 13.0	548.4 ± 37.5
PD-1-040913-5.3	5.80 ± 0.05	0.051 ± 0.001	0	0	33.9 ± 0.3	35.2 ± 2.2	871.9 ± 39.0	280.8 ± 15.5	591.0 ± 41.9
PD-1-040913-5.9	6.46 ± 0.06	0.052 ± 0.001	0	0	35.0 ± 0.5	36.2 ± 2.2	969.3 ± 43.5	337.2 ± 18.0	632.1 ± 47.1
PD-1-040913-6.5	7.11 ± 0.06	0.053 ± 0.001	0	0	36.9 ± 0.7	37.7 ± 2.2	1061.7 ± 80.5	393.8 ± 20.5	667.9 ± 83.1
PD-1-040913-7.1	7.77 ± 0.06	0.052 ± 0.001	0	0	40.7 ± 1.0	40.6 ± 2.2	1166.9 ± 55.6	459.5 ± 23.5	707.4 ± 60.3
PD-1-040913-7.7	8.43 ± 0.06	0.052 ± 0.001	0	0	45.1 ± 1.4	43.9 ± 2.2	1265.9 ± 63.1	520.8 ± 25.9	745.1 ± 68.2
PD-1-040913-8.3	9.08 ± 0.07	0.053 ± 0.001	0	0	47.9 ± 1.6	46.3 ± 2.2	1352.8 ± 72.6	576.7 ± 28.2	776.1 ± 77.9
PD-1-040913-8.9	9.74 ± 0.07	0.053 ± 0.001	0	0	54.5 ± 2.0	51.1 ± 2.2	1446.5 ± 74.6	638.4 ± 30.5	808.1 ± 80.6
PD-1-040913-9.5	10.39 ± 0.07	0.052 ± 0.001	0	0	63.0 ± 2.5	57.6 ± 2.2	1546.4 ± 81.1	701.9 ± 33.6	844.5 ± 87.7
PD-1-040913-10.1	11.05 ± 0.07	0.052 ± 0.001	0	0	72.3 ± 3.0	63.7 ± 2.3	1636.6 ± 94.3	760.7 ± 36.3	875.9 ± 101.1
PD-1-040913-10.7	11.71 ± 0.08	0.051 ± 0.001	0	0	83.0 ± 3.5	72.1 ± 2.3	1734.1 ± 112.5	819.7 ± 39.1	914.4 ± 119.1
PD-1-040913-11.3	12.37 ± 0.08	0.051 ± 0.001	0	0	92.3 ± 3.7	79.7 ± 2.3	1822.0 ± 10.3	875.4 ± 40.0	946.6 ± 41.4
PD-1-040913-11.9	13.02 ± 0.08	0.051 ± 0.001	0	0	101.3 ± 4.2	86.7 ± 2.5	1922.3 ± 166.7	936.5 ± 44.4	985.8 ± 172.5

Table C.5: Comparison between frictional pressure-drop from the experimental against available friction-factor formulae (PD-1-040913)

Test ID	Fr. PD.(Pa)-Exp.	Blasius	Kondratev	Ishigai	Razumovskiy	Tarasova & Leontev	Yamashita	Popov	Kuraeva & Protopopov
PD-1-040913-1.2	218.3	180.8	148.4	122.7	137.4	147.5	95.8	125.7	301.4
PD-1-040913-1.7	282.1	250.1	204.3	167.0	187.3	203.1	132.2	168.4	400.3
PD-1-040913-2.3	344.0	315.7	257.1	210.3	235.3	257.0	169.8	208.7	492.3
PD-1-040913-2.9	401.8	375.4	304.9	251.8	280.3	308.2	209.0	245.7	575.7
PD-1-040913-3.5	456.3	432.6	350.4	292.6	324.1	358.3	249.3	281.1	655.0
PD-1-040913-4.1	503.2	485.6	392.5	332.7	366.3	406.7	291.7	314.7	729.0
PD-1-040913-4.7	548.4	532.9	430.0	371.3	405.9	452.3	335.4	345.9	795.7
PD-1-040913-5.3	591.0	576.8	464.8	407.4	442.7	495.3	378.0	374.2	857.5
PD-1-040913-5.9	632.1	619.5	498.5	444.6	479.9	538.8	424.3	402.5	918.0
PD-1-040913-6.5	667.9	658.9	529.5	480.0	515.0	579.8	470.0	429.2	973.9
PD-1-040913-7.1	707.4	696.8	559.3	520.8	553.6	624.1	526.8	459.3	1028.7
PD-1-040913-7.7	745.1	732.0	586.9	557.6	588.5	664.4	578.5	486.2	1078.6
PD-1-040913-8.3	776.1	767.4	614.9	588.4	619.1	701.1	620.3	508.3	1127.8
PD-1-040913-8.9	808.1	801.9	642.1	626.7	654.9	742.3	676.7	535.9	1176.6
PD-1-040913-9.5	844.5	837.2	670.0	668.2	693.3	786.0	739.2	565.9	1225.7
PD-1-040913-10.1	875.9	872.3	697.8	708.6	730.7	828.6	799.7	595.4	1273.6
PD-1-040913-10.7	914.4	910.1	727.7	752.1	771.0	874.4	865.3	627.1	1324.4
PD-1-040913-11.3	946.6	947.0	757.0	791.6	807.5	917.2	923.9	656.0	1373.4
PD-1-040913-11.9	985.8	992.4	793.1	838.2	851.3	968.4	991.4	690.5	1433.3

April 10th, 2013- System Pressure: 7.6 MPa, Inlet Temperature: 25-26 ℃, Inlet valve: wide open, Outlet valve: 35° closed

Table C.6: Averaged values of measured signals during experiment for each data point (PD-2-041013)

Test ID	Inlet Temperature (RTD1) (C)	Pressure (MPa)	Power (kW)	Outlet Temp (RTD2)(C)	T11 (C)	T12(C)	CO$_2$ volumetric Flow rate (m^3/s)×10^6	HE-Inlet water Temp.(C)	HE-Outlet water Temp.(C)	Water Flow rate (lpm)
PD-2-041013-1.2	24.9 ± 0.4	7.62 ± 0.02	1.32 ± 0.03	31.1 ± 0.5	32.8 ± 2.2	25.2 ± 2.2	38.8 ± 1.1	11.2 ± 2.2	28.9 ± 2.2	0.9
PD-2-041013-1.7	25.3 ± 0.4	7.61 ± 0.02	1.86 ± 0.03	31.8 ± 0.5	33.3 ± 2.2	25.3 ± 2.2	45.1 ± 1.1	11.1 ± 2.2	28.0 ± 2.2	1.6
PD-2-041013-2.3	25.5 ± 0.4	7.61 ± 0.02	2.52 ± 0.04	32.2 ± 0.5	33.6 ± 2.2	25.1 ± 2.2	50.5 ± 1.1	10.7 ± 2.2	26.3 ± 2.2	2.5
PD-2-041013-3	25.5 ± 0.4	7.61 ± 0.02	3.28 ± 0.04	32.3 ± 0.5	33.9 ± 2.2	25.3 ± 2.2	54.9 ± 1.1	8.6 ± 2.2	24.6 ± 2.2	3.2
PD-2-041013-3.5	25.4 ± 0.4	7.62 ± 0.02	3.83 ± 0.04	32.5 ± 0.5	34.1 ± 2.2	25.0 ± 2.2	57.0 ± 1.1	7.3 ± 2.2	22.6 ± 2.2	3.9
PD-2-041013-4.1	25.6 ± 0.4	7.59 ± 0.02	4.49 ± 0.05	32.6 ± 0.5	34.3 ± 2.2	25.4 ± 2.2	59.4 ± 1.1	6.4 ± 2.2	20.6 ± 2.2	5.2
PD-2-041013-4.7	25.2 ± 0.4	7.60 ± 0.02	5.15 ± 0.05	32.9 ± 0.5	34.9 ± 2.2	24.8 ± 2.2	60.6 ± 1.1	5.7 ± 2.2	18.7 ± 2.2	6.5
PD-2-041013-5.3	25.4 ± 0.4	7.60 ± 0.02	5.80 ± 0.05	33.5 ± 0.5	36.2 ± 2.2	25.2 ± 2.2	61.2 ± 1.1	5.2 ± 2.2	19.8 ± 2.2	6.9
PD-2-041013-5.9	26.3 ± 0.4	7.61 ± 0.02	6.46 ± 0.06	35.4 ± 0.5	39.5 ± 2.2	25.1 ± 2.2	60.9 ± 1.1	4.9 ± 2.2	19.1 ± 2.2	7.8
PD-2-041013-6.5	25.8 ± 0.4	7.60 ± 0.02	7.12 ± 0.06	36.9 ± 0.5	42.0 ± 2.2	24.4 ± 2.2	60.6 ± 1.1	4.5 ± 2.2	17.6 ± 2.2	9.1
PD-2-041013-7.1	26.2 ± 0.4	7.61 ± 0.02	7.77 ± 0.06	40.9 ± 0.5	47.6 ± 2.2	24.7 ± 2.2	59.7 ± 1.1	4.4 ± 2.2	17.8 ± 2.2	9.6
PD-2-041013-7.8	25.3 ± 0.4	7.60 ± 0.02	8.54 ± 0.06	44.3 ± 0.5	51.8 ± 2.2	24.9 ± 2.2	59.1 ± 1.1	4.1 ± 2.2	16.9 ± 2.2	11
PD-2-041013-8.3	25.3 ± 0.4	7.60 ± 0.02	9.09 ± 0.07	49.3 ± 0.5	58.4 ± 2.2	24.8 ± 2.2	58.4 ± 1.1	4.0 ± 2.2	16.4 ± 2.2	12.1
PD-2-041013-8.9	25.8 ± 0.4	7.61 ± 0.02	9.74 ± 0.07	59.9 ± 0.6	69.0 ± 2.3	24.6 ± 2.2	56.8 ± 1.1	4.0 ± 2.2	16.6 ± 2.2	12.4
PD-2-041013-9.5	25.9 ± 0.4	7.60 ± 0.02	10.40 ± 0.07	71.6 ± 0.6	79.1 ± 2.4	24.4 ± 2.2	55.6 ± 1.1	3.9 ± 2.2	16.3 ± 2.2	13.3
PD-2-041013-10.1	25.5 ± 0.4	7.60 ± 0.02	11.06 ± 0.07	80.8 ± 0.7	86.6 ± 2.7	24.1 ± 2.2	54.6 ± 1.1	3.8 ± 2.2	15.5 ± 2.2	14.8
PD-2-041013-10.6	25.2 ± 0.4	7.60 ± 0.02	11.60 ± 0.08	93.4 ± 0.7	94.1 ± 2.6	24.8 ± 2.2	53.9 ± 1.3	3.7 ± 2.2	15.4 ± 2.2	15.3

Table C.7: Averaged values of measured pressure-drops during experiment for each data point (PD-2-041013)

Test ID	DP2-1 (Pa)	DP2-2 (Pa)	DP2-3 (Pa)	DP2-4 (Pa)	DP2-5 (Pa)	DP3 (Pa)	DP13 (Pa)	DP10 (Pa)
PD-2-041013-1.2	104.3 ± 11.5	26.32 ± 11.49	60.38 ± 11.49	30.4 ± 11.3	39.1 ± 11.1	170.7 ± 11.5	233.5 ± 17.8	378.3 ± 126.2
PD-2-041013-1.7	127.0 ± 12.1	35.20 ± 12.09	84.15 ± 12.02	48.5 ± 11.9	48.0 ± 11.5	186.3 ± 12.1	311.1 ± 20.4	520.1 ± 129.1
PD-2-041013-2.3	149.1 ± 12.8	44.58 ± 12.80	111.16 ± 12.78	70.0 ± 12.6	61.8 ± 12.1	203.8 ± 12.8	399.9 ± 23.7	695.1 ± 131.8
PD-2-041013-3	168.2 ± 14.0	55.19 ± 14.04	140.66 ± 13.94	95.7 ± 14.0	80.4 ± 13.0	217.5 ± 14.0	498.8 ± 28.7	897.9 ± 134.2
PD-2-041013-3.5	179.1 ± 15.3	62.16 ± 15.21	159.53 ± 15.08	113.1 ± 14.9	95.7 ± 13.9	228.0 ± 15.3	564.7 ± 32.6	1039.8 ± 141.7
PD-2-041013-4.1	191.0 ± 16.6	72.94 ± 16.56	185.57 ± 15.99	137.8 ± 16.1	115.0 ± 14.7	234.1 ± 16.6	653.3 ± 34.5	1225.4 ± 142.1
PD-2-041013-4.7	200.2 ± 17.8	81.48 ± 17.79	206.70 ± 16.98	161.6 ± 17.6	130.4 ± 15.6	242.3 ± 17.8	727.6 ± 40.7	1378.0 ± 145.7
PD-2-041013-5.3	207.0 ± 19.0	93.23 ± 18.76	230.01 ± 18.33	188.4 ± 18.8	151.1 ± 16.7	243.5 ± 19.0	814.3 ± 46.1	1558.1 ± 147.3
PD-2-041013-5.9	212.1 ± 20.1	108.32 ± 19.77	255.33 ± 18.93	219.1 ± 19.4	169.2 ± 17.0	239.0 ± 20.1	905.6 ± 50.9	1758.0 ± 153.5
PD-2-041013-6.5	216.1 ± 21.4	118.17 ± 21.28	275.89 ± 20.73	245.4 ± 20.8	187.5 ± 18.4	239.8 ± 21.4	982.5 ± 56.5	1927.8 ± 156.7
PD-2-041013-7.1	218.3 ± 22.3	131.43 ± 22.08	299.49 ± 21.44	274.4 ± 21.3	207.3 ± 19.2	235.0 ± 22.3	1067.6 ± 61.7	2077.9 ± 157.6
PD-2-041013-7.8	221.3 ± 25.1	141.49 ± 23.93	323.00 ± 22.99	305.1 ± 22.5	226.5 ± 20.3	235.0 ± 25.1	1151.9 ± 72.6	2229.2 ± 162.3
PD-2-041013-8.3	222.9 ± 26.3	150.53 ± 25.36	341.93 ± 24.02	327.0 ± 24.3	241.4 ± 21.3	230.4 ± 26.3	1216.8 ± 81.4	2351.3 ± 161.9
PD-2-041013-8.9	223.4 ± 27.7	162.47 ± 26.43	367.85 ± 24.64	353.6 ± 24.7	251.4 ± 21.8	222.4 ± 27.7	1290.0 ± 85.8	2471.2 ± 148.5
PD-2-041013-9.5	224.2 ± 30.4	173.38 ± 29.48	395.24 ± 27.25	379.0 ± 26.5	258.6 ± 23.8	215.1 ± 30.4	1359.8 ± 97.5	2614.9 ± 172.1
PD-2-041013-10.1	225.3 ± 32.4	181.78 ± 31.58	420.42 ± 29.25	403.8 ± 27.1	266.6 ± 25.2	213.7 ± 32.4	1425.4 ± 103.1	2733.0 ± 171.2
PD-2-041013-10.6	237.2 ± 53.1	185.85 ± 98.38	448.25 ± 43.16	434.7 ± 41.7	269.6 ± 33.8	215.8 ± 53.1	1500.0 ± 153.8	2845.0 ± 98.6

Table C.8: Averaged values of measured wall surface temperature during experiment for each data point (PD-2-041013)

Test ID	TS21T (C)	TS21B (C)	TS22T (C)	TS22B (C)	TS23T (C)	TS23B (C)	TS24T (C)	TS24B (C)	TS25T (C)	TS25B (C)	TS26T (C)	TS26B (C)
PD-2-041013-1.2	35.6	34.0	40.3	34.8	39.2	35.2	41.3	34.9	43.7	36.1	44.4	36.7
PD-2-041013-1.7	38.5	36.1	45.4	36.8	44.0	37.2	45.7	36.7	48.5	38.1	49.3	39.0
PD-2-041013-2.3	42.8	38.5	51.8	39.6	49.2	39.9	50.5	39.1	54.4	40.8	56.1	42.3
PD-2-041013-3	49.0	42.0	59.8	43.3	56.0	43.1	57.2	41.9	62.5	44.2	65.6	46.4
PD-2-041013-3.5	54.1	44.9	66.0	46.3	61.4	45.7	62.9	44.1	69.1	46.9	73.4	50.0
PD-2-041013-4.1	61.9	49.5	74.0	50.5	68.5	49.0	70.3	46.9	77.9	50.7	84.1	55.4
PD-2-041013-4.7	69.3	54.1	82.3	54.8	76.1	52.4	78.6	49.9	87.4	54.7	95.5	61.5
PD-2-041013-5.3	78.6	60.5	92.3	60.1	84.9	56.4	88.1	53.7	99.2	60.4	110.5	70.8
PD-2-041013-5.9	89.4	68.6	105.0	66.7	95.3	61.1	100.2	59.0	114.4	69.2	130.0	85.0
PD-2-041013-6.5	98.2	75.1	116.4	72.2	104.7	65.3	110.6	63.5	127.0	76.5	145.0	95.6
PD-2-041013-7.1	108.9	83.2	130.6	79.0	116.3	70.8	124.3	70.9	144.7	88.8	166.3	113.8
PD-2-041013-7.8	120.0	91.3	144.9	86.5	128.1	76.3	137.7	77.8	161.0	100.1	185.3	129.7
PD-2-041013-8.3	129.0	98.1	157.0	92.7	138.3	81.5	150.0	85.6	176.6	112.6	203.7	146.3
PD-2-041013-8.9	141.4	107.6	173.8	101.6	152.7	89.9	168.5	99.6	200.5	133.6	231.2	172.9
PD-2-041013-9.5	153.4	116.9	189.8	110.5	166.8	98.8	186.9	114.5	223.6	154.3	257.3	198.7
PD-2-041013-10.1	164.3	125.3	204.0	119.4	179.2	106.8	202.2	126.8	242.5	170.4	277.7	218.9
PD-2-041013-10.6	170.6	133.4	204.7	120.2	188.1	114.7	217.0	139.6	260.4	186.2	296.6	238.2

Table C.9: Steady-state parameters of the loop (processed data) (PD-2-041013)

Test ID	Power (kW)	Flow rate (kg/s)	Inlet K	Outlet K*	Outlet Temp. Calculated (C)	T11(C)	Total Ch. PD (Pa)	Acc. PD.(Pa)	Fr. PD.(Pa)
PD-2-041013-1.2	1.32 ± 0.03	0.030 ± 0.001	0	8.8	31.9 ± 0.1	32.8 ± 2.2	223.1 ± 17.8	20.6 ± 2.0	202.6 ± 17.9
PD-2-041013-1.7	1.86 ± 0.03	0.034 ± 0.001	0	8.7	32.2 ± 0.1	33.3 ± 2.2	296.7 ± 20.4	38.6 ± 3.3	258.1 ± 20.7
PD-2-041013-2.3	2.52 ± 0.04	0.038 ± 0.001	0	8.9	32.3 ± 0.1	33.6 ± 2.2	381.1 ± 23.7	65.8 ± 4.9	315.3 ± 24.2
PD-2-041013-3	3.28 ± 0.04	0.041 ± 0.001	0	9.1	32.4 ± 0.1	33.9 ± 2.2	475.3 ± 28.7	103.4 ± 6.9	371.9 ± 29.5
PD-2-041013-3.5	3.83 ± 0.04	0.043 ± 0.001	0	9.3	32.7 ± 0.1	34.1 ± 2.2	538.2 ± 32.6	132.7 ± 8.4	405.6 ± 33.7
PD-2-041013-4.1	4.49 ± 0.05	0.045 ± 0.001	0	9.3	32.9 ± 0.2	34.3 ± 2.2	623.1 ± 34.5	176.3 ± 10.7	446.8 ± 36.2
PD-2-041013-4.7	5.15 ± 0.05	0.046 ± 0.001	0	9.3	33.5 ± 0.3	34.9 ± 2.2	694.3 ± 40.7	216.8 ± 12.4	477.5 ± 42.5
PD-2-041013-5.3	5.80 ± 0.05	0.046 ± 0.001	0	9.4	35.1 ± 0.5	36.2 ± 2.2	778.1 ± 46.1	266.7 ± 15.1	511.5 ± 48.5
PD-2-041013-5.9	6.46 ± 0.06	0.045 ± 0.001	0	9.5	39.3 ± 1.0	39.5 ± 2.2	867.2 ± 50.9	323.9 ± 18.6	543.3 ± 54.2
PD-2-041013-6.5	7.12 ± 0.06	0.046 ± 0.001	0	9.6	42.7 ± 1.3	42.0 ± 2.2	941.7 ± 56.5	371.9 ± 20.8	569.7 ± 60.2
PD-2-041013-7.1	7.77 ± 0.06	0.045 ± 0.001	0	9.4	50.5 ± 1.9	47.6 ± 2.2	1024.8 ± 61.7	425.3 ± 23.6	599.6 ± 66.1
PD-2-041013-7.8	8.54 ± 0.06	0.045 ± 0.001	0	9.2	56.8 ± 2.4	51.8 ± 2.2	1106.5 ± 72.6	480.7 ± 25.9	625.8 ± 77.1
PD-2-041013-8.3	9.09 ± 0.07	0.044 ± 0.001	0	9.1	65.0 ± 2.9	58.4 ± 2.2	1169.9 ± 81.4	521.5 ± 27.8	648.3 ± 86.0
PD-2-041013-8.9	9.74 ± 0.07	0.043 ± 0.001	0	9.0	81.3 ± 3.8	69.0 ± 2.3	1242.2 ± 85.8	566.0 ± 30.3	676.1 ± 91.0
PD-2-041013-9.5	10.40 ± 0.07	0.042 ± 0.001	0	9.0	96.9 ± 4.5	79.1 ± 2.4	1310.7 ± 97.5	608.6 ± 32.0	702.1 ± 102.6
PD-2-041013-10.1	11.06 ± 0.07	0.041 ± 0.001	0	8.9	109.9 ± 5.0	86.6 ± 2.7	1374.8 ± 103.1	648.1 ± 34.2	726.8 ± 108.6
PD-2-041013-10.6	11.60 ± 0.08	0.041 ± 0.001	0	8.8	121.3 ± 6.4	94.1 ± 2.6	1448.1 ± 153.8	681.2 ± 42.4	766.9 ± 159.6

* Mean outlet K factor: 9.1

Table C.10: Comparison between frictional pressure-drop from the experimental against available friction-factor formulae (PD-2-041013)

Test ID	Fr. PD.(Pa)-Exp.	Blasius	Kondratev	Ishigai	Razumovskiy	Tarasova & Leontev	Yamashita	Popov	Kuraeva & Protopopov
PD-2-041013-1.2	202.6	168.2	138.1	113.7	127.5	137.2	88.9	116.1	282.9
PD-2-041013-1.7	258.1	224.7	183.8	150.5	168.6	183.2	120.2	150.9	364.9
PD-2-041013-2.3	315.3	284.5	231.8	191.1	213.1	233.4	157.0	188.1	450.4
PD-2-041013-3	371.9	344.9	280.1	233.6	259.0	285.8	198.2	225.4	536.0
PD-2-041013-3.5	405.6	382.2	309.9	260.8	287.9	319.1	226.2	248.3	588.9
PD-2-041013-4.1	446.8	427.9	346.1	297.2	325.4	362.4	266.8	277.8	654.4
PD-2-041013-4.7	477.5	464.9	375.6	325.4	354.9	397.2	299.1	300.0	707.0
PD-2-041013-5.3	511.5	498.4	402.0	357.0	385.8	433.1	340.1	323.6	756.5
PD-2-041013-5.9	543.3	524.4	422.3	390.0	415.8	467.1	388.7	347.2	796.8
PD-2-041013-6.5	569.7	552.2	444.3	416.3	441.3	497.3	425.1	366.0	837.0
PD-2-041013-7.1	599.6	576.5	463.4	447.6	469.6	529.3	472.9	388.3	873.0
PD-2-041013-7.8	625.8	608.3	488.6	478.4	499.3	564.5	517.3	410.1	918.4
PD-2-041013-8.3	648.3	629.8	505.7	504.1	522.9	591.5	556.7	428.4	949.1
PD-2-041013-8.9	676.1	651.3	522.8	536.8	551.5	622.6	609.1	452.3	978.3
PD-2-041013-9.5	702.1	677.2	543.4	569.7	580.6	655.9	660.2	476.4	1012.7
PD-2-041013-10.1	726.8	702.1	563.4	598.1	606.5	685.7	702.7	497.6	1045.1
PD-2-041013-10.6	766.9	725.6	582.3	624.3	630.6	713.2	741.4	517.4	1075.8

April 11th, 2013- System Pressure: 7.6 MPa, Inlet Temperature: 25-26 ℃, Inlet valve: wide open, Outlet valve: 40º closed

Table C.11: Averaged values of measured signals during experiment for each data point (PD-3-041113)

Test ID	Inlet Temperature (RTD1) (C)	Pressure (MPa)	Power (kW)	Outlet Temp (RTD2)(C)	T11 (C)	T12(C)	CO_2 volumetric Flow rate $(m^3/s) \times 10^6$	HE-Inlet water Temp.(C)	HE-Outlet water Temp.(C)	Water Flow rate (lpm)
PD-3-041113-1.2	25.0 ± 0.4	7.59 ± 0.02	1.32 ± 0.03	31.0 ± 0.5	32.8 ± 2.2	25.1 ± 2.2	35.9 ± 1.8	10.5 ± 2.2	29.1 ± 2.2	0.9
PD-3-041113-1.7	24.9 ± 0.4	7.60 ± 0.02	1.86 ± 0.03	31.6 ± 0.5	33.2 ± 2.2	25.2 ± 2.2	42.5 ± 1.1	10.5 ± 2.2	27.8 ± 2.2	1.5
PD-3-041113-2.3	25.1 ± 0.4	7.60 ± 0.02	2.52 ± 0.03	32.1 ± 0.5	33.5 ± 2.2	25.1 ± 2.2	47.4 ± 1.1	10.0 ± 2.2	26.4 ± 2.2	2.2
PD-3-041113-2.9	25.4 ± 0.4	7.60 ± 0.02	3.17 ± 0.04	32.2 ± 0.5	33.7 ± 2.2	25.2 ± 2.2	50.8 ± 1.1	9.8 ± 2.2	24.5 ± 2.2	3.4
PD-3-041113-3.5	25.4 ± 0.4	7.60 ± 0.02	3.83 ± 0.04	32.4 ± 0.5	34.0 ± 2.2	24.8 ± 2.2	53.2 ± 1.1	7.3 ± 2.2	21.9 ± 2.2	4.2
PD-3-041113-4.1	25.8 ± 0.4	7.62 ± 0.02	4.49 ± 0.05	32.8 ± 0.5	34.8 ± 2.2	24.9 ± 2.2	54.6 ± 1.1	6.2 ± 2.2	20.1 ± 2.2	5.2
PD-3-041113-4.7	26.0 ± 0.4	7.61 ± 0.02	5.14 ± 0.05	33.6 ± 0.5	36.2 ± 2.2	25.1 ± 2.2	55.1 ± 1.1	5.6 ± 2.2	19.8 ± 2.2	5.9
PD-3-041113-5.4	26.2 ± 0.4	7.62 ± 0.02	5.91 ± 0.05	35.6 ± 0.5	39.6 ± 2.2	25.2 ± 2.2	54.5 ± 1.1	5.1 ± 2.2	19.5 ± 2.2	7.2
PD-3-041113-5.9	26.0 ± 0.4	7.61 ± 0.02	6.46 ± 0.06	37.6 ± 0.5	42.9 ± 2.2	25.0 ± 2.2	53.8 ± 1.1	4.8 ± 2.2	17.6 ± 2.2	8.6
PD-3-041113-6.5	26.0 ± 0.4	7.61 ± 0.02	7.12 ± 0.06	42.0 ± 0.5	48.7 ± 2.2	25.0 ± 2.2	52.7 ± 1.1	4.6 ± 2.2	17.2 ± 2.2	9.2
PD-3-041113-7.1	26.0 ± 0.4	7.61 ± 0.02	7.77 ± 0.06	48.3 ± 0.5	56.0 ± 2.2	25.0 ± 2.2	51.7 ± 1.1	4.5 ± 2.2	16.8 ± 2.2	10.2
PD-3-041113-7.7	26.0 ± 0.4	7.61 ± 0.02	8.43 ± 0.06	57.5 ± 0.6	65.5 ± 2.3	25.1 ± 2.2	50.3 ± 1.1	4.3 ± 2.2	16.5 ± 2.2	11
PD-3-041113-8.3	25.8 ± 0.4	7.60 ± 0.02	9.09 ± 0.07	68.2 ± 0.6	77.6 ± 2.2	24.8 ± 2.2	49.1 ± 1.1	4.1 ± 2.2	16.2 ± 2.2	12
PD-3-041113-8.9	25.8 ± 0.4	7.62 ± 0.02	9.74 ± 0.07	82.7 ± 0.7	86.2 ± 2.5	24.9 ± 2.2	47.9 ± 1.1	4.1 ± 2.2	16.1 ± 2.2	12.3

172

Table C.12: Averaged values of measured pressure-drops during experiment for each data point (PD-3-041113)

Test ID	DP2-1 (Pa)	DP2-2 (Pa)	DP2-3 (Pa)	DP2-4 (Pa)	DP2-5 (Pa)	DP3 (Pa)	DP13 (Pa)	DP10 (Pa)
PD-3-041113-1.2	97.4 ± 12.5	24.55 ± 12.75	53.37 ± 12.83	27.3 ± 11.8	40.4 ± 11.9	174.2 ± 12.5	251.9 ± 27.5	672.6 ± 127.6
PD-3-041113-1.7	117.6 ± 12.5	32.27 ± 12.53	74.13 ± 12.44	42.0 ± 12.0	48.0 ± 11.8	190.9 ± 12.5	319.5 ± 22.9	880.0 ± 135.1
PD-3-041113-2.3	136.6 ± 13.5	41.08 ± 13.60	98.39 ± 13.43	61.2 ± 13.0	62.0 ± 12.5	204.2 ± 13.5	400.9 ± 28.1	1152.4 ± 138.4
PD-3-041113-2.9	150.8 ± 14.7	50.07 ± 14.75	122.26 ± 14.36	80.9 ± 13.9	77.5 ± 13.2	213.7 ± 14.7	480.1 ± 33.5	1428.8 ± 146.1
PD-3-041113-3.5	162.0 ± 16.2	59.00 ± 16.11	144.49 ± 15.47	101.0 ± 15.1	94.6 ± 14.2	222.1 ± 16.2	556.5 ± 38.0	1692.8 ± 177.4
PD-3-041113-4.1	169.5 ± 17.3	68.98 ± 17.62	165.97 ± 17.08	122.5 ± 16.3	113.3 ± 15.3	224.8 ± 17.3	633.4 ± 42.7	1922.3 ± 164.1
PD-3-041113-4.7	174.6 ± 18.7	79.80 ± 18.61	186.62 ± 18.37	145.2 ± 17.4	133.6 ± 16.3	229.9 ± 18.7	710.0 ± 48.3	2193.1 ± 161.1
PD-3-041113-5.4	178.6 ± 20.0	92.62 ± 19.82	209.05 ± 19.39	174.7 ± 17.7	150.2 ± 17.2	228.2 ± 20.0	791.8 ± 51.1	2504.8 ± 231.4
PD-3-041113-5.9	179.9 ± 21.4	102.24 ± 21.46	224.81 ± 20.79	194.9 ± 19.4	168.5 ± 18.1	224.1 ± 21.4	855.2 ± 58.0	2708.1 ± 169.0
PD-3-041113-6.5	180.9 ± 22.8	113.21 ± 22.74	243.87 ± 21.96	218.8 ± 20.1	185.2 ± 18.9	219.9 ± 22.8	925.4 ± 63.4	2929.6 ± 175.7
PD-3-041113-7.1	181.7 ± 25.7	123.13 ± 24.95	264.06 ± 23.18	241.6 ± 20.7	199.9 ± 19.6	215.9 ± 25.7	992.3 ± 75.2	3129.2 ± 181.4
PD-3-041113-7.7	182.1 ± 27.3	132.47 ± 26.44	286.19 ± 24.46	264.7 ± 22.3	210.6 ± 20.8	209.6 ± 27.3	1056.6 ± 81.3	3289.5 ± 185.2
PD-3-041113-8.3	182.7 ± 29.3	140.42 ± 29.25	309.38 ± 27.48	288.6 ± 23.6	217.1 ± 22.7	205.7 ± 29.3	1117.4 ± 93.7	3463.3 ± 194.6
PD-3-041113-8.9	178.4 ± 37.5	148.82 ± 51.64	334.12 ± 55.38	311.9 ± 32.3	227.8 ± 36.6	205.4 ± 37.5	1179.9 ± 151.9	3582.2 ± 120.6

Table C.13: Averaged values of measured wall surface temperature during experiment for each data point (PD-3-041113)

Test ID	TS21T (C)	TS21B (C)	TS22T (C)	TS22B (C)	TS23T (C)	TS23B (C)	TS24T (C)	TS24B (C)	TS25T (C)	TS25B (C)	TS26T (C)	TS26B (C)
PD-3-041113-1.2	35.7	34.1	41.2	35.0	40.5	35.2	42.3	34.8	45.2	36.0	45.7	36.5
PD-3-041113-1.7	38.9	35.9	46.6	37.1	45.6	37.3	47.6	36.7	51.1	38.2	51.2	39.0
PD-3-041113-2.3	43.7	38.6	53.9	40.3	51.9	40.2	53.4	39.3	57.6	41.2	58.3	42.2
PD-3-041113-2.9	50.2	42.1	62.0	44.0	58.5	43.4	59.7	41.9	65.1	44.4	67.2	46.1
PD-3-041113-3.5	57.5	46.2	70.8	48.4	65.8	46.8	67.2	44.9	73.9	48.1	77.8	51.0
PD-3-041113-4.1	66.7	51.8	81.3	53.8	74.5	50.8	76.4	48.5	84.7	53.0	91.1	58.2
PD-3-041113-4.7	76.5	58.4	92.7	59.7	83.7	55.1	86.4	52.5	97.1	59.0	106.6	67.8
PD-3-041113-5.4	88.6	67.0	107.8	67.5	96.1	60.8	100.2	58.5	114.2	68.9	128.6	83.2
PD-3-041113-5.9	97.1	73.6	118.8	73.3	105.2	65.0	110.6	63.3	127.1	76.9	144.7	95.2
PD-3-041113-6.5	107.9	82.0	133.1	81.0	117.5	70.9	125.0	71.1	145.5	90.0	167.1	114.4
PD-3-041113-7.1	119.1	90.7	147.9	89.2	130.5	77.3	140.7	80.7	165.5	105.9	191.2	135.9
PD-3-041113-7.7	130.9	99.9	163.5	98.1	144.4	85.0	158.1	93.1	188.3	125.2	218.2	162.1
PD-3-041113-8.3	142.6	107.8	178.7	106.6	158.3	93.3	175.8	106.7	210.9	145.0	244.4	186.8
PD-3-041113-8.9	154.0	117.0	193.5	116.0	172.2	103.9	196.0	124.0	236.7	168.4	273.6	215.9

Table C.14: Steady-state parameters of the loop (processed data) (PD-3-041113)

Test ID	Power (kW)	Flow rate (kg/s)	Inlet K	Outlet K*	Outlet Temp. Calculated (C)	T11(C)	Total Ch. PD (Pa)	Acc. PD.(Pa)	Fr. PD.(Pa)
PD-3-041113-1.2	1.32 ± 0.03	0.027 ± 0.001	0	25.6	31.9 ± 0.1	32.8 ± 2.2	243.0 ± 27.5	20.1 ± 2.8	223.0 ± 27.7
PD-3-041113-1.7	1.86 ± 0.03	0.032 ± 0.001	0	21.9	32.2 ± 0.1	33.2 ± 2.2	306.5 ± 22.9	36.9 ± 3.2	269.6 ± 23.1
PD-3-041113-2.3	2.52 ± 0.03	0.036 ± 0.001	0	21.1	32.3 ± 0.1	33.5 ± 2.2	384.0 ± 28.1	62.9 ± 4.8	321.1 ± 28.5
PD-3-041113-2.9	3.17 ± 0.04	0.038 ± 0.001	0	20.7	32.4 ± 0.1	33.7 ± 2.2	459.6 ± 33.5	94.7 ± 6.6	364.9 ± 34.1
PD-3-041113-3.5	3.83 ± 0.04	0.040 ± 0.001	0	20.3	32.7 ± 0.2	34.0 ± 2.2	532.8 ± 38.0	129.7 ± 8.6	403.0 ± 39.0
PD-3-041113-4.1	4.49 ± 0.05	0.041 ± 0.001	0	19.6	33.6 ± 0.3	34.8 ± 2.2	606.9 ± 42.7	170.2 ± 10.9	436.7 ± 44.1
PD-3-041113-4.7	5.14 ± 0.05	0.041 ± 0.001	0	19.5	35.4 ± 0.5	36.2 ± 2.2	681.0 ± 48.3	214.4 ± 13.1	466.5 ± 50.1
PD-3-041113-5.4	5.91 ± 0.05	0.041 ± 0.001	0	19.7	40.0 ± 1.1	39.6 ± 2.2	760.6 ± 51.1	267.2 ± 15.8	493.4 ± 53.5
PD-3-041113-5.9	6.46 ± 0.06	0.040 ± 0.001	0	19.6	44.6 ± 1.5	42.9 ± 2.2	822.5 ± 58.0	304.6 ± 17.9	517.9 ± 60.7
PD-3-041113-6.5	7.12 ± 0.06	0.039 ± 0.001	0	19.4	53.0 ± 2.3	48.7 ± 2.2	891.2 ± 63.4	348.9 ± 20.5	542.3 ± 66.6
PD-3-041113-7.1	7.77 ± 0.06	0.039 ± 0.001	0	19.0	63.9 ± 3.0	56.0 ± 2.2	956.6 ± 75.2	392.1 ± 22.7	564.5 ± 78.6
PD-3-041113-7.7	8.43 ± 0.06	0.038 ± 0.001	0	18.6	78.5 ± 3.9	65.5 ± 2.3	1019.7 ± 81.3	431.6 ± 24.7	588.1 ± 85.0
PD-3-041113-8.3	9.09 ± 0.07	0.037 ± 0.001	0	18.4	94.3 ± 4.7	77.6 ± 2.2	1079.3 ± 93.7	468.6 ± 26.6	610.7 ± 97.5
PD-3-041113-8.9	9.74 ± 0.07	0.036 ± 0.001	0	18.0	113.4 ± 5.6	86.2 ± 2.5	1141.0 ± 151.9	500.2 ± 28.6	640.9 ± 154.6

* Mean outlet K factor: 20.1

Table C.15: Comparison between frictional pressure-drop from the experimental against available friction-factor formulae (PD-3-041113)

Test ID	Fr. PD.(Pa)-Exp.	Blasius	Kondratev	Ishigai	Razumovskiy	Tarasova & Leontev	Yamashita	Popov	Kuraeva & Protopopov
PD-3-041113-1.2	223.0	146.9	120.7	99.3	111.4	120.2	78.3	100.9	251.3
PD-3-041113-1.7	269.6	205.0	167.8	136.7	153.3	167.1	109.3	136.6	336.5
PD-3-041113-2.3	321.1	258.5	210.8	173.0	193.1	212.2	142.7	169.4	414.0
PD-3-041113-2.9	364.9	304.3	247.4	206.6	228.8	253.0	176.6	198.3	480.5
PD-3-041113-3.5	403.0	345.3	280.1	237.8	261.5	290.7	210.0	224.2	540.0
PD-3-041113-4.1	436.7	379.7	307.5	267.3	291.3	325.2	245.4	247.3	591.1
PD-3-041113-4.7	466.5	409.5	330.9	295.6	318.9	357.1	282.1	268.5	635.7
PD-3-041113-5.4	493.4	434.5	350.6	324.1	345.4	387.8	323.7	288.7	674.2
PD-3-041113-5.9	517.9	452.4	364.7	344.4	364.2	409.5	353.6	303.0	701.0
PD-3-041113-6.5	542.3	472.5	380.6	369.5	387.0	435.5	392.0	320.7	731.0
PD-3-041113-7.1	564.5	494.3	397.9	396.3	411.4	463.2	433.0	340.0	762.5
PD-3-041113-7.7	588.1	514.5	414.0	423.0	435.5	490.0	474.8	359.4	790.7
PD-3-041113-8.3	610.7	536.3	431.5	450.2	459.7	517.4	515.9	379.6	820.0
PD-3-041113-8.9	640.9	557.3	448.4	476.9	483.5	544.1	556.5	399.9	847.2

April 12th, 2013- System Pressure: 7.6 MPa, Inlet Temperature: 25-26 ℃, Inlet valve: wide open, Outlet valve: 30º closed

Table C.16: Averaged values of measured signals during experiment for each data point (PD-4-041213)

Test ID	Inlet Temperature (RTD1) (C)	Pressure (MPa)	Power (kW)	Outlet Temp (RTD2)(C)	T11 (C)	T12(C)	CO_2 volumetric Flow rate $(m^3/s) \times 10^6$	HE-Inlet water Temp.(C)	HE-Outlet water Temp.(C)	Water Flow rate (lpm)
PD-4-041213-1.25	25.0 ± 0.4	7.62 ± 0.02	1.37 ± 0.03	30.9 ± 0.5	32.6 ± 2.2	25.4 ± 2.2	40.7 ± 1.0	10.4 ± 2.2	29.1 ± 2.2	0.9
PD-4-041213-1.7	25.1 ± 0.4	7.59 ± 0.02	1.86 ± 0.03	31.3 ± 0.5	32.8 ± 2.2	25.2 ± 2.2	46.4 ± 1.1	10.6 ± 2.2	28.0 ± 2.2	1.5
PD-4-041213-2.3	25.4 ± 0.4	7.61 ± 0.02	2.52 ± 0.03	31.7 ± 0.5	33.2 ± 2.2	25.2 ± 2.2	52.0 ± 1.1	10.4 ± 2.2	26.7 ± 2.2	2.3
PD-4-041213-2.9	25.7 ± 0.4	7.60 ± 0.02	3.17 ± 0.04	31.9 ± 0.5	33.3 ± 2.2	25.4 ± 2.2	56.3 ± 1.1	8.9 ± 2.2	24.7 ± 2.2	3.1
PD-4-041213-3.5	25.5 ± 0.4	7.61 ± 0.02	3.83 ± 0.04	32.1 ± 0.5	33.6 ± 2.2	25.2 ± 2.2	59.3 ± 1.1	7.5 ± 2.2	22.1 ± 2.2	4.2
PD-4-041213-4.1	25.5 ± 0.4	7.60 ± 0.02	4.49 ± 0.05	32.2 ± 0.5	33.9 ± 2.2	25.2 ± 2.2	61.7 ± 1.1	6.6 ± 2.2	20.2 ± 2.2	5.4
PD-4-041213-4.6	25.4 ± 0.4	7.60 ± 0.02	5.03 ± 0.05	32.5 ± 0.5	34.4 ± 2.2	25.1 ± 2.2	63.1 ± 1.1	6.0 ± 2.2	19.7 ± 2.2	6.1
PD-4-041213-5.3	25.5 ± 0.4	7.61 ± 0.02	5.80 ± 0.05	33.1 ± 0.5	35.6 ± 2.2	25.1 ± 2.2	64.3 ± 1.0	5.5 ± 2.2	20.1 ± 2.2	6.9
PD-4-041213-5.8	26.1 ± 0.4	7.62 ± 0.02	6.35 ± 0.06	34.2 ± 0.5	37.5 ± 2.2	25.2 ± 2.2	64.5 ± 1.1	5.0 ± 2.2	19.2 ± 2.2	7.6
PD-4-041213-6.5	25.5 ± 0.4	7.61 ± 0.02	7.11 ± 0.06	35.5 ± 0.5	39.9 ± 2.2	25.1 ± 2.2	64.7 ± 1.1	4.7 ± 2.2	17.9 ± 2.2	8.9
PD-4-041213-7.1	25.6 ± 0.4	7.61 ± 0.02	7.77 ± 0.06	37.9 ± 0.5	43.4 ± 2.2	25.2 ± 2.2	64.4 ± 1.1	4.6 ± 2.2	17.7 ± 2.2	9.7
PD-4-041213-7.7	25.7 ± 0.4	7.61 ± 0.02	8.43 ± 0.06	41.4 ± 0.5	48.0 ± 2.2	25.2 ± 2.2	63.9 ± 1.1	4.5 ± 2.2	17.8 ± 2.2	10.3
PD-4-041213-8.3	25.6 ± 0.4	7.60 ± 0.02	9.08 ± 0.07	45.8 ± 0.5	53.9 ± 2.2	24.7 ± 2.2	63.2 ± 1.1	4.3 ± 2.2	17.1 ± 2.2	11.6
PD-4-041213-8.9	25.7 ± 0.4	7.61 ± 0.02	9.74 ± 0.07	52.2 ± 0.5	60.3 ± 2.3	25.1 ± 2.2	62.4 ± 1.1	4.2 ± 2.2	16.8 ± 2.2	12.4
PD-4-041213-9.5	25.7 ± 0.4	7.62 ± 0.02	10.39 ± 0.07	59.9 ± 0.6	67.4 ± 2.4	25.1 ± 2.2	61.5 ± 1.1	4.1 ± 2.2	16.8 ± 2.2	12.9
PD-4-041213-10.1	25.4 ± 0.4	7.61 ± 0.02	11.05 ± 0.07	69.1 ± 0.6	77.1 ± 2.3	25.0 ± 2.2	60.7 ± 1.1	4.0 ± 2.2	16.2 ± 2.2	14.4
PD-4-041213-10.7	25.4 ± 0.4	7.61 ± 0.02	11.71 ± 0.08	79.9 ± 0.7	87.4 ± 2.4	24.9 ± 2.2	60.0 ± 1.2	4.1 ± 2.2	16.4 ± 2.2	14.9
PD-4-041213-11.3	25.4 ± 0.4	7.62 ± 0.02	12.36 ± 0.08	91.1 ± 0.7	96.9 ± 2.4	25.1 ± 2.2	58.9 ± 1.3	4.0 ± 2.2	15.9 ± 2.2	16.1
PD-4-041213-11.9	25.1 ± 0.4	7.61 ± 0.02	13.02 ± 0.08	103.0 ± 0.7	104.4 ± 2.5	24.6 ± 2.2	58.1 ± 1.3	3.9 ± 2.2	15.1 ± 2.2	18

Table C.17: Averaged values of measured pressure-drops during experiment for each data point (PD-4-041213)

Test ID	DP2-1 (Pa)	DP2-2 (Pa)	DP2-3 (Pa)	DP2-4 (Pa)	DP2-5 (Pa)	DP3 (Pa)	DP13 (Pa)	DP10 (Pa)
PD-4-041213-1.25	107.8 ± 11.4	28.16 ± 11.41	67.02 ± 11.40	36.4 ± 11.4	38.5 ± 11.0	170.6 ± 11.4	252.6 ± 15.0	283.5 ± 135.2
PD-4-041213-1.7	128.8 ± 12.4	36.04 ± 12.32	89.52 ± 12.40	53.4 ± 12.3	46.7 ± 11.8	184.3 ± 12.4	325.4 ± 27.6	374.1 ± 136.1
PD-4-041213-2.3	152.2 ± 12.6	45.63 ± 12.58	118.12 ± 12.51	75.6 ± 12.8	61.2 ± 11.9	203.5 ± 12.6	419.1 ± 22.1	503.5 ± 132.7
PD-4-041213-2.9	171.6 ± 13.5	55.91 ± 13.54	146.46 ± 13.36	99.6 ± 13.7	77.2 ± 12.6	217.2 ± 13.5	512.8 ± 25.2	649.8 ± 142.3
PD-4-041213-3.5	186.5 ± 14.6	65.01 ± 14.75	171.07 ± 14.53	122.5 ± 15.2	93.1 ± 13.5	228.8 ± 14.6	596.6 ± 29.4	772.6 ± 134.1
PD-4-041213-4.1	199.9 ± 15.8	75.81 ± 15.67	197.85 ± 15.22	148.1 ± 16.4	111.0 ± 14.3	236.2 ± 15.8	687.8 ± 33.8	905.3 ± 136.6
PD-4-041213-4.6	209.0 ± 16.8	84.07 ± 16.66	217.75 ± 16.28	169.1 ± 17.6	128.0 ± 15.1	242.5 ± 16.8	760.1 ± 37.3	1002.7 ± 140.3
PD-4-041213-5.3	219.6 ± 18.3	97.08 ± 18.05	246.18 ± 17.20	201.0 ± 18.7	149.0 ± 15.9	248.1 ± 18.3	862.1 ± 42.6	1143.4 ± 141.0
PD-4-041213-5.8	225.5 ± 19.0	108.92 ± 18.72	267.91 ± 17.96	227.4 ± 19.4	166.5 ± 16.8	246.1 ± 19.0	942.4 ± 46.3	1265.7 ± 163.8
PD-4-041213-6.5	232.9 ± 20.8	120.80 ± 20.32	294.05 ± 19.89	259.7 ± 20.7	186.4 ± 18.3	248.3 ± 20.8	1037.5 ± 54.0	1399.5 ± 145.9
PD-4-041213-7.1	237.8 ± 21.7	133.74 ± 20.93	319.19 ± 20.50	289.9 ± 21.6	208.3 ± 18.8	246.9 ± 21.7	1130.3 ± 61.4	1508.7 ± 148.4
PD-4-041213-7.7	241.4 ± 23.3	145.94 ± 22.70	343.70 ± 21.51	319.6 ± 24.0	228.4 ± 19.7	244.0 ± 23.3	1218.1 ± 68.1	1616.7 ± 158.8
PD-4-041213-8.3	245.1 ± 24.9	157.89 ± 23.91	369.24 ± 23.04	350.3 ± 24.5	246.1 ± 21.0	240.7 ± 24.9	1305.4 ± 77.1	1720.4 ± 152.4
PD-4-041213-8.9	247.9 ± 27.0	169.29 ± 25.58	394.33 ± 24.21	380.2 ± 25.5	260.6 ± 22.0	237.0 ± 27.0	1386.6 ± 83.9	1810.8 ± 153.7
PD-4-041213-9.5	250.3 ± 29.2	180.37 ± 28.35	420.42 ± 26.12	409.1 ± 26.6	273.8 ± 23.4	232.1 ± 29.2	1466.2 ± 93.1	1891.7 ± 179.3
PD-4-041213-10.1	259.3 ± 36.5	187.13 ± 65.76	448.96 ± 38.50	445.1 ± 36.1	279.5 ± 26.9	230.1 ± 36.5	1549.2 ± 121.9	1970.9 ± 158.4
PD-4-041213-10.7	263.6 ± 49.5	197.75 ± 76.43	481.70 ± 36.04	472.7 ± 38.8	289.1 ± 30.6	224.7 ± 49.5	1631.7 ± 136.7	2046.5 ± 159.5
PD-4-041213-11.3	271.1 ± 71.7	207.46 ± 102.83	514.73 ± 37.46	500.5 ± 43.1	298.0 ± 37.1	220.5 ± 71.7	1716.0 ± 170.8	2117.4 ± 174.1
PD-4-041213-11.9	283.3 ± 96.8	221.86 ± 127.93	545.32 ± 40.87	535.2 ± 44.5	301.6 ± 43.8	217.3 ± 96.8	1809.2 ± 218.0	2188.4 ± 93.5

Table C.18: Averaged values of measured wall surface temperature during experiment for each data point (PD-4-041213)

Test ID	TS21T (C)	TS21B (C)	TS22T (C)	TS22B (C)	TS23T (C)	TS23B (C)	TS24T (C)	TS24B (C)	TS25T (C)	TS25B (C)	TS26T (C)	TS26B (C)
PD-4-041213-1.25	35.4	33.9	40.4	34.6	39.4	35.2	40.8	34.8	43.4	35.9	43.9	36.5
PD-4-041213-1.7	37.9	35.5	44.6	36.4	43.3	36.8	44.2	36.2	47.3	37.7	48.0	38.5
PD-4-041213-2.3	42.2	38.1	50.9	39.2	48.5	39.6	48.6	38.5	53.1	40.4	54.8	41.7
PD-4-041213-2.9	47.3	41.1	57.3	42.4	53.8	42.3	53.9	40.8	59.7	43.2	62.6	45.1
PD-4-041213-3.5	53.0	44.4	64.2	45.9	60.1	45.3	60.3	43.3	67.6	46.4	71.8	49.2
PD-4-041213-4.1	60.0	48.5	71.4	49.8	66.9	48.5	67.4	46.0	76.1	49.8	82.0	54.2
PD-4-041213-4.6	66.0	52.4	77.6	53.4	73.1	51.2	73.9	48.5	83.9	53.2	91.5	59.1
PD-4-041213-5.3	75.7	58.9	87.7	58.7	82.6	55.4	84.4	52.4	96.3	59.0	107.1	68.4
PD-4-041213-5.8	83.6	64.8	96.7	63.2	90.3	59.0	93.1	56.1	107.2	65.1	121.3	78.2
PD-4-041213-6.5	93.2	71.6	108.3	69.1	100.0	63.5	104.2	60.5	120.4	72.2	137.1	89.1
PD-4-041213-7.1	102.5	78.8	120.1	75.0	109.8	67.9	115.8	66.0	134.7	81.2	154.3	102.4
PD-4-041213-7.7	112.4	86.4	133.2	81.5	120.6	73.0	128.3	72.8	150.6	92.4	173.2	118.6
PD-4-041213-8.3	122.4	93.8	146.3	88.3	131.4	78.3	141.4	80.3	167.1	104.8	192.3	135.6
PD-4-041213-8.9	133.0	101.7	160.5	96.3	143.1	84.5	155.9	90.0	185.1	119.8	213.2	155.0
PD-4-041213-9.5	144.0	109.9	174.9	104.5	155.3	91.3	171.1	100.9	203.9	135.9	234.3	175.2
PD-4-041213-10.1	153.9	117.4	185.5	109.3	165.9	98.7	186.0	112.5	222.5	151.6	254.5	194.7
PD-4-041213-10.7	163.4	125.0	198.3	115.8	179.0	107.4	202.8	126.7	243.1	170.0	276.8	217.4
PD-4-041213-11.3	169.7	130.7	206.4	121.5	191.2	116.5	219.2	140.8	262.5	187.7	297.7	238.9
PD-4-041213-11.9	173.8	135.1	212.9	126.7	203.8	125.9	235.8	155.4	281.3	205.5	318.3	260.6

Table C.19: Steady-state parameters of the loop (processed data) (PD-4-041213)

Test ID	Power (kW)	Flow rate (kg/s)	Inlet K	Outlet K	Outlet Temp. Calculated (C)	T11(C)	Total Ch. PD (Pa)	Acc. PD.(Pa)	Fr. PD.(Pa)
PD-4-041213-1.25	1.37 ± 0.03	0.031 ± 0.001	0	3.9	31.9 ± 0.1	32.6 ± 2.2	241.3 ± 15.0	22.6 ± 2.1	218.7 ± 15.2
PD-4-041213-1.7	1.86 ± 0.03	0.035 ± 0.001	0	4.1	32.1 ± 0.1	32.8 ± 2.2	310.2 ± 27.6	39.0 ± 3.4	271.3 ± 27.8
PD-4-041213-2.3	2.52 ± 0.03	0.039 ± 0.001	0	4.6	32.3 ± 0.1	33.2 ± 2.2	399.3 ± 22.1	66.4 ± 5.0	332.9 ± 22.6
PD-4-041213-2.9	3.17 ± 0.04	0.042 ± 0.001	0	5.1	32.3 ± 0.1	33.3 ± 2.2	488.5 ± 25.2	100.3 ± 6.8	388.2 ± 26.1
PD-4-041213-3.5	3.83 ± 0.04	0.045 ± 0.001	0	5.3	32.5 ± 0.1	33.6 ± 2.2	568.4 ± 29.4	135.7 ± 8.5	432.7 ± 30.6
PD-4-041213-4.1	4.49 ± 0.05	0.047 ± 0.001	0	5.4	32.7 ± 0.2	33.9 ± 2.2	655.7 ± 33.8	178.1 ± 10.5	477.6 ± 35.4
PD-4-041213-4.6	5.03 ± 0.05	0.048 ± 0.001	0	5.4	33.2 ± 0.2	34.4 ± 2.2	725.1 ± 37.3	214.5 ± 12.2	510.6 ± 39.2
PD-4-041213-5.3	5.80 ± 0.05	0.049 ± 0.001	0	5.4	34.5 ± 0.4	35.6 ± 2.2	823.4 ± 42.6	271.6 ± 14.9	551.8 ± 45.1
PD-4-041213-5.8	6.35 ± 0.06	0.048 ± 0.001	0	5.6	36.7 ± 0.6	37.5 ± 2.2	901.4 ± 46.3	319.7 ± 17.5	581.7 ± 49.5
PD-4-041213-6.5	7.11 ± 0.06	0.049 ± 0.001	0	5.5	39.3 ± 0.9	39.9 ± 2.2	993.1 ± 54.0	378.4 ± 20.0	614.7 ± 57.5
PD-4-041213-7.1	7.77 ± 0.06	0.049 ± 0.001	0	5.4	43.8 ± 1.3	43.4 ± 2.2	1083.3 ± 61.4	435.4 ± 22.5	647.9 ± 65.4
PD-4-041213-7.7	8.43 ± 0.06	0.048 ± 0.001	0	5.3	49.9 ± 1.8	48.0 ± 2.2	1168.8 ± 68.1	491.5 ± 25.3	677.3 ± 72.6
PD-4-041213-8.3	9.08 ± 0.07	0.048 ± 0.001	0	5.2	57.1 ± 2.2	53.9 ± 2.2	1253.7 ± 77.1	547.0 ± 27.3	706.6 ± 81.8
PD-4-041213-8.9	9.74 ± 0.07	0.047 ± 0.001	0	5.0	66.9 ± 2.8	60.3 ± 2.3	1332.9 ± 83.9	599.8 ± 29.9	733.1 ± 89.1
PD-4-041213-9.5	10.39 ± 0.07	0.046 ± 0.001	0	4.9	78.1 ± 3.3	67.4 ± 2.4	1410.8 ± 93.1	649.4 ± 31.7	761.4 ± 98.4
PD-4-041213-10.1	11.05 ± 0.07	0.046 ± 0.001	0	4.7	88.8 ± 3.9	77.1 ± 2.3	1491.8 ± 121.9	698.0 ± 34.4	793.8 ± 126.7
PD-4-041213-10.7	11.71 ± 0.08	0.045 ± 0.001	0	4.5	101.8 ± 4.5	87.4 ± 2.4	1572.3 ± 136.7	746.7 ± 38.0	825.6 ± 141.9
PD-4-041213-11.3	12.36 ± 0.08	0.045 ± 0.001	0	4.4	116.9 ± 5.4	96.9 ± 2.4	1655.4 ± 170.8	787.0 ± 42.7	868.4 ± 176.0
PD-4-041213-11.9	13.02 ± 0.08	0.044 ± 0.001	0	4.3	130.3 ± 6.3	104.4 ± 2.5	1747.0 ± 218.0	829.4 ± 47.6	917.6 ± 223.1

* Mean outlet K factor: 4.9

Table C.20: Comparison between frictional pressure-drop from the experimental against available friction-factor formulae (PD-4-041213)

Test ID	Fr. PD.(Pa)-Exp.	Blasius	Kondratev	Ishigai	Razumovskiy	Tarasova & Leontev	Yamashita	Popov	Kuraeva & Protopopov
PD-4-041213-1.25	218.7	182.4	149.6	123.9	138.7	149.0	97.2	126.6	303.8
PD-4-041213-1.7	271.3	236.2	193.1	158.1	177.2	192.3	125.7	159.0	381.0
PD-4-041213-2.3	332.9	298.0	242.7	200.1	223.2	244.0	163.5	197.6	468.8
PD-4-041213-2.9	388.2	355.4	288.7	240.6	266.9	293.8	202.4	233.3	549.8
PD-4-041213-3.5	432.7	405.1	328.3	275.7	304.6	337.3	237.6	263.3	619.4
PD-4-041213-4.1	477.6	452.2	365.8	311.7	342.3	381.0	276.8	292.8	686.0
PD-4-041213-4.6	510.6	487.4	393.6	339.1	370.7	414.2	307.9	314.6	735.8
PD-4-041213-5.3	551.8	530.8	428.0	376.9	408.5	458.4	354.7	343.3	798.7
PD-4-041213-5.8	581.7	557.4	448.8	405.9	435.9	489.9	395.2	364.5	838.7
PD-4-041213-6.5	614.7	595.7	479.1	439.8	469.5	529.7	439.8	389.4	893.5
PD-4-041213-7.1	647.9	626.1	503.0	472.7	500.5	565.6	487.2	413.0	938.0
PD-4-041213-7.7	677.3	654.9	525.7	505.3	530.8	600.7	536.0	435.9	980.1
PD-4-041213-8.3	706.6	684.7	549.3	538.8	561.9	636.8	586.4	459.6	1022.8
PD-4-041213-8.9	733.1	713.3	571.9	573.2	593.4	672.6	639.0	484.3	1063.0
PD-4-041213-9.5	761.4	740.8	593.7	606.7	624.0	707.3	690.7	508.4	1100.9
PD-4-041213-10.1	793.8	770.8	617.6	640.5	655.1	743.2	741.7	533.0	1141.5
PD-4-041213-10.7	825.6	804.2	644.2	678.8	689.9	783.4	799.4	561.2	1185.9
PD-4-041213-11.3	868.4	830.9	665.6	711.9	719.6	816.4	848.4	587.1	1218.5
PD-4-041213-11.9	917.6	861.4	690.1	746.2	751.2	852.2	899.0	613.1	1257.0

April 17th, 2013- System Pressure: 7.6 MPa, Inlet Temperature: 25-26 ℃, Inlet valve: 30° closed, Outlet valve: wide open

Table C.21: Averaged values of measured signals during experiment for each data point (PD-5-041713)

Test ID	Inlet Temperature (RTD1) (C)	Pressure (MPa)	Power (kW)	Outlet Temp (RTD2)(C)	T11 (C)	T12(C)	CO$_2$ volumetric Flow rate (m^3/s)×10^6	HE-Inlet water Temp.(C)	HE-Outlet water Temp.(C)	Water Flow rate (lpm)
PD-5-041713-1.2	24.8 ± 0.4	7.61 ± 0.02	1.32 ± 0.03	30.5 ± 0.5	32.1 ± 2.2	25.3 ± 2.2	39.1 ± 1.2	8.3 ± 2.2	29.6 ± 2.2	0.6
PD-5-041713-1.75	25.2 ± 0.4	7.61 ± 0.02	1.92 ± 0.03	31.2 ± 0.5	32.7 ± 2.2	25.5 ± 2.2	47.1 ± 1.1	9.7 ± 2.2	28.9 ± 2.2	1.3
PD-5-041713-2.3	25.6 ± 0.4	7.60 ± 0.02	2.52 ± 0.03	31.5 ± 0.5	32.9 ± 2.2	25.2 ± 2.2	53.8 ± 1.1	9.6 ± 2.2	27.3 ± 2.2	2.1
PD-5-041713-2.9	25.6 ± 0.4	7.60 ± 0.02	3.17 ± 0.04	31.6 ± 0.5	33.1 ± 2.2	25.3 ± 2.2	57.0 ± 1.1	9.4 ± 2.2	25.9 ± 2.2	3
PD-5-041713-3.5	25.6 ± 0.4	7.59 ± 0.02	3.83 ± 0.04	31.7 ± 0.5	33.3 ± 2.2	25.0 ± 2.2	60.3 ± 1.2	9.0 ± 2.2	23.9 ± 2.2	4.1
PD-5-041713-4.1	25.9 ± 0.4	7.60 ± 0.02	4.48 ± 0.05	32.1 ± 0.5	33.8 ± 2.2	24.9 ± 2.2	62.8 ± 1.2	7.7 ± 2.2	22.3 ± 2.2	5
PD-5-041713-4.7	25.8 ± 0.4	7.61 ± 0.02	5.14 ± 0.05	32.4 ± 0.5	34.4 ± 2.2	25.5 ± 2.2	64.7 ± 1.2	6.8 ± 2.2	21.2 ± 2.2	5.7
PD-5-041713-5.3	25.7 ± 0.4	7.61 ± 0.02	5.79 ± 0.05	32.8 ± 0.5	35.2 ± 2.2	25.5 ± 2.2	65.8 ± 1.2	5.9 ± 2.2	19.4 ± 2.2	7
PD-5-041713-5.9	25.8 ± 0.4	7.60 ± 0.02	6.45 ± 0.06	33.6 ± 0.5	36.7 ± 2.2	24.6 ± 2.2	66.9 ± 1.2	5.6 ± 2.2	20.1 ± 2.2	7.5
PD-5-041713-6.5	25.7 ± 0.4	7.59 ± 0.02	7.11 ± 0.06	34.6 ± 0.5	38.6 ± 2.2	24.9 ± 2.2	67.6 ± 1.2	5.2 ± 2.2	19.4 ± 2.2	8.4
PD-5-041713-7.1	25.9 ± 0.4	7.59 ± 0.02	7.76 ± 0.06	36.9 ± 0.5	41.8 ± 2.2	25.3 ± 2.2	67.8 ± 1.1	5.1 ± 2.2	18.4 ± 2.2	9.6
PD-5-041713-7.7	26.0 ± 0.4	7.61 ± 0.02	8.42 ± 0.06	39.7 ± 0.5	45.7 ± 2.2	25.1 ± 2.2	67.7 ± 1.2	4.9 ± 2.2	18.2 ± 2.2	10.4
PD-5-041713-8.3	25.9 ± 0.4	7.60 ± 0.02	9.07 ± 0.07	43.1 ± 0.5	50.2 ± 2.2	24.6 ± 2.2	67.6 ± 1.2	4.6 ± 2.2	17.7 ± 2.2	11.3
PD-5-041713-8.9	26.0 ± 0.4	7.61 ± 0.02	9.73 ± 0.07	48.3 ± 0.5	56.7 ± 2.2	25.0 ± 2.2	67.1 ± 1.1	4.4 ± 2.2	17.7 ± 2.2	11.9
PD-5-041713-9.5	25.9 ± 0.4	7.62 ± 0.02	10.39 ± 0.07	53.5 ± 0.6	61.9 ± 2.2	24.8 ± 2.2	66.7 ± 1.1	4.3 ± 2.2	17.2 ± 2.2	13
PD-5-041713-10.1	26.1 ± 0.4	7.62 ± 0.02	11.04 ± 0.07	61.6 ± 0.6	70.8 ± 2.3	24.8 ± 2.2	66.2 ± 1.1	4.3 ± 2.2	16.9 ± 2.2	14.1
PD-5-041713-10.7	26.0 ± 0.4	7.61 ± 0.02	11.70 ± 0.08	70.3 ± 0.6	78.7 ± 2.3	25.0 ± 2.2	65.6 ± 1.1	4.2 ± 2.2	16.6 ± 2.2	15
PD-5-041713-11.3	26.0 ± 0.4	7.61 ± 0.02	12.36 ± 0.08	80.3 ± 0.7	86.7 ± 2.4	25.2 ± 2.2	64.3 ± 1.4	4.0 ± 2.2	17.1 ± 2.2	14.7
PD-5-041713-12.7	26.1 ± 0.4	7.61 ± 0.02	13.89 ± 0.08	106.2 ± 0.8	112.5 ± 2.5	24.9 ± 2.2	65.0 ± 1.1	3.9 ± 2.2	15.6 ± 2.2	18.5

Table C.22: Averaged values of measured pressure-drops during experiment for each data point (PD-5-041713)

Test ID	DP2-1 (Pa)	DP2-2 (Pa)	DP2-3 (Pa)	DP2-4 (Pa)	DP2-5 (Pa)	DP3 (Pa)	DP13 (Pa)	DP10 (Pa)
PD-5-041713-1.2	91.3 ± 12.1	26.76 ± 11.99	61.54 ± 12.06	32.7 ± 11.5	39.7 ± 11.5	293.8 ± 12.1	238.3 ± 22.9	215.4 ± 122.4
PD-5-041713-1.75	118.9 ± 11.8	36.97 ± 11.71	90.28 ± 11.60	53.9 ± 11.9	50.3 ± 11.3	351.9 ± 11.8	331.5 ± 18.4	263.3 ± 144.4
PD-5-041713-2.3	144.2 ± 12.4	47.31 ± 12.29	120.17 ± 12.16	77.4 ± 12.7	63.0 ± 11.7	404.3 ± 12.4	428.5 ± 20.7	327.7 ± 123.5
PD-5-041713-2.9	164.0 ± 13.3	57.46 ± 13.24	148.66 ± 13.03	100.9 ± 13.8	79.5 ± 12.4	444.8 ± 13.3	522.8 ± 24.3	388.8 ± 127.2
PD-5-041713-3.5	181.7 ± 14.2	68.14 ± 14.07	176.98 ± 14.03	126.7 ± 15.1	95.8 ± 13.3	480.0 ± 14.2	617.9 ± 28.0	457.1 ± 135.3
PD-5-041713-4.1	196.9 ± 15.2	79.75 ± 15.25	204.99 ± 14.80	153.4 ± 16.4	114.9 ± 14.0	508.6 ± 15.2	714.8 ± 31.7	524.8 ± 133.7
PD-5-041713-4.7	209.1 ± 16.5	90.71 ± 16.50	231.14 ± 15.93	180.2 ± 17.8	133.4 ± 14.9	529.8 ± 16.5	806.4 ± 36.2	575.5 ± 137.4
PD-5-041713-5.3	220.1 ± 18.1	101.85 ± 17.70	256.71 ± 17.05	208.4 ± 19.4	153.4 ± 15.9	547.3 ± 18.1	899.3 ± 42.6	631.2 ± 139.0
PD-5-041713-5.9	231.0 ± 18.7	114.53 ± 18.50	284.41 ± 17.80	239.6 ± 20.3	176.0 ± 16.6	559.4 ± 18.7	1001.2 ± 46.8	679.3 ± 129.9
PD-5-041713-6.5	239.8 ± 20.2	127.12 ± 19.52	310.84 ± 19.13	271.7 ± 21.0	194.6 ± 17.8	568.8 ± 20.2	1096.7 ± 51.7	733.4 ± 140.7
PD-5-041713-7.1	247.0 ± 22.3	141.32 ± 21.39	338.77 ± 20.86	305.0 ± 23.2	216.2 ± 19.3	568.0 ± 22.3	1198.1 ± 61.8	784.2 ± 132.3
PD-5-041713-7.7	254.0 ± 23.1	153.81 ± 22.50	365.24 ± 21.95	337.4 ± 23.5	236.4 ± 20.2	569.8 ± 23.1	1293.7 ± 68.8	823.9 ± 132.2
PD-5-041713-8.3	260.1 ± 25.9	166.30 ± 25.18	392.14 ± 24.28	371.4 ± 25.4	256.1 ± 22.0	569.2 ± 25.9	1389.8 ± 75.6	853.0 ± 133.4
PD-5-041713-8.9	266.4 ± 26.2	178.56 ± 25.25	419.99 ± 24.76	406.5 ± 27.0	274.3 ± 22.5	563.9 ± 26.2	1486.0 ± 82.1	887.7 ± 119.2
PD-5-041713-9.5	271.6 ± 27.8	189.42 ± 27.23	447.23 ± 26.31	438.9 ± 28.1	291.0 ± 23.7	561.2 ± 27.8	1575.9 ± 88.7	919.1 ± 154.5
PD-5-041713-10.1	277.4 ± 30.3	202.79 ± 29.91	480.19 ± 27.97	474.9 ± 29.3	301.3 ± 25.1	549.8 ± 30.3	1671.1 ± 98.1	957.1 ± 135.5
PD-5-041713-10.7	287.3 ± 41.0	212.36 ± 57.87	513.73 ± 33.18	507.9 ± 34.9	312.5 ± 29.8	548.7 ± 41.0	1765.4 ± 111.4	989.1 ± 145.7
PD-5-041713-11.3	295.4 ± 57.4	224.32 ± 68.78	548.48 ± 30.02	537.5 ± 36.4	323.6 ± 32.7	539.2 ± 57.4	1858.4 ± 121.5	1015.6 ± 163.2
PD-5-041713-12.7	316.0 ± 87.5	256.74 ± 75.11	632.79 ± 28.44	608.8 ± 35.5	345.7 ± 40.6	525.5 ± 87.5	2083.6 ± 145.7	1085.1 ± 88.2

Table C.23: Averaged values of measured wall surface temperature during experiment for each data point (PD-5-041713)

Test ID	TS21T (C)	TS21B (C)	TS22T (C)	TS22B (C)	TS23T (C)	TS23B (C)	TS24T (C)	TS24B (C)	TS25T (C)	TS25B (C)	TS26T (C)	TS26B (C)
PD-5-041713-1.2	34.9	33.5	40.0	34.1	39.0	34.6	40.4	34.2	43.0	35.4	43.8	36.0
PD-5-041713-1.75	38.1	35.5	45.2	36.3	43.8	36.9	44.2	36.2	47.7	37.6	48.7	38.5
PD-5-041713-2.3	41.9	37.9	50.5	38.9	47.9	39.3	47.8	38.2	52.1	40.0	54.2	41.4
PD-5-041713-2.9	46.9	40.8	56.8	42.0	53.2	42.1	52.9	40.4	58.6	42.9	61.9	44.8
PD-5-041713-3.5	52.6	44.1	63.1	45.3	59.0	45.0	58.8	42.8	65.9	45.9	70.5	48.8
PD-5-041713-4.1	59.3	48.4	69.5	49.2	65.7	48.1	65.9	45.6	74.5	49.6	81.1	54.0
PD-5-041713-4.7	66.3	52.9	76.7	53.1	72.8	51.4	73.5	48.5	83.7	53.6	92.4	60.0
PD-5-041713-5.3	73.6	58.0	84.7	57.4	80.3	54.7	81.5	51.5	93.5	58.1	104.7	67.2
PD-5-041713-5.9	81.5	63.7	93.4	62.0	88.1	58.3	90.3	55.0	104.5	63.7	118.2	76.1
PD-5-041713-6.5	89.5	69.6	102.7	66.7	96.2	61.9	99.5	58.7	115.8	69.8	131.9	85.5
PD-5-041713-7.1	98.5	76.6	113.8	72.0	105.5	66.2	110.5	63.9	129.8	78.4	148.6	98.3
PD-5-041713-7.7	107.3	83.2	124.9	77.6	114.9	70.7	121.8	69.6	143.8	87.7	165.0	111.8
PD-5-041713-8.3	116.3	89.4	136.4	83.3	124.6	75.3	133.2	75.9	158.1	97.8	181.7	126.3
PD-5-041713-8.9	126.2	96.6	149.1	89.5	135.3	80.7	146.5	84.3	174.5	110.9	200.5	143.7
PD-5-041713-9.5	135.8	103.9	161.4	96.1	145.7	86.2	159.1	92.6	190.0	123.4	217.9	159.6
PD-5-041713-10.1	146.5	111.9	175.3	103.7	157.3	93.1	174.2	104.0	208.4	139.5	238.4	179.7
PD-5-041713-10.7	155.1	119.1	186.4	110.0	168.2	100.5	189.0	115.8	226.5	155.2	257.9	199.1
PD-5-041713-11.3	161.2	124.4	198.5	116.7	180.5	108.9	204.5	129.0	244.9	171.9	278.0	219.8
PD-5-041713-12.7	171.3	135.3	228.1	135.4	210.0	130.4	240.9	160.7	285.3	211.2	323.1	268.1

184

Table C.24: Steady-state parameters of the loop (processed data) (PD-5-041713)

Test ID	Power (kW)	Flow rate (kg/s)	Inlet K*	Outlet K	Outlet Temp. Calculated (C)	T11(C)	Total Ch. PD (Pa)	Acc. PD.(Pa)	Fr. PD.(Pa)
PD-5-041713-1.2	1.32 ± 0.03	0.030 ± 0.001	5.0	0	31.8 ± 0.1	32.1 ± 2.2	227.8 ± 22.9	20.6 ± 2.1	207.3 ± 23.0
PD-5-041713-1.75	1.92 ± 0.03	0.036 ± 0.001	4.7	0	32.2 ± 0.1	32.7 ± 2.2	315.8 ± 18.4	40.8 ± 3.5	275.0 ± 18.7
PD-5-041713-2.3	2.52 ± 0.03	0.041 ± 0.001	4.6	0	32.2 ± 0.1	32.9 ± 2.2	407.5 ± 20.7	68.0 ± 5.1	339.4 ± 21.3
PD-5-041713-2.9	3.17 ± 0.04	0.043 ± 0.001	4.9	0	32.3 ± 0.1	33.1 ± 2.2	498.0 ± 24.3	100.7 ± 6.9	397.3 ± 25.2
PD-5-041713-3.5	3.83 ± 0.04	0.045 ± 0.001	5.0	0	32.4 ± 0.1	33.3 ± 2.2	588.9 ± 28.0	138.3 ± 9.0	450.7 ± 29.4
PD-5-041713-4.1	4.48 ± 0.05	0.047 ± 0.001	5.1	0	32.8 ± 0.2	33.8 ± 2.2	681.9 ± 31.7	181.7 ± 11.3	500.2 ± 33.7
PD-5-041713-4.7	5.14 ± 0.05	0.049 ± 0.001	5.1	0	33.3 ± 0.2	34.4 ± 2.2	769.7 ± 36.2	227.3 ± 13.7	542.3 ± 38.7
PD-5-041713-5.3	5.79 ± 0.05	0.050 ± 0.001	5.2	0	34.3 ± 0.4	35.2 ± 2.2	859.2 ± 42.6	275.9 ± 16.2	583.3 ± 45.6
PD-5-041713-5.9	6.45 ± 0.06	0.050 ± 0.001	5.2	0	35.8 ± 0.6	36.7 ± 2.2	957.5 ± 46.8	331.0 ± 19.0	626.5 ± 50.6
PD-5-041713-6.5	7.11 ± 0.06	0.051 ± 0.001	5.2	0	37.8 ± 0.8	38.6 ± 2.2	1049.6 ± 51.7	387.9 ± 21.3	661.6 ± 55.9
PD-5-041713-7.1	7.76 ± 0.06	0.051 ± 0.001	5.2	0	41.7 ± 1.1	41.8 ± 2.2	1147.9 ± 61.8	449.3 ± 23.5	698.6 ± 66.1
PD-5-041713-7.7	8.42 ± 0.06	0.051 ± 0.001	5.3	0	46.5 ± 1.5	45.7 ± 2.2	1240.6 ± 68.8	507.5 ± 26.6	733.1 ± 73.7
PD-5-041713-8.3	9.07 ± 0.07	0.051 ± 0.001	5.3	0	52.0 ± 1.9	50.2 ± 2.2	1333.8 ± 75.6	567.7 ± 29.1	766.1 ± 81.0
PD-5-041713-8.9	9.73 ± 0.07	0.050 ± 0.001	5.3	0	60.0 ± 2.4	56.7 ± 2.2	1427.4 ± 82.1	627.1 ± 31.1	800.4 ± 87.8
PD-5-041713-9.5	10.39 ± 0.07	0.050 ± 0.001	5.3	0	67.8 ± 2.8	61.9 ± 2.2	1514.8 ± 88.7	683.3 ± 33.2	831.5 ± 94.7
PD-5-041713-10.1	11.04 ± 0.07	0.050 ± 0.001	5.3	0	78.4 ± 3.3	70.8 ± 2.3	1607.6 ± 98.1	742.1 ± 35.6	865.5 ± 104.3
PD-5-041713-10.7	11.70 ± 0.08	0.049 ± 0.001	5.4	0	88.9 ± 3.7	78.7 ± 2.3	1699.6 ± 111.4	796.3 ± 37.0	903.3 ± 117.3
PD-5-041713-11.3	12.36 ± 0.08	0.048 ± 0.001	5.5	0	102.9 ± 4.9	86.7 ± 2.4	1791.3 ± 121.5	841.5 ± 46.4	949.8 ± 130.1
PD-5-041713-12.7	13.89 ± 0.08	0.049 ± 0.001	5.0	0	126.6 ± 4.8	112.5 ± 2.5	2009.2 ± 145.7	978.4 ± 43.4	1030.8 ± 152.0

* Mean inlet K factor: 5.1

Table C.25: Comparison between frictional pressure-drop from the experimental against available friction-factor formulae (PD-5-041713)

Test ID	Fr. PD.(Pa)-Exp.	Blasius	Kondratev	Ishigai	Razumovskiy	Tarasova & Leontev	Yamashita	Popov	Kuraeva & Protopopov
PD-5-041713-1.2	207.3	170.1	139.6	116.3	130.0	139.4	91.4	119.1	286.0
PD-5-041713-1.75	275.0	242.5	198.2	162.7	182.1	197.6	129.6	163.6	390.1
PD-5-041713-2.3	339.4	314.3	255.9	211.0	235.4	257.1	172.0	208.7	491.2
PD-5-041713-2.9	397.3	362.5	294.3	245.3	272.2	299.3	205.8	238.3	559.2
PD-5-041713-3.5	450.7	415.0	336.2	283.2	312.7	345.8	244.0	270.8	632.6
PD-5-041713-4.1	500.2	463.7	374.9	321.2	352.3	391.3	285.3	302.2	701.6
PD-5-041713-4.7	542.3	508.3	410.2	356.2	388.5	433.5	325.0	330.3	764.4
PD-5-041713-5.3	583.3	548.4	442.0	389.4	422.3	473.0	364.7	356.0	821.3
PD-5-041713-5.9	626.5	589.8	474.7	425.9	458.7	515.4	410.6	383.8	880.3
PD-5-041713-6.5	661.6	629.3	505.9	461.6	494.0	556.8	457.0	410.6	936.6
PD-5-041713-7.1	698.6	665.7	534.5	499.2	529.8	598.3	509.5	438.0	989.3
PD-5-041713-7.7	733.1	699.4	561.1	534.4	563.2	637.0	559.4	463.5	1037.6
PD-5-041713-8.3	766.1	735.3	589.4	571.5	598.6	678.0	612.6	490.5	1088.3
PD-5-041713-8.9	800.4	768.9	615.9	609.9	634.2	718.8	669.7	518.2	1135.6
PD-5-041713-9.5	831.5	802.7	642.7	646.3	668.5	758.3	723.4	544.6	1182.3
PD-5-041713-10.1	865.5	839.8	672.1	688.9	708.0	803.3	787.4	575.7	1232.8
PD-5-041713-10.7	903.3	874.6	699.8	728.1	744.0	844.9	846.4	604.2	1279.6
PD-5-041713-11.3	949.8	901.3	721.1	762.9	774.6	879.2	899.4	630.8	1312.4
PD-5-041713-12.7	1030.8	1012.7	809.7	876.1	881.5	1004.3	1064.6	714.0	1460.4

April 18th, 2013- System Pressure: 7.6 MPa, Inlet Temperature: 25-26 ℃, Inlet valve: 40º closed, Outlet valve: wide open

Table C.26: Averaged values of measured signals during experiment for each data point (PD-6-041813)

Test ID	Inlet Temperature (RTD1) (C)	Pressure (MPa)	Power (kW)	Outlet Temp (RTD2)(C)	T11 (C)	T12(C)	CO_2 volumetric Flow rate $(m^3/s) \times 10^6$	HE-Inlet water Temp.(C)	HE-Outlet water Temp.(C)	Water Flow rate (lpm)
PD-6-041813-1.6	25.4 ± 0.4	7.59 ± 0.02	1.75 ± 0.03	30.8 ± 0.5	32.3 ± 2.2	25.5 ± 2.2	43.7 ± 1.1	8.5 ± 2.2	28.7 ± 2.2	1.2
PD-6-041813-2.3	25.5 ± 0.4	7.60 ± 0.02	2.52 ± 0.04	31.2 ± 0.5	32.7 ± 2.2	25.2 ± 2.2	50.4 ± 1.1	9.3 ± 2.2	26.6 ± 2.2	2.2
PD-6-041813-2.9	25.8 ± 0.4	7.61 ± 0.02	3.17 ± 0.04	31.4 ± 0.5	32.9 ± 2.2	25.5 ± 2.2	54.2 ± 1.1	9.0 ± 2.2	25.7 ± 2.2	2.9
PD-6-041813-3.5	26.1 ± 0.4	7.61 ± 0.02	3.83 ± 0.04	31.7 ± 0.5	33.4 ± 2.2	26.1 ± 2.2	57.1 ± 1.1	9.1 ± 2.2	24.6 ± 2.2	3.8
PD-6-041813-4.1	25.8 ± 0.4	7.60 ± 0.02	4.48 ± 0.05	31.9 ± 0.5	33.8 ± 2.2	25.5 ± 2.2	59.3 ± 1.1	7.7 ± 2.2	21.5 ± 2.2	5.3
PD-6-041813-4.75	25.8 ± 0.4	7.59 ± 0.02	5.19 ± 0.05	32.4 ± 0.5	34.8 ± 2.2	25.4 ± 2.2	61.2 ± 1.2	6.2 ± 2.2	19.9 ± 2.2	6.1
PD-6-041813-5.3	26.0 ± 0.4	7.61 ± 0.02	5.80 ± 0.05	33.4 ± 0.5	36.5 ± 2.2	25.1 ± 2.2	62.3 ± 1.3	5.8 ± 2.2	20.1 ± 2.2	6.9
PD-6-041813-5.9	25.9 ± 0.4	7.62 ± 0.02	6.45 ± 0.06	34.7 ± 0.5	38.5 ± 2.2	25.6 ± 2.2	62.3 ± 1.1	5.6 ± 2.2	19.7 ± 2.2	7.6
PD-6-041813-6.5	26.3 ± 0.4	7.63 ± 0.02	7.11 ± 0.06	37.7 ± 0.5	42.4 ± 2.2	25.2 ± 2.2	62.9 ± 1.1	5.4 ± 2.2	19.6 ± 2.2	8.2
PD-6-041813-7.1	25.9 ± 0.4	7.61 ± 0.02	7.76 ± 0.06	39.6 ± 0.5	45.9 ± 2.2	25.2 ± 2.2	63.3 ± 1.1	5.1 ± 2.2	17.9 ± 2.2	10
PD-6-041813-7.7	25.8 ± 0.4	7.61 ± 0.02	8.42 ± 0.06	43.2 ± 0.5	50.2 ± 2.2	25.3 ± 2.2	63.2 ± 1.1	4.8 ± 2.2	17.5 ± 2.2	10.7
PD-6-041813-8.3	25.7 ± 0.4	7.61 ± 0.02	9.08 ± 0.07	48.1 ± 0.5	55.1 ± 2.3	25.5 ± 2.2	62.9 ± 1.1	4.7 ± 2.2	17.3 ± 2.2	11.5
PD-6-041813-8.9	25.8 ± 0.4	7.62 ± 0.02	9.73 ± 0.07	54.8 ± 0.6	63.3 ± 2.2	25.5 ± 2.2	62.6 ± 1.1	4.6 ± 2.2	17.4 ± 2.2	12.2
PD-6-041813-9.5	25.8 ± 0.4	7.62 ± 0.02	10.39 ± 0.07	62.1 ± 0.6	71.2 ± 2.2	25.2 ± 2.2	62.2 ± 1.2	4.3 ± 2.2	17.3 ± 2.2	12.8
PD-6-041813-10.1	25.9 ± 0.4	7.62 ± 0.02	11.05 ± 0.07	71.3 ± 0.6	80.1 ± 2.3	25.4 ± 2.2	61.8 ± 1.2	4.4 ± 2.2	16.9 ± 2.2	13.9
PD-6-041813-10.7	26.3 ± 0.4	7.61 ± 0.02	11.70 ± 0.08	84.1 ± 0.7	93.1 ± 2.2	26.0 ± 2.2	62.2 ± 1.1	4.2 ± 2.2	16.7 ± 2.2	14.8
PD-6-041813-11.3	26.3 ± 0.4	7.62 ± 0.02	12.36 ± 0.08	95.2 ± 0.7	102.3 ± 2.5	26.1 ± 2.2	61.5 ± 1.1	4.1 ± 2.2	16.4 ± 2.2	15.7
PD-6-041813-11.9	26.0 ± 0.4	7.62 ± 0.02	13.02 ± 0.08	105.7 ± 0.8	110.0 ± 2.8	25.9 ± 2.2	60.6 ± 1.1	4.1 ± 2.2	16.3 ± 2.2	16.4

Table C.27: Averaged values of measured pressure-drops during experiment for each data point (PD-6-041813)

Test ID	DP2-1 (Pa)	DP2-2 (Pa)	DP2-3 (Pa)	DP2-4 (Pa)	DP2-5 (Pa)	DP3 (Pa)	DP13 (Pa)	DP10 (Pa)
PD-6-041813-1.6	140.5 ± 12.3	13.91 ± 12.50	81.18 ± 12.54	30.3 ± 12.0	102.8 ± 11.7	632.6 ± 12.3	306.8 ± 19.3	329.5 ± 165.2
PD-6-041813-2.3	166.7 ± 14.3	24.96 ± 14.14	113.37 ± 14.30	54.9 ± 14.0	119.7 ± 13.2	786.9 ± 14.3	413.7 ± 39.0	397.7 ± 125.0
PD-6-041813-2.9	184.0 ± 15.8	35.22 ± 15.47	140.15 ± 15.38	77.9 ± 15.3	133.5 ± 14.1	881.2 ± 15.8	501.4 ± 50.4	467.7 ± 124.8
PD-6-041813-3.5	198.8 ± 15.3	46.45 ± 15.53	166.87 ± 15.14	101.9 ± 15.6	151.7 ± 14.0	954.7 ± 15.3	593.0 ± 35.4	533.9 ± 135.7
PD-6-041813-4.1	212.1 ± 16.6	56.83 ± 16.56	192.21 ± 16.28	127.0 ± 16.9	170.7 ± 14.9	1023.6 ± 16.6	682.6 ± 39.6	587.6 ± 117.8
PD-6-041813-4.75	224.2 ± 17.6	69.39 ± 17.70	220.04 ± 17.01	157.1 ± 18.0	190.3 ± 15.7	1073.8 ± 17.6	781.6 ± 41.4	641.7 ± 129.5
PD-6-041813-5.3	234.2 ± 18.2	80.87 ± 18.10	244.13 ± 17.63	183.8 ± 18.6	210.1 ± 16.2	1103.2 ± 18.2	870.9 ± 45.5	691.9 ± 125.6
PD-6-041813-5.9	242.9 ± 19.6	91.49 ± 19.22	267.85 ± 19.27	211.7 ± 20.0	226.8 ± 17.6	1130.0 ± 19.6	956.0 ± 48.7	735.9 ± 156.8
PD-6-041813-6.5	250.9 ± 19.4	105.72 ± 19.19	295.46 ± 18.73	243.8 ± 20.8	246.4 ± 17.2	1132.5 ± 19.4	1054.8 ± 52.8	784.9 ± 184.0
PD-6-041813-7.1	258.8 ± 22.1	117.18 ± 21.84	321.23 ± 21.36	274.4 ± 22.6	266.9 ± 19.5	1158.0 ± 22.1	1148.5 ± 61.4	832.0 ± 132.7
PD-6-041813-7.7	265.1 ± 23.8	128.65 ± 23.40	347.09 ± 22.23	305.9 ± 23.3	284.9 ± 20.2	1162.1 ± 23.8	1238.8 ± 68.8	864.6 ± 134.1
PD-6-041813-8.3	270.6 ± 24.9	140.61 ± 24.69	373.65 ± 23.65	338.0 ± 24.3	302.1 ± 21.5	1157.4 ± 24.9	1329.4 ± 74.4	906.0 ± 134.9
PD-6-041813-8.9	276.8 ± 26.2	152.03 ± 25.70	400.65 ± 24.51	371.6 ± 26.4	317.1 ± 22.4	1148.3 ± 26.2	1419.6 ± 89.4	933.7 ± 135.1
PD-6-041813-9.5	283.0 ± 29.7	162.68 ± 29.35	428.04 ± 27.43	405.7 ± 28.0	329.8 ± 24.7	1138.5 ± 29.7	1507.8 ± 101.8	964.7 ± 135.8
PD-6-041813-10.1	289.1 ± 31.9	173.77 ± 31.54	456.79 ± 29.04	438.9 ± 29.5	340.7 ± 26.1	1121.8 ± 31.9	1594.8 ± 110.9	995.8 ± 136.2
PD-6-041813-10.7	295.7 ± 35.7	187.54 ± 35.86	494.76 ± 32.74	469.7 ± 31.0	346.2 ± 28.5	1088.4 ± 35.7	1687.9 ± 123.8	1034.2 ± 160.2
PD-6-041813-11.3	301.0 ± 36.8	198.92 ± 35.92	523.67 ± 31.93	500.8 ± 31.0	353.2 ± 28.3	1076.9 ± 36.8	1769.8 ± 118.0	1047.3 ± 129.3
PD-6-041813-11.9	308.5 ± 50.3	212.03 ± 45.60	560.01 ± 31.16	526.0 ± 32.7	363.8 ± 32.6	1065.5 ± 50.3	1861.2 ± 118.5	1038.2 ± 91.9

Table C.28: Averaged values of measured wall surface temperature during experiment for each data point (PD-6-041813)

Test ID	TS21T (C)	TS21B (C)	TS22T (C)	TS22B (C)	TS23T (C)	TS23B (C)	TS24T (C)	TS24B (C)	TS25T (C)	TS25B (C)	TS26T (C)	TS26B (C)
PD-6-041813-1.6	37.7	34.9	44.9	35.7	43.5	36.2	44.3	35.5	47.2	37.0	47.9	37.9
PD-6-041813-2.3	43.0	38.1	52.4	39.0	49.8	39.5	49.6	38.3	54.0	40.3	56.5	41.6
PD-6-041813-2.9	49.0	41.6	59.7	42.5	55.8	42.4	55.8	40.9	61.4	43.6	65.3	45.6
PD-6-041813-3.5	56.0	45.8	67.5	46.4	62.5	45.8	62.8	43.8	70.0	47.2	75.8	50.9
PD-6-041813-4.1	62.6	50.0	74.7	50.3	69.5	48.9	69.9	46.4	78.5	50.8	86.2	56.3
PD-6-041813-4.75	71.0	55.6	83.4	55.1	77.6	52.6	78.6	49.6	89.4	55.8	100.0	64.3
PD-6-041813-5.3	78.6	61.2	91.9	59.6	85.3	56.2	87.5	53.2	100.4	61.8	113.9	73.8
PD-6-041813-5.9	86.7	67.1	101.7	64.7	93.9	60.1	97.2	57.3	112.5	68.6	128.6	84.1
PD-6-041813-6.5	96.0	74.2	113.5	70.4	103.9	64.9	109.1	63.4	127.7	78.5	147.1	98.5
PD-6-041813-7.1	104.2	80.1	123.4	75.4	112.1	68.8	118.9	67.8	139.9	85.9	161.3	109.8
PD-6-041813-7.7	113.3	86.9	135.2	81.3	122.0	73.6	130.7	74.4	154.6	96.4	178.7	124.8
PD-6-041813-8.3	122.9	94.1	147.6	87.5	132.4	78.8	143.4	82.1	170.6	108.8	197.0	141.3
PD-6-041813-8.9	133.0	101.7	160.7	94.4	143.7	85.0	157.4	91.9	188.1	123.4	217.1	160.1
PD-6-041813-9.5	143.0	109.4	173.7	101.4	154.8	91.6	171.5	102.3	205.6	138.2	236.5	178.7
PD-6-041813-10.1	153.8	117.1	187.4	109.1	166.9	99.2	186.7	114.6	224.4	154.8	257.1	199.0
PD-6-041813-10.7	165.7	125.9	202.7	118.0	180.4	108.9	204.6	131.1	246.3	175.3	280.7	224.1
PD-6-041813-11.3	176.5	134.4	216.6	127.5	193.3	118.1	220.7	144.8	264.7	192.5	300.7	245.2
PD-6-041813-11.9	180.9	138.9	228.4	136.2	205.6	127.2	235.6	158.0	281.8	208.3	319.2	264.8

Table C.29: Steady-state parameters of the loop (processed data) (PD-6-041813)

Test ID	Power (kW)	Flow rate (kg/s)	Inlet K*	Outlet K	Outlet Temp. Calculated (C)	T11(C)	Total Ch. PD (Pa)	Acc. PD.(Pa)	Fr. PD.(Pa)
PD-6-041813-1.6	1.75 ± 0.03	0.033 ± 0.001	19.1	0	32.1 ± 0.1	32.3 ± 2.2	293.4 ± 19.3	35.2 ± 3.2	258.2 ± 19.5
PD-6-041813-2.3	2.52 ± 0.04	0.038 ± 0.001	18.9	0	32.3 ± 0.1	32.7 ± 2.2	394.9 ± 39.0	65.8 ± 5.0	329.1 ± 39.3
PD-6-041813-2.9	3.17 ± 0.04	0.041 ± 0.001	18.9	0	32.4 ± 0.1	32.9 ± 2.2	478.6 ± 50.4	98.8 ± 6.9	379.8 ± 50.8
PD-6-041813-3.5	3.83 ± 0.04	0.043 ± 0.001	19.0	0	32.7 ± 0.2	33.4 ± 2.2	566.5 ± 35.4	137.1 ± 9.1	429.4 ± 36.6
PD-6-041813-4.1	4.48 ± 0.05	0.045 ± 0.001	19.0	0	33.0 ± 0.2	33.8 ± 2.2	652.5 ± 39.6	176.7 ± 11.0	475.8 ± 41.1
PD-6-041813-4.75	5.19 ± 0.05	0.046 ± 0.001	18.9	0	33.8 ± 0.3	34.8 ± 2.2	747.6 ± 41.4	226.3 ± 14.0	521.4 ± 43.7
PD-6-041813-5.3	5.80 ± 0.05	0.047 ± 0.001	18.9	0	35.3 ± 0.5	36.5 ± 2.2	833.9 ± 45.5	272.8 ± 17.0	561.1 ± 48.6
PD-6-041813-5.9	6.45 ± 0.06	0.047 ± 0.001	19.4	0	37.8 ± 0.8	38.5 ± 2.2	916.4 ± 48.7	321.2 ± 18.2	595.2 ± 52.0
PD-6-041813-6.5	7.11 ± 0.06	0.047 ± 0.001	19.3	0	42.2 ± 1.2	42.4 ± 2.2	1012.1 ± 52.8	380.1 ± 20.8	632.0 ± 56.8
PD-6-041813-7.1	7.76 ± 0.06	0.047 ± 0.001	19.4	0	45.5 ± 1.5	45.9 ± 2.2	1102.5 ± 61.4	434.2 ± 23.1	668.3 ± 65.6
PD-6-041813-7.7	8.42 ± 0.06	0.047 ± 0.001	19.5	0	51.1 ± 1.9	50.2 ± 2.2	1190.2 ± 68.8	489.5 ± 25.7	700.7 ± 73.4
PD-6-041813-8.3	9.08 ± 0.07	0.047 ± 0.001	19.5	0	58.2 ± 2.4	55.1 ± 2.3	1278.1 ± 74.4	545.4 ± 28.1	732.7 ± 79.5
PD-6-041813-8.9	9.73 ± 0.07	0.047 ± 0.001	19.6	0	67.3 ± 2.9	63.3 ± 2.2	1365.9 ± 89.4	600.9 ± 30.4	765.0 ± 94.4
PD-6-041813-9.5	10.39 ± 0.07	0.047 ± 0.001	19.6	0	77.2 ± 3.5	71.2 ± 2.2	1451.6 ± 101.8	654.9 ± 34.5	796.7 ± 107.5
PD-6-041813-10.1	11.05 ± 0.07	0.046 ± 0.001	19.6	0	88.7 ± 4.0	80.1 ± 2.3	1536.4 ± 110.9	707.1 ± 36.4	829.3 ± 116.7
PD-6-041813-10.7	11.70 ± 0.08	0.046 ± 0.001	18.8	0	100.7 ± 4.2	93.1 ± 2.2	1626.4 ± 123.8	767.5 ± 36.9	858.9 ± 129.2
PD-6-041813-11.3	12.36 ± 0.08	0.046 ± 0.001	19.0	0	114.2 ± 4.8	102.3 ± 2.5	1706.4 ± 118.0	812.2 ± 39.4	894.3 ± 124.4
PD-6-041813-11.9	13.02 ± 0.08	0.045 ± 0.001	19.2	0	127.1 ± 5.2	110.0 ± 2.8	1796.3 ± 118.5	854.2 ± 41.0	942.1 ± 125.4

* Mean inlet K factor: 19.2

Table C.30: Comparison between frictional pressure-drop from the experimental against available friction-factor formulae (PD-6-041813)

Test ID	Fr. PD.(Pa)-Exp.	Blasius	Kondratev	Ishigai	Razumovskiy	Tarasova & Leontev	Yamashita	Popov	Kuraeva & Protopopov
PD-6-041813-1.6	258.2	211.1	172.7	142.3	159.2	172.6	113.7	143.0	345.6
PD-6-041813-2.3	329.1	283.4	231.0	190.7	212.5	232.7	156.6	187.7	448.9
PD-6-041813-2.9	379.8	335.2	272.3	227.9	252.4	278.2	193.4	220.1	522.9
PD-6-041813-3.5	429.4	382.1	309.6	263.8	290.1	321.3	231.7	250.1	590.1
PD-6-041813-4.1	475.8	427.0	345.4	297.2	325.2	362.2	267.4	277.6	653.6
PD-6-041813-4.75	521.4	473.4	382.2	334.5	363.6	406.9	310.8	307.2	719.9
PD-6-041813-5.3	561.1	509.3	410.6	366.6	395.5	444.0	351.0	331.7	772.2
PD-6-041813-5.9	595.2	537.8	433.1	394.3	422.3	475.3	388.4	352.0	814.1
PD-6-041813-6.5	632.0	576.3	463.5	433.4	459.8	518.5	441.9	381.0	870.3
PD-6-041813-7.1	668.3	613.8	493.1	467.0	493.1	557.6	486.5	406.0	923.4
PD-6-041813-7.7	700.7	647.1	519.5	501.2	525.7	595.4	535.2	430.9	971.1
PD-6-041813-8.3	732.7	680.8	546.1	536.9	559.4	634.4	587.1	456.8	1018.8
PD-6-041813-8.9	765.0	715.3	573.5	575.3	595.3	675.4	643.6	484.9	1067.2
PD-6-041813-9.5	796.7	750.3	601.2	613.6	631.2	716.4	699.9	513.1	1115.2
PD-6-041813-10.1	829.3	785.4	629.1	653.1	667.7	758.2	758.5	542.4	1162.5
PD-6-041813-10.7	858.9	834.4	668.1	704.5	715.6	814.5	834.6	579.8	1229.7
PD-6-041813-11.3	894.3	866.5	693.7	741.4	749.3	852.8	889.3	607.7	1270.7
PD-6-041813-11.9	942.1	895.4	716.9	774.4	779.5	887.0	938.0	633.0	1306.7

April 24th, 2013- System Pressure: 8.5 MPa, Inlet Temperature: 25-26 ℃, Inlet valve: wide open, Outlet valve: wide open

Table C.31: Averaged values of measured signals during experiment for each data point (PD-7-042413)

Test ID	Inlet Temperature (RTD1) (C)	Pressure (MPa)	Power (kW)	Outlet Temp (RTD2)(C)	T11 (C)	T12(C)	CO_2 volumetric Flow rate $(m^3/s) \times 10^6$	HE-Inlet water Temp.(C)	HE-Outlet water Temp.(C)	Water Flow rate (lpm)
PD-7-042413-1.2	25.1 ± 0.4	8.51 ± 0.02	1.32 ± 0.03	33.1 ± 0.5	34.8 ± 2.2	25.2 ± 2.2	38.0 ± 1.1	9.9 ± 2.2	31.1 ± 2.2	0.6
PD-7-042413-1.7	24.9 ± 0.4	8.51 ± 0.02	1.86 ± 0.03	34.1 ± 0.5	36.0 ± 2.2	24.6 ± 2.2	44.7 ± 1.1	10.8 ± 2.2	29.4 ± 2.2	1.4
PD-7-042413-2.3	24.9 ± 0.4	8.51 ± 0.02	2.52 ± 0.04	35.1 ± 0.5	37.0 ± 2.2	24.6 ± 2.2	50.4 ± 1.1	10.2 ± 2.2	27.6 ± 2.2	2.2
PD-7-042413-2.9	25.3 ± 0.4	8.51 ± 0.02	3.17 ± 0.04	36.0 ± 0.5	37.9 ± 2.2	25.2 ± 2.2	55.3 ± 1.1	10.3 ± 2.2	26.7 ± 2.2	2.9
PD-7-042413-3.5	25.2 ± 0.4	8.51 ± 0.02	3.83 ± 0.04	36.5 ± 0.5	38.5 ± 2.2	25.1 ± 2.2	59.0 ± 1.2	9.7 ± 2.2	24.9 ± 2.2	3.9
PD-7-042413-4.1	25.6 ± 0.4	8.51 ± 0.02	4.48 ± 0.05	37.1 ± 0.5	39.2 ± 2.2	24.5 ± 2.2	62.2 ± 1.2	8.2 ± 2.2	23.1 ± 2.2	4.8
PD-7-042413-4.8	25.6 ± 0.4	8.50 ± 0.02	5.25 ± 0.05	37.6 ± 0.5	39.9 ± 2.2	24.9 ± 2.2	65.0 ± 1.2	6.9 ± 2.2	21.2 ± 2.2	5.9
PD-7-042413-5.3	25.5 ± 0.4	8.49 ± 0.02	5.80 ± 0.05	38.0 ± 0.5	40.6 ± 2.2	24.9 ± 2.2	66.8 ± 1.2	6.5 ± 2.2	20.3 ± 2.2	6.9
PD-7-042413-5.9	25.6 ± 0.4	8.50 ± 0.02	6.45 ± 0.06	38.8 ± 0.5	41.8 ± 2.2	24.5 ± 2.2	68.1 ± 1.2	6.0 ± 2.2	20.1 ± 2.2	7.8
PD-7-042413-6.5	26.3 ± 0.4	8.51 ± 0.02	7.11 ± 0.06	40.2 ± 0.5	43.8 ± 2.2	24.5 ± 2.2	69.2 ± 1.2	5.6 ± 2.2	20.0 ± 2.2	8.2
PD-7-042413-7.1	26.4 ± 0.4	8.50 ± 0.02	7.76 ± 0.06	41.7 ± 0.5	46.1 ± 2.2	24.6 ± 2.2	69.7 ± 1.2	5.1 ± 2.2	19.3 ± 2.2	9
PD-7-042413-7.7	26.2 ± 0.4	8.50 ± 0.02	8.42 ± 0.06	43.2 ± 0.5	48.7 ± 2.2	24.9 ± 2.2	70.2 ± 1.2	5.0 ± 2.2	18.8 ± 2.2	10
PD-7-042413-8.52	26.1 ± 0.4	8.52 ± 0.02	9.32 ± 0.07	46.4 ± 0.5	53.0 ± 2.2	25.4 ± 2.2	70.4 ± 1.2	4.8 ± 2.2	18.6 ± 2.2	11.1
PD-7-042413-9.5	25.7 ± 0.4	8.50 ± 0.02	10.39 ± 0.07	51.1 ± 0.6	58.9 ± 2.2	24.9 ± 2.2	70.4 ± 1.2	4.5 ± 2.2	17.5 ± 2.2	13.1
PD-7-042413-10.1	25.7 ± 0.4	8.51 ± 0.02	11.04 ± 0.07	55.3 ± 0.6	63.1 ± 2.3	25.0 ± 2.2	70.0 ± 1.2	4.4 ± 2.2	17.4 ± 2.2	13.7
PD-7-042413-10.7	25.7 ± 0.4	8.49 ± 0.02	11.70 ± 0.08	60.4 ± 0.6	69.3 ± 2.2	24.7 ± 2.2	69.5 ± 1.3	4.2 ± 2.2	16.8 ± 2.2	14.9
PD-7-042413-11.3	25.8 ± 0.4	8.52 ± 0.02	12.36 ± 0.08	67.0 ± 0.6	75.3 ± 2.4	24.9 ± 2.2	68.9 ± 1.3	4.2 ± 2.2	16.8 ± 2.2	15.6

Table C.32: Averaged values of measured pressure-drops during experiment for each data point (PD-7-042413)

Test ID	DP2-1 (Pa)	DP2-2 (Pa)	DP2-3 (Pa)	DP2-4 (Pa)	DP2-5 (Pa)	DP3 (Pa)	DP13 (Pa)	DP10 (Pa)
PD-7-042413-1.2	112.2 ± 11.0	21.85 ± 11.02	56.44 ± 10.96	24.5 ± 11.0	43.6 ± 10.8	297.0 ± 11.0	235.1 ± 13.3	240.4 ± 118.6
PD-7-042413-1.7	136.8 ± 11.5	30.24 ± 11.52	79.41 ± 11.40	41.4 ± 11.6	50.9 ± 11.1	316.1 ± 11.5	310.8 ± 16.7	273.9 ± 122.9
PD-7-042413-2.3	162.7 ± 12.2	39.57 ± 12.14	106.34 ± 11.97	62.8 ± 12.3	62.9 ± 11.5	338.3 ± 12.2	400.6 ± 20.4	318.3 ± 123.7
PD-7-042413-2.9	184.5 ± 12.9	48.83 ± 12.86	133.11 ± 12.67	85.2 ± 13.1	75.4 ± 12.0	355.2 ± 12.9	488.2 ± 24.3	365.4 ± 123.6
PD-7-042413-3.5	203.3 ± 13.9	57.74 ± 13.92	158.66 ± 13.47	107.5 ± 14.4	90.5 ± 12.8	367.7 ± 13.9	573.6 ± 29.6	411.8 ± 118.4
PD-7-042413-4.1	220.2 ± 15.4	67.68 ± 15.51	185.69 ± 15.16	132.4 ± 16.0	106.3 ± 14.1	381.3 ± 15.4	663.2 ± 33.7	457.8 ± 125.7
PD-7-042413-4.8	236.4 ± 16.8	78.89 ± 16.88	215.19 ± 16.19	162.1 ± 17.2	126.4 ± 15.0	389.7 ± 16.8	765.0 ± 36.3	514.5 ± 126.6
PD-7-042413-5.3	247.9 ± 17.6	87.07 ± 17.41	237.40 ± 16.53	184.9 ± 18.2	139.9 ± 15.4	396.2 ± 17.6	840.0 ± 40.2	555.4 ± 147.2
PD-7-042413-5.9	258.0 ± 19.1	97.14 ± 18.95	261.66 ± 18.00	211.7 ± 19.9	161.4 ± 16.7	402.8 ± 19.1	929.1 ± 44.5	608.1 ± 126.7
PD-7-042413-6.5	267.8 ± 20.1	109.52 ± 19.92	289.03 ± 19.01	242.8 ± 21.4	180.3 ± 17.7	405.5 ± 20.1	1025.0 ± 48.6	660.4 ± 146.7
PD-7-042413-7.1	269.3 ± 99.2	121.92 ± 109.06	315.06 ± 115.49	274.1 ± 34.9	198.8 ± 68.3	414.1 ± 99.2	1112.6 ± 136.9	716.6 ± 133.9
PD-7-042413-7.7	283.0 ± 51.3	131.62 ± 51.67	340.47 ± 52.54	305.6 ± 27.3	220.0 ± 33.8	415.2 ± 51.3	1210.8 ± 76.4	755.0 ± 132.0
PD-7-042413-8.52	292.8 ± 26.3	145.82 ± 26.29	374.61 ± 25.59	347.3 ± 24.9	247.2 ± 22.8	415.6 ± 26.3	1333.6 ± 73.1	812.1 ± 131.0
PD-7-042413-9.5	301.6 ± 28.5	163.96 ± 28.35	416.45 ± 27.48	399.3 ± 26.5	279.2 ± 24.4	414.2 ± 28.5	1481.8 ± 85.3	879.6 ± 133.7
PD-7-042413-10.1	305.4 ± 30.8	174.62 ± 29.99	441.69 ± 28.46	429.7 ± 27.8	295.3 ± 25.4	414.2 ± 30.8	1565.6 ± 92.2	917.9 ± 142.4
PD-7-042413-10.7	309.9 ± 30.9	187.61 ± 31.04	470.46 ± 29.80	464.3 ± 29.7	311.8 ± 26.6	409.9 ± 30.9	1659.8 ± 99.5	951.5 ± 144.6
PD-7-042413-11.3	313.5 ± 33.0	199.42 ± 32.66	497.42 ± 31.31	494.4 ± 30.2	325.4 ± 27.6	409.7 ± 33.0	1743.3 ± 106.7	975.0 ± 87.0

Table C.33: Averaged values of measured wall surface temperature during experiment for each data point (PD-7-042413)

Test ID	TS21T (C)	TS21B (C)	TS22T (C)	TS22B (C)	TS23T (C)	TS23B (C)	TS24T (C)	TS24B (C)	TS25T (C)	TS25B (C)	TS26T (C)	TS26B (C)
PD-7-042413-1.2	36.9	34.9	41.9	36.3	41.4	37.3	42.4	37.5	46.0	39.3	47.3	40.3
PD-7-042413-1.7	39.8	37.4	46.1	38.9	45.2	39.8	46.3	39.8	50.3	41.6	52.2	42.7
PD-7-042413-2.3	43.1	40.1	51.4	41.6	49.9	42.6	50.9	42.1	56.1	44.3	58.5	46.1
PD-7-042413-2.9	46.9	42.8	57.4	44.5	55.2	45.5	56.1	44.6	62.7	47.3	66.3	49.9
PD-7-042413-3.5	50.9	45.4	63.2	47.4	60.6	48.3	61.8	47.1	69.9	50.3	74.6	54.0
PD-7-042413-4.1	56.1	48.5	69.2	50.8	66.8	51.4	68.2	49.8	77.8	53.9	83.9	58.7
PD-7-042413-4.8	62.7	52.4	76.2	54.8	74.5	55.0	76.3	52.9	87.4	58.4	95.4	64.8
PD-7-042413-5.3	67.7	55.4	81.5	57.8	80.0	57.6	81.9	55.1	94.5	61.6	104.0	69.4
PD-7-042413-5.9	75.0	59.9	89.3	62.0	87.7	61.1	90.4	58.4	104.5	66.5	116.0	76.6
PD-7-042413-6.5	83.9	65.8	98.4	66.9	96.4	65.2	99.9	62.5	115.8	72.8	130.2	86.0
PD-7-042413-7.1	92.2	71.7	106.9	72.0	102.6	69.1	109.6	66.6	127.4	79.1	144.1	95.6
PD-7-042413-7.7	100.6	77.8	121.1	77.0	112.4	72.9	118.6	70.7	138.3	85.0	157.0	104.5
PD-7-042413-8.52	112.2	86.5	135.8	84.2	125.3	78.7	132.3	77.4	155.1	95.6	176.7	120.1
PD-7-042413-9.5	126.2	97.4	155.4	93.1	140.4	85.9	149.5	86.5	176.2	110.2	200.9	140.7
PD-7-042413-10.1	135.4	104.5	161.0	99.2	150.4	91.0	160.9	93.5	190.2	121.1	217.0	155.1
PD-7-042413-10.7	144.8	111.8	173.1	105.6	160.6	96.6	173.1	101.6	205.5	133.3	234.2	171.0
PD-7-042413-11.3	154.7	119.3	186.1	112.5	171.5	102.9	186.4	111.0	221.6	146.7	251.8	188.0

Table C.34: Steady-state parameters of the loop (processed data) (PD-7-042413)

Test ID	Power (kW)	Flow rate (kg/s)	Inlet K	Outlet K	Outlet Temp. Calculated (C)	T11(C)	Total Ch. PD (Pa)	Acc. PD.(Pa)	Fr. PD.(Pa)
PD-7-042413-1.2	1.32 ± 0.03	0.030 ± 0.001	0	0	34.7 ± 0.3	34.8 ± 2.2	225.1 ± 13.3	16.9 ± 1.6	208.2 ± 13.4
PD-7-042413-1.7	1.86 ± 0.03	0.035 ± 0.001	0	0	35.6 ± 0.2	36.0 ± 2.2	296.6 ± 16.7	30.3 ± 2.4	266.2 ± 16.8
PD-7-042413-2.3	2.52 ± 0.04	0.040 ± 0.001	0	0	36.4 ± 0.2	37.0 ± 2.2	381.9 ± 20.4	51.1 ± 3.7	330.8 ± 20.7
PD-7-042413-2.9	3.17 ± 0.04	0.043 ± 0.001	0	0	37.1 ± 0.2	37.9 ± 2.2	464.9 ± 24.3	78.1 ± 5.2	386.8 ± 24.9
PD-7-042413-3.5	3.83 ± 0.04	0.046 ± 0.001	0	0	37.6 ± 0.2	38.5 ± 2.2	546.2 ± 29.6	108.5 ± 7.2	437.6 ± 30.5
PD-7-042413-4.1	4.48 ± 0.05	0.049 ± 0.001	0	0	38.3 ± 0.2	39.2 ± 2.2	631.5 ± 33.7	145.7 ± 8.9	485.9 ± 34.8
PD-7-042413-4.8	5.25 ± 0.05	0.051 ± 0.001	0	0	38.9 ± 0.3	39.9 ± 2.2	728.8 ± 36.3	192.2 ± 11.2	536.6 ± 38.0
PD-7-042413-5.3	5.80 ± 0.05	0.052 ± 0.001	0	0	39.5 ± 0.3	40.6 ± 2.2	800.5 ± 40.2	228.5 ± 13.0	572.0 ± 42.3
PD-7-042413-5.9	6.45 ± 0.06	0.053 ± 0.001	0	0	40.8 ± 0.4	41.8 ± 2.2	886.2 ± 44.5	275.6 ± 15.6	610.5 ± 47.1
PD-7-042413-6.5	7.11 ± 0.06	0.053 ± 0.001	0	0	43.1 ± 0.6	43.8 ± 2.2	978.6 ± 48.6	330.9 ± 17.9	647.7 ± 51.8
PD-7-042413-7.1	7.76 ± 0.06	0.054 ± 0.001	0	0	45.6 ± 0.8	46.1 ± 2.2	1063.1 ± 136.9	385.2 ± 19.9	678.0 ± 138.3
PD-7-042413-7.7	8.42 ± 0.06	0.054 ± 0.001	0	0	48.5 ± 1.0	48.7 ± 2.2	1158.1 ± 76.4	439.6 ± 22.0	718.5 ± 79.5
PD-7-042413-8.52	9.32 ± 0.07	0.055 ± 0.001	0	0	53.7 ± 1.4	53.0 ± 2.2	1276.9 ± 73.1	514.4 ± 25.2	762.5 ± 77.3
PD-7-042413-9.5	10.39 ± 0.07	0.055 ± 0.001	0	0	61.3 ± 1.9	58.9 ± 2.2	1420.4 ± 85.3	607.1 ± 29.5	813.2 ± 90.3
PD-7-042413-10.1	11.04 ± 0.07	0.055 ± 0.001	0	0	68.0 ± 2.3	63.1 ± 2.3	1501.7 ± 92.2	661.9 ± 31.3	839.8 ± 97.4
PD-7-042413-10.7	11.70 ± 0.08	0.054 ± 0.001	0	0	75.7 ± 2.8	69.3 ± 2.2	1593.4 ± 99.5	719.8 ± 35.6	873.6 ± 105.7
PD-7-042413-11.3	12.36 ± 0.08	0.054 ± 0.001	0	0	85.0 ± 3.3	75.3 ± 2.4	1674.9 ± 106.7	771.9 ± 38.2	903.1 ± 113.3

Table C.35: Comparison between frictional pressure-drop from the experimental against available friction-factor formulae (PD-7-042413)

Test ID	Fr. PD.(Pa)-Exp.	Blasius	Kondratev	Ishigai	Razumovskiy	Tarasova & Leontev	Yamashita	Popov	Kuraeva & Protopopov
PD-7-042413-1.2	208.2	164.8	135.5	127.6	137.9	142.7	105.3	132.9	283.8
PD-7-042413-1.7	266.2	225.6	184.8	162.3	178.7	188.4	129.6	167.9	370.2
PD-7-042413-2.3	330.8	287.3	234.5	199.6	221.4	236.6	159.3	203.6	455.9
PD-7-042413-2.9	386.8	346.3	281.8	237.8	263.9	284.9	193.0	238.4	537.3
PD-7-042413-3.5	437.6	400.1	324.9	273.5	303.2	330.0	226.1	270.2	611.2
PD-7-042413-4.1	485.9	451.6	365.8	310.5	342.7	375.4	263.3	301.7	682.6
PD-7-042413-4.8	536.6	506.6	409.6	350.4	385.1	424.7	305.1	334.6	758.7
PD-7-042413-5.3	572.0	545.2	440.3	379.1	415.4	460.1	336.4	357.9	812.2
PD-7-042413-5.9	610.5	584.4	471.3	411.3	448.2	498.6	375.0	382.6	867.8
PD-7-042413-6.5	647.7	623.3	501.8	447.6	483.8	540.1	421.7	409.8	924.1
PD-7-042413-7.1	678.0	658.2	529.3	480.5	515.9	577.7	465.3	433.9	974.4
PD-7-042413-7.7	718.5	694.3	557.8	513.4	548.2	615.9	509.1	458.0	1025.6
PD-7-042413-8.52	762.5	741.0	594.6	558.3	591.7	667.0	570.9	490.4	1092.3
PD-7-042413-9.5	813.2	796.3	638.2	613.2	644.4	729.2	649.3	529.3	1171.0
PD-7-042413-10.1	839.8	826.2	661.8	646.4	675.4	764.9	698.4	553.2	1213.2
PD-7-042413-10.7	873.6	858.8	687.5	683.1	709.6	804.3	753.7	579.4	1258.8
PD-7-042413-11.3	903.1	889.1	711.5	718.4	742.1	841.5	807.1	604.9	1300.5

May 1st, 2013- System Pressure: 8.5 MPa, Inlet Temperature: 25-26 ℃, Inlet valve: wide open, Outlet valve: 30º closed

Table C.36: Averaged values of measured signals during experiment for each data point (PD-8-050113)

Test ID	Inlet Temperature (RTD1) (C)	Pressure (MPa)	Power (kW)	Outlet Temp (RTD2)(C)	T11 (C)	T12(C)	CO_2 volumetric Flow rate $(m^3/s) \times 10^6$	HE-Inlet water Temp.(C)	HE-Outlet water Temp.(C)	Water Flow rate (lpm)
PD-8-050113-1.2	24.9 ± 0.4	8.49 ± 0.02	1.32 ± 0.03	32.8 ± 0.5	34.5 ± 2.2	25.3 ± 2.2	36.8 ± 1.2	10.1 ± 2.2	30.6 ± 2.2	0.7
PD-8-050113-1.7	25.1 ± 0.4	8.50 ± 0.02	1.86 ± 0.03	34.0 ± 0.5	35.8 ± 2.2	24.8 ± 2.2	44.1 ± 1.1	11.1 ± 2.2	29.1 ± 2.2	1.5
PD-8-050113-2.3	25.3 ± 0.4	8.49 ± 0.02	2.52 ± 0.03	34.9 ± 0.5	36.9 ± 2.2	24.8 ± 2.2	49.7 ± 1.1	10.7 ± 2.2	27.8 ± 2.2	2.2
PD-8-050113-2.9	25.1 ± 0.4	8.50 ± 0.02	3.18 ± 0.04	35.6 ± 0.5	37.5 ± 2.2	24.8 ± 2.2	53.8 ± 1.1	10.5 ± 2.2	25.9 ± 2.2	3.2
PD-8-050113-3.5	25.1 ± 0.4	8.49 ± 0.02	3.83 ± 0.04	36.2 ± 0.5	38.2 ± 2.2	24.7 ± 2.2	57.1 ± 1.2	9.4 ± 2.2	24.3 ± 2.2	4.1
PD-8-050113-4.1	25.8 ± 0.4	8.51 ± 0.02	4.49 ± 0.05	37.0 ± 0.5	39.2 ± 2.2	24.5 ± 2.2	59.7 ± 1.2	7.4 ± 2.2	23.3 ± 2.2	4.5
PD-8-050113-4.7	25.8 ± 0.4	8.50 ± 0.02	5.14 ± 0.05	37.6 ± 0.5	40.1 ± 2.2	24.9 ± 2.2	61.5 ± 1.2	6.8 ± 2.2	21.4 ± 2.2	5.6
PD-8-050113-5.3	25.9 ± 0.4	8.50 ± 0.02	5.80 ± 0.05	38.5 ± 0.5	41.5 ± 2.2	24.5 ± 2.2	62.9 ± 1.2	6.3 ± 2.2	20.3 ± 2.2	6.7
PD-8-050113-5.9	26.2 ± 0.4	8.50 ± 0.02	6.46 ± 0.06	39.9 ± 0.5	43.6 ± 2.2	24.7 ± 2.2	63.7 ± 1.2	5.9 ± 2.2	20.8 ± 2.2	7.3
PD-8-050113-6.5	26.2 ± 0.4	8.50 ± 0.02	7.11 ± 0.06	41.6 ± 0.5	46.2 ± 2.2	25.1 ± 2.2	63.9 ± 1.2	5.5 ± 2.2	19.8 ± 2.2	8.3
PD-8-050113-7.2	25.9 ± 0.4	8.50 ± 0.02	7.88 ± 0.06	44.0 ± 0.5	49.8 ± 2.2	24.6 ± 2.2	63.9 ± 1.2	5.3 ± 2.2	18.5 ± 2.2	9.8
PD-8-050113-7.7	26.1 ± 0.4	8.50 ± 0.02	8.42 ± 0.06	47.0 ± 0.5	53.7 ± 2.2	24.6 ± 2.2	63.6 ± 1.2	5.4 ± 2.2	18.6 ± 2.2	10.4
PD-8-050113-8.3	26.3 ± 0.4	8.52 ± 0.02	9.08 ± 0.07	51.5 ± 0.6	59.0 ± 2.2	25.0 ± 2.2	62.8 ± 1.3	5.2 ± 2.2	18.5 ± 2.2	11.1
PD-8-050113-8.9	26.0 ± 0.4	8.51 ± 0.02	9.74 ± 0.07	56.0 ± 0.6	64.7 ± 2.2	24.5 ± 2.2	62.6 ± 1.4	5.2 ± 2.2	17.7 ± 2.2	12.6
PD-8-050113-9.5	26.0 ± 0.4	8.51 ± 0.02	10.39 ± 0.07	62.4 ± 0.6	71.6 ± 2.2	24.4 ± 2.2	61.6 ± 1.3	5.0 ± 2.2	17.4 ± 2.2	13.4
PD-8-050113-10.1	26.0 ± 0.4	8.51 ± 0.02	11.05 ± 0.07	70.1 ± 0.6	81.1 ± 2.2	24.3 ± 2.2	61.2 ± 1.2	4.9 ± 2.2	17.1 ± 2.2	14.7
PD-8-050113-10.7	26.1 ± 0.4	8.50 ± 0.02	11.70 ± 0.08	79.7 ± 0.7	89.4 ± 2.3	24.5 ± 2.2	60.4 ± 1.2	4.7 ± 2.2	17.5 ± 2.2	14.5
PD-8-050113-11.3	26.3 ± 0.4	8.50 ± 0.02	12.36 ± 0.08	93.8 ± 0.7	101.5 ± 2.3	25.1 ± 2.2	59.2 ± 1.3	4.7 ± 2.2	17.6 ± 2.2	15.1
PD-8-050113-11.9	25.9 ± 0.4	8.50 ± 0.02	13.02 ± 0.08	104.5 ± 0.8	111.1 ± 2.4	24.8 ± 2.2	59.2 ± 1.2	4.7 ± 2.2	16.7 ± 2.2	17.1
PD-8-050113-12.4	25.8 ± 0.4	8.51 ± 0.02	13.57 ± 0.08	116.5 ± 0.8	120.3 ± 2.4	25.0 ± 2.2	56.7 ± 2.8	4.7 ± 2.2	16.2 ± 2.2	18.4

Table C.37: Averaged values of measured pressure-drops during experiment for each data point (PD-8-050113)

Test ID	DP2-1 (Pa)	DP2-2 (Pa)	DP2-3 (Pa)	DP2-4 (Pa)	DP2-5 (Pa)	DP3 (Pa)	DP13 (Pa)	DP10 (Pa)
PD-8-050113-1.2	94.3 ± 11.4	26.25 ± 11.79	55.47 ± 11.81	36.5 ± 11.3	62.7 ± 11.2	322.2 ± 11.4	226.9 ± 16.1	362.4 ± 126.6
PD-8-050113-1.7	118.9 ± 12.2	34.86 ± 12.59	78.83 ± 12.52	53.4 ± 11.9	71.8 ± 11.8	342.3 ± 12.2	304.7 ± 21.4	458.1 ± 126.4
PD-8-050113-2.3	141.9 ± 12.4	43.99 ± 12.45	104.56 ± 12.28	73.8 ± 12.3	82.4 ± 11.7	360.4 ± 12.4	388.9 ± 22.3	569.7 ± 125.8
PD-8-050113-2.9	161.0 ± 13.2	52.33 ± 13.23	128.69 ± 12.96	94.3 ± 13.2	95.2 ± 12.2	375.1 ± 13.2	469.3 ± 25.3	679.4 ± 127.9
PD-8-050113-3.5	177.1 ± 14.3	60.93 ± 14.38	152.63 ± 14.24	115.5 ± 14.4	110.9 ± 13.3	386.0 ± 14.3	550.1 ± 31.0	793.0 ± 132.4
PD-8-050113-4.1	191.7 ± 15.6	70.91 ± 16.05	177.74 ± 15.60	139.4 ± 15.9	128.5 ± 14.3	397.2 ± 15.6	635.1 ± 34.6	919.3 ± 143.2
PD-8-050113-4.7	202.4 ± 17.0	80.34 ± 17.25	201.06 ± 17.07	163.6 ± 17.4	146.8 ± 15.6	401.2 ± 17.0	716.5 ± 40.0	1036.5 ± 137.9
PD-8-050113-5.3	212.4 ± 17.5	89.97 ± 17.83	224.37 ± 17.10	189.2 ± 18.0	165.7 ± 15.6	406.9 ± 17.5	799.4 ± 41.2	1157.2 ± 136.5
PD-8-050113-5.9	220.3 ± 18.9	100.54 ± 18.92	248.27 ± 18.05	216.8 ± 19.1	181.8 ± 16.5	410.0 ± 18.9	880.8 ± 46.2	1281.0 ± 142.6
PD-8-050113-6.5	226.6 ± 20.3	110.39 ± 20.03	270.54 ± 19.75	244.1 ± 20.1	201.8 ± 17.8	410.1 ± 20.3	961.5 ± 52.5	1405.1 ± 145.6
PD-8-050113-7.2	232.8 ± 22.2	119.76 ± 21.78	297.15 ± 20.90	276.0 ± 20.7	225.1 ± 18.8	410.0 ± 22.2	1053.4 ± 58.0	1544.7 ± 148.6
PD-8-050113-7.7	235.8 ± 22.8	128.75 ± 22.18	316.17 ± 21.89	299.6 ± 22.8	241.0 ± 19.7	411.0 ± 22.8	1120.7 ± 64.2	1641.2 ± 132.6
PD-8-050113-8.3	239.0 ± 24.6	138.58 ± 24.42	339.45 ± 23.70	326.8 ± 23.6	257.4 ± 21.1	415.4 ± 24.6	1196.3 ± 71.8	1741.9 ± 164.1
PD-8-050113-8.9	242.5 ± 26.1	146.42 ± 25.45	363.94 ± 24.56	355.0 ± 24.5	272.6 ± 21.9	418.2 ± 26.1	1271.2 ± 79.3	1837.6 ± 151.8
PD-8-050113-9.5	245.4 ± 27.5	156.40 ± 27.47	388.60 ± 25.75	383.1 ± 25.0	285.7 ± 22.7	408.9 ± 27.5	1345.9 ± 86.3	1909.8 ± 154.1
PD-8-050113-10.1	248.3 ± 29.8	169.60 ± 29.19	413.39 ± 27.32	411.7 ± 26.2	295.5 ± 24.0	399.5 ± 29.8	1422.9 ± 96.5	1998.7 ± 151.9
PD-8-050113-10.7	249.0 ± 31.2	183.14 ± 30.83	438.57 ± 28.54	438.3 ± 27.0	302.9 ± 25.0	391.6 ± 31.2	1495.8 ± 99.4	2078.5 ± 158.7
PD-8-050113-11.3	257.9 ± 46.6	195.32 ± 84.80	466.50 ± 44.66	467.2 ± 38.3	306.6 ± 29.7	382.4 ± 46.6	1575.9 ± 143.1	2159.7 ± 180.0
PD-8-050113-11.9	265.3 ± 66.1	205.55 ± 123.16	493.32 ± 56.03	493.7 ± 46.3	317.0 ± 35.4	377.6 ± 66.1	1655.5 ± 195.2	2236.8 ± 160.6
PD-8-050113-12.4	281.4 ± 105.2	213.82 ± 184.35	511.73 ± 69.54	510.6 ± 58.4	326.5 ± 46.8	377.0 ± 105.2	1722.8 ± 288.2	2281.6 ± 91.3

Table C.38: Averaged values of measured wall surface temperature during experiment for each data point (PD-8-050113)

Test ID	TS21T (C)	TS21B (C)	TS22T (C)	TS22B (C)	TS23T (C)	TS23B (C)	TS24T (C)	TS24B (C)	TS25T (C)	TS25B (C)	TS26T (C)	TS26B (C)
PD-8-050113-1.2	36.8	34.8	42.1	36.1	41.7	37.0	42.8	37.2	46.4	38.9	47.6	39.8
PD-8-050113-1.7	39.9	37.5	46.9	38.8	45.9	39.7	46.9	39.5	51.0	41.4	52.4	42.7
PD-8-050113-2.3	43.5	40.2	52.9	41.6	51.3	42.6	51.9	42.0	57.5	44.3	59.7	46.7
PD-8-050113-2.9	47.4	42.7	59.1	44.4	56.8	45.3	57.6	44.5	64.5	47.4	67.9	50.5
PD-8-050113-3.5	52.2	45.6	65.8	47.6	62.9	48.4	63.9	47.0	72.5	50.8	77.1	55.0
PD-8-050113-4.1	58.7	49.5	73.3	51.6	70.2	51.9	71.4	50.2	81.4	55.2	87.9	60.8
PD-8-050113-4.7	65.6	53.5	81.4	55.6	77.6	55.4	79.4	53.2	90.9	59.6	99.2	67.2
PD-8-050113-5.3	73.3	58.2	89.3	60.0	85.6	59.1	88.0	56.7	101.1	64.6	111.9	74.8
PD-8-050113-5.9	82.3	64.1	98.4	65.0	94.4	63.1	97.5	60.8	112.7	70.8	126.4	84.2
PD-8-050113-6.5	91.5	70.3	110.0	70.3	103.7	67.4	107.7	65.3	124.9	77.6	141.7	94.5
PD-8-050113-7.2	102.1	77.9	152.4	76.8	114.6	72.5	119.7	70.8	139.5	86.1	159.3	107.2
PD-8-050113-7.7	110.3	84.3	170.8	82.1	123.5	76.7	129.7	76.2	152.1	94.8	174.4	119.8
PD-8-050113-8.3	120.2	92.0	154.8	88.8	134.6	82.2	142.3	83.5	168.2	106.7	193.4	136.4
PD-8-050113-8.9	129.8	99.4	179.1	95.5	145.2	87.7	154.4	90.8	183.6	118.3	211.2	152.1
PD-8-050113-9.5	140.1	107.3	196.5	102.8	156.6	94.0	168.1	99.9	200.8	132.3	231.0	170.2
PD-8-050113-10.1	150.2	115.2	196.4	110.2	168.4	100.8	182.5	110.3	218.6	147.3	251.1	189.4
PD-8-050113-10.7	161.3	123.6	199.8	118.7	181.1	108.8	198.1	122.8	238.2	164.4	272.8	211.0
PD-8-050113-11.3	170.9	131.2	208.7	123.9	192.6	118.3	215.6	137.9	259.9	183.7	295.6	234.7
PD-8-050113-11.9	178.7	137.3	214.0	127.1	203.4	126.5	230.3	150.2	277.8	199.4	314.3	253.8
PD-8-050113-12.4	180.4	139.7	210.2	126.4	213.0	134.6	244.4	163.7	295.1	215.6	332.6	273.1

Table C.39: Steady-state parameters of the loop (processed data) (PD-8-050113)

Test ID	Power (kW)	Flow rate (kg/s)	Inlet K	Outlet K*	Outlet Temp. Calculated (C)	T11(C)	Total Ch. PD (Pa)	Acc. PD.(Pa)	Fr. PD.(Pa)
PD-8-050113-1.2	1.32 ± 0.03	0.029 ± 0.001	0	9.5	34.7 ± 0.3	34.5 ± 2.2	217.5 ± 16.1	16.5 ± 1.6	201.0 ± 16.2
PD-8-050113-1.7	1.86 ± 0.03	0.035 ± 0.001	0	7.5	35.7 ± 0.2	35.8 ± 2.2	290.9 ± 21.4	30.6 ± 2.4	260.3 ± 21.6
PD-8-050113-2.3	2.52 ± 0.03	0.039 ± 0.001	0	6.8	36.5 ± 0.2	36.9 ± 2.2	370.7 ± 22.3	51.9 ± 3.8	318.8 ± 22.6
PD-8-050113-2.9	3.18 ± 0.04	0.042 ± 0.001	0	6.5	37.1 ± 0.2	37.5 ± 2.2	447.1 ± 25.3	77.0 ± 5.2	370.1 ± 25.8
PD-8-050113-3.5	3.83 ± 0.04	0.045 ± 0.001	0	6.4	37.6 ± 0.2	38.2 ± 2.2	524.1 ± 31.0	107.1 ± 6.9	417.0 ± 31.8
PD-8-050113-4.1	4.49 ± 0.05	0.047 ± 0.001	0	6.4	38.5 ± 0.2	39.2 ± 2.2	605.4 ± 34.6	144.4 ± 9.1	461.0 ± 35.7
PD-8-050113-4.7	5.14 ± 0.05	0.048 ± 0.001	0	6.3	39.3 ± 0.3	40.1 ± 2.2	683.5 ± 40.0	183.9 ± 11.0	499.7 ± 41.5
PD-8-050113-5.3	5.80 ± 0.05	0.049 ± 0.001	0	6.3	40.6 ± 0.4	41.5 ± 2.2	763.2 ± 41.2	226.7 ± 13.6	536.5 ± 43.4
PD-8-050113-5.9	6.46 ± 0.06	0.049 ± 0.001	0	6.3	42.6 ± 0.6	43.6 ± 2.2	841.7 ± 46.2	274.4 ± 15.5	567.3 ± 48.7
PD-8-050113-6.5	7.11 ± 0.06	0.049 ± 0.001	0	6.3	45.3 ± 0.9	46.2 ± 2.2	919.9 ± 52.5	322.1 ± 18.3	597.8 ± 55.6
PD-8-050113-7.2	7.88 ± 0.06	0.050 ± 0.001	0	6.3	49.2 ± 1.2	49.8 ± 2.2	1009.0 ± 58.0	378.1 ± 20.9	630.9 ± 61.6
PD-8-050113-7.7	8.42 ± 0.06	0.049 ± 0.001	0	6.2	53.9 ± 1.6	53.7 ± 2.2	1074.4 ± 64.2	421.3 ± 23.4	653.1 ± 68.3
PD-8-050113-8.3	9.08 ± 0.07	0.049 ± 0.001	0	6.1	61.1 ± 2.1	59.0 ± 2.2	1148.2 ± 71.8	470.8 ± 26.1	677.4 ± 76.4
PD-8-050113-8.9	9.74 ± 0.07	0.049 ± 0.001	0	5.9	67.7 ± 2.8	64.7 ± 2.2	1220.7 ± 79.3	521.0 ± 31.0	699.7 ± 85.1
PD-8-050113-9.5	10.39 ± 0.07	0.048 ± 0.001	0	5.7	77.5 ± 3.1	71.6 ± 2.2	1293.8 ± 86.3	567.7 ± 30.8	726.2 ± 91.6
PD-8-050113-10.1	11.05 ± 0.07	0.047 ± 0.001	0	5.5	87.4 ± 3.6	81.1 ± 2.2	1368.7 ± 96.5	616.2 ± 32.3	752.6 ± 101.7
PD-8-050113-10.7	11.70 ± 0.08	0.047 ± 0.001	0	5.3	99.4 ± 4.2	89.4 ± 2.3	1439.9 ± 99.4	662.0 ± 34.8	777.9 ± 105.3
PD-8-050113-11.3	12.36 ± 0.08	0.046 ± 0.001	0	5.2	115.0 ± 5.1	101.5 ± 2.3	1519.0 ± 143.1	700.7 ± 38.8	818.3 ± 148.2
PD-8-050113-11.9	13.02 ± 0.08	0.046 ± 0.001	0	5.1	124.1 ± 5.1	111.1 ± 2.4	1596.3 ± 195.2	746.8 ± 38.1	849.4 ± 198.9
PD-8-050113-12.4	13.57 ± 0.08	0.044 ± 0.002	0	5.1	143.1 ± 12.7	120.3 ± 2.4	1664.6 ± 288.2	759.3 ± 88.2	905.3 ± 301.4

* Mean outlet K factor: 6.2

Table C.40: Comparison between frictional pressure-drop from the experimental against available friction-factor formulae (PD-8-050113)

Test ID	Fr. PD.(Pa)-Exp.	Blasius	Kondratev	Ishigai	Razumovskiy	Tarasova & Leontev	Yamashita	Popov	Kuraeva & Protopopov
PD-8-050113-1.2	201.0	156.2	128.5	120.5	130.4	135.1	99.3	125.6	270.7
PD-8-050113-1.7	260.3	220.1	180.3	157.9	174.0	183.7	126.2	163.0	362.1
PD-8-050113-2.3	318.8	279.6	228.2	194.0	215.2	230.5	155.7	197.1	445.1
PD-8-050113-2.9	370.1	331.9	270.2	227.0	252.2	272.9	184.6	227.0	517.4
PD-8-050113-3.5	417.0	380.1	308.7	259.2	287.4	313.7	215.3	254.8	584.4
PD-8-050113-4.1	461.0	424.6	344.1	292.7	322.6	354.4	250.9	282.4	647.6
PD-8-050113-4.7	499.7	464.0	375.4	322.5	353.7	391.1	284.4	305.9	703.5
PD-8-050113-5.3	536.5	501.4	405.0	352.7	384.6	427.4	320.0	329.2	757.0
PD-8-050113-5.9	567.3	534.5	431.1	382.6	414.2	462.2	358.7	351.2	805.6
PD-8-050113-6.5	597.8	563.0	453.5	409.8	440.5	493.4	395.9	370.5	847.8
PD-8-050113-7.2	630.9	595.4	479.1	440.3	470.0	529.4	439.7	390.8	896.2
PD-8-050113-7.7	653.1	616.9	496.0	464.9	492.7	556.0	476.7	407.6	928.8
PD-8-050113-8.3	677.4	639.8	514.1	493.5	518.9	585.3	519.4	428.6	962.2
PD-8-050113-8.9	699.7	670.0	537.9	524.5	548.2	620.0	565.1	450.1	1006.0
PD-8-050113-9.5	726.2	692.8	555.9	553.3	574.2	649.7	610.1	470.4	1038.6
PD-8-050113-10.1	752.6	722.9	579.8	587.0	605.7	685.5	660.1	495.1	1080.4
PD-8-050113-10.7	777.9	750.7	601.9	620.1	635.4	720.0	710.7	519.2	1118.5
PD-8-050113-11.3	818.3	773.9	620.4	651.4	662.8	750.6	758.9	542.9	1148.2
PD-8-050113-11.9	849.4	808.5	648.1	686.0	695.5	789.2	809.5	568.0	1195.7
PD-8-050113-12.4	905.3	808.5	648.4	697.7	703.7	794.9	827.7	579.4	1188.6

May 2nd, 2013- System Pressure: 7.6 MPa, Inlet Temperature: 25-26 ºC, Inlet valve: 44º closed, Outlet valve: wide open

Table C.41: Averaged values of measured signals during experiment for each data point (PD-9-050213)

Test ID	Inlet Temperature (RTD1) (C)	Pressure (MPa)	Power (kW)	Outlet Temp (RTD2)(C)	T11 (C)	T12(C)	CO_2 volumetric Flow rate $(m^3/s)\times10^6$	HE-Inlet water Temp.(C)	HE-Outlet water Temp.(C)	Water Flow rate (lpm)
PD-9-050213-2.9	25.5 ± 0.4	7.59 ± 0.02	3.17 ± 0.04	30.5 ± 0.5	32.3 ± 2.2	25.0 ± 2.2	50.1 ± 1.1	9.1 ± 2.2	24.2 ± 2.2	3.4
PD-9-050213-3.5	25.6 ± 0.4	7.60 ± 0.02	3.83 ± 0.04	31.0 ± 0.5	33.1 ± 2.2	25.2 ± 2.2	52.4 ± 1.1	8.8 ± 2.2	23.1 ± 2.2	4.3
PD-9-050213-4.1	25.3 ± 0.4	7.61 ± 0.02	4.49 ± 0.05	31.7 ± 0.5	34.2 ± 2.2	24.9 ± 2.2	53.8 ± 1.1	8.0 ± 2.2	21.2 ± 2.2	5.5
PD-9-050213-4.7	25.6 ± 0.4	7.61 ± 0.02	5.14 ± 0.05	33.2 ± 0.5	36.4 ± 2.2	25.0 ± 2.2	55.0 ± 1.1	7.0 ± 2.2	20.5 ± 2.2	6.2
PD-9-050213-5.3	25.5 ± 0.4	7.61 ± 0.02	5.80 ± 0.05	34.8 ± 0.5	39.2 ± 2.2	24.8 ± 2.2	56.0 ± 1.1	6.5 ± 2.2	19.1 ± 2.2	7.5
PD-9-050213-5.9	25.6 ± 0.4	7.61 ± 0.02	6.45 ± 0.06	37.9 ± 0.5	43.3 ± 2.2	24.7 ± 2.2	56.6 ± 1.1	5.9 ± 2.2	17.8 ± 2.2	8.8
PD-9-050213-6.5	25.6 ± 0.4	7.61 ± 0.02	7.11 ± 0.06	41.9 ± 0.5	48.5 ± 2.2	24.8 ± 2.2	56.6 ± 1.2	5.5 ± 2.2	17.4 ± 2.2	9.6
PD-9-050213-7.1	25.6 ± 0.4	7.61 ± 0.02	7.77 ± 0.06	47.2 ± 0.5	54.9 ± 2.2	24.8 ± 2.2	56.8 ± 1.1	5.3 ± 2.2	17.3 ± 2.2	10.5
PD-9-050213-7.7	25.8 ± 0.4	7.60 ± 0.02	8.42 ± 0.06	54.4 ± 0.6	62.6 ± 2.2	24.8 ± 2.2	56.7 ± 1.2	5.2 ± 2.2	16.9 ± 2.2	11.5
PD-9-050213-8.3	25.9 ± 0.4	7.61 ± 0.02	9.08 ± 0.07	63.2 ± 0.6	71.7 ± 2.2	24.9 ± 2.2	56.5 ± 1.1	5.1 ± 2.2	17.2 ± 2.2	11.9
PD-9-050213-8.9	25.8 ± 0.4	7.61 ± 0.02	9.74 ± 0.07	72.3 ± 0.6	81.0 ± 2.3	24.6 ± 2.2	56.1 ± 1.2	4.9 ± 2.2	16.6 ± 2.2	13.2
PD-9-050213-9.5	26.0 ± 0.4	7.61 ± 0.02	10.39 ± 0.07	85.1 ± 0.7	94.1 ± 2.2	24.9 ± 2.2	55.7 ± 1.2	4.9 ± 2.2	17.0 ± 2.2	13.5
PD-9-050213-10.1	25.8 ± 0.4	7.62 ± 0.02	11.05 ± 0.07	95.0 ± 0.7	104.3 ± 2.2	24.6 ± 2.2	55.4 ± 1.2	4.8 ± 2.2	16.1 ± 2.2	15.3
PD-9-050213-10.7	25.7 ± 0.4	7.62 ± 0.02	11.71 ± 0.08	107.5 ± 0.8	114.4 ± 2.3	24.5 ± 2.2	54.7 ± 1.1	4.6 ± 2.2	16.3 ± 2.2	15.6

Table C.42: Averaged values of measured pressure-drops during experiment for each data point (PD-9-050213)

Test ID	DP2-1 (Pa)	DP2-2 (Pa)	DP2-3 (Pa)	DP2-4 (Pa)	DP2-5 (Pa)	DP3 (Pa)	DP13 (Pa)	DP10 (Pa)
PD-9-050213-2.9	124.3 ± 14.2	31.88 ± 14.35	80.30 ± 14.17	87.7 ± 13.9	76.7 ± 13.1	1492.1 ± 14.2	460.1 ± 27.6	749.7 ± 155.5
PD-9-050213-3.5	136.6 ± 14.5	41.98 ± 14.20	103.23 ± 14.03	109.9 ± 14.9	93.1 ± 13.2	1607.8 ± 14.5	541.6 ± 30.9	769.7 ± 118.7
PD-9-050213-4.1	147.3 ± 21.8	51.23 ± 21.88	124.51 ± 21.47	132.9 ± 19.9	109.8 ± 18.7	1708.9 ± 21.8	620.1 ± 89.6	802.7 ± 126.5
PD-9-050213-4.7	157.6 ± 18.0	63.88 ± 18.48	149.27 ± 18.29	160.0 ± 17.8	126.5 ± 16.4	1770.2 ± 18.0	708.6 ± 48.0	854.6 ± 127.0
PD-9-050213-5.3	166.1 ± 19.0	74.82 ± 19.72	172.36 ± 19.27	187.7 ± 19.0	143.6 ± 17.3	1829.5 ± 19.0	793.5 ± 51.9	898.4 ± 132.4
PD-9-050213-5.9	173.4 ± 20.0	87.61 ± 20.43	196.51 ± 19.90	217.1 ± 19.9	161.4 ± 17.9	1853.9 ± 20.0	882.4 ± 55.6	950.0 ± 132.6
PD-9-050213-6.5	180.7 ± 21.3	99.43 ± 21.94	220.70 ± 21.55	241.6 ± 22.0	183.3 ± 19.4	1872.5 ± 21.3	969.7 ± 62.0	993.3 ± 125.7
PD-9-050213-7.1	186.5 ± 23.0	110.42 ± 23.15	241.29 ± 22.30	276.7 ± 23.7	195.3 ± 20.1	1875.8 ± 23.0	1050.9 ± 70.7	1037.3 ± 136.0
PD-9-050213-7.7	193.4 ± 23.7	120.50 ± 23.88	254.11 ± 22.67	325.1 ± 24.6	211.4 ± 20.8	1866.3 ± 23.7	1142.1 ± 74.6	1066.3 ± 136.4
PD-9-050213-8.3	203.1 ± 24.6	128.76 ± 25.34	283.71 ± 23.81	357.4 ± 25.5	223.5 ± 21.8	1851.6 ± 24.6	1231.3 ± 75.9	1048.5 ± 135.9
PD-9-050213-8.9	210.5 ± 26.6	138.77 ± 26.36	313.41 ± 24.29	384.0 ± 26.3	232.9 ± 22.5	1843.1 ± 26.6	1312.7 ± 89.8	1045.0 ± 130.8
PD-9-050213-9.5	218.7 ± 27.4	149.16 ± 26.69	345.78 ± 24.67	411.3 ± 26.4	239.9 ± 23.0	1810.5 ± 27.4	1395.8 ± 92.1	1045.8 ± 136.4
PD-9-050213-10.1	224.8 ± 29.9	158.70 ± 28.71	372.22 ± 26.39	442.1 ± 27.7	248.4 ± 24.9	1803.8 ± 29.9	1475.9 ± 103.1	1063.4 ± 137.2
PD-9-050213-10.7	231.3 ± 32.0	156.64 ± 31.43	416.45 ± 27.39	467.6 ± 29.4	255.4 ± 25.3	1779.6 ± 32.0	1555.4 ± 105.4	1070.0 ± 96.6

Table C.43: Averaged values of measured wall surface temperature during experiment for each data point (PD-9-050213)

Test ID	TS21T (C)	TS21B (C)	TS22T (C)	TS22B (C)	TS23T (C)	TS23B (C)	TS24T (C)	TS24B (C)	TS25T (C)	TS25B (C)	TS26T (C)	TS26B (C)
PD-9-050213-2.9	52.0	43.0	64.3	43.2	59.5	42.7	58.6	40.8	65.0	44.0	68.8	47.3
PD-9-050213-3.5	59.5	47.9	73.4	47.7	66.9	46.3	66.5	44.0	75.2	48.6	81.0	54.0
PD-9-050213-4.1	66.7	52.9	82.5	52.2	74.7	50.0	75.0	47.3	85.7	53.5	93.8	61.6
PD-9-050213-4.7	75.2	59.2	92.3	57.6	83.5	54.2	85.1	51.7	98.7	60.7	110.8	73.1
PD-9-050213-5.3	83.5	65.3	102.4	62.8	92.3	58.5	95.1	56.2	111.5	68.1	127.2	84.7
PD-9-050213-5.9	93.7	72.0	113.7	68.7	102.1	63.2	106.8	62.2	126.8	78.1	146.0	99.5
PD-9-050213-6.5	102.3	79.0	125.5	74.7	112.3	68.1	119.1	69.0	142.5	89.3	164.9	115.7
PD-9-050213-7.1	111.2	86.1	137.9	80.9	123.1	73.6	132.1	77.2	159.3	102.2	185.1	133.5
PD-9-050213-7.7	121.4	93.6	150.8	87.8	134.6	80.0	146.6	87.2	177.9	117.6	206.7	153.6
PD-9-050213-8.3	131.9	101.5	164.2	95.2	146.8	87.2	162.0	98.9	197.3	134.4	228.9	174.5
PD-9-050213-8.9	142.2	109.4	177.3	102.7	158.7	94.7	176.9	110.7	216.1	150.5	249.6	194.6
PD-9-050213-9.5	153.6	118.5	191.8	111.4	172.4	104.5	195.0	126.5	238.6	170.9	273.8	219.4
PD-9-050213-10.1	164.1	125.8	204.9	119.6	184.6	113.0	210.2	139.4	256.9	187.2	293.3	239.3
PD-9-050213-10.7	175.2	134.7	218.9	128.6	197.9	123.2	226.9	154.3	276.4	205.6	314.7	261.7

Table C.44: Steady-state parameters of the loop (processed data) (PD-9-050213)

Test ID	Power (kW)	Flow rate (kg/s)	Inlet K	Outlet K	Outlet Temp. Calculated (C)	T11(C)	Total Ch. PD (Pa)	Acc. PD.(Pa)	Fr. PD.(Pa)
PD-9-050213-2.9	3.17 ± 0.04	0.038 ± 0.001	43.9	0	32.4 ± 0.2	32.3 ± 2.2	440.1 ± 27.6	94.8 ± 6.6	345.3 ± 28.4
PD-9-050213-3.5	3.83 ± 0.04	0.040 ± 0.001	43.6	0	32.8 ± 0.2	33.1 ± 2.2	518.4 ± 30.9	129.6 ± 8.6	388.8 ± 32.1
PD-9-050213-4.1	4.49 ± 0.05	0.041 ± 0.001	43.9	0	33.5 ± 0.3	34.2 ± 2.2	594.0 ± 89.6	166.0 ± 10.7	428.0 ± 90.3
PD-9-050213-4.7	5.14 ± 0.05	0.041 ± 0.001	44.1	0	35.1 ± 0.5	36.4 ± 2.2	679.7 ± 48.0	211.2 ± 13.3	468.5 ± 49.8
PD-9-050213-5.3	5.80 ± 0.05	0.042 ± 0.001	44.0	0	37.2 ± 0.8	39.2 ± 2.2	761.6 ± 51.9	256.9 ± 15.4	504.6 ± 54.2
PD-9-050213-5.9	6.45 ± 0.06	0.043 ± 0.001	43.9	0	40.9 ± 1.2	43.3 ± 2.2	847.6 ± 55.6	307.6 ± 18.6	540.0 ± 58.6
PD-9-050213-6.5	7.11 ± 0.06	0.043 ± 0.001	44.2	0	46.1 ± 1.7	48.5 ± 2.2	932.3 ± 62.0	357.9 ± 22.1	574.5 ± 65.8
PD-9-050213-7.1	7.77 ± 0.06	0.043 ± 0.001	44.1	0	52.7 ± 2.2	54.9 ± 2.2	1010.8 ± 70.7	410.3 ± 23.3	600.5 ± 74.4
PD-9-050213-7.7	8.42 ± 0.06	0.043 ± 0.001	44.1	0	61.4 ± 2.9	62.6 ± 2.2	1099.4 ± 74.6	463.0 ± 27.4	636.4 ± 79.5
PD-9-050213-8.3	9.08 ± 0.07	0.042 ± 0.001	44.1	0	71.8 ± 3.4	71.7 ± 2.2	1186.3 ± 75.9	513.4 ± 28.5	672.9 ± 81.1
PD-9-050213-8.9	9.74 ± 0.07	0.042 ± 0.001	44.6	0	83.0 ± 4.0	81.0 ± 2.3	1265.6 ± 89.8	561.0 ± 31.3	704.6 ± 95.1
PD-9-050213-9.5	10.39 ± 0.07	0.042 ± 0.001	44.5	0	96.9 ± 4.7	94.1 ± 2.2	1346.6 ± 92.1	608.6 ± 34.0	738.0 ± 98.1
PD-9-050213-10.1	11.05 ± 0.07	0.042 ± 0.001	44.5	0	108.7 ± 5.3	104.3 ± 2.2	1424.6 ± 103.1	654.0 ± 37.0	770.6 ± 109.5
PD-9-050213-10.7	11.71 ± 0.08	0.041 ± 0.001	45.0	0	123.9 ± 5.6	114.4 ± 2.3	1502.5 ± 105.4	694.3 ± 37.0	808.2 ± 111.7

* Mean inlet K factor: 44.2

Table C.45: Comparison between frictional pressure-drop from the experimental against available friction-factor formulae (PD-9-050213)

Test ID	Fr. PD.(Pa)-Exp.	Blasius	Kondratev	Ishigai	Razumovskiy	Tarasova & Leontev	Yamashita	Popov	Kuraeva & Protopopov
PD-9-050213-2.9	345.3	297.8	242.1	203.0	224.5	248.3	174.4	194.5	471.8
PD-9-050213-3.5	388.8	337.9	274.2	233.5	256.5	285.3	207.6	219.5	530.4
PD-9-050213-4.1	428.0	372.8	302.0	260.7	284.7	318.3	238.5	241.2	581.3
PD-9-050213-4.7	468.5	407.7	329.6	292.1	315.8	354.5	278.0	265.1	633.5
PD-9-050213-5.3	504.6	443.5	358.0	323.0	346.9	390.8	317.0	288.6	686.0
PD-9-050213-5.9	540.0	478.4	385.6	356.3	379.2	428.6	361.7	313.2	737.7
PD-9-050213-6.5	574.5	509.8	410.4	387.9	409.5	463.8	406.1	336.3	784.0
PD-9-050213-7.1	600.5	544.3	437.7	422.8	442.9	502.5	455.3	361.9	834.2
PD-9-050213-7.7	636.4	578.2	464.7	459.2	477.3	542.0	508.2	388.6	883.2
PD-9-050213-8.3	672.9	611.8	491.3	495.7	511.6	581.2	561.6	415.3	930.7
PD-9-050213-8.9	704.6	643.3	516.4	530.3	544.1	618.2	612.5	441.1	974.2
PD-9-050213-9.5	738.0	677.9	544.0	569.3	579.6	659.4	670.6	469.8	1021.7
PD-9-050213-10.1	770.6	711.8	571.1	605.0	613.0	697.9	722.2	496.7	1067.1
PD-9-050213-10.7	808.2	742.0	595.3	639.5	644.7	733.5	772.4	523.4	1105.5

May 3rd, 2013- System Pressure: 9.5 MPa, Inlet Temperature: 25-26 ℃, Inlet valve: wide open, Outlet valve: wide open

Table C.46: Averaged values of measured signals during experiment for each data point (PD-10-050313)

Test ID	Inlet Temperature (RTD1) (C)	Pressure (MPa)	Power (kW)	Outlet Temp (RTD2)(C)	T11 (C)	T12(C)	CO_2 volumetric Flow rate $(m^3/s)\times10^6$	HE-Inlet water Temp.(C)	HE-Outlet water Temp.(C)	Water Flow rate (lpm)
PD-10-050313-1.2	25.2 ± 0.5	9.47 ± 0.02	1.32 ± 0.03	35.0 ± 0.5	36.7 ± 2.2	25.5 ± 2.2	35.7 ± 1.1	11.0 ± 2.2	32.3 ± 2.2	0.6
PD-10-050313-1.7	25.3 ± 0.4	9.48 ± 0.02	1.86 ± 0.03	36.6 ± 0.5	38.6 ± 2.2	24.9 ± 2.2	43.4 ± 1.0	11.9 ± 2.2	30.3 ± 2.2	1.5
PD-10-050313-2.3	25.2 ± 0.4	9.50 ± 0.02	2.52 ± 0.04	38.0 ± 0.5	40.3 ± 2.2	25.1 ± 2.2	48.9 ± 1.1	11.1 ± 2.2	29.0 ± 2.2	2.1
PD-10-050313-2.9	25.3 ± 0.4	9.52 ± 0.02	3.18 ± 0.04	39.4 ± 0.5	41.7 ± 2.2	25.1 ± 2.2	53.3 ± 1.2	11.1 ± 2.2	27.8 ± 2.2	2.8
PD-10-050313-3.5	25.5 ± 0.4	9.50 ± 0.02	3.83 ± 0.04	40.5 ± 0.5	42.8 ± 2.2	25.1 ± 2.2	57.1 ± 1.1	10.3 ± 2.2	26.2 ± 2.2	3.7
PD-10-050313-4.1	25.6 ± 0.4	9.49 ± 0.02	4.49 ± 0.05	41.4 ± 0.5	43.9 ± 2.2	25.0 ± 2.2	60.3 ± 1.1	8.8 ± 2.2	24.6 ± 2.2	4.4
PD-10-050313-4.7	25.5 ± 0.4	9.51 ± 0.02	5.15 ± 0.05	42.3 ± 0.5	45.0 ± 2.2	25.0 ± 2.2	62.7 ± 1.1	7.7 ± 2.2	22.9 ± 2.2	5.4
PD-10-050313-5.3	25.6 ± 0.4	9.51 ± 0.02	5.80 ± 0.05	43.2 ± 0.5	46.2 ± 2.2	24.9 ± 2.2	64.9 ± 1.1	6.9 ± 2.2	21.2 ± 2.2	6.6
PD-10-050313-5.9	25.5 ± 0.4	9.50 ± 0.02	6.46 ± 0.06	44.1 ± 0.5	47.3 ± 2.2	24.6 ± 2.2	66.6 ± 1.2	6.3 ± 2.2	20.3 ± 2.2	7.5
PD-10-050313-6.5	25.5 ± 0.4	9.49 ± 0.02	7.12 ± 0.06	45.0 ± 0.5	48.9 ± 2.2	24.3 ± 2.2	68.1 ± 1.2	5.9 ± 2.2	19.8 ± 2.2	8.6
PD-10-050313-7.1	25.7 ± 0.4	9.51 ± 0.02	7.77 ± 0.06	46.7 ± 0.5	50.9 ± 2.2	24.8 ± 2.2	69.0 ± 1.3	5.7 ± 2.2	19.4 ± 2.2	9.2
PD-10-050313-7.7	25.6 ± 0.4	9.50 ± 0.02	8.43 ± 0.06	48.1 ± 0.5	53.0 ± 2.2	25.1 ± 2.2	69.7 ± 1.3	5.4 ± 2.2	18.8 ± 2.2	10.2
PD-10-050313-8.3	25.3 ± 0.4	9.49 ± 0.02	9.09 ± 0.07	49.7 ± 0.5	55.6 ± 2.2	24.6 ± 2.2	70.3 ± 1.2	5.3 ± 2.2	18.2 ± 2.2	11.5
PD-10-050313-8.9	25.6 ± 0.4	9.50 ± 0.02	9.74 ± 0.07	53.0 ± 0.6	59.8 ± 2.2	25.8 ± 2.2	70.6 ± 1.1	5.3 ± 2.2	18.3 ± 2.2	12.2
PD-10-050313-9.8	25.9 ± 0.4	9.50 ± 0.02	10.73 ± 0.07	59.1 ± 0.6	66.3 ± 2.2	26.0 ± 2.2	70.5 ± 1.1	5.2 ± 2.2	18.1 ± 2.2	13.5
PD-10-050313-10.7	25.9 ± 0.4	9.50 ± 0.02	11.71 ± 0.08	63.4 ± 0.6	72.7 ± 2.2	24.6 ± 2.2	70.7 ± 1.3	5.1 ± 2.2	17.5 ± 2.2	15.4
PD-10-050313-11.3	25.9 ± 0.4	9.49 ± 0.02	12.37 ± 0.08	68.2 ± 0.6	78.6 ± 2.2	24.5 ± 2.2	70.5 ± 1.4	4.9 ± 2.2	17.7 ± 2.2	15.8
PD-10-050313-11.9	25.9 ± 0.4	9.51 ± 0.02	13.03 ± 0.08	74.1 ± 0.6	85.0 ± 2.2	24.6 ± 2.2	70.0 ± 1.2	4.8 ± 2.2	17.2 ± 2.2	17.1
PD-10-050313-12.5	26.1 ± 0.4	9.52 ± 0.02	13.69 ± 0.08	81.4 ± 0.7	92.0 ± 2.3	24.8 ± 2.2	70.0 ± 1.3	4.8 ± 2.2	17.0 ± 2.2	18

Table C.47: Averaged values of measured pressure-drops during experiment for each data point (PD-10-050313)

Test ID	DP2-1 (Pa)	DP2-2 (Pa)	DP2-3 (Pa)	DP2-4 (Pa)	DP2-5 (Pa)	DP3 (Pa)	DP13 (Pa)	DP10 (Pa)
PD-10-050313-1.2	102.2 ± 10.8	19.59 ± 10.90	51.87 ± 10.86	23.2 ± 11.0	41.8 ± 10.7	452.2 ± 10.8	224.9 ± 12.4	-11.4 ± 124.7
PD-10-050313-1.7	127.5 ± 11.1	28.14 ± 11.19	74.90 ± 11.13	39.3 ± 11.3	49.2 ± 10.9	474.8 ± 11.1	299.7 ± 14.2	22.8 ± 118.7
PD-10-050313-2.3	151.5 ± 11.8	36.53 ± 11.83	98.69 ± 11.66	57.3 ± 11.9	59.0 ± 11.2	498.4 ± 11.8	378.2 ± 18.0	58.7 ± 119.0
PD-10-050313-2.9	172.5 ± 12.3	44.73 ± 12.43	122.10 ± 12.24	76.5 ± 12.7	71.0 ± 11.7	519.1 ± 12.3	457.0 ± 20.6	94.9 ± 120.3
PD-10-050313-3.5	191.7 ± 13.3	53.53 ± 13.37	147.14 ± 12.87	98.2 ± 13.7	85.0 ± 12.2	532.5 ± 13.3	540.4 ± 25.8	133.8 ± 120.4
PD-10-050313-4.1	208.5 ± 14.4	62.07 ± 14.43	171.02 ± 13.94	120.1 ± 14.7	98.2 ± 13.1	545.0 ± 14.4	620.2 ± 30.2	178.9 ± 121.4
PD-10-050313-4.7	223.1 ± 15.8	70.16 ± 16.24	193.92 ± 15.52	141.6 ± 16.2	112.5 ± 14.3	556.4 ± 15.8	697.5 ± 35.1	218.8 ± 120.5
PD-10-050313-5.3	236.0 ± 17.3	78.56 ± 17.55	216.91 ± 16.90	164.1 ± 18.1	129.5 ± 15.5	566.7 ± 17.3	777.2 ± 41.5	264.6 ± 118.8
PD-10-050313-5.9	247.3 ± 18.6	87.27 ± 19.11	239.75 ± 18.07	188.4 ± 18.3	146.3 ± 16.4	573.5 ± 18.6	857.3 ± 43.1	303.6 ± 119.5
PD-10-050313-6.5	257.5 ± 19.8	96.45 ± 19.98	263.23 ± 19.15	214.3 ± 19.7	162.2 ± 17.4	579.0 ± 19.8	938.4 ± 47.3	345.0 ± 121.5
PD-10-050313-7.1	265.8 ± 21.0	105.71 ± 21.44	285.52 ± 20.32	239.9 ± 21.1	180.2 ± 18.4	585.1 ± 21.0	1018.7 ± 52.6	389.3 ± 124.9
PD-10-050313-7.7	271.6 ± 34.3	115.32 ± 37.91	308.51 ± 43.87	267.1 ± 22.3	198.8 ± 31.3	591.0 ± 34.3	1099.9 ± 67.6	425.3 ± 121.6
PD-10-050313-8.3	241.2 ± 113.4	125.31 ± 117.56	332.54 ± 138.03	294.0 ± 31.6	223.6 ± 85.7	597.1 ± 113.4	1157.7 ± 150.6	484.6 ± 132.1
PD-10-050313-8.9	21.6 ± 331.9	132.53 ± 301.58	365.46 ± 327.75	315.7 ± 107.8	281.8 ± 184.3	600.9 ± 331.9	1091.0 ± 350.9	559.0 ± 177.0
PD-10-050313-9.8	84.5 ± 392.5	146.01 ± 289.81	395.06 ± 286.89	363.5 ± 173.5	319.6 ± 160.5	618.1 ± 392.5	1269.3 ± 343.2	621.3 ± 153.2
PD-10-050313-10.7	302.9 ± 30.4	167.70 ± 30.23	429.01 ± 29.30	415.1 ± 27.6	289.5 ± 25.5	588.4 ± 30.4	1527.5 ± 82.9	623.5 ± 127.9
PD-10-050313-11.3	306.5 ± 31.0	179.21 ± 30.98	454.86 ± 29.76	445.8 ± 28.4	302.8 ± 26.1	586.3 ± 31.0	1609.8 ± 94.2	662.6 ± 129.1
PD-10-050313-11.9	310.2 ± 33.3	189.94 ± 33.69	480.49 ± 32.20	474.9 ± 30.3	315.4 ± 28.0	587.6 ± 33.3	1689.0 ± 101.6	697.5 ± 128.1
PD-10-050313-12.5	313.4 ± 33.9	201.51 ± 33.97	508.53 ± 31.87	504.1 ± 29.7	326.4 ± 27.7	585.5 ± 33.9	1769.7 ± 102.6	725.7 ± 87.2

Table C.48: Averaged values of measured wall surface temperature during experiment for each data point (PD-10-050313)

Test ID	TS21T (C)	TS21B (C)	TS22T (C)	TS22B (C)	TS23T (C)	TS23B (C)	TS24T (C)	TS24B (C)	TS25T (C)	TS25B (C)	TS26T (C)	TS26B (C)
PD-10-050313-1.2	37.9	35.8	43.7	37.5	43.8	38.8	44.6	39.7	49.2	42.0	51.2	43.6
PD-10-050313-1.7	41.4	38.7	48.1	40.8	48.2	42.0	49.0	42.6	54.3	45.1	56.8	46.9
PD-10-050313-2.3	45.3	41.9	53.9	44.2	53.3	45.5	54.3	45.7	61.0	48.5	63.9	50.7
PD-10-050313-2.9	49.2	45.0	59.8	47.4	58.7	48.7	59.9	48.6	67.7	51.9	71.1	54.7
PD-10-050313-3.5	53.1	48.0	65.6	50.5	64.2	51.8	65.7	51.4	74.7	55.1	79.1	59.1
PD-10-050313-4.1	57.3	50.9	71.2	53.7	70.0	54.8	71.8	54.1	82.4	58.6	88.4	63.9
PD-10-050313-4.7	62.0	53.7	77.1	57.0	76.3	58.1	78.4	57.0	90.9	62.3	98.2	69.2
PD-10-050313-5.3	67.2	57.0	83.4	60.5	83.0	61.3	85.6	60.1	99.9	66.4	108.6	74.9
PD-10-050313-5.9	73.0	60.5	90.2	64.3	90.0	64.6	93.1	63.1	109.1	70.7	119.7	81.1
PD-10-050313-6.5	79.6	64.4	97.5	68.3	97.4	68.2	101.2	66.4	118.9	75.6	131.2	88.3
PD-10-050313-7.1	87.5	69.3	106.1	72.9	105.8	72.2	110.2	70.4	129.8	81.8	144.1	96.9
PD-10-050313-7.7	95.5	74.4	114.6	77.5	113.7	76.0	119.1	74.3	140.4	88.0	156.8	105.6
PD-10-050313-8.3	103.9	79.7	122.8	82.1	119.6	80.0	127.7	78.4	151.0	94.1	169.9	114.6
PD-10-050313-8.9	111.8	86.2	127.4	86.1	125.5	84.5	136.0	84.4	164.0	103.0	186.4	127.3
PD-10-050313-9.8	118.1	94.4	140.7	93.9	140.1	91.9	153.3	93.6	184.3	117.3	210.2	147.6
PD-10-050313-10.7	140.8	108.0	166.9	105.3	160.6	98.9	170.4	102.1	202.5	130.4	230.3	165.5
PD-10-050313-11.3	149.8	115.3	178.6	111.5	170.7	104.2	181.8	109.5	216.7	141.6	246.0	180.0
PD-10-050313-11.9	159.3	122.8	190.9	118.2	181.1	110.1	194.0	117.9	231.8	153.7	262.4	195.7
PD-10-050313-12.5	169.0	131.5	204.2	125.3	192.1	116.9	207.2	127.8	247.8	167.4	280.1	213.1

Table C.49: Steady-state parameters of the loop (processed data) (PD-10-050313)

Test ID	Power (kW)	Flow rate (kg/s)	Inlet K	Outlet K	Outlet Temp. Calculated (C)	T11(C)	Total Ch. PD (Pa)	Acc. PD.(Pa)	Fr. PD.(Pa)
PD-10-050313-1.2	1.32 ± 0.03	0.029 ± 0.001	0	0	37.2 ± 0.4	36.7 ± 2.2	215.9 ± 12.4	14.2 ± 1.3	201.7 ± 12.5
PD-10-050313-1.7	1.86 ± 0.03	0.035 ± 0.001	0	0	38.5 ± 0.3	38.6 ± 2.2	286.2 ± 14.2	26.0 ± 2.0	260.1 ± 14.3
PD-10-050313-2.3	2.52 ± 0.04	0.039 ± 0.001	0	0	40.0 ± 0.3	40.3 ± 2.2	360.5 ± 18.0	43.0 ± 3.1	317.5 ± 18.2
PD-10-050313-2.9	3.18 ± 0.04	0.043 ± 0.001	0	0	41.3 ± 0.3	41.7 ± 2.2	435.4 ± 20.6	64.3 ± 4.3	371.1 ± 21.0
PD-10-050313-3.5	3.83 ± 0.04	0.046 ± 0.001	0	0	42.3 ± 0.3	42.8 ± 2.2	514.8 ± 25.8	90.5 ± 5.7	424.3 ± 26.5
PD-10-050313-4.1	4.49 ± 0.05	0.048 ± 0.001	0	0	43.2 ± 0.3	43.9 ± 2.2	590.7 ± 30.2	120.1 ± 7.1	470.6 ± 31.0
PD-10-050313-4.7	5.15 ± 0.05	0.050 ± 0.001	0	0	44.2 ± 0.3	45.0 ± 2.2	664.4 ± 35.1	152.4 ± 8.6	512.0 ± 36.2
PD-10-050313-5.3	5.80 ± 0.05	0.052 ± 0.001	0	0	45.4 ± 0.3	46.2 ± 2.2	740.5 ± 41.5	188.9 ± 10.3	551.6 ± 42.8
PD-10-050313-5.9	6.46 ± 0.06	0.053 ± 0.001	0	0	46.6 ± 0.4	47.3 ± 2.2	817.2 ± 43.1	228.4 ± 12.2	588.8 ± 44.8
PD-10-050313-6.5	7.12 ± 0.06	0.055 ± 0.001	0	0	48.0 ± 0.5	48.9 ± 2.2	894.8 ± 47.3	272.0 ± 14.6	622.8 ± 49.5
PD-10-050313-7.1	7.77 ± 0.06	0.055 ± 0.001	0	0	50.3 ± 0.7	50.9 ± 2.2	972.1 ± 52.6	318.0 ± 17.6	654.0 ± 55.4
PD-10-050313-7.7	8.43 ± 0.06	0.056 ± 0.001	0	0	52.7 ± 0.9	53.0 ± 2.2	1050.2 ± 67.6	365.8 ± 20.3	684.3 ± 70.6
PD-10-050313-8.3	9.09 ± 0.07	0.057 ± 0.001	0	0	55.2 ± 1.0	55.6 ± 2.2	1105.0 ± 150.6	414.2 ± 20.4	690.8 ± 152.0
PD-10-050313-8.9	9.74 ± 0.07	0.057 ± 0.001	0	0	59.2 ± 1.2	59.8 ± 2.2	1035.5 ± 350.9	466.8 ± 21.3	568.6 ± 351.5
PD-10-050313-9.8	10.73 ± 0.07	0.056 ± 0.001	0	0	67.1 ± 1.6	66.3 ± 2.2	1209.9 ± 343.2	548.2 ± 24.0	661.7 ± 344.0
PD-10-050313-10.7	11.71 ± 0.08	0.056 ± 0.001	0	0	75.7 ± 2.3	72.7 ± 2.2	1463.9 ± 82.9	629.5 ± 30.5	834.3 ± 88.4
PD-10-050313-11.3	12.37 ± 0.08	0.056 ± 0.001	0	0	82.5 ± 2.8	78.6 ± 2.2	1543.7 ± 94.2	682.9 ± 35.0	860.8 ± 100.5
PD-10-050313-11.9	13.03 ± 0.08	0.056 ± 0.001	0	0	90.7 ± 3.0	85.0 ± 2.2	1620.8 ± 101.6	732.7 ± 34.5	888.2 ± 107.3
PD-10-050313-12.5	13.69 ± 0.08	0.056 ± 0.001	0	0	99.3 ± 3.5	92.0 ± 2.3	1699.0 ± 102.6	785.3 ± 38.9	913.7 ± 109.7

Table C.50: Comparison between frictional pressure-drop from the experimental against available friction-factor formulae (PD-10-050313)

Test ID	Fr. PD.(Pa)-Exp.	Blasius	Kondratev	Ishigai	Razumovskiy	Tarasova & Leontev	Yamashita	Popov	Kuraeva & Protopopov
PD-10-050313-1.2	201.7	150.9	124.3	127.4	134.3	136.6	111.0	132.3	264.0
PD-10-050313-1.7	260.1	216.8	177.8	170.2	182.9	188.5	141.8	177.2	362.2
PD-10-050313-2.3	317.5	275.4	225.1	203.4	222.0	232.5	164.8	210.5	443.9
PD-10-050313-2.9	371.1	328.0	267.4	234.7	258.0	273.5	189.8	240.0	515.7
PD-10-050313-3.5	424.3	380.0	309.1	267.3	294.7	315.5	218.3	269.6	586.4
PD-10-050313-4.1	470.6	428.2	347.5	299.1	329.6	355.8	248.0	297.5	652.1
PD-10-050313-4.7	512.0	472.3	382.7	329.2	362.3	393.8	277.7	323.1	712.5
PD-10-050313-5.3	551.6	514.9	416.6	359.7	394.9	431.7	309.7	348.1	771.1
PD-10-050313-5.9	588.8	554.9	448.3	389.2	426.0	468.4	342.3	371.6	826.6
PD-10-050313-6.5	622.8	595.3	480.3	420.4	458.3	506.5	378.3	395.9	883.0
PD-10-050313-7.1	654.0	629.4	507.2	449.7	487.6	541.2	415.1	417.5	931.9
PD-10-050313-7.7	684.3	663.5	534.1	479.0	516.9	576.0	452.6	439.0	980.5
PD-10-050313-8.3	690.8	696.9	560.5	507.9	545.7	610.3	490.2	460.1	1027.9
PD-10-050313-8.9	568.6	728.4	585.3	539.6	576.1	645.8	534.0	483.0	1073.8
PD-10-050313-9.8	661.7	773.8	621.0	587.8	621.7	699.0	603.9	517.1	1140.0
PD-10-050313-10.7	834.3	824.1	660.6	638.7	670.1	756.2	677.0	552.8	1211.6
PD-10-050313-11.3	860.8	855.3	685.2	672.1	701.6	792.9	726.6	576.5	1255.8
PD-10-050313-11.9	888.2	883.6	707.5	704.4	731.4	827.3	775.4	599.3	1295.6
PD-10-050313-12.5	913.7	918.6	735.3	742.2	766.4	868.5	831.7	626.3	1344.6

May 10th, 2013- System Pressure: 7.6 MPa, Inlet Temperature: 20-21 °C, Inlet valve: wide open, Outlet valve: wide open

Table C.51: Averaged values of measured signals during experiment for each data point (PD-11-051013)

Test ID	Inlet Temperature (RTD1) (C)	Pressure (MPa)	Power (kW)	Outlet Temp (RTD2)(C)	T11 (C)	T12(C)	CO_2 volumetric Flow rate $(m^3/s) \times 10^6$	HE-Inlet water Temp.(C)	HE-Outlet water Temp.(C)	Water Flow rate (lpm)
PD-11-051013-1.2	19.9 ± 0.4	7.60 ± 0.02	1.31 ± 0.03	28.4 ± 0.5	30.1 ± 2.2	19.3 ± 2.2	38.0 ± 1.3	8.2 ± 2.2	24.4 ± 2.2	1.1
PD-11-051013-1.7	20.0 ± 0.4	7.61 ± 0.02	1.86 ± 0.03	29.7 ± 0.5	31.6 ± 2.2	19.7 ± 2.2	44.5 ± 1.1	10.1 ± 2.2	22.0 ± 2.2	2.4
PD-11-051013-2.3	20.1 ± 0.4	7.61 ± 0.02	2.51 ± 0.03	30.6 ± 0.5	32.4 ± 2.2	19.4 ± 2.2	50.2 ± 1.1	9.4 ± 2.2	20.5 ± 2.2	3.6
PD-11-051013-2.9	20.3 ± 0.4	7.59 ± 0.02	3.17 ± 0.04	31.1 ± 0.5	32.8 ± 2.2	19.4 ± 2.2	54.9 ± 1.2	9.2 ± 2.2	19.0 ± 2.2	5.3
PD-11-051013-3.5	20.3 ± 0.4	7.61 ± 0.02	3.82 ± 0.04	31.5 ± 0.5	33.1 ± 2.2	19.5 ± 2.2	58.8 ± 1.2	7.4 ± 2.2	18.6 ± 2.2	5.5
PD-11-051013-4.1	20.7 ± 0.4	7.61 ± 0.02	4.48 ± 0.05	31.7 ± 0.5	33.3 ± 2.2	19.8 ± 2.2	62.3 ± 1.2	7.0 ± 2.2	17.6 ± 2.2	7
PD-11-051013-4.85	20.9 ± 0.4	7.59 ± 0.02	5.30 ± 0.05	31.8 ± 0.5	33.4 ± 2.2	19.9 ± 2.2	65.6 ± 1.2	6.4 ± 2.2	16.5 ± 2.2	8.8
PD-11-051013-5.3	20.9 ± 0.4	7.60 ± 0.02	5.79 ± 0.05	32.0 ± 0.5	33.6 ± 2.2	19.8 ± 2.2	67.0 ± 1.2	5.9 ± 2.2	15.6 ± 2.2	10
PD-11-051013-5.95	21.0 ± 0.4	7.60 ± 0.02	6.50 ± 0.06	32.2 ± 0.5	34.1 ± 2.2	19.9 ± 2.2	68.8 ± 1.2	5.5 ± 2.2	14.8 ± 2.2	11.8
PD-11-051013-6.5	21.0 ± 0.4	7.60 ± 0.02	7.10 ± 0.06	32.4 ± 0.5	34.5 ± 2.2	19.8 ± 2.2	70.1 ± 1.4	5.4 ± 2.2	14.4 ± 2.2	13.4
PD-11-051013-7.1	20.8 ± 0.4	7.59 ± 0.02	7.75 ± 0.06	32.7 ± 0.5	35.4 ± 2.2	19.9 ± 2.2	71.1 ± 1.2	5.2 ± 2.2	13.8 ± 2.2	15.4
PD-11-051013-7.7	20.2 ± 0.4	7.61 ± 0.02	8.41 ± 0.06	33.2 ± 0.5	36.3 ± 2.2	19.9 ± 2.2	71.6 ± 1.3	4.9 ± 2.2	12.7 ± 2.2	18.6
PD-11-051013-8.3	20.6 ± 0.4	7.61 ± 0.02	9.07 ± 0.07	34.3 ± 0.5	38.4 ± 2.2	20.2 ± 2.2	71.9 ± 1.3	4.9 ± 2.2	12.8 ± 2.2	19.4
PD-11-051013-8.9	20.8 ± 0.4	7.61 ± 0.02	9.72 ± 0.07	36.0 ± 0.5	41.2 ± 2.2	20.4 ± 2.2	72.0 ± 1.2	4.8 ± 2.2	12.5 ± 2.2	21.6
PD-11-051013-9.5	20.9 ± 0.4	7.61 ± 0.02	10.38 ± 0.07	38.3 ± 0.5	44.7 ± 2.2	20.4 ± 2.2	71.6 ± 1.2	4.6 ± 2.2	12.1 ± 2.2	23.5
PD-11-051013-10.1	21.0 ± 0.4	7.61 ± 0.02	11.03 ± 0.07	41.5 ± 0.5	49.1 ± 2.2	20.5 ± 2.2	70.5 ± 1.5	4.5 ± 2.2	11.7 ± 2.2	25.8
PD-11-051013-10.75	21.3 ± 0.4	7.60 ± 0.02	11.74 ± 0.08	46.6 ± 0.5	55.1 ± 2.3	20.7 ± 2.2	70.2 ± 1.4	4.5 ± 2.2	11.5 ± 2.2	27.9

Table C.52: Averaged values of measured pressure-drops during experiment for each data point (PD-11-051013)

Test ID	DP2-1 (Pa)	DP2-2 (Pa)	DP2-3 (Pa)	DP2-4 (Pa)	DP2-5 (Pa)	DP3 (Pa)	DP13 (Pa)	DP10 (Pa)	DP7 (Pa)
PD-11-051013-1.2	70.7 ± 11.0	31.58 ± 11.17	69.08 ± 11.24	49.4 ± 11.2	17.1 ± 11.0	31.7 ± 11.0	243.6 ± 13.7	63.9 ± 83.6	36.8 ± 10.5
PD-11-051013-1.7	92.8 ± 11.6	39.92 ± 11.79	91.15 ± 11.95	65.5 ± 11.9	23.6 ± 11.6	49.4 ± 11.6	319.8 ± 16.2	95.2 ± 86.2	47.0 ± 10.6
PD-11-051013-2.3	116.0 ± 12.2	48.51 ± 12.37	116.84 ± 12.57	85.8 ± 12.6	33.2 ± 12.3	68.0 ± 12.2	408.3 ± 17.9	138.9 ± 90.5	58.9 ± 10.6
PD-11-051013-2.9	136.0 ± 12.9	56.74 ± 13.05	143.29 ± 13.29	107.9 ± 13.6	46.1 ± 13.2	83.0 ± 12.9	499.0 ± 19.9	186.1 ± 92.1	70.7 ± 10.7
PD-11-051013-3.5	152.5 ± 14.1	64.26 ± 14.21	168.12 ± 14.32	130.0 ± 15.0	63.3 ± 14.4	97.3 ± 14.1	588.1 ± 24.0	234.8 ± 103.8	81.7 ± 10.8
PD-11-051013-4.1	167.5 ± 14.9	73.23 ± 14.88	195.37 ± 15.14	156.4 ± 15.8	79.4 ± 15.1	109.4 ± 14.9	683.0 ± 23.9	294.8 ± 111.6	92.8 ± 10.9
PD-11-051013-4.85	183.0 ± 16.2	84.69 ± 16.14	228.42 ± 15.97	190.0 ± 18.0	102.6 ± 16.7	120.3 ± 16.2	801.2 ± 25.8	370.3 ± 124.2	104.4 ± 11.0
PD-11-051013-5.3	190.9 ± 17.1	91.56 ± 16.77	246.97 ± 16.78	210.3 ± 19.2	117.8 ± 17.8	127.0 ± 17.1	870.8 ± 27.7	412.7 ± 122.3	110.2 ± 11.0
PD-11-051013-5.95	201.2 ± 18.2	102.69 ± 17.89	274.25 ± 17.61	242.4 ± 20.6	140.6 ± 18.7	133.5 ± 18.2	975.6 ± 30.4	477.3 ± 143.7	118.5 ± 11.2
PD-11-051013-6.5	209.2 ± 19.9	112.32 ± 18.77	297.52 ± 18.34	270.7 ± 22.2	159.9 ± 20.4	137.0 ± 19.9	1065.3 ± 32.6	530.6 ± 152.4	125.3 ± 11.2
PD-11-051013-7.1	217.0 ± 20.5	123.02 ± 19.47	322.28 ± 19.10	302.2 ± 23.3	183.8 ± 20.9	137.9 ± 20.5	1165.0 ± 32.4	569.8 ± 166.1	132.9 ± 11.5
PD-11-051013-7.7	223.9 ± 22.2	130.71 ± 20.41	342.68 ± 20.48	330.2 ± 24.3	204.8 ± 22.2	144.2 ± 22.2	1249.9 ± 35.7	607.2 ± 166.9	137.0 ± 11.7
PD-11-051013-8.3	230.5 ± 22.5	144.10 ± 20.94	369.92 ± 20.41	367.2 ± 25.0	228.3 ± 22.7	143.6 ± 22.5	1359.1 ± 36.3	661.9 ± 179.1	142.0 ± 11.6
PD-11-051013-8.9	236.9 ± 23.5	156.93 ± 21.11	396.35 ± 20.99	404.2 ± 26.0	252.2 ± 23.6	145.8 ± 23.5	1466.6 ± 38.7	717.2 ± 188.6	146.2 ± 11.8
PD-11-051013-9.5	242.5 ± 24.1	169.39 ± 21.79	422.42 ± 21.74	441.5 ± 26.7	275.7 ± 24.5	143.6 ± 24.1	1572.7 ± 41.1	771.2 ± 195.6	149.4 ± 12.0
PD-11-051013-10.1	247.1 ± 24.8	182.11 ± 22.51	449.76 ± 22.41	480.1 ± 27.5	298.4 ± 25.3	139.3 ± 24.8	1679.8 ± 44.1	819.0 ± 208.8	151.8 ± 12.2
PD-11-051013-10.75	251.9 ± 25.0	196.83 ± 22.82	482.31 ± 23.61	523.2 ± 28.7	320.1 ± 25.9	133.2 ± 25.0	1797.7 ± 46.3	867.7 ± 216.8	153.7 ± 12.3

Table C.53: Averaged values of measured wall surface temperature during experiment for each data point (PD-11-051013)

Test ID	TS21T (C)	TS21B (C)	TS22T (C)	TS22B (C)	TS23T (C)	TS23B (C)	TS24T (C)	TS24B (C)	TS25T (C)	TS25B (C)	TS26T (C)	TS26B (C)
PD-11-051013-1.2	32.3	29.9	36.7	31.5	36.3	32.6	37.5	33.0	42.1	34.4	43.3	35.1
PD-11-051013-1.7	35.5	32.8	41.1	34.4	40.4	35.4	42.3	35.0	47.2	36.5	48.6	37.5
PD-11-051013-2.3	38.6	35.5	46.6	36.8	45.7	37.8	47.3	37.1	53.1	39.0	54.6	40.4
PD-11-051013-2.9	42.4	37.6	52.3	39.5	50.6	40.4	51.8	39.3	58.6	41.5	60.2	43.4
PD-11-051013-3.5	46.9	40.2	58.3	42.6	55.8	43.3	57.1	41.6	64.7	44.3	67.0	46.7
PD-11-051013-4.1	52.4	43.4	64.6	46.2	61.7	46.3	62.5	43.9	70.9	47.1	74.3	50.2
PD-11-051013-4.85	60.3	48.0	72.7	51.0	69.6	50.3	70.2	46.8	79.8	50.9	84.7	55.1
PD-11-051013-5.3	65.5	51.0	77.7	54.2	74.8	52.7	75.4	48.8	85.6	53.4	91.9	58.6
PD-11-051013-5.95	74.0	56.3	85.7	59.0	82.8	56.5	83.4	51.7	95.0	57.5	103.6	64.7
PD-11-051013-6.5	81.4	61.2	92.8	63.3	89.6	59.6	90.4	54.2	103.4	61.4	114.0	70.7
PD-11-051013-7.1	89.6	67.0	101.3	68.1	97.3	63.2	98.3	57.2	113.3	65.9	126.1	78.2
PD-11-051013-7.7	97.0	72.0	109.6	72.7	104.8	66.6	106.4	60.3	122.9	70.4	137.4	85.3
PD-11-051013-8.3	106.6	79.6	120.4	78.2	113.9	70.6	115.8	64.3	135.1	77.2	152.2	96.3
PD-11-051013-8.9	116.0	87.0	131.4	83.9	123.1	74.7	125.8	68.8	147.8	84.8	166.9	108.0
PD-11-051013-9.5	125.3	94.3	143.0	89.5	132.6	79.0	136.2	74.1	161.1	93.6	182.5	121.3
PD-11-051013-10.1	135.3	102.0	155.4	95.6	142.7	83.7	147.6	80.4	175.6	104.4	199.1	136.5
PD-11-051013-10.75	146.6	110.7	169.8	102.8	153.9	89.4	161.0	88.9	192.9	118.3	218.6	155.1

Table C.54: Steady-state parameters of the loop (processed data) (PD-11-051013)

Test ID	Power (kW)	Flow rate (kg/s)	Inlet K	Outlet K	Outlet Temp. Calculated (C)	T11(C)	Total Ch. PD (Pa)	Acc. PD.(Pa)	Fr. PD.(Pa)
PD-11-051013-1.2	1.31 ± 0.03	0.031 ± 0.001	0	0	30.1 ± 0.3	30.1 ± 2.2	233.3 ± 13.7	15.4 ± 1.5	217.8 ± 13.8
PD-11-051013-1.7	1.86 ± 0.03	0.036 ± 0.001	0	0	31.2 ± 0.2	31.6 ± 2.2	305.3 ± 16.2	28.2 ± 2.3	277.1 ± 16.4
PD-11-051013-2.3	2.51 ± 0.03	0.041 ± 0.001	0	0	31.8 ± 0.1	32.4 ± 2.2	389.2 ± 17.9	48.5 ± 3.6	340.8 ± 18.2
PD-11-051013-2.9	3.17 ± 0.04	0.045 ± 0.001	0	0	32.1 ± 0.1	32.8 ± 2.2	475.4 ± 19.9	75.1 ± 5.3	400.2 ± 20.6
PD-11-051013-3.5	3.82 ± 0.04	0.048 ± 0.001	0	0	32.3 ± 0.1	33.1 ± 2.2	560.1 ± 24.0	106.3 ± 7.0	453.8 ± 25.0
PD-11-051013-4.1	4.48 ± 0.05	0.051 ± 0.001	0	0	32.4 ± 0.1	33.3 ± 2.2	650.3 ± 23.9	145.1 ± 9.0	505.2 ± 25.5
PD-11-051013-4.85	5.30 ± 0.05	0.053 ± 0.001	0	0	32.4 ± 0.1	33.4 ± 2.2	763.2 ± 25.8	199.2 ± 11.5	564.0 ± 28.3
PD-11-051013-5.3	5.79 ± 0.05	0.054 ± 0.001	0	0	32.6 ± 0.1	33.6 ± 2.2	829.8 ± 27.7	233.0 ± 12.9	596.9 ± 30.5
PD-11-051013-5.95	6.50 ± 0.06	0.056 ± 0.001	0	0	33.0 ± 0.2	34.1 ± 2.2	930.4 ± 30.4	287.9 ± 15.6	642.5 ± 34.2
PD-11-051013-6.5	7.10 ± 0.06	0.057 ± 0.001	0	0	33.4 ± 0.3	34.5 ± 2.2	1016.3 ± 32.6	337.9 ± 19.8	678.4 ± 38.1
PD-11-051013-7.1	7.75 ± 0.06	0.058 ± 0.001	0	0	34.1 ± 0.4	35.4 ± 2.2	1112.2 ± 32.4	394.5 ± 20.7	717.7 ± 38.4
PD-11-051013-7.7	8.41 ± 0.06	0.059 ± 0.001	0	0	35.1 ± 0.5	36.3 ± 2.2	1193.8 ± 35.7	445.4 ± 25.0	748.5 ± 43.6
PD-11-051013-8.3	9.07 ± 0.07	0.058 ± 0.001	0	0	37.4 ± 0.7	38.4 ± 2.2	1299.6 ± 36.3	514.6 ± 26.7	785.0 ± 45.1
PD-11-051013-8.9	9.72 ± 0.07	0.058 ± 0.001	0	0	40.4 ± 1.0	41.2 ± 2.2	1403.6 ± 38.7	582.9 ± 29.0	820.7 ± 48.3
PD-11-051013-9.5	10.38 ± 0.07	0.058 ± 0.001	0	0	44.6 ± 1.4	44.7 ± 2.2	1506.7 ± 41.1	651.2 ± 32.5	855.5 ± 52.4
PD-11-051013-10.1	11.03 ± 0.07	0.057 ± 0.001	0	0	50.7 ± 2.1	49.1 ± 2.2	1611.4 ± 44.1	718.2 ± 41.6	893.3 ± 60.7
PD-11-051013-10.75	11.74 ± 0.08	0.057 ± 0.001	0	0	58.1 ± 2.5	55.1 ± 2.3	1725.9 ± 46.3	796.1 ± 43.1	929.8 ± 63.3

Table C.55: Comparison between frictional pressure-drop from the experimental against available friction-factor formulae (PD-11-051013)

Test ID	Fr. PD.(Pa)-Exp.	Blasius	Kondratev	Ishigai	Razumovskiy	Tarasova & Leontev	Yamashita	Popov	Kuraeva & Protopopov
PD-11-051013-1.2	217.8	171.3	141.0	121.5	134.8	141.8	95.0	127.3	288.5
PD-11-051013-1.7	277.1	231.5	189.8	151.5	171.5	184.8	114.8	156.4	371.3
PD-11-051013-2.3	340.8	293.6	239.9	186.7	212.5	232.2	142.5	189.5	456.4
PD-11-051013-2.9	400.2	353.1	287.7	223.8	254.3	280.3	174.7	223.2	538.0
PD-11-051013-3.5	453.8	408.7	332.2	260.1	294.3	326.4	207.8	255.4	614.3
PD-11-051013-4.1	505.2	465.5	377.4	299.1	336.7	375.5	246.0	288.9	692.5
PD-11-051013-4.85	564.0	529.1	428.0	344.7	385.2	432.4	293.5	326.3	780.4
PD-11-051013-5.3	596.9	561.7	453.8	369.2	410.9	462.7	320.8	345.8	826.1
PD-11-051013-5.95	642.5	610.6	492.5	407.6	450.5	509.6	365.2	375.5	894.9
PD-11-051013-6.5	678.4	651.7	524.9	440.6	484.3	549.7	404.7	400.6	952.8
PD-11-051013-7.1	717.7	693.4	557.9	475.1	519.2	591.6	448.0	426.1	1012.1
PD-11-051013-7.7	748.5	728.2	585.4	502.8	547.5	626.0	483.2	446.3	1061.0
PD-11-051013-8.3	785.0	765.2	614.3	541.4	584.2	669.1	537.7	473.5	1115.9
PD-11-051013-8.9	820.7	802.2	643.3	579.8	620.7	712.1	592.7	500.7	1170.3
PD-11-051013-9.5	855.5	835.4	669.3	616.9	655.4	752.6	648.2	526.6	1219.1
PD-11-051013-10.1	893.3	861.3	689.5	652.1	686.7	788.6	704.5	550.7	1257.7
PD-11-051013-10.75	929.8	904.5	723.5	700.8	732.1	841.2	778.3	585.0	1319.4

May 13th, 2013- System Pressure: 7.6 MPa, Inlet Temperature: 20-21 ℃, Inlet valve: wide open, Outlet valve: 30º closed

Table C.56: Averaged values of measured signals during experiment for each data point (PD-12-051313)

Test ID	Inlet Temperature (RTD1) (C)	Pressure (MPa)	Power (kW)	Outlet Temp (RTD2)(C)	T11 (C)	T12(C)	CO_2 volumetric Flow rate $(m^3/s) \times 10^6$	HE-Inlet water Temp.(C)	HE-Outlet water Temp.(C)	Water Flow rate (lpm)
PD-12-051313-1.2	20.3 ± 0.4	7.61 ± 0.02	1.32 ± 0.03	28.7 ± 0.5	30.4 ± 2.2	19.9 ± 2.2	37.0 ± 1.4	9.6 ± 2.2	24.5 ± 2.2	1.2
PD-12-051313-1.7	20.0 ± 0.4	7.60 ± 0.02	1.86 ± 0.03	29.7 ± 0.5	31.6 ± 2.2	19.6 ± 2.2	43.6 ± 1.1	10.0 ± 2.2	21.7 ± 2.2	2.5
PD-12-051313-2.35	20.5 ± 0.4	7.60 ± 0.02	2.57 ± 0.04	30.7 ± 0.5	32.4 ± 2.2	20.1 ± 2.2	49.7 ± 1.1	9.7 ± 2.2	20.5 ± 2.2	3.8
PD-12-051313-2.9	20.5 ± 0.4	7.60 ± 0.02	3.17 ± 0.04	31.1 ± 0.5	32.7 ± 2.2	20.0 ± 2.2	53.9 ± 1.2	8.3 ± 2.2	19.1 ± 2.2	4.8
PD-12-051313-3.5	20.6 ± 0.4	7.60 ± 0.02	3.82 ± 0.04	31.4 ± 0.5	33.0 ± 2.2	19.9 ± 2.2	57.5 ± 1.2	7.6 ± 2.2	17.7 ± 2.2	6.2
PD-12-051313-4.2	20.5 ± 0.4	7.59 ± 0.02	4.59 ± 0.05	31.6 ± 0.5	33.1 ± 2.2	19.6 ± 2.2	60.6 ± 1.2	6.7 ± 2.2	15.8 ± 2.2	8.5
PD-12-051313-4.7	20.8 ± 0.4	7.61 ± 0.02	5.14 ± 0.05	31.9 ± 0.5	33.4 ± 2.2	20.0 ± 2.2	62.3 ± 1.2	6.5 ± 2.2	15.2 ± 2.2	9.9
PD-12-051313-5.3	21.0 ± 0.4	7.60 ± 0.02	5.79 ± 0.05	32.0 ± 0.5	33.7 ± 2.2	20.0 ± 2.2	64.1 ± 1.1	6.2 ± 2.2	14.8 ± 2.2	11.4
PD-12-051313-5.9	21.1 ± 0.4	7.61 ± 0.02	6.45 ± 0.06	32.3 ± 0.5	34.4 ± 2.2	20.0 ± 2.2	65.2 ± 1.4	6.1 ± 2.2	14.6 ± 2.2	13
PD-12-051313-6.5	21.0 ± 0.4	7.60 ± 0.02	7.10 ± 0.06	32.6 ± 0.5	35.2 ± 2.2	19.9 ± 2.2	66.2 ± 1.4	5.9 ± 2.2	14.1 ± 2.2	14.7
PD-12-051313-7.1	20.8 ± 0.4	7.60 ± 0.02	7.76 ± 0.06	33.3 ± 0.5	36.5 ± 2.2	19.8 ± 2.2	66.0 ± 1.2	5.8 ± 2.2	13.8 ± 2.2	16.6
PD-12-051313-7.7	21.0 ± 0.4	7.62 ± 0.02	8.41 ± 0.06	34.7 ± 0.5	39.0 ± 2.2	19.9 ± 2.2	66.6 ± 1.2	5.7 ± 2.2	13.3 ± 2.2	18.9
PD-12-051313-8.3	21.0 ± 0.4	7.62 ± 0.02	9.07 ± 0.07	36.6 ± 0.5	42.0 ± 2.2	19.9 ± 2.2	65.9 ± 1.3	5.6 ± 2.2	12.9 ± 2.2	21.1
PD-12-051313-8.9	21.0 ± 0.4	7.62 ± 0.02	9.72 ± 0.07	39.4 ± 0.5	46.2 ± 2.2	20.0 ± 2.2	65.7 ± 1.2	5.4 ± 2.2	12.4 ± 2.2	23.8
PD-12-051313-9.5	21.2 ± 0.4	7.61 ± 0.02	10.38 ± 0.07	44.0 ± 0.5	52.6 ± 2.2	20.4 ± 2.2	64.5 ± 1.2	5.4 ± 2.2	12.0 ± 2.2	26.6

Table C.57: Averaged values of measured pressure-drops during experiment for each data point (PD-12-051313)

Test ID	DP2-1 (Pa)	DP2-2 (Pa)	DP2-3 (Pa)	DP2-4 (Pa)	DP2-5 (Pa)	DP3 (Pa)	DP13 (Pa)	DP10 (Pa)	DP7 (Pa)
PD-12-051313-1.2	80.0 ± 11.8	25.79 ± 12.62	59.76 ± 12.90	37.8 ± 11.6	26.7 ± 11.7	109.8 ± 11.8	229.7 ± 19.9	187.0 ± 78.5	41.3 ± 10.8
PD-12-051313-1.7	100.8 ± 12.8	33.67 ± 13.58	80.91 ± 13.89	53.4 ± 12.3	33.2 ± 12.4	125.6 ± 12.8	302.7 ± 27.6	259.4 ± 78.7	50.6 ± 11.4
PD-12-051313-2.35	124.1 ± 13.3	42.77 ± 13.78	107.94 ± 14.03	74.6 ± 13.2	45.3 ± 13.1	143.4 ± 13.3	396.5 ± 31.8	366.0 ± 79.5	63.9 ± 12.1
PD-12-051313-2.9	140.5 ± 14.1	49.77 ± 14.43	130.49 ± 14.67	93.7 ± 14.4	59.2 ± 14.0	156.4 ± 14.1	476.4 ± 36.1	463.3 ± 79.4	74.4 ± 12.9
PD-12-051313-3.5	155.5 ± 15.0	57.44 ± 15.68	154.52 ± 15.91	115.8 ± 15.5	72.5 ± 15.1	169.6 ± 15.0	559.1 ± 39.8	572.8 ± 80.9	84.9 ± 13.5
PD-12-051313-4.2	169.7 ± 16.9	66.69 ± 17.74	182.03 ± 17.42	142.9 ± 17.0	93.7 ± 16.6	179.3 ± 16.9	659.4 ± 43.3	707.4 ± 81.3	95.6 ± 14.2
PD-12-051313-4.7	178.3 ± 18.1	73.98 ± 19.10	201.58 ± 18.96	163.6 ± 19.0	111.9 ± 18.3	187.9 ± 18.1	734.6 ± 52.2	806.4 ± 81.9	102.7 ± 15.7
PD-12-051313-5.3	187.4 ± 20.2	83.67 ± 20.95	225.89 ± 20.35	190.8 ± 20.6	129.8 ± 19.5	192.2 ± 20.2	823.5 ± 60.0	928.4 ± 83.0	111.1 ± 17.4
PD-12-051313-5.9	195.0 ± 21.9	93.59 ± 22.43	249.27 ± 21.77	218.9 ± 22.1	148.1 ± 21.5	196.5 ± 21.9	911.8 ± 67.5	1045.7 ± 84.0	118.1 ± 19.4
PD-12-051313-6.5	201.6 ± 23.3	103.79 ± 23.97	272.32 ± 23.40	248.3 ± 23.3	169.4 ± 22.3	197.4 ± 23.3	1003.2 ± 73.4	1161.4 ± 85.9	124.1 ± 20.8
PD-12-051313-7.1	207.6 ± 25.3	113.57 ± 26.76	294.22 ± 26.44	277.4 ± 24.8	189.9 ± 24.6	199.3 ± 25.3	1091.2 ± 90.8	1270.9 ± 86.4	128.3 ± 25.0
PD-12-051313-7.7	212.9 ± 26.9	124.71 ± 28.04	316.89 ± 27.75	309.2 ± 25.8	210.7 ± 25.6	200.1 ± 26.9	1184.0 ± 100.3	1389.4 ± 88.1	132.7 ± 27.4
PD-12-051313-8.3	216.4 ± 28.7	135.43 ± 30.20	338.99 ± 29.91	340.7 ± 27.1	233.5 ± 27.6	197.2 ± 28.7	1275.5 ± 112.3	1513.3 ± 89.5	135.0 ± 30.0
PD-12-051313-8.9	220.1 ± 32.2	146.48 ± 34.56	362.30 ± 33.61	374.3 ± 28.4	254.5 ± 29.5	195.7 ± 32.2	1369.0 ± 130.2	1624.8 ± 90.8	137.1 ± 34.4
PD-12-051313-9.5	164.6 ± 93.7	159.08 ± 124.50	384.30 ± 156.24	417.1 ± 100.5	354.6 ± 103.5	195.3 ± 93.7	1492.4 ± 425.8	1734.7 ± 93.0	138.9 ± 68.8

Table C.58: Averaged values of measured wall surface temperature during experiment for each data point (PD-12-051313)

Test ID	TS21T (C)	TS21B (C)	TS22T (C)	TS22B (C)	TS23T (C)	TS23B (C)	TS24T (C)	TS24B (C)	TS25T (C)	TS25B (C)	TS26T (C)	TS26B (C)
PD-12-051313-1.2	32.6	30.4	37.3	31.9	36.9	32.9	38.4	33.2	42.6	34.5	43.7	35.2
PD-12-051313-1.7	35.4	32.9	41.7	34.4	41.1	35.3	43.3	35.0	48.0	36.5	49.3	37.5
PD-12-051313-2.35	39.3	35.8	48.3	37.2	47.5	38.2	49.3	37.4	54.9	39.5	55.5	41.0
PD-12-051313-2.9	43.0	37.9	53.9	39.9	52.3	40.7	53.8	39.5	60.2	41.9	61.4	43.9
PD-12-051313-3.5	48.0	40.9	60.5	43.2	58.0	43.7	59.2	41.9	66.6	44.7	68.7	47.3
PD-12-051313-4.2	54.8	44.7	68.4	47.4	65.3	47.4	66.4	44.6	74.7	48.2	78.1	51.7
PD-12-051313-4.7	60.8	48.3	74.7	51.0	71.4	50.3	72.1	46.9	81.3	51.2	86.1	55.7
PD-12-051313-5.3	69.0	53.0	82.6	55.6	78.8	53.8	79.4	49.6	90.0	54.9	96.5	61.1
PD-12-051313-5.9	77.7	58.6	91.1	60.5	86.8	57.6	87.5	52.6	99.7	59.2	108.6	68.0
PD-12-051313-6.5	86.6	64.7	100.3	65.8	95.1	61.2	96.0	55.7	109.9	63.9	121.3	75.9
PD-12-051313-7.1	95.5	71.1	110.0	71.1	103.7	65.0	105.0	59.2	120.7	69.4	134.9	84.7
PD-12-051313-7.7	105.4	78.5	121.3	76.9	113.2	69.3	115.1	63.5	133.4	76.6	150.6	96.2
PD-12-051313-8.3	115.4	86.2	133.6	83.2	123.3	73.9	126.0	68.5	146.8	84.9	166.7	108.8
PD-12-051313-8.9	125.7	94.1	146.6	89.6	133.6	78.7	137.5	74.4	161.5	95.1	184.1	123.8
PD-12-051313-9.5	134.7	101.9	156.2	94.9	140.5	84.2	150.6	82.3	178.9	108.6	204.6	142.5

Table C.59: Steady-state parameters of the loop (processed data) (PD-12-051313)

Test ID	Power (kW)	Flow rate (kg/s)	Inlet K	Outlet K*	Outlet Temp. Calculated (C)	T11(C)	Total Ch. PD (Pa)	Acc. PD.(Pa)	Fr. PD.(Pa)
PD-12-051313-1.2	1.32 ± 0.03	0.030 ± 0.001	0	5.6	30.5 ± 0.3	30.4 ± 2.2	219.9 ± 19.9	15.5 ± 1.7	204.5 ± 20.0
PD-12-051313-1.7	1.86 ± 0.03	0.036 ± 0.001	0	5.0	31.2 ± 0.2	31.6 ± 2.2	288.7 ± 27.6	28.1 ± 2.3	260.6 ± 27.7
PD-12-051313-2.35	2.57 ± 0.04	0.040 ± 0.001	0	5.0	32.0 ± 0.1	32.4 ± 2.2	377.7 ± 31.8	51.2 ± 3.8	326.5 ± 32.0
PD-12-051313-2.9	3.17 ± 0.04	0.044 ± 0.001	0	5.0	32.1 ± 0.1	32.7 ± 2.2	453.5 ± 36.1	75.6 ± 5.4	377.9 ± 36.5
PD-12-051313-3.5	3.82 ± 0.04	0.047 ± 0.001	0	5.0	32.3 ± 0.1	33.0 ± 2.2	532.1 ± 39.8	107.6 ± 7.1	424.4 ± 40.4
PD-12-051313-4.2	4.59 ± 0.05	0.049 ± 0.001	0	5.0	32.3 ± 0.1	33.1 ± 2.2	627.8 ± 43.3	149.9 ± 9.2	477.9 ± 44.3
PD-12-051313-4.7	5.14 ± 0.05	0.051 ± 0.001	0	5.0	32.6 ± 0.1	33.4 ± 2.2	699.9 ± 52.2	184.8 ± 10.7	515.2 ± 53.3
PD-12-051313-5.3	5.79 ± 0.05	0.052 ± 0.001	0	5.0	32.8 ± 0.2	33.7 ± 2.2	785.2 ± 60.0	231.0 ± 12.8	554.1 ± 61.4
PD-12-051313-5.9	6.45 ± 0.06	0.053 ± 0.001	0	5.0	33.3 ± 0.2	34.4 ± 2.2	870.1 ± 67.5	280.7 ± 17.3	589.4 ± 69.6
PD-12-051313-6.5	7.10 ± 0.06	0.054 ± 0.001	0	4.9	34.1 ± 0.4	35.2 ± 2.2	958.0 ± 73.4	333.4 ± 20.3	624.5 ± 76.1
PD-12-051313-7.1	7.76 ± 0.06	0.054 ± 0.001	0	4.8	35.5 ± 0.5	36.5 ± 2.2	1043.4 ± 90.8	386.8 ± 21.2	656.6 ± 93.3
PD-12-051313-7.7	8.41 ± 0.06	0.054 ± 0.001	0	4.7	38.0 ± 0.8	39.0 ± 2.2	1132.7 ± 100.3	446.9 ± 23.7	685.8 ± 103.1
PD-12-051313-8.3	9.07 ± 0.07	0.053 ± 0.001	0	4.8	41.7 ± 1.2	42.0 ± 2.2	1221.9 ± 112.3	506.4 ± 27.7	715.5 ± 115.7
PD-12-051313-8.9	9.72 ± 0.07	0.053 ± 0.001	0	4.7	46.3 ± 1.6	46.2 ± 2.2	1312.4 ± 130.2	568.8 ± 29.7	743.6 ± 133.6
PD-12-051313-9.5	10.38 ± 0.07	0.052 ± 0.001	0	4.7	53.9 ± 2.2	52.6 ± 2.2	1433.9 ± 425.8	630.5 ± 33.1	803.3 ± 427.1

*Mean outlet K factor: 5.0

Table C.60: Comparison between frictional pressure-drop from the experimental against available friction-factor formulae (PD-12-051313)

Test ID	Fr. PD.(Pa)-Exp.	Blasius	Kondratev	Ishigai	Razumovskiy	Tarasova & Leontev	Yamashita	Popov	Kuraeva & Protopopov
PD-12-051313-1.2	204.5	163.0	134.2	114.0	126.9	134.2	88.6	119.1	275.6
PD-12-051313-1.7	260.6	223.7	183.4	145.9	165.4	178.5	110.8	150.4	360.2
PD-12-051313-2.35	326.5	289.5	236.4	184.1	209.4	229.5	141.7	185.7	451.1
PD-12-051313-2.9	377.9	342.4	278.9	217.3	246.7	272.4	170.7	215.8	524.2
PD-12-051313-3.5	424.4	394.1	320.3	251.7	284.3	316.0	203.1	245.7	595.9
PD-12-051313-4.2	477.9	449.4	364.4	289.3	325.1	363.9	240.8	277.1	672.6
PD-12-051313-4.7	515.2	485.1	392.7	316.5	353.5	397.2	270.6	299.0	723.4
PD-12-051313-5.3	554.1	527.8	426.6	349.6	387.9	437.8	308.5	324.8	784.2
PD-12-051313-5.9	589.4	565.2	456.0	381.1	419.7	475.5	347.2	348.4	838.4
PD-12-051313-6.5	624.5	604.0	486.7	413.5	452.4	514.6	387.9	372.4	894.5
PD-12-051313-7.1	656.6	631.2	508.0	440.4	478.2	545.4	425.7	391.0	935.2
PD-12-051313-7.7	685.8	668.3	537.3	476.0	512.7	586.3	474.2	416.6	989.9
PD-12-051313-8.3	715.5	693.6	557.0	505.7	540.1	618.4	519.7	436.8	1028.6
PD-12-051313-8.9	743.6	726.5	582.9	541.0	573.3	657.6	572.2	461.3	1077.3
PD-12-051313-9.5	803.3	751.0	602.0	574.8	603.4	691.8	626.7	484.6	1114.0

May 22nd, 2013- System Pressure: 9.5 MPa, Inlet Temperature: 20-21 ℃, Inlet valve: wide open, Outlet valve: wide open

Table C.61: Averaged values of measured signals during experiment for each data point (PD-13-052213)

Test ID	Inlet Temperature (RTD1) (C)	Pressure (MPa)	Power (kW)	Outlet Temp (RTD2)(C)	T11 (C)	T12(C)	CO$_2$ volumetric Flow rate (m^3/s)×10^6	HE-Inlet water Temp.(C)	HE-Outlet water Temp.(C)	Water Flow rate (lpm)
PD-13-052213-1.3	20.7 ± 0.4	9.50 ± 0.02	1.42 ± 0.03	32.5 ± 0.5	34.0 ± 2.2	20.7 ± 2.2	35.1 ± 1.1	11.4 ± 2.2	26.1 ± 2.2	1.2
PD-13-052213-1.7	20.9 ± 0.4	9.52 ± 0.02	1.86 ± 0.03	34.2 ± 0.5	36.1 ± 2.2	20.8 ± 2.2	40.6 ± 1.1	12.3 ± 2.2	24.2 ± 2.2	2.2
PD-13-052213-2.3	21.0 ± 0.4	9.50 ± 0.02	2.51 ± 0.03	36.0 ± 0.5	38.3 ± 2.2	20.3 ± 2.2	46.3 ± 1.1	11.5 ± 2.2	22.1 ± 2.2	3.6
PD-13-052213-2.9	20.9 ± 0.4	9.50 ± 0.02	3.17 ± 0.04	37.4 ± 0.5	40.0 ± 2.2	20.0 ± 2.2	51.0 ± 1.1	10.9 ± 2.2	19.9 ± 2.2	5.7
PD-13-052213-3.5	20.9 ± 0.4	9.51 ± 0.02	3.82 ± 0.04	38.6 ± 0.5	41.2 ± 2.2	20.0 ± 2.2	54.6 ± 1.1	9.7 ± 2.2	19.3 ± 2.2	6.5
PD-13-052213-4.1	21.0 ± 0.4	9.51 ± 0.02	4.48 ± 0.05	39.7 ± 0.5	42.3 ± 2.2	20.3 ± 2.2	58.0 ± 1.1	8.9 ± 2.2	18.9 ± 2.2	7.2
PD-13-052213-4.7	20.8 ± 0.4	9.48 ± 0.02	5.13 ± 0.05	40.5 ± 0.5	43.1 ± 2.2	20.2 ± 2.2	60.8 ± 1.2	8.3 ± 2.2	17.3 ± 2.2	9.5
PD-13-052213-5.4	20.7 ± 0.4	9.49 ± 0.02	5.89 ± 0.05	41.4 ± 0.5	44.3 ± 2.2	20.4 ± 2.2	63.4 ± 1.2	7.8 ± 2.2	16.4 ± 2.2	11.5
PD-13-052213-5.9	20.7 ± 0.4	9.49 ± 0.02	6.44 ± 0.06	42.0 ± 0.5	45.1 ± 2.2	20.4 ± 2.2	65.1 ± 1.2	7.7 ± 2.2	15.1 ± 2.2	14.9
PD-13-052213-6.5	20.7 ± 0.4	9.50 ± 0.02	7.10 ± 0.06	42.9 ± 0.5	46.2 ± 2.2	20.6 ± 2.2	66.7 ± 1.2	7.5 ± 2.2	14.6 ± 2.2	17
PD-13-052213-7.1	20.7 ± 0.4	9.49 ± 0.02	7.75 ± 0.06	43.7 ± 0.5	47.5 ± 2.2	20.6 ± 2.2	68.2 ± 1.2	7.3 ± 2.2	13.8 ± 2.2	20.7
PD-13-052213-7.7	21.0 ± 0.4	9.51 ± 0.02	8.41 ± 0.06	45.0 ± 0.5	49.2 ± 2.2	21.1 ± 2.2	69.2 ± 1.1	7.3 ± 2.2	13.7 ± 2.2	22.5
PD-13-052213-8.3	21.1 ± 0.4	9.51 ± 0.02	9.06 ± 0.07	46.3 ± 0.5	51.1 ± 2.2	21.2 ± 2.2	70.1 ± 1.1	7.1 ± 2.2	13.2 ± 2.2	25.6
PD-13-052213-8.75	21.4 ± 0.4	9.50 ± 0.02	9.55 ± 0.07	47.6 ± 0.5	52.9 ± 2.2	21.5 ± 2.2	70.7 ± 1.1	7.2 ± 2.2	13.1 ± 2.2	27.6

Table C.62: Averaged values of measured pressure-drops during experiment for each data point (PD-13-052213)

Test ID	DP2-1 (Pa)	DP2-2 (Pa)	DP2-3 (Pa)	DP2-4 (Pa)	DP2-5 (Pa)	DP3 (Pa)	DP13 (Pa)	DP10 (Pa)	DP7 (Pa)
PD-13-052213-1.3	111.2 ± 10.8	8.43 ± 11.01	35.67 ± 11.12	4.8 ± 11.0	58.5 ± 10.9	391.6 ± 10.8	211.5 ± 12.5	194.3 ± 78.3	55.5 ± 10.5
PD-13-052213-1.7	127.5 ± 11.3	14.29 ± 11.81	51.16 ± 12.01	15.4 ± 11.4	64.0 ± 11.3	415.4 ± 11.3	265.4 ± 14.4	215.3 ± 78.6	62.4 ± 10.6
PD-13-052213-2.3	148.9 ± 12.3	22.68 ± 13.48	74.10 ± 13.72	32.8 ± 12.2	71.6 ± 12.3	437.2 ± 12.3	343.0 ± 19.1	245.8 ± 78.6	72.3 ± 10.8
PD-13-052213-2.9	169.0 ± 13.5	30.32 ± 15.17	96.43 ± 15.52	50.8 ± 13.1	82.1 ± 13.3	460.8 ± 13.5	420.0 ± 25.8	277.7 ± 78.8	81.7 ± 11.4
PD-13-052213-3.5	185.4 ± 14.3	37.22 ± 15.88	117.16 ± 16.12	68.9 ± 13.9	93.7 ± 13.9	479.4 ± 14.3	492.7 ± 31.0	307.4 ± 78.8	90.7 ± 11.9
PD-13-052213-4.1	200.3 ± 15.2	44.65 ± 16.93	139.06 ± 17.30	89.1 ± 15.0	107.8 ± 14.6	494.6 ± 15.2	569.8 ± 38.7	341.9 ± 79.0	99.9 ± 12.9
PD-13-052213-4.7	213.9 ± 17.9	51.77 ± 20.08	160.62 ± 20.43	110.0 ± 16.6	120.9 ± 17.0	507.1 ± 17.9	644.3 ± 51.5	374.8 ± 79.2	107.0 ± 15.1
PD-13-052213-5.4	227.8 ± 19.7	59.71 ± 23.16	185.18 ± 23.56	134.7 ± 18.6	137.9 ± 19.2	523.3 ± 19.7	728.6 ± 55.2	414.8 ± 79.6	115.6 ± 15.9
PD-13-052213-5.9	237.0 ± 20.9	65.82 ± 24.22	203.01 ± 24.52	153.7 ± 19.5	150.8 ± 19.9	531.9 ± 20.9	791.5 ± 60.1	445.8 ± 79.2	120.7 ± 16.9
PD-13-052213-6.5	245.9 ± 22.8	73.40 ± 26.19	223.60 ± 26.50	177.1 ± 21.1	168.6 ± 22.1	541.3 ± 22.8	867.4 ± 66.9	481.3 ± 79.7	127.0 ± 18.3
PD-13-052213-7.1	254.3 ± 24.0	81.50 ± 27.23	245.42 ± 27.05	202.9 ± 22.8	187.6 ± 22.6	548.2 ± 24.0	947.8 ± 74.2	523.2 ± 80.2	132.9 ± 19.8
PD-13-052213-7.7	261.5 ± 26.0	89.87 ± 29.88	266.33 ± 30.60	228.8 ± 23.9	207.3 ± 24.7	555.5 ± 26.0	1027.5 ± 77.1	562.4 ± 80.4	138.4 ± 21.2
PD-13-052213-8.3	268.6 ± 28.4	98.91 ± 32.20	288.97 ± 31.68	257.1 ± 25.3	224.2 ± 26.1	560.2 ± 28.4	1108.9 ± 88.7	603.5 ± 80.2	143.3 ± 23.8
PD-13-052213-8.75	273.1 ± 29.9	106.41 ± 34.07	306.48 ± 34.50	280.0 ± 26.5	237.8 ± 27.7	561.4 ± 29.9	1173.2 ± 97.8	635.4 ± 90.8	147.2 ± 26.1

Table C.63: Averaged values of measured wall surface temperature during experiment for each data point (PD-13-052213)

Test ID	TS21T (C)	TS21B (C)	TS22T (C)	TS22B (C)	TS23T (C)	TS23B (C)	TS24T (C)	TS24B (C)	TS25T (C)	TS25B (C)	TS26T (C)	TS26B (C)
PD-13-052213-1.3	35.0	32.6	41.5	34.7	41.8	36.2	42.4	37.4	48.5	40.3	50.8	42.3
PD-13-052213-1.7	38.1	35.3	45.6	37.6	46.0	39.2	46.5	40.4	53.3	43.3	56.0	45.3
PD-13-052213-2.3	42.4	38.7	51.4	41.4	51.3	43.0	51.9	43.7	60.1	46.9	63.3	49.1
PD-13-052213-2.9	46.2	41.8	57.1	44.8	56.4	46.4	57.0	46.7	66.7	50.0	69.9	52.7
PD-13-052213-3.5	49.9	44.8	62.9	47.9	61.9	49.5	62.7	49.5	73.7	53.3	76.9	56.6
PD-13-052213-4.1	53.8	47.8	69.1	51.1	67.6	52.6	68.5	52.2	81.0	56.5	84.3	60.8
PD-13-052213-4.7	57.6	50.3	74.7	54.0	73.2	55.4	74.4	54.8	88.4	59.7	92.8	65.3
PD-13-052213-5.4	62.9	53.7	81.7	57.9	80.5	59.1	81.9	58.1	97.9	63.9	104.8	71.0
PD-13-052213-5.9	67.1	56.2	86.8	60.8	85.8	61.7	87.5	60.4	105.0	67.0	113.1	75.3
PD-13-052213-6.5	73.0	59.8	93.7	64.7	93.0	65.2	95.0	63.5	114.4	71.3	123.6	81.3
PD-13-052213-7.1	79.4	63.7	100.7	68.8	100.4	68.7	103.0	66.7	123.5	75.7	134.3	87.6
PD-13-052213-7.7	87.2	68.6	109.0	73.5	108.6	72.8	111.4	70.4	133.8	81.5	147.0	95.6
PD-13-052213-8.3	95.6	73.8	117.4	78.5	117.0	76.7	119.9	74.1	143.9	87.4	159.3	103.9
PD-13-052213-8.75	102.6	78.3	124.6	82.4	123.6	79.8	126.6	77.3	152.0	92.3	169.2	111.0

Table C.64: Steady-state parameters of the loop (processed data) (PD-13-052213)

Test ID	Power (kW)	Flow rate (kg/s)	Inlet K	Outlet K	Outlet Temp. Calculated (C)	T11(C)	Total Ch. PD (Pa)	Acc. PD.(Pa)	Fr. PD.(Pa)
PD-13-052213-1.3	1.42 ± 0.03	0.030 ± 0.001	0	0	35.1 ± 0.5	34.0 ± 2.2	202.5 ± 12.5	13.3 ± 1.2	189.1 ± 12.5
PD-13-052213-1.7	1.86 ± 0.03	0.034 ± 0.001	0	0	36.6 ± 0.4	36.1 ± 2.2	253.2 ± 14.4	21.3 ± 1.6	231.9 ± 14.5
PD-13-052213-2.3	2.51 ± 0.03	0.039 ± 0.001	0	0	38.3 ± 0.3	38.3 ± 2.2	326.7 ± 19.1	35.9 ± 2.5	290.8 ± 19.3
PD-13-052213-2.9	3.17 ± 0.04	0.043 ± 0.001	0	0	39.7 ± 0.3	40.0 ± 2.2	399.7 ± 25.8	53.8 ± 3.5	345.9 ± 26.1
PD-13-052213-3.5	3.82 ± 0.04	0.046 ± 0.001	0	0	40.8 ± 0.3	41.2 ± 2.2	468.7 ± 31.0	74.9 ± 4.6	393.9 ± 31.4
PD-13-052213-4.1	4.48 ± 0.05	0.049 ± 0.001	0	0	41.8 ± 0.2	42.3 ± 2.2	542.0 ± 38.7	100.6 ± 5.8	441.4 ± 39.1
PD-13-052213-4.7	5.13 ± 0.05	0.051 ± 0.001	0	0	42.5 ± 0.3	43.1 ± 2.2	612.8 ± 51.5	128.8 ± 7.5	484.0 ± 52.1
PD-13-052213-5.4	5.89 ± 0.05	0.053 ± 0.001	0	0	43.6 ± 0.3	44.3 ± 2.2	692.9 ± 55.2	166.0 ± 9.4	527.0 ± 56.0
PD-13-052213-5.9	6.44 ± 0.06	0.055 ± 0.001	0	0	44.3 ± 0.3	45.1 ± 2.2	752.9 ± 60.1	195.6 ± 11.0	557.2 ± 61.1
PD-13-052213-6.5	7.10 ± 0.06	0.056 ± 0.001	0	0	45.4 ± 0.4	46.2 ± 2.2	825.4 ± 66.9	234.4 ± 12.5	591.0 ± 68.0
PD-13-052213-7.1	7.75 ± 0.06	0.057 ± 0.001	0	0	46.5 ± 0.4	47.5 ± 2.2	902.4 ± 74.2	277.3 ± 14.4	625.1 ± 75.5
PD-13-052213-7.7	8.41 ± 0.06	0.058 ± 0.001	0	0	48.4 ± 0.5	49.2 ± 2.2	978.8 ± 77.1	323.1 ± 16.0	655.7 ± 78.8
PD-13-052213-8.3	9.06 ± 0.07	0.059 ± 0.001	0	0	50.3 ± 0.7	51.1 ± 2.2	1057.0 ± 88.7	372.8 ± 18.0	684.2 ± 90.5
PD-13-052213-8.75	9.55 ± 0.07	0.059 ± 0.001	0	0	52.2 ± 0.8	52.9 ± 2.2	1118.8 ± 97.8	413.7 ± 19.6	705.2 ± 99.7

Table C.65: Comparison between frictional pressure-drop from the experimental against available friction-factor formulae (PD-13-052213)

Test ID	Fr. PD.(Pa)-Exp.	Blasius	Kondratev	Ishigai	Razumovskiy	Tarasova & Leontev	Yamashita	Popov	Kuraeva & Protopopov
PD-13-052213-1.3	189.1	153.9	126.9	132.1	138.7	140.5	115.8	137.6	268.3
PD-13-052213-1.7	231.9	201.0	165.2	162.7	173.5	177.4	137.1	170.2	339.6
PD-13-052213-2.3	290.8	259.4	212.4	193.8	211.2	219.5	155.8	202.8	421.7
PD-13-052213-2.9	345.9	314.1	256.5	223.4	246.6	259.9	176.5	231.9	495.4
PD-13-052213-3.5	393.9	362.4	295.4	250.6	278.4	296.8	198.0	257.2	559.9
PD-13-052213-4.1	441.4	410.9	334.2	279.9	311.6	335.4	223.4	283.3	624.8
PD-13-052213-4.7	484.0	457.1	371.1	308.5	343.7	372.9	249.4	308.3	686.6
PD-13-052213-5.4	527.0	506.7	410.7	341.1	379.4	415.0	281.5	335.6	753.8
PD-13-052213-5.9	557.2	541.3	438.2	364.8	405.0	445.3	305.9	354.9	801.0
PD-13-052213-6.5	591.0	579.3	468.4	392.4	434.2	480.0	336.5	376.4	853.8
PD-13-052213-7.1	625.1	618.1	499.1	421.4	464.4	516.2	369.8	398.6	907.8
PD-13-052213-7.7	655.7	653.4	527.0	450.4	493.9	551.3	405.5	420.1	958.3
PD-13-052213-8.3	684.2	688.0	554.3	480.1	523.5	586.8	443.5	441.5	1008.1
PD-13-052213-8.75	705.2	714.7	575.2	504.4	547.4	615.3	475.8	458.8	1046.8

May 23rd, 2013- System Pressure: 7.6 MPa, Inlet Temperature: 20-21 ℃, Inlet valve: wide open, Outlet valve: 40º closed

Table C.66: Averaged values of measured signals during experiment for each data point (PD-14-052313)

Test ID	Inlet Temperature (RTD1) (C)	Pressure (MPa)	Power (kW)	Outlet Temp (RTD2)(C)	T11 (C)	T12(C)	CO_2 volumetric Flow rate $(m^3/s)\times10^6$	HE-Inlet water Temp.(C)	HE-Outlet water Temp.(C)	Water Flow rate (lpm)
PD-14-052313-1.8	20.9 ± 0.4	7.58 ± 0.02	1.97 ± 0.03	29.4 ± 0.5	31.1 ± 2.2	20.4 ± 2.2	42.1 ± 1.1	10.9 ± 2.2	21.6 ± 2.2	2.9
PD-14-052313-2.6	20.8 ± 0.4	7.62 ± 0.02	2.84 ± 0.04	30.3 ± 0.5	31.8 ± 2.2	20.4 ± 2.2	47.8 ± 1.1	10.6 ± 2.2	18.9 ± 2.2	5.6
PD-14-052313-3	20.9 ± 0.4	7.61 ± 0.02	3.28 ± 0.04	30.4 ± 0.5	32.0 ± 2.2	20.4 ± 2.2	49.8 ± 1.1	9.7 ± 2.2	18.1 ± 2.2	6.5
PD-14-052313-3.5	20.9 ± 0.4	7.59 ± 0.02	3.82 ± 0.04	30.5 ± 0.5	32.1 ± 2.2	20.4 ± 2.2	51.7 ± 1.1	9.1 ± 2.2	17.3 ± 2.2	7.8
PD-14-052313-4.1	20.9 ± 0.4	7.61 ± 0.02	4.48 ± 0.05	30.9 ± 0.5	32.6 ± 2.2	20.5 ± 2.2	53.2 ± 1.1	8.7 ± 2.2	16.4 ± 2.2	9.8
PD-14-052313-4.7	20.9 ± 0.4	7.61 ± 0.02	5.13 ± 0.05	31.2 ± 0.5	33.4 ± 2.2	20.4 ± 2.2	53.9 ± 1.1	8.2 ± 2.2	15.4 ± 2.2	12.2
PD-14-052313-5.3	20.9 ± 0.4	7.61 ± 0.02	5.79 ± 0.05	31.9 ± 0.5	34.7 ± 2.2	20.4 ± 2.2	53.9 ± 1.1	8.0 ± 2.2	14.4 ± 2.2	15.4
PD-14-052313-5.9	20.9 ± 0.4	7.60 ± 0.02	6.44 ± 0.06	33.1 ± 0.5	37.1 ± 2.2	20.2 ± 2.2	53.4 ± 1.1	7.5 ± 2.2	13.5 ± 2.2	18.6
PD-14-052313-6.8	21.0 ± 0.4	7.62 ± 0.02	7.43 ± 0.06	37.8 ± 0.5	44.5 ± 2.2	20.2 ± 2.2	51.4 ± 1.1	7.2 ± 2.2	12.7 ± 2.2	23.3

Table C.67: Averaged values of measured pressure-drops during experiment for each data point (PD-14-052313)

Test ID	DP2-1 (Pa)	DP2-2 (Pa)	DP2-3 (Pa)	DP2-4 (Pa)	DP2-5 (Pa)	DP3 (Pa)	DP13 (Pa)	DP10 (Pa)	DP7 (Pa)
PD-14-052313-1.8	93.4 ± 12.4	33.04 ± 12.96	76.91 ± 13.13	51.2 ± 12.3	39.8 ± 12.3	130.7 ± 12.4	290.6 ± 22.4	814.4 ± 298.6	55.4 ± 10.9
PD-14-052313-2.6	113.7 ± 13.6	42.34 ± 14.13	103.88 ± 14.09	73.5 ± 13.4	56.5 ± 13.1	151.6 ± 13.6	386.5 ± 27.1	1156.0 ± 258.2	68.8 ± 11.2
PD-14-052313-3	121.5 ± 13.9	47.34 ± 14.42	117.97 ± 14.36	86.2 ± 13.8	67.0 ± 13.5	157.3 ± 13.9	437.0 ± 28.3	1343.2 ± 236.5	75.7 ± 11.2
PD-14-052313-3.5	129.1 ± 14.7	53.78 ± 15.22	135.01 ± 15.19	102.3 ± 14.6	79.7 ± 14.3	161.6 ± 14.7	497.3 ± 32.0	1573.7 ± 253.8	83.2 ± 11.4
PD-14-052313-4.1	136.7 ± 15.5	61.48 ± 15.81	154.01 ± 15.71	121.8 ± 15.9	98.1 ± 15.1	166.9 ± 15.5	569.9 ± 34.6	1835.8 ± 308.6	90.6 ± 11.5
PD-14-052313-4.7	142.4 ± 16.3	69.83 ± 16.68	172.48 ± 16.27	143.2 ± 16.7	115.1 ± 15.7	169.0 ± 16.3	641.1 ± 35.1	2105.0 ± 295.0	96.8 ± 11.7
PD-14-052313-5.3	146.6 ± 17.2	78.20 ± 17.32	190.33 ± 16.88	165.7 ± 17.8	134.4 ± 16.5	169.1 ± 17.2	713.6 ± 36.9	2366.9 ± 298.6	101.9 ± 11.8
PD-14-052313-5.9	149.8 ± 18.1	87.17 ± 18.11	208.45 ± 17.62	190.0 ± 19.2	152.4 ± 17.5	165.7 ± 18.1	786.4 ± 38.8	2639.3 ± 305.8	105.6 ± 11.9
PD-14-052313-6.8	88.0 ± 156.9	99.63 ± 127.21	231.04 ± 155.38	231.9 ± 96.9	262.3 ± 98.5	162.6 ± 156.9	912.1 ± 241.7	3045.5 ± 303.9	109.5 ± 36.7

Table C.68: Averaged values of measured wall surface temperature during experiment for each data point (PD-14-052313)

Test ID	TS21T (C)	TS21B (C)	TS22T (C)	TS22B (C)	TS23T (C)	TS23B (C)	TS24T (C)	TS24B (C)	TS25T (C)	TS25B (C)	TS26T (C)	TS26B (C)
PD-14-052313-1.8	36.7	33.3	45.4	34.4	45.2	35.3	46.3	34.7	51.8	36.5	52.5	37.7
PD-14-052313-2.6	43.4	37.3	55.3	38.7	54.1	39.4	54.4	38.3	60.9	40.6	61.2	42.6
PD-14-052313-3	47.7	39.7	60.7	41.3	58.7	41.6	58.5	40.0	65.5	42.8	66.4	45.3
PD-14-052313-3.5	54.1	43.2	68.1	44.8	65.0	44.6	64.0	42.3	72.1	45.7	74.2	49.0
PD-14-052313-4.1	62.5	48.1	77.7	49.7	73.2	48.4	72.0	45.5	81.4	49.9	85.1	54.6
PD-14-052313-4.7	71.8	53.9	88.3	55.1	81.8	52.6	80.7	48.8	91.9	54.5	97.8	61.9
PD-14-052313-5.3	81.9	60.7	100.4	61.3	91.5	57.1	90.6	52.7	103.7	60.3	113.3	71.5
PD-14-052313-5.9	92.6	68.4	113.6	68.1	101.9	62.0	101.3	57.2	117.3	67.6	131.5	83.6
PD-14-052313-6.8	109.2	81.1	132.0	78.2	116.1	70.4	120.3	67.1	142.9	84.5	164.6	109.7

Table C.69: Steady-state parameters of the loop (processed data) (PD-14-052313)

Test ID	Power (kW)	Flow rate (kg/s)	Inlet K	Outlet K*	Outlet Temp. Calculated (C)	T11(C)	Total Ch. PD (Pa)	Acc. PD.(Pa)	Fr. PD.(Pa)
PD-14-052313-1.8	1.97 ± 0.03	0.034 ± 0.001	0	20.0	31.7 ± 0.1	31.1 ± 2.2	277.4 ± 22.4	32.0 ± 2.7	245.4 ± 22.6
PD-14-052313-2.6	2.84 ± 0.04	0.039 ± 0.001	0	19.8	32.3 ± 0.1	31.8 ± 2.2	368.5 ± 27.1	61.1 ± 4.6	307.4 ± 27.5
PD-14-052313-3	3.28 ± 0.04	0.040 ± 0.001	0	19.9	32.3 ± 0.1	32.0 ± 2.2	416.8 ± 28.3	79.9 ± 5.6	336.9 ± 28.9
PD-14-052313-3.5	3.82 ± 0.04	0.042 ± 0.001	0	20.0	32.3 ± 0.1	32.1 ± 2.2	474.5 ± 32.0	106.2 ± 7.0	368.3 ± 32.8
PD-14-052313-4.1	4.48 ± 0.05	0.043 ± 0.001	0	19.9	32.6 ± 0.1	32.6 ± 2.2	544.4 ± 34.6	140.4 ± 8.9	404.0 ± 35.7
PD-14-052313-4.7	5.13 ± 0.05	0.044 ± 0.001	0	19.9	33.0 ± 0.2	33.4 ± 2.2	613.2 ± 35.1	178.4 ± 11.3	434.8 ± 36.9
PD-14-052313-5.3	5.79 ± 0.05	0.044 ± 0.001	0	19.9	34.1 ± 0.4	34.7 ± 2.2	683.6 ± 36.9	219.9 ± 13.4	463.7 ± 39.2
PD-14-052313-5.9	6.44 ± 0.06	0.043 ± 0.001	0	19.9	36.3 ± 0.7	37.1 ± 2.2	754.5 ± 38.8	265.0 ± 16.4	489.4 ± 42.1
PD-14-052313-6.8	7.43 ± 0.06	0.042 ± 0.001	0	20.0	44.6 ± 1.6	44.5 ± 2.2	878.2 ± 241.7	334.1 ± 20.0	544.1 ± 242.5

*Mean outlet K factor: 19.9

Table C.70: Comparison between frictional pressure-drop from the experimental against available friction-factor formulae (PD-14-052313)

Test ID	Fr. PD.(Pa)-Exp.	Blasius	Kondratev	Ishigai	Razumovskiy	Tarasova & Leontev	Yamashita	Popov	Kuraeva & Protopopov
PD-14-052313-1.8	245.4	210.3	172.4	136.6	154.8	168.3	105.1	139.0	341.6
PD-14-052313-2.6	307.4	275.5	224.9	176.1	199.6	220.3	139.1	174.8	433.5
PD-14-052313-3	336.9	303.9	247.7	195.0	220.2	244.4	157.3	190.8	474.1
PD-14-052313-3.5	368.3	335.4	272.9	216.9	243.8	272.3	180.1	208.5	519.5
PD-14-052313-4.1	404.0	367.4	298.3	241.3	269.2	302.4	207.8	227.6	566.6
PD-14-052313-4.7	434.8	395.1	320.2	264.6	292.6	330.4	236.6	244.7	608.5
PD-14-052313-5.3	463.7	417.2	337.6	286.2	313.4	355.3	266.4	259.5	643.3
PD-14-052313-5.9	489.4	437.2	353.3	308.2	333.9	379.8	299.1	274.2	675.4
PD-14-052313-6.8	544.1	458.7	370.0	340.4	362.1	412.1	351.7	295.4	711.6

May 24th, 2013- System Pressure: 8.5 MPa, Inlet Temperature: 20-21 °C, Inlet valve: wide open, Outlet valve: wide open

Table C.71: Averaged values of measured signals during experiment for each data point (PD-15-052413)

Test ID	Inlet Temperature (RTD1) (C)	Pressure (MPa)	Power (kW)	Outlet Temp (RTD2)(C)	T11 (C)	T12(C)	CO_2 volumetric Flow rate $(m^3/s) \times 10^6$	HE-Inlet water Temp.(C)	HE-Outlet water Temp.(C)	Water Flow rate (lpm)
PD-15-052413-1.25	20.3 ± 0.4	8.52 ± 0.02	1.86 ± 0.03	31.6 ± 0.5	33.7 ± 2.2	19.7 ± 2.2	41.7 ± 1.4	11.5 ± 2.2	21.6 ± 2.2	2.9
PD-15-052413-1.7	20.6 ± 0.4	8.52 ± 0.03	1.37 ± 0.03	30.4 ± 0.5	32.1 ± 2.2	20.0 ± 2.2	35.6 ± 1.4	10.1 ± 2.2	25.1 ± 2.2	1.2
PD-15-052413-2.3	20.6 ± 0.4	8.52 ± 0.02	2.52 ± 0.03	33.1 ± 0.5	35.2 ± 2.2	20.1 ± 2.2	47.0 ± 1.3	11.2 ± 2.2	21.0 ± 2.2	4
PD-15-052413-2.9	20.4 ± 0.4	8.51 ± 0.02	3.17 ± 0.04	34.0 ± 0.5	36.1 ± 2.2	19.6 ± 2.2	51.9 ± 1.3	9.9 ± 2.2	19.5 ± 2.2	5.3
PD-15-052413-3.5	20.7 ± 0.4	8.50 ± 0.02	3.83 ± 0.04	34.8 ± 0.5	36.8 ± 2.2	20.0 ± 2.2	56.2 ± 1.4	9.4 ± 2.2	18.7 ± 2.2	6.7
PD-15-052413-4.1	20.8 ± 0.4	8.51 ± 0.02	4.48 ± 0.05	35.4 ± 0.5	37.5 ± 2.2	20.2 ± 2.2	59.6 ± 1.4	8.9 ± 2.2	17.8 ± 2.2	8.4
PD-15-052413-4.7	21.0 ± 0.4	8.50 ± 0.02	5.14 ± 0.05	36.0 ± 0.5	38.1 ± 2.2	20.5 ± 2.2	62.5 ± 1.4	8.5 ± 2.2	17.2 ± 2.2	10
PD-15-052413-5.3	21.0 ± 0.4	8.50 ± 0.02	5.79 ± 0.05	36.4 ± 0.5	38.7 ± 2.2	20.7 ± 2.2	64.9 ± 1.3	8.1 ± 2.2	16.4 ± 2.2	11.8
PD-15-052413-5.9	21.0 ± 0.4	8.51 ± 0.02	6.45 ± 0.06	37.0 ± 0.5	39.6 ± 2.2	20.9 ± 2.2	66.5 ± 1.4	7.9 ± 2.2	15.5 ± 2.2	14.4
PD-15-052413-6.5	21.0 ± 0.4	8.50 ± 0.02	7.11 ± 0.06	37.5 ± 0.5	40.4 ± 2.2	21.0 ± 2.2	68.2 ± 1.4	7.8 ± 2.2	14.7 ± 2.2	17.9
PD-15-052413-7.1	21.0 ± 0.4	8.50 ± 0.02	7.76 ± 0.06	38.3 ± 0.5	41.6 ± 2.2	21.1 ± 2.2	69.1 ± 1.3	7.7 ± 2.2	14.0 ± 2.2	21.2
PD-15-052413-7.7	21.3 ± 0.4	8.52 ± 0.02	8.42 ± 0.06	39.5 ± 0.5	43.5 ± 2.2	21.5 ± 2.2	69.8 ± 1.4	7.7 ± 2.2	13.8 ± 2.2	24
PD-15-052413-8.3	21.5 ± 0.4	8.53 ± 0.02	9.07 ± 0.07	41.0 ± 0.5	45.6 ± 2.2	21.7 ± 2.2	69.9 ± 1.3	7.8 ± 2.2	13.4 ± 2.2	27.5

Table C.72: Averaged values of measured pressure-drops during experiment for each data point (PD-15-052413)

Test ID	DP2-1 (Pa)	DP2-2 (Pa)	DP2-3 (Pa)	DP2-4 (Pa)	DP2-5 (Pa)	DP3 (Pa)	DP13 (Pa)	DP10 (Pa)	DP7 (Pa)
PD-15-052413-1.25	120.0 ± 11.2	24.45 ± 11.40	69.93 ± 11.51	36.5 ± 11.5	47.9 ± 11.3	285.2 ± 11.2	290.5 ± 15.1	289.1 ± 78.5	55.1 ± 10.6
PD-15-052413-1.7	100.4 ± 10.9	17.42 ± 11.04	50.81 ± 11.09	22.8 ± 11.1	41.8 ± 10.9	263.5 ± 10.9	223.2 ± 12.6	264.6 ± 78.3	46.9 ± 10.5
PD-15-052413-2.3	141.2 ± 11.7	32.85 ± 11.94	93.26 ± 12.07	54.9 ± 12.2	57.7 ± 11.8	304.1 ± 11.7	372.2 ± 17.0	324.8 ± 78.5	66.3 ± 10.6
PD-15-052413-2.9	161.0 ± 12.2	40.53 ± 12.46	116.99 ± 12.63	74.6 ± 13.0	69.0 ± 12.4	320.6 ± 12.2	454.8 ± 18.2	359.3 ± 78.8	76.9 ± 10.7
PD-15-052413-3.5	178.2 ± 12.8	48.50 ± 13.04	141.58 ± 13.22	96.1 ± 13.8	82.5 ± 13.2	334.0 ± 12.8	539.8 ± 20.2	400.7 ± 78.9	87.6 ± 10.7
PD-15-052413-4.1	193.7 ± 13.6	56.35 ± 14.02	165.60 ± 14.21	118.1 ± 15.2	97.9 ± 14.2	347.7 ± 13.6	624.2 ± 22.0	443.9 ± 79.1	96.7 ± 10.8
PD-15-052413-4.7	206.7 ± 14.4	64.62 ± 14.65	189.79 ± 14.95	142.1 ± 16.4	112.1 ± 15.2	357.9 ± 14.4	707.6 ± 23.3	488.9 ± 79.3	105.7 ± 10.9
PD-15-052413-5.3	218.1 ± 15.4	72.66 ± 15.61	212.89 ± 15.79	166.3 ± 17.8	128.0 ± 16.2	366.5 ± 15.4	789.5 ± 26.3	533.6 ± 79.5	113.4 ± 10.9
PD-15-052413-5.9	228.3 ± 16.2	80.96 ± 16.44	235.93 ± 16.53	192.1 ± 19.4	145.3 ± 17.6	375.5 ± 16.2	873.0 ± 27.0	580.0 ± 79.9	120.5 ± 11.0
PD-15-052413-6.5	237.2 ± 17.5	89.82 ± 17.78	259.29 ± 17.40	220.2 ± 21.3	166.6 ± 19.0	380.3 ± 17.5	962.5 ± 29.8	625.3 ± 79.9	127.4 ± 11.2
PD-15-052413-7.1	245.1 ± 17.9	99.23 ± 18.14	282.49 ± 18.10	249.5 ± 22.1	188.3 ± 19.2	384.4 ± 17.9	1052.8 ± 31.1	673.7 ± 80.4	133.2 ± 11.2
PD-15-052413-7.7	252.4 ± 18.6	109.45 ± 18.56	306.25 ± 18.49	280.1 ± 23.0	211.0 ± 20.0	388.1 ± 18.6	1146.0 ± 31.4	721.6 ± 81.7	139.5 ± 11.3
PD-15-052413-8.3	258.7 ± 19.7	120.32 ± 18.71	330.43 ± 18.74	312.1 ± 23.6	230.8 ± 20.7	389.2 ± 19.7	1238.3 ± 33.2	770.9 ± 91.2	143.9 ± 11.5

Table C.73: Averaged values of measured wall surface temperature during experiment for each data point (PD-15-052413)

Test ID	TS21T (C)	TS21B (C)	TS22T (C)	TS22B (C)	TS23T (C)	TS23B (C)	TS24T (C)	TS24B (C)	TS25T (C)	TS25B (C)	TS26T (C)	TS26B (C)
PD-15-052413-1.25	36.4	33.8	43.0	35.8	42.8	37.0	43.6	37.6	49.2	39.7	51.1	40.9
PD-15-052413-1.7	33.6	31.5	39.3	33.2	39.4	34.5	39.7	35.3	45.0	37.4	46.6	38.6
PD-15-052413-2.3	40.3	37.2	48.9	39.2	48.1	40.4	48.7	40.3	55.7	42.6	57.4	44.4
PD-15-052413-2.9	43.4	39.9	54.3	41.8	53.0	43.0	53.2	42.6	61.7	45.3	64.0	48.0
PD-15-052413-3.5	47.3	42.6	60.3	44.8	58.4	45.8	58.5	45.0	68.7	48.4	71.9	52.0
PD-15-052413-4.1	51.6	45.5	66.4	48.0	64.1	48.8	64.1	47.6	76.0	51.6	80.3	56.0
PD-15-052413-4.7	56.6	48.5	72.8	51.4	70.2	51.9	70.3	50.2	84.0	55.0	89.1	60.7
PD-15-052413-5.3	62.2	51.8	79.0	55.1	76.9	55.1	77.2	52.9	92.2	58.7	98.9	65.6
PD-15-052413-5.9	68.7	55.5	85.8	59.1	84.1	58.5	84.6	55.9	100.9	62.8	109.3	71.3
PD-15-052413-6.5	75.9	59.6	93.0	63.4	91.5	62.0	92.2	58.9	110.2	66.9	120.0	77.5
PD-15-052413-7.1	84.0	64.6	101.1	68.1	99.5	65.6	100.2	62.1	120.0	71.7	132.0	84.7
PD-15-052413-7.7	93.0	70.7	110.3	73.3	108.0	69.6	109.0	65.9	130.7	77.4	145.1	93.5
PD-15-052413-8.3	102.4	77.4	120.2	78.7	116.9	73.6	118.2	70.0	142.0	84.0	159.0	103.4

Table C.74: Steady-state parameters of the loop (processed data) (PD-15-052413)

Test ID	Power (kW)	Flow rate (kg/s)	Inlet K	Outlet K	Outlet Temp. Calculated (C)	T11(C)	Total Ch. PD (Pa)	Acc. PD.(Pa)	Fr. PD.(Pa)
PD-15-052413-1.25	1.86 ± 0.03	0.035 ± 0.001	0	0	34.0 ± 0.3	33.7 ± 2.2	277.6 ± 15.1	24.0 ± 2.2	253.6 ± 15.2
PD-15-052413-1.7	1.37 ± 0.03	0.030 ± 0.001	0	0	33.0 ± 0.4	32.1 ± 2.2	214.0 ± 12.6	14.3 ± 1.5	199.8 ± 12.7
PD-15-052413-2.3	2.52 ± 0.03	0.039 ± 0.001	0	0	35.5 ± 0.2	35.2 ± 2.2	355.4 ± 17.0	41.0 ± 3.3	314.4 ± 17.3
PD-15-052413-2.9	3.17 ± 0.04	0.043 ± 0.001	0	0	36.2 ± 0.2	36.1 ± 2.2	433.7 ± 18.2	61.7 ± 4.7	372.0 ± 18.8
PD-15-052413-3.5	3.83 ± 0.04	0.047 ± 0.001	0	0	36.8 ± 0.2	36.8 ± 2.2	514.3 ± 20.2	88.4 ± 6.7	425.9 ± 21.3
PD-15-052413-4.1	4.48 ± 0.05	0.049 ± 0.001	0	0	37.3 ± 0.2	37.5 ± 2.2	594.5 ± 22.0	118.9 ± 8.3	475.6 ± 23.5
PD-15-052413-4.7	5.14 ± 0.05	0.052 ± 0.001	0	0	37.8 ± 0.2	38.1 ± 2.2	673.9 ± 23.3	154.5 ± 10.3	519.4 ± 25.5
PD-15-052413-5.3	5.79 ± 0.05	0.054 ± 0.001	0	0	38.2 ± 0.2	38.7 ± 2.2	751.8 ± 26.3	192.8 ± 11.8	559.0 ± 28.8
PD-15-052413-5.9	6.45 ± 0.06	0.055 ± 0.001	0	0	39.0 ± 0.3	39.6 ± 2.2	831.8 ± 27.0	234.8 ± 14.5	597.1 ± 30.7
PD-15-052413-6.5	7.11 ± 0.06	0.056 ± 0.001	0	0	39.7 ± 0.3	40.4 ± 2.2	917.5 ± 29.8	281.4 ± 16.9	636.0 ± 34.2
PD-15-052413-7.1	7.76 ± 0.06	0.057 ± 0.001	0	0	40.8 ± 0.4	41.6 ± 2.2	1004.5 ± 31.1	330.8 ± 19.1	673.7 ± 36.6
PD-15-052413-7.7	8.42 ± 0.06	0.057 ± 0.001	0	0	42.7 ± 0.6	43.5 ± 2.2	1094.4 ± 31.4	385.4 ± 22.9	709.0 ± 38.9
PD-15-052413-8.3	9.07 ± 0.07	0.057 ± 0.001	0	0	45.3 ± 0.8	45.6 ± 2.2	1183.8 ± 33.2	442.1 ± 24.1	741.8 ± 41.1

Table C.75: Comparison between frictional pressure-drop from the experimental against available friction-factor formulae (PD-15-052413)

Test ID	Fr. PD.(Pa)-Exp.	Blasius	Kondratev	Ishigai	Razumovskiy	Tarasova & Leontev	Yamashita	Popov	Kuraeva & Protopopov
PD-15-052413-1.25	253.6	209.4	171.9	158.0	171.9	178.2	127.5	165.6	349.0
PD-15-052413-1.7	199.8	155.1	127.8	127.7	135.6	138.4	109.1	133.1	269.6
PD-15-052413-2.3	314.4	264.4	216.4	183.8	204.4	216.7	143.5	190.7	423.0
PD-15-052413-2.9	372.0	322.5	263.2	216.9	243.0	261.0	169.1	222.1	501.6
PD-15-052413-3.5	425.9	379.2	308.6	251.1	281.8	306.0	198.5	252.9	578.1
PD-15-052413-4.1	475.6	431.3	350.3	284.4	318.8	349.0	229.1	282.1	648.8
PD-15-052413-4.7	519.4	480.7	389.7	317.6	354.9	391.3	261.8	310.0	716.3
PD-15-052413-5.3	559.0	527.1	426.6	349.5	389.3	432.0	294.7	336.1	779.9
PD-15-052413-5.9	597.1	566.9	458.1	379.2	420.4	468.9	327.9	359.3	835.5
PD-15-052413-6.5	636.0	609.8	492.1	411.6	454.2	509.2	365.0	384.3	895.5
PD-15-052413-7.1	673.7	644.9	519.8	440.8	483.7	544.5	401.6	405.6	945.9
PD-15-052413-7.7	709.0	679.8	547.3	472.8	515.2	581.9	443.7	428.8	997.0
PD-15-052413-8.3	741.8	710.0	570.9	503.2	544.2	616.3	486.5	450.0	1041.9

May 27th, 2013 (I) - System Pressure: 9.5 MPa, Inlet Temperature: 20-21 °C, Inlet valve: wide open, Outlet valve: 31° closed

Table C.76: Averaged values of measured signals during experiment for each data point (PD-16-052713(I))

Test ID	Inlet Temperature (RTD1) (C)	Pressure (MPa)	Power (kW)	Outlet Temp (RTD2)(C)	T11 (C)	T12(C)	CO$_2$ volumetric Flow rate (m^3/s)×10^6	HE-Inlet water Temp.(C)	HE-Outlet water Temp.(C)	Water Flow rate (lpm)
PD-16-052713(I)-1.2	20.3 ± 0.4	9.51 ± 0.02	1.31 ± 0.03	31.7 ± 0.5	33.4 ± 2.2	19.9 ± 2.2	29.5 ± 3.0	11.7 ± 2.2	24.8 ± 2.2	1.4
PD-16-052713(I)-1.8	20.9 ± 0.4	9.48 ± 0.02	1.97 ± 0.03	34.4 ± 0.5	36.2 ± 2.2	21.0 ± 2.2	39.9 ± 1.1	12.2 ± 2.2	23.8 ± 2.2	2.4
PD-16-052713(I)-2.3	20.7 ± 0.4	9.49 ± 0.02	2.52 ± 0.03	35.6 ± 0.5	38.0 ± 2.2	20.1 ± 2.2	44.7 ± 1.2	11.6 ± 2.2	20.9 ± 2.2	4.2
PD-16-052713(I)-2.9	20.8 ± 0.4	9.51 ± 0.02	3.17 ± 0.04	37.1 ± 0.5	39.7 ± 2.2	19.9 ± 2.2	49.3 ± 1.1	11.0 ± 2.2	19.2 ± 2.2	6.3
PD-16-052713(I)-3.5	20.7 ± 0.4	9.51 ± 0.02	3.83 ± 0.04	38.3 ± 0.5	40.9 ± 2.2	19.8 ± 2.2	52.5 ± 1.1	10.0 ± 2.2	18.5 ± 2.2	7.4
PD-16-052713(I)-4.2	20.9 ± 0.4	9.50 ± 0.02	4.48 ± 0.05	39.5 ± 0.5	42.1 ± 2.2	19.9 ± 2.2	55.4 ± 1.1	9.5 ± 2.2	17.8 ± 2.2	8.9
PD-16-052713(I)-4.7	21.0 ± 0.4	9.50 ± 0.02	5.14 ± 0.05	40.5 ± 0.5	43.3 ± 2.2	20.0 ± 2.2	58.0 ± 1.2	9.0 ± 2.2	16.7 ± 2.2	11.2
PD-16-052713(I)-5.3	21.2 ± 0.4	9.51 ± 0.02	5.79 ± 0.05	41.6 ± 0.5	44.7 ± 2.2	20.4 ± 2.2	59.9 ± 1.2	8.8 ± 2.2	16.2 ± 2.2	13.1
PD-16-052713(I)-5.9	21.1 ± 0.4	9.50 ± 0.02	6.45 ± 0.06	42.5 ± 0.5	45.9 ± 2.2	20.3 ± 2.2	61.5 ± 1.2	8.6 ± 2.2	15.0 ± 2.2	17.3
PD-16-052713(I)-6.5	21.5 ± 0.4	9.50 ± 0.02	7.11 ± 0.06	43.8 ± 0.5	47.7 ± 2.2	20.8 ± 2.2	62.5 ± 1.3	8.7 ± 2.2	14.8 ± 2.2	19.6
PD-16-052713(I)-7.1	21.4 ± 0.4	9.51 ± 0.02	7.76 ± 0.06	45.2 ± 0.5	49.8 ± 2.2	20.7 ± 2.2	63.3 ± 1.2	8.5 ± 2.2	13.9 ± 2.2	24.5
PD-16-052713(I)-7.7	21.7 ± 0.4	9.53 ± 0.02	8.42 ± 0.06	47.8 ± 0.5	52.6 ± 2.2	21.3 ± 2.2	63.3 ± 1.2	8.5 ± 2.2	13.7 ± 2.2	27.8

Table C.77: Averaged values of measured pressure-drops during experiment for each data point (PD-16-052713(I))

Test ID	DP2-1 (Pa)	DP2-2 (Pa)	DP2-3 (Pa)	DP2-4 (Pa)	DP2-5 (Pa)	DP3 (Pa)	DP13 (Pa)	DP10 (Pa)	DP7 (Pa)
PD-16-052713(I)-1.2	84.9 ± 10.8	48.38 ± 10.90	25.04 ± 10.97	-26.5 ± 10.9	36.6 ± 10.8	455.3 ± 10.8	189.7 ± 13.2	289.3 ± 78.9	53.3 ± 10.5
PD-16-052713(I)-1.8	105.2 ± 11.2	57.45 ± 11.39	46.53 ± 11.56	-11.1 ± 11.4	43.7 ± 11.2	473.0 ± 11.2	264.4 ± 16.4	381.9 ± 79.9	62.7 ± 10.6
PD-16-052713(I)-2.3	122.5 ± 11.6	63.96 ± 11.91	64.36 ± 12.08	2.7 ± 11.9	50.8 ± 11.6	493.5 ± 11.6	327.3 ± 18.2	466.9 ± 80.2	70.8 ± 10.7
PD-16-052713(I)-2.9	140.1 ± 12.1	71.18 ± 12.56	84.83 ± 12.67	19.5 ± 12.5	62.4 ± 12.1	514.5 ± 12.1	400.7 ± 20.1	569.8 ± 81.2	79.7 ± 10.7
PD-16-052713(I)-3.5	154.1 ± 12.5	77.93 ± 12.95	104.12 ± 13.16	36.9 ± 13.3	74.3 ± 12.7	529.8 ± 12.5	469.6 ± 21.6	665.0 ± 82.1	87.7 ± 10.8
PD-16-052713(I)-4.2	166.8 ± 13.2	84.94 ± 13.66	124.15 ± 13.88	56.0 ± 14.3	88.5 ± 13.4	543.3 ± 13.2	541.6 ± 23.8	773.5 ± 82.7	95.9 ± 10.8
PD-16-052713(I)-4.7	178.5 ± 13.9	92.07 ± 14.43	144.42 ± 14.55	76.3 ± 15.2	104.7 ± 14.3	555.1 ± 13.9	615.0 ± 25.5	883.6 ± 83.8	103.3 ± 10.9
PD-16-052713(I)-5.3	187.6 ± 14.8	99.21 ± 15.23	163.85 ± 15.10	97.2 ± 16.0	121.2 ± 15.0	563.2 ± 14.8	685.8 ± 27.0	984.6 ± 84.9	109.9 ± 11.0
PD-16-052713(I)-5.9	195.9 ± 15.7	106.40 ± 16.13	183.21 ± 15.86	119.4 ± 17.3	137.0 ± 16.0	571.8 ± 15.7	755.9 ± 30.0	1106.4 ± 86.1	115.8 ± 11.2
PD-16-052713(I)-6.5	201.9 ± 16.6	114.60 ± 16.56	203.42 ± 16.43	143.6 ± 18.3	154.0 ± 17.0	573.9 ± 16.6	829.6 ± 30.5	1219.2 ± 88.8	121.4 ± 11.3
PD-16-052713(I)-7.1	208.1 ± 17.1	122.02 ± 17.14	222.37 ± 17.17	167.1 ± 19.5	170.9 ± 18.1	578.3 ± 17.1	900.3 ± 32.3	1335.4 ± 89.2	126.1 ± 11.4
PD-16-052713(I)-7.7	189.9 ± 58.4	131.68 ± 83.89	240.34 ± 120.02	191.5 ± 28.8	214.4 ± 88.1	588.2 ± 58.4	975.6 ± 126.9	1445.5 ± 103.0	129.8 ± 34.0

236

Table C.78: Averaged values of measured wall surface temperature during experiment for each data point (PD-16-052713(I))

Test ID	TS21T (C)	TS21B (C)	TS22T (C)	TS22B (C)	TS23T (C)	TS23B (C)	TS24T (C)	TS24B (C)	TS25T (C)	TS25B (C)	TS26T (C)	TS26B (C)
PD-16-052713(I)-1.2	33.9	31.7	41.0	33.6	41.1	35.0	41.7	36.4	47.7	39.2	49.9	41.0
PD-16-052713(I)-1.8	39.2	36.1	48.0	38.3	47.8	39.7	48.8	40.7	55.7	43.6	58.2	45.6
PD-16-052713(I)-2.3	42.3	38.7	52.8	41.1	52.2	42.6	53.1	43.3	61.4	46.4	64.5	48.8
PD-16-052713(I)-2.9	46.4	42.0	59.1	44.5	58.1	46.0	58.7	46.4	68.8	49.8	71.4	52.9
PD-16-052713(I)-3.5	50.4	45.0	65.7	47.7	64.4	49.2	65.0	49.4	76.5	53.3	79.1	57.2
PD-16-052713(I)-4.2	54.8	48.0	72.4	51.0	70.8	52.4	71.5	52.4	84.7	56.9	87.8	61.8
PD-16-052713(I)-4.7	59.9	51.2	79.4	54.6	77.6	55.6	78.5	55.4	93.3	60.9	97.1	67.1
PD-16-052713(I)-5.3	65.9	54.7	87.1	58.6	85.1	59.4	86.0	58.7	102.7	65.2	108.0	73.2
PD-16-052713(I)-5.9	72.4	58.4	94.8	62.7	92.7	62.9	93.9	62.0	112.3	69.7	120.2	79.7
PD-16-052713(I)-6.5	80.7	63.4	103.6	67.6	101.6	67.0	102.9	65.9	123.2	75.5	133.7	88.0
PD-16-052713(I)-7.1	89.1	68.3	112.6	72.5	110.3	71.1	111.9	69.9	134.1	81.7	147.4	96.7
PD-16-052713(I)-7.7	98.6	74.5	122.1	78.5	117.7	75.9	121.1	74.9	146.6	89.5	163.1	108.0

Table C.79: Steady-state parameters of the loop (processed data) (PD-16-052713(I))

Test ID	Power (kW)	Flow rate (kg/s)	Inlet K	Outlet K*	Outlet Temp. Calculated (C)	T11(C)	Total Ch. PD (Pa)	Acc. PD.(Pa)	Fr. PD.(Pa)
PD-16-052713(I)-1.2	1.31 ± 0.03	0.025 ± 0.003	0	11.6	35.9 ± 1.1	33.4 ± 2.2	183.2 ± 13.2	10.6 ± 2.7	172.6 ± 13.5
PD-16-052713(I)-1.8	1.97 ± 0.03	0.034 ± 0.001	0	7.1	37.3 ± 0.4	36.2 ± 2.2	252.5 ± 16.4	23.1 ± 1.8	229.4 ± 16.5
PD-16-052713(I)-2.3	2.52 ± 0.03	0.038 ± 0.001	0	6.8	38.6 ± 0.4	38.0 ± 2.2	311.9 ± 18.2	35.0 ± 2.7	276.9 ± 18.4
PD-16-052713(I)-2.9	3.17 ± 0.04	0.042 ± 0.001	0	6.7	40.0 ± 0.3	39.7 ± 2.2	381.6 ± 20.1	52.9 ± 3.6	328.6 ± 20.4
PD-16-052713(I)-3.5	3.83 ± 0.04	0.044 ± 0.001	0	6.7	41.2 ± 0.3	40.9 ± 2.2	447.2 ± 21.6	73.9 ± 4.8	373.3 ± 22.2
PD-16-052713(I)-4.2	4.48 ± 0.05	0.047 ± 0.001	0	6.8	42.2 ± 0.3	42.1 ± 2.2	515.8 ± 23.8	99.2 ± 6.2	416.7 ± 24.6
PD-16-052713(I)-4.7	5.14 ± 0.05	0.049 ± 0.001	0	6.8	43.2 ± 0.3	43.3 ± 2.2	585.8 ± 25.5	128.2 ± 7.9	457.6 ± 26.7
PD-16-052713(I)-5.3	5.79 ± 0.05	0.050 ± 0.001	0	6.7	44.3 ± 0.3	44.7 ± 2.2	653.5 ± 27.0	160.9 ± 9.6	492.6 ± 28.6
PD-16-052713(I)-5.9	6.45 ± 0.06	0.052 ± 0.001	0	6.9	45.4 ± 0.4	45.9 ± 2.2	720.5 ± 30.0	196.3 ± 11.5	524.3 ± 32.1
PD-16-052713(I)-6.5	7.11 ± 0.06	0.052 ± 0.001	0	6.8	47.0 ± 0.5	47.7 ± 2.2	791.3 ± 30.5	237.6 ± 14.8	553.7 ± 33.9
PD-16-052713(I)-7.1	7.76 ± 0.06	0.053 ± 0.001	0	6.9	49.0 ± 0.7	49.8 ± 2.2	859.3 ± 32.3	278.6 ± 15.9	580.7 ± 36.0
PD-16-052713(I)-7.7	8.42 ± 0.06	0.053 ± 0.001	0	6.9	52.0 ± 0.9	52.6 ± 2.2	932.5 ± 126.9	323.3 ± 18.0	609.2 ± 128.2

*Mean outlet K factor: 6.8

Table C.80: Comparison between frictional pressure-drop from the experimental against available friction-factor formulae (PD-16-052713(I))

Test ID	Fr. PD.(Pa)-Exp.	Blasius	Kondratev	Ishigai	Razumovskiy	Tarasova & Leontev	Yamashita	Popov	Kuraeva & Protopopov
PD-16-052713(I)-1.2	172.6	113.8	94.2	100.3	104.7	105.8	89.6	104.1	205.6
PD-16-052713(I)-1.8	229.4	196.0	161.1	154.7	166.2	170.8	128.2	162.0	331.8
PD-16-052713(I)-2.3	276.9	244.6	200.5	181.6	198.4	206.6	145.6	190.0	400.2
PD-16-052713(I)-2.9	328.6	297.2	242.9	210.2	232.4	245.6	166.1	217.8	471.6
PD-16-052713(I)-3.5	373.3	340.0	277.3	234.1	260.3	278.4	185.5	239.3	529.1
PD-16-052713(I)-4.2	416.7	382.8	311.6	260.1	289.7	312.9	208.9	262.0	587.3
PD-16-052713(I)-4.7	457.6	425.5	345.6	287.5	319.9	348.4	235.0	285.1	645.5
PD-16-052713(I)-5.3	492.6	461.7	374.4	312.5	346.8	380.4	261.7	305.0	696.0
PD-16-052713(I)-5.9	524.3	497.2	402.7	337.7	373.6	412.6	289.5	324.5	745.9
PD-16-052713(I)-6.5	553.7	529.1	427.9	363.4	399.7	444.0	321.1	343.0	792.3
PD-16-052713(I)-7.1	580.7	558.8	451.3	387.8	424.3	473.8	352.0	360.5	835.6
PD-16-052713(I)-7.7	609.2	581.6	469.2	410.8	446.2	500.1	384.9	376.0	870.8

May 27th, 2013 (II) - System Pressure: 9.5 MPa, Inlet Temperature: 20-21 ºC, Inlet valve: wide open, Outlet valve: 40º closed

Table C.81: Averaged values of measured signals during experiment for each data point (PD-17-052713(II))

Test ID	Inlet Temperature (RTD1) (C)	Pressure (MPa)	Power (kW)	Outlet Temp (RTD2)(C)	T11 (C)	T12(C)	CO$_2$ volumetric Flow rate (m^3/s)$\times 10^6$	HE-Inlet water Temp.(C)	HE-Outlet water Temp.(C)	Water Flow rate (lpm)
PD-17-052713(II)-1.7	20.5 ± 0.4	8.51 ± 0.02	1.86 ± 0.03	31.7 ± 0.5	34.1 ± 2.2	19.8 ± 2.2	39.3 ± 1.1	11.1 ± 2.2	21.5 ± 2.2	3
PD-17-052713(II)-2.3	20.8 ± 0.4	8.52 ± 0.02	2.52 ± 0.04	33.3 ± 0.5	35.4 ± 2.2	20.4 ± 2.2	44.6 ± 1.1	11.4 ± 2.2	19.7 ± 2.2	5
PD-17-052713(II)-2.9	20.9 ± 0.4	8.52 ± 0.02	3.17 ± 0.04	34.2 ± 0.5	36.3 ± 2.2	20.5 ± 2.2	48.0 ± 1.1	10.9 ± 2.2	18.4 ± 2.2	7.1
PD-17-052713(II)-3.5	21.0 ± 0.4	8.51 ± 0.02	3.83 ± 0.04	34.9 ± 0.5	37.1 ± 2.2	20.5 ± 2.2	50.4 ± 1.2	9.9 ± 2.2	17.6 ± 2.2	8.4
PD-17-052713(II)-4.1	21.0 ± 0.4	8.51 ± 0.02	4.48 ± 0.05	35.6 ± 0.5	37.9 ± 2.2	20.5 ± 2.2	52.5 ± 1.2	9.6 ± 2.2	16.6 ± 2.2	10.9
PD-17-052713(II)-4.7	21.3 ± 0.4	8.51 ± 0.02	5.14 ± 0.05	36.5 ± 0.5	39.1 ± 2.2	20.6 ± 2.2	53.9 ± 1.2	9.4 ± 2.2	15.6 ± 2.2	14.2
PD-17-052713(II)-5.3	21.2 ± 0.4	8.51 ± 0.02	5.79 ± 0.05	37.4 ± 0.5	40.5 ± 2.2	20.4 ± 2.2	54.7 ± 1.2	9.0 ± 2.2	14.7 ± 2.2	17.5
PD-17-052713(II)-5.9	21.5 ± 0.4	8.53 ± 0.02	6.45 ± 0.06	39.0 ± 0.5	42.8 ± 2.2	21.0 ± 2.2	54.7 ± 1.3	9.0 ± 2.2	14.5 ± 2.2	19.9
PD-17-052713(II)-6.5	21.7 ± 0.4	8.51 ± 0.02	7.10 ± 0.06	41.5 ± 0.5	46.3 ± 2.2	21.5 ± 2.2	53.8 ± 1.2	8.9 ± 2.2	13.9 ± 2.2	24.4
PD-17-052713(II)-6.5	21.7 ± 0.4	8.51 ± 0.02	7.10 ± 0.06	41.3 ± 0.5	46.4 ± 2.2	21.4 ± 2.2	54.0 ± 1.3	8.8 ± 2.2	13.8 ± 2.2	24.4
PD-17-052713(II)-7.1	21.7 ± 0.4	8.52 ± 0.02	7.76 ± 0.06	45.2 ± 0.5	50.9 ± 2.2	22.3 ± 2.2	53.2 ± 1.1	8.7 ± 2.2	13.4 ± 2.2	27.7

Table C.82: Averaged values of measured pressure-drops during experiment for each data point (PD-17-052713(II))

Test ID	DP2-1 (Pa)	DP2-2 (Pa)	DP2-3 (Pa)	DP2-4 (Pa)	DP2-5 (Pa)	DP3 (Pa)	DP13 (Pa)	DP10 (Pa)	DP7 (Pa)
PD-17-052713(II)-1.7	88.1 ± 11.7	62.79 ± 12.16	52.97 ± 12.40	1.7 ± 11.7	35.3 ± 11.6	368.7 ± 11.7	253.6 ± 20.2	698.9 ± 82.4	54.4 ± 10.8
PD-17-052713(II)-2.3	103.6 ± 12.4	70.48 ± 12.88	72.20 ± 13.07	17.3 ± 12.4	45.1 ± 12.3	378.1 ± 12.4	320.7 ± 23.5	913.2 ± 84.8	64.2 ± 10.9
PD-17-052713(II)-2.9	116.6 ± 13.0	77.52 ± 13.46	91.30 ± 13.58	33.9 ± 13.2	56.1 ± 12.8	385.4 ± 13.0	386.8 ± 26.2	1132.3 ± 86.3	73.7 ± 11.0
PD-17-052713(II)-3.5	127.1 ± 14.0	84.35 ± 14.57	110.25 ± 14.58	51.6 ± 14.0	71.4 ± 13.5	389.5 ± 14.0	455.5 ± 29.4	1358.4 ± 90.2	82.4 ± 11.2
PD-17-052713(II)-4.1	135.4 ± 14.7	91.24 ± 15.27	128.71 ± 15.24	70.4 ± 15.0	88.5 ± 14.4	393.2 ± 14.7	524.6 ± 30.3	1587.1 ± 93.5	89.7 ± 11.3
PD-17-052713(II)-4.7	142.4 ± 15.5	98.81 ± 15.94	147.58 ± 15.69	91.0 ± 16.4	104.5 ± 15.3	395.9 ± 15.5	594.2 ± 33.5	1829.7 ± 97.8	96.8 ± 11.4
PD-17-052713(II)-5.3	147.4 ± 16.6	105.97 ± 16.98	164.57 ± 16.63	111.4 ± 17.2	119.1 ± 16.0	399.5 ± 16.6	658.2 ± 33.9	2057.2 ± 101.3	101.9 ± 11.6
PD-17-052713(II)-5.9	150.9 ± 17.1	114.28 ± 17.32	182.32 ± 17.18	133.7 ± 18.3	135.7 ± 16.8	398.9 ± 17.1	726.0 ± 37.0	2288.6 ± 102.9	107.3 ± 11.7
PD-17-052713(II)-6.5	130.4 ± 78.3	124.00 ± 91.04	199.51 ± 120.55	157.0 ± 40.2	180.7 ± 82.2	399.3 ± 78.3	800.1 ± 133.9	2548.9 ± 105.0	111.1 ± 31.3
PD-17-052713(II)-6.5	133.1 ± 72.9	123.79 ± 83.63	199.50 ± 110.58	157.6 ± 38.3	177.0 ± 75.6	399.9 ± 72.9	799.4 ± 123.2	2550.9 ± 97.3	110.4 ± 28.9
PD-17-052713(II)-7.1	33.5 ± 238.5	129.00 ± 224.58	214.14 ± 276.44	178.6 ± 137.3	367.4 ± 176.0	397.4 ± 238.5	930.0 ± 349.3	2810.3 ± 190.4	115.0 ± 68.1

Table C.83: Averaged values of measured wall surface temperature during experiment for each data point (PD-17-052713(II))

Test ID	TS21T (C)	TS21B (C)	TS22T (C)	TS22B (C)	TS23T (C)	TS23B (C)	TS24T (C)	TS24B (C)	TS25T (C)	TS25B (C)	TS26T (C)	TS26B (C)
PD-17-052713(II)-1.7	37.2	34.3	45.1	36.0	44.8	37.0	46.1	37.4	51.8	39.5	53.2	41.0
PD-17-052713(II)-2.3	41.3	37.7	52.3	39.3	52.2	40.3	53.0	40.4	60.1	42.9	61.2	44.9
PD-17-052713(II)-2.9	45.9	40.6	59.9	42.4	59.3	43.4	59.7	43.2	68.3	46.3	69.5	49.3
PD-17-052713(II)-3.5	51.4	43.6	68.0	45.9	66.4	46.8	66.5	46.2	76.7	49.9	79.0	54.2
PD-17-052713(II)-4.1	58.2	47.4	76.9	50.0	74.2	50.5	74.2	49.4	86.1	54.1	89.5	59.8
PD-17-052713(II)-4.7	66.5	52.0	86.6	54.8	82.9	54.5	82.7	53.0	96.3	58.9	101.5	66.7
PD-17-052713(II)-5.3	75.5	57.2	97.2	60.0	92.0	58.7	92.0	56.9	107.5	64.5	115.0	74.7
PD-17-052713(II)-5.9	86.5	64.0	109.8	66.7	102.6	63.8	102.9	61.7	120.9	72.0	132.4	86.1
PD-17-052713(II)-6.5	97.8	72.0	122.4	73.9	111.3	69.2	114.0	67.2	135.5	81.1	151.9	100.0
PD-17-052713(II)-6.5	97.6	71.8	122.3	73.8	111.5	69.2	114.0	67.1	135.2	80.7	151.7	99.6
PD-17-052713(II)-7.1	108.8	80.3	130.5	79.4	118.4	74.2	124.3	73.6	151.6	92.1	173.1	117.0

Table C.84: Steady-state parameters of the loop (processed data) (PD-17-052713(II))

Test ID	Power (kW)	Flow rate (kg/s)	Inlet K	Outlet K*	Outlet Temp. Calculated (C)	T11(C)	Total Ch. PD (Pa)	Acc. PD.(Pa)	Fr. PD.(Pa)
PD-17-052713(II)-1.7	1.86 ± 0.03	0.033 ± 0.001	0	20.1	34.6 ± 0.3	34.1 ± 2.2	242.1 ± 20.2	23.5 ± 2.0	218.5 ± 20.3
PD-17-052713(II)-2.3	2.52 ± 0.04	0.037 ± 0.001	0	19.4	35.8 ± 0.2	35.4 ± 2.2	305.4 ± 23.5	40.6 ± 3.1	264.8 ± 23.7
PD-17-052713(II)-2.9	3.17 ± 0.04	0.040 ± 0.001	0	19.5	36.7 ± 0.2	36.3 ± 2.2	368.4 ± 26.2	61.6 ± 4.4	306.7 ± 26.5
PD-17-052713(II)-3.5	3.83 ± 0.04	0.042 ± 0.001	0	19.7	37.4 ± 0.2	37.1 ± 2.2	434.2 ± 29.4	87.1 ± 6.1	347.1 ± 30.0
PD-17-052713(II)-4.1	4.48 ± 0.05	0.043 ± 0.001	0	19.6	38.0 ± 0.2	37.9 ± 2.2	500.4 ± 30.3	116.6 ± 7.8	383.8 ± 31.3
PD-17-052713(II)-4.7	5.14 ± 0.05	0.044 ± 0.001	0	19.7	38.9 ± 0.3	39.1 ± 2.2	567.4 ± 33.5	151.0 ± 9.7	416.4 ± 34.9
PD-17-052713(II)-5.3	5.79 ± 0.05	0.045 ± 0.001	0	19.6	40.0 ± 0.4	40.5 ± 2.2	628.9 ± 33.9	187.2 ± 12.1	441.7 ± 36.0
PD-17-052713(II)-5.9	6.45 ± 0.06	0.045 ± 0.001	0	19.5	42.3 ± 0.7	42.8 ± 2.2	694.8 ± 37.0	228.3 ± 15.4	466.5 ± 40.1
PD-17-052713(II)-6.5	7.10 ± 0.06	0.044 ± 0.001	0	19.8	46.1 ± 1.1	46.3 ± 2.2	767.3 ± 133.9	272.0 ± 17.8	495.4 ± 135.1
PD-17-052713(II)-6.5	7.10 ± 0.06	0.044 ± 0.001	0	19.8	45.9 ± 1.1	46.4 ± 2.2	766.6 ± 123.2	272.2 ± 18.0	494.3 ± 124.5
PD-17-052713(II)-7.1	7.76 ± 0.06	0.044 ± 0.001	0	20.0	51.4 ± 1.5	50.9 ± 2.2	895.5 ± 349.3	315.2 ± 18.4	580.3 ± 349.8

*Mean outlet K factor: 19.7

Table C.85: Comparison between frictional pressure-drop from the experimental against available friction-factor formulae (PD-17-052713(II))

Test ID	Fr. PD.(Pa)-Exp.	Blasius	Kondratev	Ishigai	Razumovskiy	Tarasova & Leontev	Yamashita	Popov	Kuraeva & Protopopov
PD-17-052713(II)-1.7	218.5	188.7	155.1	138.0	151.6	158.5	109.5	144.4	317.2
PD-17-052713(II)-2.3	264.8	241.7	197.9	164.9	184.3	197.0	128.6	169.8	390.0
PD-17-052713(II)-2.9	306.7	283.6	231.6	188.8	211.9	229.7	149.0	190.8	448.0
PD-17-052713(II)-3.5	347.1	319.6	260.4	211.4	237.0	259.6	171.0	209.4	498.5
PD-17-052713(II)-4.1	383.8	354.6	288.3	235.3	262.7	290.3	195.8	228.6	548.5
PD-17-052713(II)-4.7	416.4	385.5	312.9	258.9	287.2	319.5	223.0	246.5	593.9
PD-17-052713(II)-5.3	441.7	412.9	334.7	280.8	309.6	346.5	250.1	262.4	634.7
PD-17-052713(II)-5.9	466.5	433.5	350.8	301.7	329.4	370.5	280.0	276.2	667.6
PD-17-052713(II)-6.5	495.4	448.7	362.6	321.3	346.9	391.4	311.2	288.4	693.3
PD-17-052713(II)-6.5	494.3	450.6	364.1	322.3	348.1	392.8	311.9	289.3	695.7
PD-17-052713(II)-7.1	580.3	467.1	377.0	343.4	367.1	415.0	344.9	303.5	722.4

May 29th, 2013 - System Pressure: 7.6 MPa, Inlet Temperature: 20-21 ℃, Inlet valve: 45º closed, Outlet valve: wide open

Table C.86: Averaged values of measured signals during experiment for each data point (PD-18-052913)

Test ID	Inlet Temperature (RTD1) (C)	Pressure (MPa)	Power (kW)	Outlet Temp (RTD2)(C)	T11 (C)	T12(C)	CO_2 volumetric Flow rate $(m^3/s)\times10^6$	HE-Inlet water Temp.(C)	HE-Outlet water Temp.(C)	Water Flow rate (lpm)
PD-18-052913-1.6	20.9 ± 0.4	7.60 ± 0.02	1.75 ± 0.03	28.4 ± 0.5	30.0 ± 2.2	20.8 ± 2.2	36.5 ± 1.2	12.3 ± 2.2	20.5 ± 2.2	3.4
PD-18-052913-2.3	21.1 ± 0.4	7.58 ± 0.02	2.52 ± 0.03	28.8 ± 0.5	30.4 ± 2.2	20.6 ± 2.2	42.9 ± 1.1	11.3 ± 2.2	18.1 ± 2.2	6.2
PD-18-052913-2.9	21.0 ± 0.4	7.62 ± 0.02	3.18 ± 0.04	29.4 ± 0.5	31.0 ± 2.2	20.3 ± 2.2	46.0 ± 1.1	10.4 ± 2.2	17.2 ± 2.2	7.9
PD-18-052913-3.5	21.1 ± 0.4	7.62 ± 0.02	3.83 ± 0.04	29.7 ± 0.5	31.5 ± 2.2	20.3 ± 2.2	48.4 ± 1.1	9.7 ± 2.2	16.5 ± 2.2	9.7
PD-18-052913-4.1	21.3 ± 0.4	7.62 ± 0.02	4.49 ± 0.05	30.3 ± 0.5	32.5 ± 2.2	20.5 ± 2.2	50.3 ± 1.1	9.4 ± 2.2	16.0 ± 2.2	11.7
PD-18-052913-4.7	21.2 ± 0.4	7.60 ± 0.02	5.15 ± 0.05	30.9 ± 0.5	33.7 ± 2.2	20.4 ± 2.2	51.6 ± 1.1	9.1 ± 2.2	14.6 ± 2.2	16.4
PD-18-052913-5.3	21.3 ± 0.4	7.62 ± 0.02	5.80 ± 0.05	32.2 ± 0.5	35.9 ± 2.2	20.5 ± 2.2	52.3 ± 1.1	9.0 ± 2.2	14.1 ± 2.2	19.4
PD-18-052913-5.9	21.2 ± 0.4	7.63 ± 0.02	6.46 ± 0.06	34.2 ± 0.5	38.8 ± 2.2	20.6 ± 2.2	52.8 ± 1.2	8.9 ± 2.2	13.6 ± 2.2	23.9
PD-18-052913-6.3	21.4 ± 0.4	7.62 ± 0.02	6.90 ± 0.06	36.2 ± 0.5	42.4 ± 2.2	20.8 ± 2.2	52.8 ± 1.2	8.8 ± 2.2	13.2 ± 2.2	28

Table C.87: Averaged values of measured pressure-drops during experiment for each data point (PD-18-052913)

Test ID	DP2-1 (Pa)	DP2-2 (Pa)	DP2-3 (Pa)	DP2-4 (Pa)	DP2-5 (Pa)	DP3 (Pa)	DP13 (Pa)	DP10 (Pa)	DP7 (Pa)
PD-18-052913-1.6	105.6 ± 13.0	53.27 ± 14.07	88.17 ± 14.35	24.9 ± 12.3	9.4 ± 12.8	1172.7 ± 13.0	237.1 ± 25.3	-151.1 ± 78.8	49.9 ± 11.3
PD-18-052913-2.3	119.5 ± 13.5	61.88 ± 13.95	111.31 ± 14.10	43.6 ± 13.2	23.9 ± 13.2	1498.0 ± 13.5	316.8 ± 29.3	-1.1 ± 80.2	66.0 ± 11.4
PD-18-052913-2.9	132.4 ± 13.8	71.10 ± 14.23	130.45 ± 14.57	38.6 ± 14.9	62.7 ± 14.7	1707.6 ± 13.8	390.7 ± 31.5	94.3 ± 79.7	79.4 ± 11.5
PD-18-052913-3.5	143.0 ± 14.8	79.49 ± 15.09	151.23 ± 15.17	49.5 ± 15.1	88.3 ± 14.5	1879.4 ± 14.8	460.4 ± 34.6	638.1 ± 171.4	86.4 ± 11.6
PD-18-052913-4.1	153.1 ± 15.4	89.11 ± 15.72	172.60 ± 15.75	73.4 ± 16.1	103.5 ± 15.3	2011.4 ± 15.4	540.7 ± 37.1	789.2 ± 82.2	91.0 ± 11.8
PD-18-052913-4.7	161.1 ± 16.1	98.08 ± 16.29	193.38 ± 16.49	99.2 ± 18.5	89.9 ± 16.2	2124.8 ± 16.1	591.5 ± 39.7	831.7 ± 83.9	96.3 ± 11.9
PD-18-052913-5.3	169.4 ± 16.8	108.04 ± 17.01	214.20 ± 17.24	127.2 ± 19.2	95.2 ± 17.0	2203.6 ± 16.8	664.1 ± 40.1	842.0 ± 84.3	101.3 ± 12.0
PD-18-052913-5.9	176.9 ± 17.4	117.79 ± 17.56	234.82 ± 17.89	155.9 ± 20.9	112.4 ± 17.9	2262.5 ± 17.4	748.0 ± 42.9	844.6 ± 84.4	105.8 ± 12.2
PD-18-052913-6.3	174.5 ± 79.8	123.47 ± 88.37	225.31 ± 85.41	204.5 ± 39.3	130.1 ± 43.3	2292.7 ± 79.8	806.9 ± 115.8	847.5 ± 102.9	107.8 ± 23.6

Table C.88: Averaged values of measured wall surface temperature during experiment for each data point (PD-18-052913)

Test ID	TS21T (C)	TS21B (C)	TS22T (C)	TS22B (C)	TS23T (C)	TS23B (C)	TS24T (C)	TS24B (C)	TS25T (C)	TS25B (C)	TS26T (C)	TS26B (C)
PD-18-052913-1.6	34.2	30.8	48.8	33.3	47.4	34.7	46.8	33.8	52.0	35.2	52.6	36.4
PD-18-052913-2.3	48.1	37.4	61.9	41.0	57.3	39.6	55.2	37.1	60.8	38.9	60.6	40.8
PD-18-052913-2.9	55.8	43.1	66.5	43.2	62.8	41.7	60.3	39.7	67.4	42.6	68.7	45.6
PD-18-052913-3.5	63.4	48.4	76.4	47.8	70.1	45.4	67.2	42.8	76.2	46.8	79.5	51.3
PD-18-052913-4.1	70.5	53.6	86.2	52.8	77.6	49.2	75.0	46.3	86.2	51.5	92.1	58.8
PD-18-052913-4.7	80.7	60.9	97.4	58.9	86.1	53.3	83.6	49.7	97.1	56.8	105.6	67.4
PD-18-052913-5.3	87.8	67.1	107.3	64.0	94.6	57.5	93.0	54.0	109.5	63.7	122.0	78.6
PD-18-052913-5.9	95.1	73.0	117.9	69.4	103.9	61.9	103.2	58.8	123.0	72.0	139.5	91.4
PD-18-052913-6.3	100.7	78.0	123.7	73.0	108.6	65.1	110.4	62.8	132.8	78.5	152.6	101.3

Table C.89: Steady-state parameters of the loop (processed data) (PD-18-052913)

Test ID	Power (kW)	Flow rate (kg/s)	Inlet K	Outlet K*	Outlet Temp. Calculated (C)	T11(C)	Total Ch. PD (Pa)	Acc. PD.(Pa)	Fr. PD.(Pa)
PD-18-052913-1.6	1.75 ± 0.03	0.030 ± 0.001	0	50.6	31.9 ± 0.1	30.0 ± 2.2	227.2 ± 25.3	25.0 ± 2.5	202.1 ± 25.4
PD-18-052913-2.3	2.52 ± 0.03	0.035 ± 0.001	0	49.9	32.1 ± 0.1	30.4 ± 2.2	302.4 ± 29.3	49.6 ± 3.9	252.8 ± 29.6
PD-18-052913-2.9	3.18 ± 0.04	0.037 ± 0.001	0	50.8	32.4 ± 0.1	31.0 ± 2.2	373.1 ± 31.5	74.5 ± 5.4	298.7 ± 32.0
PD-18-052913-3.5	3.83 ± 0.04	0.039 ± 0.001	0	51.7	32.5 ± 0.1	31.5 ± 2.2	439.9 ± 34.6	105.0 ± 7.3	334.9 ± 35.3
PD-18-052913-4.1	4.49 ± 0.05	0.041 ± 0.001	0	52.2	32.9 ± 0.2	32.5 ± 2.2	517.3 ± 37.1	140.5 ± 9.5	376.8 ± 38.3
PD-18-052913-4.7	5.15 ± 0.05	0.042 ± 0.001	0	52.8	33.4 ± 0.3	33.7 ± 2.2	565.3 ± 39.7	179.4 ± 11.6	385.8 ± 41.3
PD-18-052913-5.3	5.80 ± 0.05	0.042 ± 0.001	0	53.7	34.9 ± 0.5	35.9 ± 2.2	635.3 ± 40.1	221.8 ± 14.2	413.5 ± 42.5
PD-18-052913-5.9	6.46 ± 0.06	0.043 ± 0.001	0	54.2	37.2 ± 0.8	38.8 ± 2.2	716.6 ± 42.9	266.5 ± 17.5	450.0 ± 46.3
PD-18-052913-6.3	6.90 ± 0.06	0.043 ± 0.001	0	55.3	39.8 ± 1.1	42.4 ± 2.2	773.8 ± 115.8	300.4 ± 18.7	473.4 ± 117.3

*Mean outlet K factor: 52.4

Table C.90: Comparison between frictional pressure-drop from the experimental against available friction-factor formulae (PD-18-052913)

Test ID	Fr. PD.(Pa)-Exp.	Blasius	Kondratev	Ishigai	Razumovskiy	Tarasova & Leontev	Yamashita	Popov	Kuraeva & Protopopov
PD-18-052913-1.6	202.1	163.7	134.5	108.5	122.3	132.6	84.8	110.2	274.7
PD-18-052913-2.3	252.8	226.2	185.0	143.9	163.3	181.1	114.2	141.9	364.5
PD-18-052913-2.9	298.7	266.2	217.2	171.3	193.2	215.2	140.0	166.2	422.8
PD-18-052913-3.5	334.9	303.3	246.9	198.0	221.7	248.5	168.0	188.2	477.3
PD-18-052913-4.1	376.8	339.1	275.4	225.9	250.6	282.2	199.1	210.6	530.4
PD-18-052913-4.7	385.8	372.9	302.3	252.8	278.2	315.0	231.0	231.1	580.7
PD-18-052913-5.3	413.5	402.6	325.8	279.3	304.6	345.9	264.9	251.1	625.8
PD-18-052913-5.9	450.0	432.2	349.2	306.5	331.3	377.4	300.8	271.2	670.4
PD-18-052913-6.3	473.4	450.9	363.9	326.4	350.2	399.1	328.7	285.7	699.0

May 30th, 2013 - System Pressure: 8.5 MPa, Inlet Temperature: 20-21 ℃, Inlet valve: 46º closed, Outlet valve: wide open

Table C.91: Averaged values of measured signals during experiment for each data point (PD-19-053013)

Test ID	Inlet Temperature (RTD1) (C)	Pressure (MPa)	Power (kW)	Outlet Temp (RTD2)(C)	T11 (C)	T12(C)	CO_2 volumetric Flow rate $(m^3/s) \times 10^6$	HE-Inlet water Temp.(C)	HE-Outlet water Temp.(C)	Water Flow rate (lpm)
PD-19-053013-2.65	20.5 ± 0.4	8.48 ± 0.02	2.90 ± 0.04	33.1 ± 0.5	35.1 ± 2.2	19.6 ± 2.2	41.5 ± 1.2	10.5 ± 2.2	17.5 ± 2.2	7
PD-19-053013-2.9	20.4 ± 0.4	8.50 ± 0.02	3.17 ± 0.04	33.4 ± 0.5	35.6 ± 2.2	19.5 ± 2.2	43.0 ± 1.2	10.1 ± 2.2	16.9 ± 2.2	7.9
PD-19-053013-3.5	20.5 ± 0.4	8.50 ± 0.02	3.83 ± 0.04	34.3 ± 0.5	36.6 ± 2.2	19.4 ± 2.2	45.7 ± 1.1	9.7 ± 2.2	15.7 ± 2.2	10.9
PD-19-053013-4.1	20.4 ± 0.4	8.51 ± 0.02	4.49 ± 0.05	35.1 ± 0.5	37.8 ± 2.2	19.4 ± 2.2	47.7 ± 1.1	9.3 ± 2.2	14.6 ± 2.2	14.9
PD-19-053013-4.7	20.5 ± 0.4	8.51 ± 0.02	5.14 ± 0.05	36.2 ± 0.5	39.4 ± 2.2	19.8 ± 2.2	49.1 ± 1.2	9.1 ± 2.2	14.3 ± 2.2	16.7
PD-19-053013-5.3	20.8 ± 0.4	8.51 ± 0.02	5.80 ± 0.05	37.7 ± 0.5	41.7 ± 2.2	20.2 ± 2.2	50.5 ± 1.2	8.9 ± 2.2	13.8 ± 2.2	20.6
PD-19-053013-5.9	21.1 ± 0.4	8.52 ± 0.02	6.45 ± 0.06	40.0 ± 0.5	44.7 ± 2.2	20.5 ± 2.2	51.2 ± 1.1	8.8 ± 2.2	13.7 ± 2.2	22.8
PD-19-053013-6.5	21.2 ± 0.4	8.49 ± 0.02	7.11 ± 0.06	43.3 ± 0.5	49.1 ± 2.2	21.2 ± 2.2	51.8 ± 1.1	8.8 ± 2.2	13.1 ± 2.2	28

Table C.92: Averaged values of measured pressure-drops during experiment for each data point (PD-19-053013)

Test ID	DP2-1 (Pa)	DP2-2 (Pa)	DP2-3 (Pa)	DP2-4 (Pa)	DP2-5 (Pa)	DP3 (Pa)	DP13 (Pa)	DP10 (Pa)	DP7 (Pa)
PD-19-053013-2.65	117.1 ± 13.4	6.60 ± 13.89	77.66 ± 14.09	73.0 ± 12.9	22.3 ± 13.0	1720.0 ± 13.4	317.4 ± 29.7	434.1 ± 79.3	67.2 ± 11.6
PD-19-053013-2.9	122.0 ± 13.7	8.66 ± 14.16	84.41 ± 14.40	79.5 ± 13.2	27.5 ± 13.2	1818.7 ± 13.7	342.3 ± 31.1	450.5 ± 79.2	70.2 ± 11.6
PD-19-053013-3.5	132.0 ± 14.4	15.45 ± 15.16	102.58 ± 15.19	97.2 ± 14.1	41.3 ± 13.9	2018.8 ± 14.4	408.8 ± 35.6	497.7 ± 79.3	77.9 ± 11.9
PD-19-053013-4.1	140.8 ± 15.0	22.46 ± 15.81	120.78 ± 15.80	116.3 ± 14.8	56.2 ± 14.6	2189.8 ± 15.0	475.8 ± 37.5	548.6 ± 79.9	85.2 ± 12.0
PD-19-053013-4.7	148.2 ± 15.5	30.10 ± 15.82	139.57 ± 15.75	137.2 ± 16.0	71.4 ± 15.1	2313.3 ± 15.5	545.5 ± 38.4	591.1 ± 79.9	91.9 ± 11.9
PD-19-053013-5.3	155.8 ± 16.1	38.79 ± 16.43	160.09 ± 16.37	160.8 ± 16.5	88.6 ± 15.7	2420.9 ± 16.1	622.2 ± 38.4	640.1 ± 80.3	98.3 ± 12.0
PD-19-053013-5.9	162.3 ± 16.6	47.93 ± 16.78	180.03 ± 17.07	185.0 ± 17.5	106.4 ± 16.3	2488.1 ± 16.6	699.3 ± 40.2	681.7 ± 80.7	103.8 ± 12.0
PD-19-053013-6.5	101.5 ± 209.5	58.08 ± 253.15	199.46 ± 275.88	209.6 ± 93.1	218.4 ± 155.6	2528.8 ± 209.5	805.2 ± 322.1	759.9 ± 108.7	110.1 ± 71.6

Table C.93: Averaged values of measured wall surface temperature during experiment for each data point (PD-19-053013)

Test ID	TS21T (C)	TS21B (C)	TS22T (C)	TS22B (C)	TS23T (C)	TS23B (C)	TS24T (C)	TS24B (C)	TS25T (C)	TS25B (C)	TS26T (C)	TS26B (C)
PD-19-053013-2.65	45.3	39.5	61.8	40.8	61.6	41.9	61.4	41.9	69.8	45.4	71.6	48.6
PD-19-053013-2.9	47.8	40.9	65.5	42.4	64.8	43.4	64.5	43.3	73.6	47.2	75.7	50.9
PD-19-053013-3.5	54.3	44.9	75.0	46.7	72.9	47.3	72.0	46.8	82.9	51.6	86.5	56.9
PD-19-053013-4.1	61.7	49.5	84.8	51.4	81.0	51.3	80.0	50.4	92.8	56.4	98.2	63.8
PD-19-053013-4.7	70.3	55.0	95.5	57.0	89.8	55.8	88.8	54.4	103.8	62.1	111.6	72.3
PD-19-053013-5.3	79.5	61.4	106.8	63.1	98.8	60.4	98.1	58.8	115.8	68.9	126.6	82.6
PD-19-053013-5.9	89.2	68.4	118.9	69.7	108.6	65.4	108.4	64.0	129.2	77.1	144.0	95.2
PD-19-053013-6.5	97.0	75.5	120.9	73.1	111.1	69.2	116.2	69.5	143.3	87.0	163.2	110.1

Table C.94: Steady-state parameters of the loop (processed data) (PD-19-053013)

Test ID	Power (kW)	Flow rate (kg/s)	Inlet K	Outlet K	Outlet Temp. Calculated (C)	T11(C)	Total Ch. PD (Pa)	Acc. PD.(Pa)	Fr. PD.(Pa)
PD-19-053013-2.65	2.90 ± 0.04	0.034 ± 0.001	0	61.6	36.8 ± 0.2	35.1 ± 2.2	303.3 ± 29.7	50.3 ± 4.3	253.0 ± 30.0
PD-19-053013-2.9	3.17 ± 0.04	0.036 ± 0.001	0	61.0	37.1 ± 0.2	35.6 ± 2.2	327.0 ± 31.1	59.0 ± 4.8	268.0 ± 31.5
PD-19-053013-3.5	3.83 ± 0.04	0.038 ± 0.001	0	61.3	37.8 ± 0.2	36.6 ± 2.2	390.7 ± 35.6	83.7 ± 5.9	307.0 ± 36.1
PD-19-053013-4.1	4.49 ± 0.05	0.040 ± 0.001	0	61.7	38.5 ± 0.2	37.8 ± 2.2	454.9 ± 37.5	112.1 ± 7.7	342.8 ± 38.2
PD-19-053013-4.7	5.14 ± 0.05	0.041 ± 0.001	0	62.2	39.6 ± 0.4	39.4 ± 2.2	522.1 ± 38.4	144.6 ± 10.0	377.5 ± 39.7
PD-19-053013-5.3	5.80 ± 0.05	0.042 ± 0.001	0	62.5	41.2 ± 0.5	41.7 ± 2.2	596.1 ± 38.4	182.4 ± 12.3	413.7 ± 40.3
PD-19-053013-5.9	6.45 ± 0.06	0.042 ± 0.001	0	63.0	43.8 ± 0.8	44.7 ± 2.2	670.7 ± 40.2	222.9 ± 14.5	447.8 ± 42.7
PD-19-053013-6.5	7.11 ± 0.06	0.043 ± 0.001	0	62.7	47.0 ± 1.1	49.1 ± 2.2	774.0 ± 322.1	267.8 ± 15.9	506.2 ± 322.5

*Mean outlet K factor: 62.0

Table C.95: Comparison between frictional pressure-drop from the experimental against available friction-factor formulae (PD-19-053013)

Test ID	Fr. PD.(Pa)-Exp.	Blasius	Kondratev	Ishigai	Razumovskiy	Tarasova & Leontev	Yamashita	Popov	Kuraeva & Protopopov
PD-19-053013-2.65	253.0	220.8	180.8	147.6	165.5	179.7	117.2	148.6	359.9
PD-19-053013-2.9	268.0	238.7	195.2	158.4	177.8	194.0	126.6	158.3	385.4
PD-19-053013-3.5	307.0	274.9	224.2	182.0	203.7	224.5	149.6	178.1	437.5
PD-19-053013-4.1	342.8	308.6	251.3	205.6	229.0	254.4	174.4	197.3	486.8
PD-19-053013-4.7	377.5	338.2	274.8	228.3	252.6	282.4	200.7	214.8	530.9
PD-19-053013-5.3	413.7	370.2	300.2	254.4	279.2	313.8	232.1	234.6	578.8
PD-19-053013-5.9	447.8	398.1	322.3	279.7	304.1	343.3	265.0	253.2	621.6
PD-19-053013-6.5	506.2	428.7	346.5	308.3	332.2	375.8	302.4	274.8	667.5

June 6th, 2013 - System Pressure: 8.5 MPa, Inlet Temperature: 29-30 ℃, Inlet valve: wide open, Outlet valve: wide open (Zero K factor)

Table C.96: Averaged values of measured signals during experiment for each data point (PD-20-060613)

Test ID	Inlet Temperature (RTD1) (C)	Pressure (MPa)	Power (kW)	Outlet Temp (RTD2)(C)	T11 (C)	T12(C)	CO_2 volumetric Flow rate $(m^3/s) \times 10^6$	HE-Inlet water Temp.(C)	HE-Outlet water Temp.(C)	Water Flow rate (lpm)
PD-20-060613-1.1	28.8 ± 0.4	8.49 ± 0.02	1.21 ± 0.02	32.6 ± 0.5	34.1 ± 2.2	29.6 ± 2.2	43.2 ± 1.2	14.2 ± 2.2	32.0 ± 2.2	0.8
PD-20-060613-1.7	29.6 ± 0.5	8.52 ± 0.03	1.86 ± 0.03	34.0 ± 0.5	35.6 ± 2.2	30.5 ± 2.2	51.7 ± 1.3	15.9 ± 2.2	32.0 ± 2.2	1.5
PD-20-060613-2.3	29.6 ± 0.5	8.49 ± 0.03	2.52 ± 0.03	34.7 ± 0.5	36.6 ± 2.2	30.0 ± 2.2	58.1 ± 1.2	14.9 ± 2.2	30.5 ± 2.2	2.5
PD-20-060613-2.9	29.9 ± 0.4	8.50 ± 0.02	3.17 ± 0.04	36.0 ± 0.5	38.1 ± 2.2	30.3 ± 2.2	61.8 ± 1.2	15.1 ± 2.2	30.0 ± 2.2	3.2
PD-20-060613-3.5	29.8 ± 0.4	8.51 ± 0.02	3.83 ± 0.04	37.1 ± 0.5	39.7 ± 2.2	30.1 ± 2.2	64.4 ± 1.2	13.2 ± 2.2	29.6 ± 2.2	3.6
PD-20-060613-4.1	30.0 ± 0.4	8.53 ± 0.02	4.49 ± 0.05	39.3 ± 0.5	42.7 ± 2.2	30.3 ± 2.2	66.4 ± 1.3	13.0 ± 2.2	29.1 ± 2.2	4.4
PD-20-060613-4.7	29.9 ± 0.4	8.49 ± 0.02	5.14 ± 0.05	41.3 ± 0.5	45.3 ± 2.2	29.9 ± 2.2	67.7 ± 1.3	12.6 ± 2.2	27.8 ± 2.2	5.4
PD-20-060613-5.3	30.0 ± 0.4	8.53 ± 0.02	5.80 ± 0.05	44.6 ± 0.5	49.3 ± 2.2	30.1 ± 2.2	68.5 ± 1.3	12.3 ± 2.2	27.2 ± 2.2	6.2
PD-20-060613-5.9	29.8 ± 0.4	8.51 ± 0.02	6.45 ± 0.06	47.9 ± 0.5	53.6 ± 2.2	29.8 ± 2.2	69.0 ± 1.5	12.0 ± 2.2	25.7 ± 2.2	7.6
PD-20-060613-6.5	29.8 ± 0.4	8.51 ± 0.02	7.11 ± 0.06	53.0 ± 0.6	59.3 ± 2.2	29.9 ± 2.2	69.2 ± 1.3	11.8 ± 2.2	25.4 ± 2.2	8.4
PD-20-060613-7.1	29.8 ± 0.4	8.49 ± 0.02	7.77 ± 0.06	58.6 ± 0.6	66.2 ± 2.2	29.7 ± 2.2	69.2 ± 1.5	11.6 ± 2.2	24.4 ± 2.2	9.9
PD-20-060613-7.7	29.8 ± 0.4	8.50 ± 0.02	8.43 ± 0.06	65.2 ± 0.6	73.5 ± 2.2	30.0 ± 2.2	69.3 ± 1.4	11.4 ± 2.2	23.4 ± 2.2	11.5
PD-20-060613-8.3	29.8 ± 0.4	8.51 ± 0.02	9.08 ± 0.07	73.2 ± 0.6	81.5 ± 2.2	30.1 ± 2.2	69.0 ± 1.3	11.3 ± 2.2	22.6 ± 2.2	13
PD-20-060613-8.9	29.8 ± 0.4	8.49 ± 0.02	9.74 ± 0.07	83.5 ± 0.7	91.0 ± 2.2	30.2 ± 2.2	68.7 ± 1.4	11.0 ± 2.2	22.3 ± 2.2	13.9
PD-20-060613-9.5	29.9 ± 0.4	8.52 ± 0.02	10.40 ± 0.07	93.7 ± 0.7	101.3 ± 2.2	30.3 ± 2.2	68.4 ± 1.3	11.0 ± 2.2	21.9 ± 2.2	15.2
PD-20-060613-10.1	29.8 ± 0.4	8.51 ± 0.02	11.06 ± 0.07	103.9 ± 0.7	112.0 ± 2.2	30.0 ± 2.2	68.0 ± 1.3	11.0 ± 2.2	21.9 ± 2.2	16.3

Table C.97: Averaged values of measured pressure-drops during experiment for each data point (PD-20-060613)

Test ID	DP2-1 (Pa)	DP2-2 (Pa)	DP2-3 (Pa)	DP2-4 (Pa)	DP2-5 (Pa)	DP3 (Pa)	DP13 (Pa)	DP10 (Pa)	DP7 (Pa)
PD-20-060613-1.1	99.0 ± 10.9	31.13 ± 11.01	69.76 ± 11.07	38.7 ± 11.3	45.7 ± 11.0	341.0 ± 10.9	285.0 ± 12.9	403.4 ± 78.5	65.2 ± 10.5
PD-20-060613-1.7	124.6 ± 11.2	43.75 ± 11.42	100.94 ± 11.52	63.7 ± 12.0	60.4 ± 11.5	356.7 ± 11.2	393.8 ± 14.1	468.4 ± 79.2	82.1 ± 10.6
PD-20-060613-2.3	148.8 ± 11.6	56.51 ± 11.86	133.09 ± 12.06	90.9 ± 12.7	72.0 ± 12.1	366.5 ± 11.6	500.7 ± 15.6	530.0 ± 80.7	95.1 ± 10.7
PD-20-060613-2.9	165.3 ± 12.0	67.90 ± 12.42	159.71 ± 12.60	115.1 ± 13.9	86.4 ± 12.8	374.2 ± 12.0	592.8 ± 18.4	587.5 ± 79.3	106.2 ± 10.7
PD-20-060613-3.5	180.9 ± 12.5	77.87 ± 12.94	185.27 ± 13.25	140.5 ± 15.0	99.9 ± 13.6	383.5 ± 12.5	680.0 ± 19.7	630.4 ± 79.3	114.3 ± 10.7
PD-20-060613-4.1	194.9 ± 13.0	89.26 ± 13.60	211.45 ± 14.10	167.5 ± 16.5	117.9 ± 14.5	388.3 ± 13.0	774.5 ± 22.2	670.2 ± 80.1	122.3 ± 10.8
PD-20-060613-4.7	206.7 ± 13.6	100.53 ± 14.34	238.14 ± 14.90	195.9 ± 17.3	133.8 ± 15.1	386.0 ± 13.6	866.7 ± 24.0	724.7 ± 80.1	128.1 ± 10.9
PD-20-060613-5.3	216.5 ± 14.1	110.35 ± 15.05	261.86 ± 15.53	222.2 ± 18.6	150.7 ± 16.2	394.4 ± 14.1	951.5 ± 25.8	763.1 ± 80.8	133.0 ± 11.0
PD-20-060613-5.9	226.1 ± 14.7	120.79 ± 15.79	287.18 ± 16.40	252.0 ± 20.4	167.0 ± 17.4	394.9 ± 14.7	1040.8 ± 27.7	799.2 ± 80.8	137.4 ± 11.1
PD-20-060613-6.5	233.5 ± 15.2	131.84 ± 16.26	311.48 ± 16.71	281.1 ± 21.3	181.5 ± 17.6	392.7 ± 15.2	1125.2 ± 28.9	819.9 ± 81.3	140.7 ± 11.4
PD-20-060613-7.1	240.7 ± 15.9	142.86 ± 16.97	336.72 ± 17.63	311.7 ± 22.0	195.0 ± 19.2	388.4 ± 15.9	1210.3 ± 29.5	854.2 ± 83.5	143.2 ± 11.4
PD-20-060613-7.7	247.3 ± 16.6	153.50 ± 17.72	361.06 ± 18.36	340.4 ± 22.9	208.2 ± 20.3	388.7 ± 16.6	1291.5 ± 31.5	871.1 ± 84.4	145.9 ± 11.8
PD-20-060613-8.3	252.8 ± 16.9	163.90 ± 18.04	385.44 ± 18.67	368.1 ± 23.6	219.2 ± 20.4	386.5 ± 16.9	1368.8 ± 33.1	897.1 ± 81.2	148.4 ± 12.0
PD-20-060613-8.9	257.0 ± 17.8	175.54 ± 18.84	411.50 ± 19.37	395.6 ± 24.7	227.5 ± 21.5	377.9 ± 17.8	1445.3 ± 33.3	912.4 ± 81.2	148.8 ± 12.0
PD-20-060613-9.5	261.7 ± 18.3	186.04 ± 19.29	436.43 ± 19.95	420.2 ± 25.6	236.1 ± 22.6	379.3 ± 18.3	1517.8 ± 33.8	927.4 ± 81.4	150.3 ± 12.1
PD-20-060613-10.1	266.0 ± 18.8	197.47 ± 19.97	463.37 ± 20.58	446.7 ± 25.8	244.2 ± 23.5	374.9 ± 18.8	1594.0 ± 34.4	934.2 ± 81.6	151.3 ± 12.3
PD-20-060613-10.7	269.8 ± 19.6	208.97 ± 20.38	490.01 ± 20.91	471.1 ± 26.6	251.0 ± 24.3	373.9 ± 19.6	1666.1 ± 35.7	934.4 ± 90.9	151.6 ± 12.4

252

Table C.98: Averaged values of measured wall surface temperature during experiment for each data point (PD-20-060613)

Test ID	TS21T (C)	TS21B (C)	TS22T (C)	TS22B (C)	TS23T (C)	TS23B (C)	TS24T (C)	TS24B (C)	TS25T (C)	TS25B (C)	TS26T (C)	TS26B (C)
PD-20-060613-1.1	36.8	35.3	41.1	35.8	39.9	36.2	38.0	36.1	42.7	37.5	43.7	38.6
PD-20-060613-1.7	41.4	38.6	46.7	39.2	45.7	39.6	43.3	39.5	50.1	41.5	52.4	43.6
PD-20-060613-2.3	45.7	41.4	51.5	42.2	50.9	42.4	48.6	42.2	57.6	45.2	61.7	48.9
PD-20-060613-2.9	51.3	45.2	58.5	45.8	57.9	45.9	55.9	45.9	67.8	50.2	74.0	56.0
PD-20-060613-3.5	57.0	49.0	65.3	49.4	64.8	49.2	63.6	49.5	77.9	55.2	86.1	62.9
PD-20-060613-4.1	63.9	53.7	73.7	53.7	73.3	53.4	73.1	54.4	90.6	62.4	101.5	73.1
PD-20-060613-4.7	70.6	58.3	81.9	57.7	81.3	57.0	82.1	58.8	102.6	69.2	116.3	83.1
PD-20-060613-5.3	78.3	63.8	91.6	62.5	90.6	61.8	92.5	64.7	116.7	77.9	133.3	95.6
PD-20-060613-5.9	85.8	69.2	101.1	67.2	99.7	66.0	103.1	70.4	129.9	86.5	149.4	107.7
PD-20-060613-6.5	94.4	75.7	112.5	73.0	110.1	71.6	115.5	78.1	146.1	98.0	168.3	123.8
PD-20-060613-7.1	103.0	82.1	124.0	78.7	120.6	77.1	127.8	86.2	162.1	110.2	186.8	140.0
PD-20-060613-7.7	111.9	88.6	136.1	85.0	131.7	83.4	140.8	95.4	178.6	123.3	205.7	156.8
PD-20-060613-8.3	121.5	95.9	149.0	91.8	143.3	90.4	154.5	105.8	196.3	137.8	225.4	175.0
PD-20-060613-8.9	131.9	103.7	163.3	99.8	156.4	98.9	170.5	118.8	216.4	155.0	247.5	196.5
PD-20-060613-9.5	142.2	111.3	177.0	107.9	169.0	107.4	185.7	131.3	235.1	171.0	267.8	216.5
PD-20-060613-10.1	152.6	119.7	190.8	116.1	181.4	116.3	200.5	144.0	253.4	187.1	287.6	236.6
PD-20-060613-10.7	162.8	126.2	204.3	124.8	193.6	125.2	214.8	156.4	270.5	202.5	306.1	255.5

June 7th, 2013 - System Pressure: 8.5 MPa, Inlet Temperature: 29-30 ℃, Inlet valve: wide open, Outlet valve: 35°closed*

*Equivalent K_{out}=9.1 (based on PD-2-041213) and K_{in}=0

Table C.99: Averaged values of measured signals during experiment for each data point (PD-21-060713)

Test ID	Inlet Temperature (RTD1) (C)	Pressure (MPa)	Power (kW)	Outlet Temp (RTD2)(C)	T11 (C)	T12(C)	CO_2 volumetric Flow rate $(m^3/s) \times 10^6$	HE-Inlet water Temp.(C)	HE-Outlet water Temp.(C)	Water Flow rate (lpm)
PD-21-060713-1.1	29.1 ± 0.4	8.52 ± 0.02	1.21 ± 0.02	33.1 ± 0.5	34.6 ± 2.2	29.5 ± 2.2	40.0 ± 1.1	16.5 ± 2.2	31.9 ± 2.2	1
PD-21-060713-1.7	28.9 ± 0.4	8.52 ± 0.02	1.86 ± 0.03	33.9 ± 0.5	35.6 ± 2.2	29.4 ± 2.2	47.4 ± 1.2	16.1 ± 2.2	30.7 ± 2.2	1.8
PD-21-060713-2.3	28.8 ± 0.4	8.51 ± 0.02	2.52 ± 0.04	34.7 ± 0.5	36.7 ± 2.2	29.3 ± 2.2	51.9 ± 1.2	16.0 ± 2.2	29.1 ± 2.2	2.9
PD-21-060713-2.9	29.0 ± 0.4	8.50 ± 0.02	3.18 ± 0.04	35.9 ± 0.5	38.2 ± 2.2	29.5 ± 2.2	55.1 ± 1.1	15.3 ± 2.2	28.2 ± 2.2	3.9
PD-21-060713-3.5	28.8 ± 0.4	8.50 ± 0.02	3.83 ± 0.04	37.2 ± 0.5	40.0 ± 2.2	29.2 ± 2.2	56.9 ± 1.2	13.0 ± 2.2	27.5 ± 2.2	4.2
PD-21-060713-4.2	29.4 ± 0.4	8.52 ± 0.02	4.60 ± 0.05	40.9 ± 0.5	44.6 ± 2.2	29.6 ± 2.2	57.8 ± 1.3	12.4 ± 2.2	27.6 ± 2.2	4.7
PD-21-060713-4.7	29.5 ± 0.4	8.51 ± 0.02	5.14 ± 0.05	44.0 ± 0.5	48.5 ± 2.2	29.6 ± 2.2	57.8 ± 1.2	12.1 ± 2.2	26.8 ± 2.2	5.5
PD-21-060713-5.3	29.4 ± 0.4	8.51 ± 0.02	5.80 ± 0.05	48.2 ± 0.5	54.1 ± 2.2	29.4 ± 2.2	57.7 ± 1.3	12.0 ± 2.2	25.4 ± 2.2	6.9
PD-21-060713-5.9	29.5 ± 0.4	8.51 ± 0.02	6.46 ± 0.06	55.5 ± 0.6	61.6 ± 2.2	29.3 ± 2.2	56.9 ± 1.4	11.6 ± 2.2	24.6 ± 2.2	7.9
PD-21-060713-6.5	29.5 ± 0.4	8.53 ± 0.02	7.12 ± 0.06	63.4 ± 0.6	70.4 ± 2.2	29.1 ± 2.2	56.5 ± 1.3	11.2 ± 2.2	24.1 ± 2.2	8.8
PD-21-060713-7.1	29.4 ± 0.5	8.53 ± 0.02	7.77 ± 0.06	72.8 ± 0.6	79.6 ± 2.2	29.4 ± 2.2	56.0 ± 1.3	11.1 ± 2.2	23.4 ± 2.2	9.9
PD-21-060713-7.7	29.4 ± 0.4	8.51 ± 0.02	8.43 ± 0.06	84.5 ± 0.7	92.0 ± 2.2	29.2 ± 2.2	55.7 ± 1.2	11.0 ± 2.2	21.8 ± 2.2	12.4

Table C.100: Averaged values of measured pressure-drops during experiment for each data point (PD-21-060713)

Test ID	DP2-1 (Pa)	DP2-2 (Pa)	DP2-3 (Pa)	DP2-4 (Pa)	DP2-5 (Pa)	DP3 (Pa)	DP13 (Pa)	DP10 (Pa)	DP7 (Pa)
PD-21-060713-1.1	97.2 ± 11.1	34.75 ± 11.24	48.62 ± 11.31	30.1 ± 11.3	46.2 ± 11.0	505.1 ± 11.1	258.8 ± 15.5	962.8 ± 79.8	30.2 ± 10.6
PD-21-060713-1.7	118.4 ± 11.4	45.47 ± 11.67	75.57 ± 11.77	51.9 ± 11.8	58.1 ± 11.4	522.6 ± 11.4	351.9 ± 17.6	1150.1 ± 81.7	42.9 ± 10.7
PD-21-060713-2.3	135.3 ± 11.9	55.56 ± 12.17	100.40 ± 12.26	73.1 ± 12.5	69.3 ± 11.9	535.5 ± 11.9	436.3 ± 20.2	1332.5 ± 82.8	52.7 ± 10.8
PD-21-060713-2.9	148.6 ± 12.4	65.83 ± 12.71	123.77 ± 12.69	94.7 ± 13.3	82.9 ± 12.6	542.4 ± 12.4	517.9 ± 22.2	1496.9 ± 84.8	62.4 ± 11.0
PD-21-060713-3.5	160.1 ± 12.9	74.99 ± 13.37	145.22 ± 13.51	115.8 ± 14.4	97.0 ± 13.1	550.4 ± 12.9	594.5 ± 24.4	1682.5 ± 86.5	70.0 ± 11.0
PD-21-060713-4.2	169.1 ± 13.3	87.10 ± 13.91	169.61 ± 14.22	142.0 ± 15.4	115.6 ± 13.8	552.8 ± 13.3	684.0 ± 28.2	1880.6 ± 89.3	78.8 ± 11.2
PD-21-060713-4.7	174.2 ± 13.8	95.26 ± 14.39	186.43 ± 14.47	161.4 ± 16.5	128.0 ± 14.4	551.2 ± 13.8	744.9 ± 29.0	2017.1 ± 90.4	82.7 ± 11.3
PD-21-060713-5.3	180.3 ± 14.4	104.27 ± 15.25	206.35 ± 15.30	185.1 ± 17.4	142.6 ± 15.4	551.3 ± 14.4	816.8 ± 30.2	2170.7 ± 92.6	86.2 ± 11.4
PD-21-060713-5.9	183.0 ± 14.6	113.05 ± 15.50	223.57 ± 15.71	207.5 ± 17.5	154.3 ± 15.7	545.8 ± 14.6	877.4 ± 31.4	2336.6 ± 94.3	87.4 ± 11.6
PD-21-060713-6.5	187.6 ± 15.6	121.24 ± 16.23	242.15 ± 16.15	230.8 ± 18.2	165.5 ± 16.2	545.1 ± 15.6	940.9 ± 32.7	2451.4 ± 98.6	89.2 ± 11.9
PD-21-060713-7.1	190.4 ± 16.1	129.92 ± 16.92	261.42 ± 17.12	252.8 ± 19.0	174.6 ± 17.0	538.2 ± 16.1	1001.6 ± 34.5	2557.1 ± 95.4	91.4 ± 12.1
PD-21-060713-7.7	193.6 ± 17.0	139.26 ± 17.48	282.62 ± 17.52	275.8 ± 19.5	183.3 ± 18.0	529.8 ± 17.0	1065.4 ± 35.9	2666.8 ± 129.2	91.5 ± 12.3

Table C.101: Averaged values of measured wall surface temperature during experiment for each data point (PD-21-060713)

Test ID	TS21T (C)	TS21B (C)	TS22T (C)	TS22B (C)	TS23T (C)	TS23B (C)	TS24T (C)	TS24B (C)	TS25T (C)	TS25B (C)	TS26T (C)	TS26B (C)
PD-21-060713-1.1	37.6	35.8	42.7	36.3	41.7	36.7	40.2	36.7	44.3	38.1	45.1	39.3
PD-21-060713-1.7	41.9	38.5	49.2	39.2	47.2	39.5	45.5	39.5	51.6	41.6	53.3	43.7
PD-21-060713-2.3	46.9	41.7	56.1	42.4	53.4	42.7	51.7	42.5	60.2	45.5	63.8	49.4
PD-21-060713-2.9	53.4	45.7	63.4	46.2	60.8	46.2	59.6	46.6	70.8	50.6	76.6	56.7
PD-21-060713-3.5	60.0	49.9	71.2	50.2	68.7	49.8	68.1	50.5	81.8	56.3	89.9	64.6
PD-21-060713-4.2	70.6	57.1	84.1	56.8	81.0	55.8	82.0	57.4	100.3	67.2	112.7	80.4
PD-21-060713-4.7	78.1	62.4	94.0	61.6	90.0	60.1	92.4	62.9	114.1	75.8	129.9	92.8
PD-21-060713-5.3	86.9	68.7	106.0	67.4	100.6	65.3	104.5	69.7	130.1	86.2	149.3	107.7
PD-21-060713-5.9	97.3	76.2	120.7	74.7	113.7	72.1	119.9	79.7	150.2	101.4	173.6	128.6
PD-21-060713-6.5	107.4	83.7	134.6	82.0	126.4	79.3	134.9	90.1	169.5	116.7	196.7	149.0
PD-21-060713-7.1	118.1	91.5	149.2	89.9	139.8	87.2	150.7	102.1	190.1	133.9	220.8	170.8
PD-21-060713-7.7	129.0	99.6	164.2	98.4	153.9	96.3	167.8	116.1	212.6	153.0	246.3	194.8

June 10th, 2013 - System Pressure: 7.6 MPa, Inlet Temperature: 29-30 ℃, Inlet valve: wide open, Outlet valve: 40°closed*

*Equivalent K_{out}=20 (average of mean K factors for 40° closed valve) and K_{in}=0

Table C.102: Averaged values of measured signals during experiment for each data point (PD-22-061013)

Test ID	Inlet Temperature (RTD1) (C)	Pressure (MPa)	Power (kW)	Outlet Temp (RTD2)(C)	T11 (C)	T12(C)	CO_2 volumetric Flow rate $(m^3/s) \times 10^6$	HE-Inlet water Temp.(C)	HE-Outlet water Temp.(C)	Water Flow rate (lpm)
PD-22-061013-1.1	28.7 ± 0.4	7.59 ± 0.02	1.21 ± 0.02	30.2 ± 0.5	31.7 ± 2.2	29.5 ± 2.2	49.6 ± 1.1	15.3 ± 2.2	30.0 ± 2.2	1
PD-22-061013-1.7	29.0 ± 0.4	7.62 ± 0.02	1.86 ± 0.03	32.9 ± 0.5	34.5 ± 2.2	29.8 ± 2.2	56.7 ± 1.2	15.4 ± 2.2	30.5 ± 2.2	1.6
PD-22-061013-2.3	29.0 ± 0.4	7.61 ± 0.03	2.52 ± 0.04	36.2 ± 0.5	38.8 ± 2.2	29.8 ± 2.2	61.2 ± 1.2	15.5 ± 2.2	30.1 ± 2.2	2.5
PD-22-061013-2.9	29.0 ± 0.4	7.60 ± 0.02	3.18 ± 0.04	40.9 ± 0.5	44.5 ± 2.2	29.8 ± 2.2	63.6 ± 1.2	14.3 ± 2.2	29.7 ± 2.2	3.1
PD-22-061013-3.5	28.9 ± 0.4	7.59 ± 0.02	3.83 ± 0.04	46.9 ± 0.5	50.8 ± 2.2	29.7 ± 2.2	65.2 ± 1.2	13.8 ± 2.2	29.1 ± 2.2	3.8
PD-22-061013-4.1	29.0 ± 0.4	7.60 ± 0.02	4.49 ± 0.05	54.8 ± 0.6	58.1 ± 2.2	29.8 ± 2.2	66.3 ± 1.2	13.3 ± 2.2	28.7 ± 2.2	4.3
PD-22-061013-4.7	29.0 ± 0.4	7.60 ± 0.02	5.15 ± 0.05	66.0 ± 0.6	69.0 ± 2.2	29.9 ± 2.2	67.0 ± 1.2	13.0 ± 2.2	28.4 ± 2.2	5
PD-22-061013-5.3	29.0 ± 0.4	7.60 ± 0.02	5.80 ± 0.05	78.2 ± 0.6	80.8 ± 2.2	29.8 ± 2.2	67.0 ± 1.3	12.8 ± 2.2	27.6 ± 2.2	5.9
PD-22-061013-5.9	29.1 ± 0.4	7.60 ± 0.02	6.46 ± 0.06	88.9 ± 0.7	90.6 ± 2.3	29.9 ± 2.2	67.2 ± 1.3	12.5 ± 2.2	26.8 ± 2.2	6.8
PD-22-061013-6.5	29.0 ± 0.4	7.60 ± 0.02	7.12 ± 0.06	102.0 ± 0.7	102.7 ± 2.2	29.9 ± 2.2	67.2 ± 1.2	12.3 ± 2.2	26.1 ± 2.2	7.7

Table C.103: Averaged values of measured pressure-drops during experiment for each data point (PD-22-061013)

Test ID	DP2-1 (Pa)	DP2-2 (Pa)	DP2-3 (Pa)	DP2-4 (Pa)	DP2-5 (Pa)	DP3 (Pa)	DP13 (Pa)	DP10 (Pa)	DP7 (Pa)
PD-22-061013-1.1	75.4 ± 11.8	71.48 ± 12.71	71.60 ± 12.21	9.0 ± 14.3	42.6 ± 11.9	203.5 ± 11.8	276.0 ± 16.1	721.3 ± 79.0	53.1 ± 10.6
PD-22-061013-1.7	98.5 ± 11.8	84.83 ± 12.78	85.62 ± 24.47	51.6 ± 12.7	50.7 ± 24.1	219.4 ± 11.8	378.0 ± 15.5	748.5 ± 78.6	63.0 ± 10.7
PD-22-061013-2.3	118.0 ± 12.9	67.35 ± 14.68	114.70 ± 14.90	110.7 ± 16.3	66.3 ± 14.0	213.6 ± 12.9	484.0 ± 21.3	716.9 ± 79.1	71.4 ± 10.9
PD-22-061013-2.9	132.9 ± 14.8	62.56 ± 18.46	156.72 ± 19.13	140.2 ± 16.1	79.0 ± 16.0	207.2 ± 14.8	578.6 ± 22.8	701.3 ± 78.8	77.7 ± 11.2
PD-22-061013-3.5	156.8 ± 18.3	72.12 ± 23.34	183.95 ± 23.86	166.4 ± 18.4	99.6 ± 18.5	206.7 ± 18.3	686.3 ± 28.0	729.8 ± 78.7	81.8 ± 11.6
PD-22-061013-4.1	172.3 ± 21.3	83.80 ± 27.15	209.30 ± 27.70	192.2 ± 19.4	108.6 ± 20.9	207.2 ± 21.3	774.1 ± 31.8	752.9 ± 79.3	84.3 ± 12.2
PD-22-061013-4.7	180.4 ± 24.4	95.01 ± 30.54	232.56 ± 30.27	217.3 ± 21.4	120.4 ± 22.7	205.4 ± 24.4	854.1 ± 35.6	778.5 ± 79.3	87.2 ± 12.7
PD-22-061013-5.3	188.4 ± 32.9	107.36 ± 41.14	257.24 ± 40.27	240.5 ± 24.4	128.5 ± 28.7	203.8 ± 32.9	931.2 ± 42.0	803.4 ± 79.5	88.5 ± 14.2
PD-22-061013-5.9	198.6 ± 33.2	117.48 ± 36.62	280.84 ± 35.88	264.4 ± 24.2	138.3 ± 26.5	201.2 ± 33.2	1008.5 ± 42.3	814.2 ± 79.9	89.8 ± 14.2
PD-22-061013-6.5	204.9 ± 73.2	130.59 ± 86.27	305.01 ± 82.01	287.7 ± 41.2	145.0 ± 54.9	201.1 ± 73.2	1082.6 ± 82.1	841.9 ± 89.5	91.6 ± 22.8

Table C.104: Averaged values of measured wall surface temperature during experiment for each data point (PD-22-061013)

Test ID	TS21T (C)	TS21B (C)	TS22T (C)	TS22B (C)	TS23T (C)	TS23B (C)	TS24T (C)	TS24B (C)	TS25T (C)	TS25B (C)	TS26T (C)	TS26B (C)
PD-22-061013-1.1	36.8	34.5	39.9	34.5	39.0	34.5	38.0	34.7	43.3	36.7	45.4	38.7
PD-22-061013-1.7	42.5	38.7	47.7	38.9	47.4	39.1	47.3	40.4	56.8	44.4	61.7	49.5
PD-22-061013-2.3	48.6	43.1	56.2	43.4	56.5	43.7	58.0	46.5	71.6	53.5	80.1	62.5
PD-22-061013-2.9	55.5	48.1	65.8	48.3	66.5	49.0	70.0	53.9	88.2	64.4	101.2	77.9
PD-22-061013-3.5	63.1	53.6	76.6	53.8	77.4	55.0	83.4	62.6	106.1	77.0	123.2	95.3
PD-22-061013-4.1	71.5	59.9	88.7	60.2	89.7	62.1	98.2	73.0	126.1	92.0	147.0	115.2
PD-22-061013-4.7	81.3	67.0	102.9	68.3	104.1	71.2	116.3	86.7	149.4	111.2	173.7	139.7
PD-22-061013-5.3	91.5	74.5	117.8	76.8	118.8	81.0	134.2	101.1	172.2	130.7	199.8	163.9
PD-22-061013-5.9	101.4	81.8	131.6	85.2	132.1	90.0	149.9	114.1	192.4	147.7	222.4	185.1
PD-22-061013-6.5	112.4	89.8	146.6	94.8	146.6	100.5	167.4	129.1	214.3	166.9	246.7	208.9

June 12th, 2013 - System Pressure: 7.6 MPa, Inlet Temperature: 29-30 ℃, Inlet valve: wide open, Outlet valve: wide open ($k_{in}=k_{out}=0$)

Table C.105: Averaged values of measured signals during experiment for each data point (PD-23-061213)

Test ID	Inlet Temperature (RTD1) (C)	Pressure (MPa)	Power (kW)	Outlet Temp (RTD2)(C)	T11 (C)	T12(C)	CO_2 volumetric Flow rate $(m^3/s) \times 10^6$	HE-Inlet water Temp.(C)	HE-Outlet water Temp.(C)	Water Flow rate (lpm)
PD-23-061213-1.1	29.0 ± 0.4	7.61 ± 0.02	1.21 ± 0.02	30.4 ± 0.5	31.7 ± 2.2	29.6 ± 2.2	47.5 ± 1.1	16.4 ± 2.2	30.1 ± 2.2	1.2
PD-23-061213-1.7	29.0 ± 0.4	7.60 ± 0.02	1.86 ± 0.03	30.6 ± 0.5	32.1 ± 2.2	29.7 ± 2.2	55.6 ± 1.1	16.3 ± 2.2	29.3 ± 2.2	2.1
PD-23-061213-2.3	29.3 ± 0.4	7.59 ± 0.02	2.52 ± 0.04	31.1 ± 0.5	32.8 ± 2.2	30.0 ± 2.2	60.9 ± 1.2	16.2 ± 2.2	28.6 ± 2.2	3.2
PD-23-061213-2.9	29.6 ± 0.4	7.59 ± 0.02	3.18 ± 0.04	32.3 ± 0.5	34.5 ± 2.2	30.2 ± 2.2	64.4 ± 1.2	15.2 ± 2.2	28.2 ± 2.2	3.8
PD-23-061213-3.5	29.6 ± 0.5	7.61 ± 0.02	3.83 ± 0.04	33.9 ± 0.5	36.7 ± 2.2	30.3 ± 2.2	66.4 ± 1.3	14.1 ± 2.2	27.6 ± 2.2	4.5
PD-23-061213-4.1	29.5 ± 0.4	7.61 ± 0.02	4.49 ± 0.05	35.7 ± 0.5	39.2 ± 2.2	30.2 ± 2.2	67.7 ± 1.3	13.4 ± 2.2	26.9 ± 2.2	5.3
PD-23-061213-4.7	29.7 ± 0.4	7.62 ± 0.02	5.15 ± 0.05	39.2 ± 0.5	43.5 ± 2.2	30.3 ± 2.2	68.8 ± 1.3	13.2 ± 2.2	26.4 ± 2.2	6.2
PD-23-061213-5.3	29.7 ± 0.4	7.61 ± 0.02	5.81 ± 0.05	44.4 ± 0.5	49.5 ± 2.2	30.2 ± 2.2	68.8 ± 1.4	12.9 ± 2.2	25.7 ± 2.2	7.2
PD-23-061213-5.9	29.4 ± 0.4	7.59 ± 0.02	6.46 ± 0.06	47.8 ± 0.5	54.0 ± 2.2	30.1 ± 2.2	69.4 ± 1.4	12.7 ± 2.2	24.4 ± 2.2	8.9
PD-23-061213-6.5	29.6 ± 0.4	7.62 ± 0.02	7.12 ± 0.06	56.1 ± 0.6	61.6 ± 2.2	30.1 ± 2.2	69.0 ± 1.4	12.4 ± 2.2	24.3 ± 2.2	9.4
PD-23-061213-7.1	29.6 ± 0.4	7.61 ± 0.02	7.78 ± 0.06	66.7 ± 0.6	72.3 ± 2.3	30.1 ± 2.2	68.7 ± 1.3	12.3 ± 2.2	23.8 ± 2.2	10.7
PD-23-061213-7.7	29.7 ± 0.4	7.61 ± 0.02	8.44 ± 0.06	78.4 ± 0.7	85.1 ± 2.2	30.1 ± 2.2	68.3 ± 1.3	12.1 ± 2.2	23.2 ± 2.2	12.2
PD-23-061213-8.3	29.5 ± 0.4	7.60 ± 0.02	9.10 ± 0.07	86.7 ± 0.7	94.9 ± 2.2	29.9 ± 2.2	68.0 ± 1.3	12.0 ± 2.2	22.0 ± 2.2	14.7
PD-23-061213-8.9	29.5 ± 0.4	7.59 ± 0.02	9.75 ± 0.07	101.7 ± 0.7	107.1 ± 2.2	30.0 ± 2.2	67.2 ± 1.2	11.8 ± 2.2	21.8 ± 2.2	15.6

Table C.106: Averaged values of measured pressure-drops during experiment for each data point (PD-23-061213)

Test ID	DP2-1 (Pa)	DP2-2 (Pa)	DP2-3 (Pa)	DP2-4 (Pa)	DP2-5 (Pa)	DP3 (Pa)	DP13 (Pa)	DP10 (Pa)	DP7 (Pa)
PD-23-061213-1.1	116.2 ± 11.0	22.07 ± 11.20	82.01 ± 11.31	72.3 ± 11.5	48.2 ± 11.2	346.7 ± 11.0	321.8 ± 13.2	212.9 ± 78.2	68.1 ± 10.5
PD-23-061213-1.7	142.6 ± 11.3	35.61 ± 11.61	115.64 ± 11.80	98.9 ± 12.4	62.4 ± 11.8	368.7 ± 11.3	437.1 ± 14.9	260.4 ± 79.8	84.0 ± 10.7
PD-23-061213-2.3	164.4 ± 11.9	49.64 ± 12.32	147.29 ± 12.43	124.6 ± 13.4	79.4 ± 12.4	378.6 ± 11.9	548.1 ± 16.9	333.1 ± 78.9	99.0 ± 10.7
PD-23-061213-2.9	181.8 ± 12.5	63.03 ± 13.07	176.59 ± 13.46	150.3 ± 14.6	96.3 ± 13.6	386.8 ± 12.5	651.1 ± 19.7	389.2 ± 79.8	111.3 ± 10.8
PD-23-061213-3.5	197.8 ± 13.0	74.66 ± 13.74	204.37 ± 14.26	177.5 ± 16.0	113.0 ± 14.3	403.6 ± 13.0	750.7 ± 22.2	434.2 ± 79.1	119.3 ± 10.9
PD-23-061213-4.1	211.5 ± 13.7	85.88 ± 14.68	230.76 ± 15.27	205.9 ± 17.8	129.0 ± 15.5	416.7 ± 13.7	846.7 ± 24.1	477.8 ± 79.2	126.5 ± 11.1
PD-23-061213-4.7	221.9 ± 14.8	97.54 ± 16.01	256.07 ± 16.41	234.8 ± 18.9	145.7 ± 16.8	425.9 ± 14.8	940.0 ± 27.4	517.7 ± 79.6	131.9 ± 11.2
PD-23-061213-5.3	231.3 ± 15.6	109.23 ± 17.07	281.48 ± 17.64	259.7 ± 20.4	166.8 ± 17.8	423.2 ± 15.6	1032.2 ± 29.1	542.9 ± 79.4	135.6 ± 11.8
PD-23-061213-5.9	242.0 ± 16.1	120.00 ± 17.60	307.95 ± 18.33	293.7 ± 21.8	181.1 ± 18.9	423.1 ± 16.1	1128.6 ± 32.6	555.2 ± 82.0	139.7 ± 11.9
PD-23-061213-6.5	247.9 ± 16.7	130.75 ± 18.43	331.97 ± 19.50	329.4 ± 22.6	186.9 ± 20.0	436.1 ± 16.7	1211.0 ± 33.6	596.6 ± 81.6	143.3 ± 12.2
PD-23-061213-7.1	253.2 ± 18.1	140.61 ± 20.21	355.83 ± 20.75	358.6 ± 24.6	197.2 ± 21.6	428.8 ± 18.1	1289.0 ± 37.4	586.8 ± 80.8	144.6 ± 12.9
PD-23-061213-7.7	258.8 ± 19.0	149.73 ± 21.15	361.65 ± 21.71	405.6 ± 24.5	203.7 ± 22.5	427.8 ± 19.0	1363.3 ± 37.0	599.2 ± 80.3	146.4 ± 13.1
PD-23-061213-8.3	266.2 ± 19.3	160.67 ± 21.24	389.60 ± 21.78	438.2 ± 25.4	215.8 ± 23.6	423.6 ± 19.3	1455.2 ± 37.6	600.0 ± 80.7	149.4 ± 13.4
PD-23-061213-8.9	268.8 ± 21.0	170.32 ± 22.87	418.51 ± 23.02	457.9 ± 26.7	221.2 ± 25.0	418.2 ± 21.0	1522.1 ± 39.4	607.2 ± 89.5	148.1 ± 14.0

Table C.107: Averaged values of measured wall surface temperature during experiment for each data point (PD-23-061213)

Test ID	TS21T (C)	TS21B (C)	TS22T (C)	TS22B (C)	TS23T (C)	TS23B (C)	TS24T (C)	TS24B (C)	TS25T (C)	TS25B (C)	TS26T (C)	TS26B (C)
PD-23-061213-1.1	35.5	33.8	39.4	34.3	37.3	34.1	35.4	33.6	38.8	34.7	39.5	35.5
PD-23-061213-1.7	39.7	36.5	43.8	37.1	42.0	36.6	39.5	35.9	44.9	37.5	46.8	39.3
PD-23-061213-2.3	45.1	40.1	49.7	40.6	48.0	39.6	45.6	38.8	53.8	41.5	57.7	45.1
PD-23-061213-2.9	51.4	44.4	57.2	44.6	55.6	43.3	54.1	42.8	65.8	47.6	72.7	54.1
PD-23-061213-3.5	57.6	48.8	65.0	48.7	63.2	46.9	62.5	47.0	77.7	53.9	87.3	63.3
PD-23-061213-4.1	64.2	53.5	73.3	52.8	71.3	50.5	71.5	51.5	90.1	61.0	102.9	73.5
PD-23-061213-4.7	72.0	59.1	83.5	57.9	81.3	55.3	83.2	58.1	105.9	71.0	122.2	87.8
PD-23-061213-5.3	80.3	65.2	94.8	63.4	92.0	60.7	96.2	66.1	123.3	83.0	143.2	104.6
PD-23-061213-5.9	87.8	70.5	104.5	68.1	100.8	64.9	106.5	72.1	136.7	92.1	158.6	117.0
PD-23-061213-6.5	97.7	77.5	118.4	75.2	113.5	72.3	122.1	83.3	157.1	108.2	181.7	138.2
PD-23-061213-7.1	108.1	85.2	133.2	83.2	127.4	80.7	139.2	96.8	178.8	127.0	206.6	161.8
PD-23-061213-7.7	118.8	93.0	147.7	91.7	141.4	89.9	156.2	111.0	200.5	145.7	230.5	185.2
PD-23-061213-8.3	128.5	100.0	160.2	98.8	152.6	97.2	169.4	121.7	217.1	159.6	248.6	202.7
PD-23-061213-8.9	140.8	109.2	176.7	109.3	168.5	109.2	188.5	139.3	241.0	181.4	274.4	229.6

June 13th, 2013 - System Pressure: 7.6 MPa, Inlet Temperature: 29-30 ℃, Inlet valve: wide open, Outlet valve: 30º closed*

*Equivalent K_{out}=5.8 (average of mean K factors for 30º closed valve) and K_{in}=0

Table C.108: Averaged values of measured signals during experiment for each data point (PD-24-061313)

Test ID	Inlet Temperature (RTD1) (C)	Pressure (MPa)	Power (kW)	Outlet Temp (RTD2)(C)	T11 (C)	T12(C)	CO_2 volumetric Flow rate $(m^3/s) \times 10^6$	HE-Inlet water Temp.(C)	HE-Outlet water Temp.(C)	Water Flow rate (lpm)
PD-24-061313-1.1	28.9 ± 0.4	7.60 ± 0.02	1.21 ± 0.02	30.2 ± 0.5	31.5 ± 2.2	29.5 ± 2.2	45.5 ± 1.0	15.6 ± 2.2	30.1 ± 2.2	1
PD-24-061313-1.7	29.1 ± 0.4	7.62 ± 0.02	1.87 ± 0.03	30.7 ± 0.5	32.2 ± 2.2	29.7 ± 2.2	53.1 ± 1.2	15.9 ± 2.2	29.6 ± 2.2	2
PD-24-061313-2.3	29.1 ± 0.4	7.60 ± 0.02	2.52 ± 0.03	31.1 ± 0.5	32.8 ± 2.2	29.4 ± 2.2	58.1 ± 1.2	15.7 ± 2.2	28.2 ± 2.2	3.2
PD-24-061313-2.7	29.0 ± 0.4	7.60 ± 0.02	2.96 ± 0.04	31.5 ± 0.5	33.5 ± 2.2	29.4 ± 2.2	59.9 ± 1.2	15.2 ± 2.2	27.5 ± 2.2	3.8
PD-24-061313-3.5	28.9 ± 0.4	7.59 ± 0.02	3.83 ± 0.04	33.1 ± 0.5	35.9 ± 2.2	29.3 ± 2.2	62.3 ± 1.3	14.3 ± 2.2	26.3 ± 2.2	5.1
PD-24-061313-4.1	28.9 ± 0.4	7.60 ± 0.02	4.49 ± 0.05	35.3 ± 0.5	39.1 ± 2.2	29.4 ± 2.2	63.3 ± 1.3	13.6 ± 2.2	25.6 ± 2.2	6.1
PD-24-061313-4.7	29.0 ± 0.4	7.62 ± 0.02	5.15 ± 0.05	38.9 ± 0.5	43.2 ± 2.2	29.4 ± 2.2	63.3 ± 1.3	13.2 ± 2.2	25.0 ± 2.2	7
PD-24-061313-5.3	29.3 ± 0.4	7.61 ± 0.02	5.81 ± 0.05	48.5 ± 0.5	53.4 ± 2.2	29.8 ± 2.2	63.1 ± 1.4	13.1 ± 2.2	24.9 ± 2.2	7.8
PD-24-061313-5.9	29.5 ± 0.4	7.62 ± 0.02	6.47 ± 0.06	61.7 ± 0.6	66.7 ± 2.2	30.1 ± 2.2	62.4 ± 1.4	13.0 ± 2.2	24.7 ± 2.2	8.6
PD-24-061313-6.5	29.4 ± 0.4	7.60 ± 0.02	7.13 ± 0.06	70.8 ± 0.6	76.4 ± 2.2	30.0 ± 2.2	62.1 ± 1.3	12.7 ± 2.2	23.9 ± 2.2	10
PD-24-061313-7.1	29.5 ± 0.4	7.62 ± 0.02	7.78 ± 0.06	85.7 ± 0.7	91.2 ± 2.2	30.1 ± 2.2	61.3 ± 1.3	12.6 ± 2.2	23.5 ± 2.2	11.2

Table C.109: Averaged values of measured pressure-drops during experiment for each data point (PD-24-061313)

Test ID	DP2-1 (Pa)	DP2-2 (Pa)	DP2-3 (Pa)	DP2-4 (Pa)	DP2-5 (Pa)	DP3 (Pa)	DP13 (Pa)	DP10 (Pa)	DP7 (Pa)
PD-24-061313-1.1	112.7 ± 11.1	28.43 ± 11.27	44.04 ± 11.31	85.9 ± 11.4	50.2 ± 11.1	482.6 ± 11.1	295.3 ± 14.0	74.0 ± 78.5	80.6 ± 10.6
PD-24-061313-1.7	137.0 ± 11.4	41.90 ± 11.62	75.26 ± 11.78	110.5 ± 12.1	65.1 ± 11.6	502.8 ± 11.4	405.3 ± 16.1	216.2 ± 80.1	96.4 ± 10.7
PD-24-061313-2.3	158.3 ± 11.9	54.02 ± 12.35	104.85 ± 12.45	134.7 ± 13.2	82.0 ± 12.4	510.0 ± 11.9	509.9 ± 18.5	324.5 ± 80.1	109.1 ± 10.8
PD-24-061313-2.7	168.9 ± 12.4	61.18 ± 12.71	121.99 ± 12.92	151.0 ± 13.9	92.7 ± 13.0	517.2 ± 12.4	572.1 ± 20.7	384.9 ± 80.5	114.6 ± 10.9
PD-24-061313-3.5	186.7 ± 13.2	75.73 ± 13.77	155.40 ± 14.09	184.0 ± 15.6	115.0 ± 14.1	524.9 ± 13.2	693.9 ± 24.0	521.0 ± 81.2	125.6 ± 11.0
PD-24-061313-4.1	198.0 ± 13.8	86.05 ± 14.37	178.59 ± 14.86	200.0 ± 17.0	142.2 ± 15.2	533.3 ± 13.8	782.2 ± 26.2	612.5 ± 82.7	132.0 ± 11.2
PD-24-061313-4.7	206.0 ± 14.6	96.20 ± 15.64	199.80 ± 15.98	221.3 ± 18.8	161.9 ± 16.2	543.8 ± 14.6	862.2 ± 28.7	700.4 ± 82.7	136.1 ± 11.6
PD-24-061313-5.3	210.6 ± 15.8	106.85 ± 17.36	220.35 ± 17.73	251.2 ± 19.9	150.8 ± 17.3	538.8 ± 15.8	917.8 ± 31.3	795.2 ± 83.0	140.0 ± 12.0
PD-24-061313-5.9	213.6 ± 17.3	115.37 ± 19.17	221.22 ± 19.86	298.7 ± 20.6	157.4 ± 19.4	534.7 ± 17.3	984.5 ± 33.7	856.8 ± 83.9	141.1 ± 12.6
PD-24-061313-6.5	219.8 ± 18.4	123.70 ± 20.36	239.54 ± 20.59	335.4 ± 21.8	168.0 ± 20.3	530.6 ± 18.4	1065.1 ± 35.1	918.1 ± 83.7	143.0 ± 12.8
PD-24-061313-7.1	223.1 ± 19.3	113.33 ± 21.65	284.39 ± 21.62	359.1 ± 22.9	180.1 ± 21.2	537.9 ± 19.3	1138.0 ± 38.5	947.2 ± 106.2	143.8 ± 13.5

Table C.110: Averaged values of measured wall surface temperature during experiment for each data point (PD-24-061313)

Test ID	TS21T (C)	TS21B (C)	TS22T (C)	TS22B (C)	TS23T (C)	TS23B (C)	TS24T (C)	TS24B (C)	TS25T (C)	TS25B (C)	TS26T (C)	TS26B (C)
PD-24-061313-1.1	35.8	33.8	40.2	33.9	38.1	34.0	36.1	33.6	39.7	34.7	40.5	35.6
PD-24-061313-1.7	40.7	37.1	45.8	37.1	43.4	36.9	41.1	36.4	47.2	38.4	49.3	40.5
PD-24-061313-2.3	45.9	40.4	51.1	40.2	49.2	39.7	47.0	39.3	55.6	42.1	59.3	45.8
PD-24-061313-2.7	49.9	43.0	55.9	42.5	53.8	41.9	51.8	41.5	62.3	45.2	67.3	50.3
PD-24-061313-3.5	58.8	49.0	67.0	47.9	64.3	46.5	63.3	46.8	78.1	53.3	86.2	62.3
PD-24-061313-4.1	66.3	54.3	76.6	52.6	73.2	50.6	73.7	51.9	92.3	61.3	104.0	74.1
PD-24-061313-4.7	74.6	60.3	87.7	58.0	83.6	55.3	85.8	58.4	108.4	71.6	124.5	88.9
PD-24-061313-5.3	85.2	68.1	103.3	65.6	98.5	63.3	104.6	71.2	133.8	91.0	155.7	115.7
PD-24-061313-5.9	96.8	76.6	120.6	74.6	115.0	73.4	125.4	87.3	161.2	114.1	187.5	145.6
PD-24-061313-6.5	106.9	83.8	134.1	81.9	127.6	81.1	140.6	99.0	180.9	130.5	209.9	166.1
PD-24-061313-7.1	118.9	92.6	150.8	91.8	144.0	92.4	160.9	116.5	206.7	153.4	238.7	194.1

June 14th, 2013 - System Pressure: 8.5 MPa, Inlet Temperature: 25-26 ºC, Inlet valve: wide open, Outlet valve: 40º closed

Table C.111: Averaged values of measured signals during experiment for each data point (PD-25-061413)

Test ID	Inlet Temperature (RTD1) (C)	Pressure (MPa)	Power (kW)	Outlet Temp (RTD2)(C)	T11 (C)	T12(C)	CO_2 volumetric Flow rate $(m^3/s) \times 10^6$	HE-Inlet water Temp.(C)	HE-Outlet water Temp.(C)	Water Flow rate (lpm)
PD-25-061413-1.2	25.3 ± 0.4	8.52 ± 0.02	1.32 ± 0.03	32.1 ± 0.5	33.5 ± 2.2	25.9 ± 2.2	34.9 ± 1.1	14.4 ± 2.2	29.1 ± 2.2	1
PD-25-061413-1.7	25.8 ± 0.4	8.51 ± 0.02	1.86 ± 0.03	33.2 ± 0.5	34.8 ± 2.2	26.3 ± 2.2	41.9 ± 1.0	15.3 ± 2.2	27.8 ± 2.2	2
PD-25-061413-2.3	25.7 ± 0.4	8.50 ± 0.02	2.52 ± 0.04	33.9 ± 0.5	35.8 ± 2.2	25.5 ± 2.2	47.1 ± 1.2	14.8 ± 2.2	25.1 ± 2.2	3.9
PD-25-061413-2.9	25.8 ± 0.4	8.52 ± 0.02	3.18 ± 0.04	34.8 ± 0.5	36.8 ± 2.2	25.5 ± 2.2	50.2 ± 1.1	13.7 ± 2.2	24.1 ± 2.2	4.9
PD-25-061413-3.5	25.6 ± 0.4	8.50 ± 0.02	3.83 ± 0.04	35.6 ± 0.5	38.0 ± 2.2	25.2 ± 2.2	52.1 ± 1.2	13.3 ± 2.2	22.4 ± 2.2	7
PD-25-061413-4.1	25.8 ± 0.4	8.50 ± 0.02	4.49 ± 0.05	36.9 ± 0.5	39.9 ± 2.2	25.3 ± 2.2	53.6 ± 1.1	12.8 ± 2.2	21.5 ± 2.2	8.6
PD-25-061413-4.7	25.9 ± 0.4	8.51 ± 0.02	5.15 ± 0.05	38.9 ± 0.5	42.6 ± 2.2	25.5 ± 2.2	53.7 ± 1.3	12.7 ± 2.2	20.7 ± 2.2	10.6
PD-25-061413-5.3	26.0 ± 0.4	8.52 ± 0.02	5.81 ± 0.05	41.8 ± 0.5	46.4 ± 2.2	25.7 ± 2.2	53.6 ± 1.2	12.3 ± 2.2	20.0 ± 2.2	12.6
PD-25-061413-5.9	25.9 ± 0.4	8.52 ± 0.02	6.46 ± 0.06	45.8 ± 0.5	51.5 ± 2.2	25.6 ± 2.2	53.0 ± 1.2	12.1 ± 2.2	19.0 ± 2.2	15.5
PD-25-061413-6.5	26.0 ± 0.4	8.52 ± 0.02	7.12 ± 0.06	51.8 ± 0.6	58.4 ± 2.2	25.8 ± 2.2	52.0 ± 1.3	12.0 ± 2.2	18.3 ± 2.2	18.6
PD-25-061413-7.1	26.0 ± 0.4	8.50 ± 0.02	7.78 ± 0.06	59.9 ± 0.6	67.0 ± 2.2	25.8 ± 2.2	51.1 ± 1.3	12.0 ± 2.2	17.4 ± 2.2	23.6

Table C.112: Averaged values of measured pressure-drops during experiment for each data point (PD-25-061413)

Test ID	DP2-1 (Pa)	DP2-2 (Pa)	DP2-3 (Pa)	DP2-4 (Pa)	DP2-5 (Pa)	DP3 (Pa)	DP13 (Pa)	DP10 (Pa)	DP7 (Pa)
PD-25-061413-1.2	112.5 ± 11.2	23.40 ± 11.45	46.53 ± 11.51	23.1 ± 11.3	37.0 ± 11.1	723.9 ± 11.2	218.3 ± 17.4	503.6 ± 81.6	58.0 ± 10.7
PD-25-061413-1.7	129.6 ± 11.7	31.62 ± 12.10	67.28 ± 12.15	39.2 ± 11.8	46.4 ± 11.6	734.7 ± 11.7	291.2 ± 19.5	726.7 ± 84.7	69.8 ± 10.7
PD-25-061413-2.3	146.9 ± 12.3	40.36 ± 12.67	90.70 ± 12.75	58.7 ± 12.5	59.1 ± 12.2	744.8 ± 12.3	373.9 ± 23.8	985.6 ± 85.9	80.3 ± 11.0
PD-25-061413-2.9	158.9 ± 13.0	47.98 ± 13.43	110.76 ± 13.39	76.8 ± 13.2	73.3 ± 12.8	755.3 ± 13.0	445.2 ± 26.3	1219.0 ± 88.9	90.1 ± 11.1
PD-25-061413-3.5	168.6 ± 13.5	56.15 ± 13.98	130.49 ± 13.91	96.6 ± 14.0	88.7 ± 13.3	759.8 ± 13.5	517.6 ± 27.4	1459.5 ± 88.2	98.1 ± 11.2
PD-25-061413-4.1	175.8 ± 14.1	64.85 ± 14.52	149.81 ± 14.31	117.5 ± 14.9	104.0 ± 13.8	760.4 ± 14.1	587.7 ± 30.6	1693.3 ± 96.8	104.6 ± 11.5
PD-25-061413-4.7	181.1 ± 14.8	73.20 ± 15.04	167.45 ± 14.91	137.8 ± 15.8	119.2 ± 14.5	764.6 ± 14.8	653.9 ± 34.2	1932.6 ± 98.8	110.1 ± 11.6
PD-25-061413-5.3	185.0 ± 15.4	81.75 ± 15.69	184.53 ± 15.42	159.2 ± 16.7	133.7 ± 15.0	764.7 ± 15.4	718.1 ± 33.7	2162.3 ± 101.2	113.7 ± 11.6
PD-25-061413-5.9	187.8 ± 16.0	90.27 ± 16.09	200.88 ± 15.90	180.7 ± 17.7	148.6 ± 15.8	764.7 ± 16.0	780.9 ± 35.4	2386.0 ± 105.6	116.4 ± 11.8
PD-25-061413-6.5	189.7 ± 16.4	98.97 ± 16.59	217.91 ± 16.34	202.8 ± 18.4	161.9 ± 16.2	760.2 ± 16.4	842.7 ± 35.9	2573.5 ± 107.9	117.7 ± 12.0
PD-25-061413-7.1	191.0 ± 17.1	107.78 ± 17.38	236.32 ± 16.97	225.1 ± 19.0	174.1 ± 16.8	753.4 ± 17.1	904.7 ± 36.9	2767.8 ± 111.3	119.4 ± 12.2

Table C.113: Averaged values of measured wall surface temperature during experiment for each data point (PD-25-061413)

Test ID	TS21T (C)	TS21B (C)	TS22T (C)	TS22B (C)	TS23T (C)	TS23B (C)	TS24T (C)	TS24B (C)	TS25T (C)	TS25B (C)	TS26T (C)	TS26B (C)
PD-25-061413-1.2	36.5	34.5	42.8	35.2	42.4	35.9	41.9	36.1	46.9	37.7	47.9	38.8
PD-25-061413-1.7	40.3	37.1	48.9	37.9	48.2	38.7	46.5	38.6	53.2	40.6	54.1	42.3
PD-25-061413-2.3	45.2	40.0	56.0	41.0	54.3	41.5	52.1	41.3	60.5	44.1	62.2	47.0
PD-25-061413-2.9	51.2	43.5	64.4	44.7	61.5	44.9	59.3	44.6	69.6	48.5	72.6	52.6
PD-25-061413-3.5	58.3	47.6	73.4	48.8	69.2	48.5	67.2	48.0	79.8	53.2	84.1	59.1
PD-25-061413-4.1	66.9	52.8	84.0	53.9	78.3	52.6	76.6	52.2	91.8	59.3	98.3	68.0
PD-25-061413-4.7	76.4	58.9	95.7	59.7	88.3	57.3	87.3	57.2	105.8	67.0	115.9	79.4
PD-25-061413-5.3	86.5	65.9	108.4	66.2	99.3	62.5	99.3	63.3	121.5	76.5	136.9	93.5
PD-25-061413-5.9	96.8	73.6	122.1	73.2	111.2	68.2	112.4	70.5	138.5	87.7	158.3	110.0
PD-25-061413-6.5	107.6	81.6	136.5	80.8	124.1	74.6	127.2	79.6	157.6	101.9	181.6	130.0
PD-25-061413-7.1	118.6	90.2	151.5	89.0	137.7	81.8	143.1	90.6	178.6	119.0	207.1	152.9

Table C.114: Steady-state parameters of the loop (processed data) (PD-25-061413)

Test ID	Power (kW)	Flow rate (kg/s)	Inlet K	Outlet K*	Outlet Temp. Calculated (C)	T11(C)	Total Ch. PD (Pa)	Acc. PD.(Pa)	Fr. PD.(Pa)
PD-25-061413-1.2	1.32 ± 0.03	0.027 ± 0.001	0	19.1	35.3 ± 0.3	33.5 ± 2.2	209.8 ± 17.4	16.3 ± 1.6	193.5 ± 17.5
PD-25-061413-1.7	1.86 ± 0.03	0.033 ± 0.001	0	18.7	36.2 ± 0.2	34.8 ± 2.2	278.7 ± 19.5	30.8 ± 2.5	247.9 ± 19.7
PD-25-061413-2.3	2.52 ± 0.04	0.037 ± 0.001	0	18.9	36.9 ± 0.2	35.8 ± 2.2	357.4 ± 23.8	51.9 ± 4.1	305.5 ± 24.1
PD-25-061413-2.9	3.18 ± 0.04	0.039 ± 0.001	0	19.1	37.7 ± 0.2	36.8 ± 2.2	425.5 ± 26.3	77.0 ± 5.2	348.5 ± 26.8
PD-25-061413-3.5	3.83 ± 0.04	0.041 ± 0.001	0	19.5	38.3 ± 0.2	38.0 ± 2.2	495.2 ± 27.4	105.9 ± 7.2	389.3 ± 28.3
PD-25-061413-4.1	4.49 ± 0.05	0.042 ± 0.001	0	19.5	39.4 ± 0.3	39.9 ± 2.2	562.8 ± 30.6	140.1 ± 9.1	422.6 ± 31.9
PD-25-061413-4.7	5.15 ± 0.05	0.042 ± 0.001	0	19.8	41.3 ± 0.5	42.6 ± 2.2	627.0 ± 34.2	175.9 ± 12.4	451.1 ± 36.4
PD-25-061413-5.3	5.81 ± 0.05	0.042 ± 0.001	0	19.9	44.3 ± 0.8	46.4 ± 2.2	689.4 ± 33.7	214.9 ± 14.0	474.5 ± 36.5
PD-25-061413-5.9	6.46 ± 0.06	0.041 ± 0.001	0	19.9	48.8 ± 1.3	51.5 ± 2.2	750.6 ± 35.4	254.3 ± 16.2	496.3 ± 39.0
PD-25-061413-6.5	7.12 ± 0.06	0.040 ± 0.001	0	19.6	55.9 ± 2.1	58.4 ± 2.2	811.0 ± 35.9	295.0 ± 20.7	516.0 ± 41.4
PD-25-061413-7.1	7.78 ± 0.06	0.040 ± 0.001	0	19.3	65.2 ± 2.9	67.0 ± 2.2	871.6 ± 36.9	336.1 ± 22.3	535.5 ± 43.1

*Mean outlet K factor: 19.4

Table C.115: Comparison between frictional pressure-drop from the experimental against available friction-factor formulae (PD-25-061413)

Test ID	Fr. PD.(Pa)-Exp.	Blasius	Kondratev	Ishigai	Razumovskiy	Tarasova & Leontev	Yamashita	Popov	Kuraeva & Protopopov
PD-25-061413-1.2	193.5	142.4	117.3	113.3	121.5	125.2	95.4	117.7	250.2
PD-25-061413-1.7	247.9	200.5	164.3	145.5	159.8	168.6	117.8	149.6	334.2
PD-25-061413-2.3	305.5	255.5	208.7	178.2	197.2	211.7	144.4	179.9	411.7
PD-25-061413-2.9	348.5	296.7	241.7	204.4	226.4	245.9	169.3	202.3	470.0
PD-25-061413-3.5	389.3	330.5	268.7	227.7	251.3	275.7	193.9	220.7	518.5
PD-25-061413-4.1	422.6	361.8	293.5	251.8	276.2	305.5	222.3	238.7	564.8
PD-25-061413-4.7	451.1	382.8	310.1	270.9	294.9	328.3	248.7	251.4	597.6
PD-25-061413-5.3	474.5	403.8	326.6	291.6	314.7	352.3	278.7	265.0	630.9
PD-25-061413-5.9	496.3	421.9	340.9	311.5	333.1	374.6	309.3	277.8	660.0
PD-25-061413-6.5	516.0	438.2	353.7	332.5	351.9	396.8	343.3	291.2	686.5
PD-25-061413-7.1	535.5	457.8	369.1	356.3	373.5	422.2	381.3	307.0	717.1

June 18th, 2013 - System Pressure: 9.5 MPa, Inlet Temperature: 33-34 ℃, Inlet valve: wide open, Outlet valve: wide open ($K_{in}=K_{out}=0$)

Table C.116: Averaged values of measured signals during experiment for each data point (PD-26-061813)

Test ID	Inlet Temperature (RTD1) (C)	Pressure (MPa)	Power (kW)	Outlet Temp (RTD2)(C)	T11 (C)	T12(C)	CO_2 volumetric Flow rate $(m^3/s) \times 10^6$	HE-Inlet water Temp.(C)	HE-Outlet water Temp.(C)	Water Flow rate (lpm)
PD-26-061813-1.2	32.7 ± 0.5	9.51 ± 0.02	1.32 ± 0.03	37.9 ± 0.5	39.5 ± 2.2	33.5 ± 2.2	46.0 ± 1.0	14.1 ± 2.2	37.2 ± 2.2	0.5
PD-26-061813-1.7	33.2 ± 0.5	9.50 ± 0.02	1.87 ± 0.03	40.2 ± 0.5	41.9 ± 2.2	34.0 ± 2.2	52.6 ± 1.3	14.4 ± 2.2	38.0 ± 2.2	0.9
PD-26-061813-2.3	33.0 ± 0.4	9.49 ± 0.02	2.52 ± 0.04	42.0 ± 0.5	44.2 ± 2.2	33.7 ± 2.2	58.2 ± 1.1	15.1 ± 2.2	36.9 ± 2.2	1.6
PD-26-061813-2.9	33.3 ± 0.5	9.51 ± 0.02	3.18 ± 0.04	45.4 ± 0.5	48.1 ± 2.2	34.2 ± 2.2	61.7 ± 1.2	14.8 ± 2.2	37.0 ± 2.2	2
PD-26-061813-3.5	33.1 ± 0.4	9.51 ± 0.02	3.84 ± 0.04	48.1 ± 0.5	51.6 ± 2.2	34.1 ± 2.2	64.3 ± 1.2	15.0 ± 2.2	35.7 ± 2.2	2.7
PD-26-061813-4.1	33.5 ± 0.5	9.52 ± 0.02	4.49 ± 0.05	53.8 ± 0.6	57.9 ± 2.2	34.5 ± 2.2	66.1 ± 1.3	14.7 ± 2.2	35.9 ± 2.2	3.1
PD-26-061813-4.7	33.4 ± 0.5	9.53 ± 0.02	5.15 ± 0.05	58.2 ± 0.6	62.8 ± 2.2	34.3 ± 2.2	67.2 ± 1.3	14.4 ± 2.2	34.9 ± 2.2	3.7
PD-26-061813-5.3	33.2 ± 0.5	9.50 ± 0.02	5.81 ± 0.05	63.5 ± 0.6	69.2 ± 2.2	34.0 ± 2.2	68.3 ± 1.3	14.1 ± 2.2	33.6 ± 2.2	4.5
PD-26-061813-5.9	33.4 ± 0.5	9.52 ± 0.02	6.47 ± 0.06	72.0 ± 0.6	77.3 ± 2.2	34.3 ± 2.2	68.6 ± 1.4	14.0 ± 2.2	33.6 ± 2.2	5
PD-26-061813-6.5	33.4 ± 0.5	9.52 ± 0.02	7.13 ± 0.06	80.1 ± 0.7	85.5 ± 2.2	34.2 ± 2.2	68.9 ± 1.3	13.9 ± 2.2	32.6 ± 2.2	5.8
PD-26-061813-7.1	33.3 ± 0.5	9.49 ± 0.02	7.78 ± 0.06	90.0 ± 0.7	96.5 ± 2.2	34.0 ± 2.2	69.1 ± 1.3	13.7 ± 2.2	31.3 ± 2.2	6.8

Table C.117: Averaged values of measured pressure-drops during experiment for each data point (PD-26-061813)

Test ID	DP2-1 (Pa)	DP2-2 (Pa)	DP2-3 (Pa)	DP2-4 (Pa)	DP2-5 (Pa)	DP3 (Pa)	DP13 (Pa)	DP10 (Pa)	DP7 (Pa)
PD-26-061813-1.2	134.6 ± 10.9	18.00 ± 10.99	69.39 ± 11.10	-2.5 ± 11.3	70.4 ± 11.0	842.1 ± 10.9	284.9 ± 12.7	702.3 ± 78.7	96.9 ± 10.5
PD-26-061813-1.7	153.3 ± 11.1	28.57 ± 11.27	94.26 ± 11.44	17.6 ± 11.9	82.2 ± 11.4	842.4 ± 11.1	369.4 ± 13.9	751.8 ± 78.9	108.7 ± 10.6
PD-26-061813-2.3	175.2 ± 11.4	39.95 ± 11.70	123.23 ± 11.94	42.7 ± 12.6	95.2 ± 12.0	850.2 ± 11.4	467.9 ± 15.2	798.7 ± 79.4	118.8 ± 10.6
PD-26-061813-2.9	190.7 ± 11.8	50.64 ± 12.19	147.96 ± 12.45	65.3 ± 13.4	109.8 ± 12.6	852.7 ± 11.8	553.5 ± 16.7	844.4 ± 79.7	127.2 ± 10.6
PD-26-061813-3.5	205.9 ± 12.2	60.67 ± 12.74	173.16 ± 13.13	89.4 ± 14.3	123.5 ± 13.2	853.9 ± 12.2	638.9 ± 19.0	869.3 ± 82.2	133.3 ± 10.7
PD-26-061813-4.1	216.5 ± 12.5	71.17 ± 13.29	196.44 ± 13.74	112.3 ± 15.6	135.3 ± 14.0	848.5 ± 12.5	715.3 ± 20.3	908.9 ± 81.0	139.6 ± 10.7
PD-26-061813-4.7	227.5 ± 12.8	80.84 ± 13.60	219.86 ± 14.34	136.4 ± 16.3	146.9 ± 14.7	849.4 ± 12.8	792.7 ± 21.8	938.1 ± 80.3	144.5 ± 10.8
PD-26-061813-5.3	237.6 ± 13.5	91.08 ± 14.45	244.32 ± 15.20	162.3 ± 17.1	158.8 ± 15.2	847.7 ± 13.5	872.6 ± 23.6	964.8 ± 80.5	149.1 ± 10.9
PD-26-061813-5.9	244.2 ± 13.8	101.01 ± 14.82	266.09 ± 15.37	184.8 ± 18.0	168.2 ± 16.1	846.1 ± 13.8	940.3 ± 24.7	977.0 ± 80.9	151.9 ± 11.1
PD-26-061813-6.5	251.2 ± 14.5	111.07 ± 15.57	289.15 ± 16.20	208.5 ± 18.6	178.6 ± 16.9	845.2 ± 14.5	1013.0 ± 25.5	1001.8 ± 81.1	154.7 ± 11.2
PD-26-061813-7.1	257.3 ± 14.8	121.50 ± 16.08	313.14 ± 16.78	232.3 ± 19.3	186.1 ± 17.6	836.4 ± 14.8	1083.2 ± 26.7	1025.0 ± 90.9	157.2 ± 11.3

Table C.118: Averaged values of measured wall surface temperature during experiment for each data point (PD-26-061813)

Test ID	TS21T (C)	TS21B (C)	TS22T (C)	TS22B (C)	TS23T (C)	TS23B (C)	TS24T (C)	TS24B (C)	TS25T (C)	TS25B (C)	TS26T (C)	TS26B (C)
PD-26-061813-1.2	42.4	41.0	46.7	41.3	46.6	41.7	45.4	42.3	51.5	44.5	53.4	46.7
PD-26-061813-1.7	46.9	44.5	52.8	44.8	52.9	45.4	51.7	46.5	60.4	49.8	63.7	53.3
PD-26-061813-2.3	51.5	47.8	59.0	48.2	59.4	48.9	58.3	50.5	70.0	55.0	74.9	60.5
PD-26-061813-2.9	57.8	52.7	67.5	52.9	68.2	53.7	68.1	56.4	83.4	63.3	90.6	71.5
PD-26-061813-3.5	63.6	56.8	75.2	56.9	76.2	57.8	76.9	61.5	95.5	70.7	105.0	81.5
PD-26-061813-4.1	71.5	62.8	85.9	62.6	87.3	64.1	89.8	69.9	113.2	82.6	127.4	98.0
PD-26-061813-4.7	78.5	67.8	95.3	67.4	96.7	69.1	100.4	76.6	127.8	92.3	146.1	111.7
PD-26-061813-5.3	85.8	73.1	105.3	72.6	106.7	74.5	111.9	84.2	143.1	103.1	164.6	126.5
PD-26-061813-5.9	95.1	80.1	118.1	79.5	119.2	81.9	127.0	95.1	162.3	118.4	187.0	146.3
PD-26-061813-6.5	103.9	86.7	130.3	86.0	131.0	89.1	140.7	105.5	180.3	132.8	207.5	164.4
PD-26-061813-7.1	113.4	93.8	143.3	93.5	143.6	97.3	155.5	117.7	199.9	149.0	229.6	184.8

June 28th, 2013 - System Pressure: 8.5 MPa, Inlet Temperature: 25-26 ℃, Inlet valve: wide open, Outlet valve: 40º closed

Table C.119: Averaged values of measured signals during experiment for each data point (PD-27-062813)

Test ID	Inlet Temperature (RTD1) (C)	Pressure (MPa)	Power (kW)	Outlet Temp (RTD2)(C)	T11 (C)	T12(C)	CO$_2$ volumetric Flow rate (m^3/s)×10^6	HE-Inlet water Temp.(C)	HE-Outlet water Temp.(C)	Water Flow rate (lpm)
PD-27-062813-1.2	25.5 ± 0.4	8.52 ± 0.02	1.32 ± 0.03	32.9 ± 0.5	34.9 ± 2.2	25.7 ± 2.2	34.6 ± 1.2	17.1 ± 2.2	27.5 ± 2.2	1.8
PD-27-062813-1.7	26.2 ± 0.4	8.52 ± 0.02	1.86 ± 0.03	34.2 ± 0.5	36.2 ± 2.2	26.5 ± 2.2	40.7 ± 1.0	17.3 ± 2.2	27.1 ± 2.2	2.8
PD-27-062813-2.3	25.9 ± 0.4	8.49 ± 0.02	2.52 ± 0.04	34.9 ± 0.5	37.0 ± 2.2	25.7 ± 2.2	45.9 ± 1.1	16.4 ± 2.2	24.3 ± 2.2	5.1
PD-27-062813-2.9	26.0 ± 0.4	8.51 ± 0.02	3.18 ± 0.04	35.8 ± 0.5	38.1 ± 2.2	25.9 ± 2.2	49.0 ± 1.1	15.6 ± 2.2	23.5 ± 2.2	6.6
PD-27-062813-3.5	26.1 ± 0.4	8.51 ± 0.02	3.83 ± 0.04	36.6 ± 0.5	39.1 ± 2.2	25.9 ± 2.2	51.3 ± 1.1	15.4 ± 2.2	22.2 ± 2.2	9.4
PD-27-062813-4.1	26.1 ± 0.4	8.48 ± 0.02	4.49 ± 0.05	37.5 ± 0.5	40.6 ± 2.2	25.9 ± 2.2	52.8 ± 1.1	15.0 ± 2.2	21.2 ± 2.2	12.4
PD-27-062813-4.7	26.5 ± 0.4	8.50 ± 0.02	5.15 ± 0.05	39.3 ± 0.5	43.3 ± 2.2	26.2 ± 2.2	53.2 ± 1.2	15.0 ± 2.2	20.6 ± 2.2	15.9
PD-27-062813-5.3	26.4 ± 0.4	8.52 ± 0.02	5.81 ± 0.05	41.8 ± 0.5	46.6 ± 2.2	26.1 ± 2.2	53.2 ± 1.2	14.8 ± 2.2	19.5 ± 2.2	21.2
PD-27-062813-5.9	26.6 ± 0.4	8.54 ± 0.02	6.46 ± 0.06	45.8 ± 0.5	52.2 ± 2.2	26.3 ± 2.2	52.5 ± 1.3	14.7 ± 2.2	18.9 ± 2.2	26.8

Table C.120: Averaged values of measured pressure-drops during experiment for each data point (PD-27-062813)

Test ID	DP2-1 (Pa)	DP2-2 (Pa)	DP2-3 (Pa)	DP2-4 (Pa)	DP2-5 (Pa)	DP3 (Pa)	DP13 (Pa)	DP10 (Pa)	DP7 (Pa)
PD-27-062813-1.2	85.6 ± 11.3	24.58 ± 11.53	51.47 ± 11.70	26.3 ± 11.3	37.3 ± 11.2	413.1 ± 11.3	220.1 ± 18.4	471.6 ± 81.1	58.6 ± 10.7
PD-27-062813-1.7	101.2 ± 11.8	32.40 ± 12.09	70.59 ± 12.20	40.7 ± 11.7	46.3 ± 11.6	425.4 ± 11.8	285.7 ± 20.6	693.5 ± 83.2	68.6 ± 10.8
PD-27-062813-2.3	117.4 ± 12.4	40.70 ± 12.81	92.38 ± 12.79	58.8 ± 12.4	58.3 ± 12.2	432.9 ± 12.4	361.4 ± 24.4	961.8 ± 85.8	78.7 ± 10.9
PD-27-062813-2.9	129.3 ± 13.1	48.34 ± 13.55	112.35 ± 13.58	76.2 ± 13.2	72.3 ± 12.8	449.8 ± 13.1	431.6 ± 27.4	1226.7 ± 87.2	88.3 ± 11.1
PD-27-062813-3.5	138.5 ± 13.8	56.45 ± 14.22	131.53 ± 14.15	95.3 ± 13.9	87.3 ± 13.4	456.8 ± 13.8	501.1 ± 28.5	1486.5 ± 89.6	96.6 ± 11.3
PD-27-062813-4.1	145.5 ± 14.2	64.53 ± 14.58	150.49 ± 14.44	115.6 ± 14.7	104.5 ± 14.0	454.9 ± 14.2	571.2 ± 30.6	1738.5 ± 94.7	101.8 ± 11.4
PD-27-062813-4.7	150.5 ± 14.8	73.24 ± 15.14	168.33 ± 14.97	136.0 ± 15.4	121.2 ± 14.4	460.3 ± 14.8	638.5 ± 31.9	1998.2 ± 95.1	107.9 ± 11.5
PD-27-062813-5.3	154.4 ± 15.7	81.45 ± 15.92	184.74 ± 15.58	156.0 ± 16.4	136.6 ± 15.2	466.6 ± 15.7	701.4 ± 34.4	2247.6 ± 98.3	112.1 ± 11.7
PD-27-062813-5.9	156.9 ± 16.3	90.21 ± 16.49	201.00 ± 16.06	177.1 ± 16.9	151.5 ± 15.5	470.0 ± 16.3	763.5 ± 36.4	2494.2 ± 163.7	115.4 ± 11.7

Table C.121: Averaged values of measured wall surface temperature during experiment for each data point (PD-27-062813)

Test ID	TS21T (C)	TS21B (C)	TS22T (C)	TS22B (C)	TS23T (C)	TS23B (C)	TS24T (C)	TS24B (C)	TS25T (C)	TS25B (C)	TS26T (C)	TS26B (C)
PD-27-062813-1.2	37.8	35.3	42.8	36.5	42.4	36.9	40.8	37.3	47.1	39.0	47.3	40.1
PD-27-062813-1.7	41.8	38.1	48.8	39.6	48.3	39.8	45.6	40.0	53.7	42.1	53.2	43.7
PD-27-062813-2.3	46.3	40.7	55.6	42.5	54.3	42.6	50.8	42.6	60.9	45.5	60.2	47.9
PD-27-062813-2.9	52.4	44.1	63.8	46.4	61.4	46.1	57.5	46.0	69.6	49.7	69.7	53.6
PD-27-062813-3.5	59.7	48.2	73.0	50.8	69.0	49.8	64.7	49.5	79.3	54.6	80.4	60.1
PD-27-062813-4.1	68.2	53.0	83.1	55.8	77.3	53.8	73.3	53.3	90.1	60.2	92.5	68.0
PD-27-062813-4.7	78.1	59.3	95.3	62.1	87.3	58.7	83.6	58.4	103.5	68.1	108.7	79.4
PD-27-062813-5.3	88.0	66.0	107.8	68.7	97.6	63.9	94.5	64.0	117.7	77.1	127.2	92.5
PD-27-062813-5.9	98.9	74.0	121.9	76.3	109.6	70.0	107.3	71.4	134.6	88.9	149.3	109.8

Table C.122: Steady-state parameters of the loop (processed data) (PD-27-062813)

Test ID	Power (kW)	Flow rate (kg/s)	Inlet K	Outlet K*	Outlet Temp. Calculated (C)	T11(C)	Total Ch. PD (Pa)	Acc. PD.(Pa)	Fr. PD.(Pa)
PD-27-062813-1.2	1.32 ± 0.03	0.027 ± 0.001	0	17.7	35.4 ± 0.3	34.9 ± 2.2	211.7 ± 18.4	16.4 ± 1.7	195.4 ± 18.4
PD-27-062813-1.7	1.86 ± 0.03	0.032 ± 0.001	0	18.5	36.5 ± 0.2	36.2 ± 2.2	273.8 ± 20.6	30.9 ± 2.5	243.0 ± 20.7
PD-27-062813-2.3	2.52 ± 0.04	0.036 ± 0.001	0	19.2	37.0 ± 0.2	37.0 ± 2.2	345.5 ± 24.4	51.7 ± 3.8	293.8 ± 24.7
PD-27-062813-2.9	3.18 ± 0.04	0.038 ± 0.001	0	20.0	37.8 ± 0.2	38.1 ± 2.2	412.7 ± 27.4	77.1 ± 5.4	335.5 ± 28.0
PD-27-062813-3.5	3.83 ± 0.04	0.040 ± 0.001	0	20.4	38.6 ± 0.2	39.1 ± 2.2	479.3 ± 28.5	107.0 ± 7.1	372.3 ± 29.4
PD-27-062813-4.1	4.49 ± 0.05	0.041 ± 0.001	0	20.4	39.6 ± 0.3	40.6 ± 2.2	546.8 ± 30.6	141.1 ± 8.9	405.6 ± 31.9
PD-27-062813-4.7	5.15 ± 0.05	0.041 ± 0.001	0	20.7	41.8 ± 0.6	43.3 ± 2.2	612.0 ± 31.9	178.8 ± 11.6	433.2 ± 34.0
PD-27-062813-5.3	5.81 ± 0.05	0.041 ± 0.001	0	20.9	45.0 ± 0.9	46.6 ± 2.2	673.0 ± 34.4	216.5 ± 14.0	456.5 ± 37.2
PD-27-062813-5.9	6.46 ± 0.06	0.040 ± 0.001	0	21.1	50.6 ± 1.5	52.2 ± 2.2	733.6 ± 36.4	256.4 ± 17.4	477.2 ± 40.3

*Mean outlet K factor: 19.4

Table C.123: Comparison between frictional pressure-drop from the experimental against available friction-factor formulae (PD-27-062813)

Test ID	Fr. PD.(Pa)-Exp.	Blasius	Kondratev	Ishigai	Razumovskiy	Tarasova & Leontev	Yamashita	Popov	Kuraeva & Protopopov
PD-27-062813-1.2	195.4	140.3	115.6	109.5	118.1	122.2	91.1	113.8	246.7
PD-27-062813-1.7	243.0	190.9	156.5	137.5	151.3	160.2	111.3	141.0	319.9
PD-27-062813-2.3	293.8	245.0	200.1	170.8	189.0	203.2	138.9	172.0	396.8
PD-27-062813-2.9	335.5	285.4	232.5	197.8	218.6	237.4	165.0	195.3	454.6
PD-27-062813-3.5	372.3	321.9	261.7	223.9	246.4	270.0	192.3	216.6	507.3
PD-27-062813-4.1	405.6	354.3	287.4	248.7	272.1	300.4	220.8	235.7	554.7
PD-27-062813-4.7	433.2	378.0	306.1	270.8	293.7	326.1	250.4	251.3	591.2
PD-27-062813-5.3	456.5	400.1	323.6	291.7	314.0	350.3	279.4	265.8	625.1
PD-27-062813-5.9	477.2	417.3	337.1	312.3	332.7	372.5	311.1	279.2	652.9

March 5th, 2013 - System Pressure: 8 MPa, Inlet Temperature: 25-26 ℃, Inlet valve: wide open, Outlet valve: wide open ($K_{in}=K_{out}=0$)

Table C.124: Averaged values of measured signals during experiment for each data point (PD-28-030513)

Test ID	Inlet Temperature (RTD1) (C)	Pressure (MPa)	Power (kW)	Outlet Temp (RTD2)(C)	T11 (C)	T12(C)	CO_2 volumetric Flow rate $(m^3/s)\times10^6$	HE-Inlet water Temp.(C)	HE-Outlet water Temp.(C)	Water Flow rate (lpm)
PD-28-030513-1.1	24.5 ± 0.4	8.01 ± 0.02	1.21 ± 0.02	31.5 ± 0.5	33.2 ± 2.2	24.4 ± 2.2	38.4 ± 1.2	9.8 ± 2.2	29.7 ± 2.2	0.6
PD-28-030513-1.7	25.0 ± 0.4	8.01 ± 0.02	1.86 ± 0.03	32.8 ± 0.5	34.6 ± 2.2	24.8 ± 2.2	41.5 ± 8.3	11.0 ± 2.2	28.8 ± 2.2	1.5
PD-28-030513-2.3	25.0 ± 0.4	8.02 ± 0.02	2.52 ± 0.03	33.6 ± 0.5	35.2 ± 2.2	25.0 ± 2.2	48.3 ± 3.7	10.7 ± 2.2	27.3 ± 2.2	2.2
PD-28-030513-2.9	24.8 ± 0.4	7.99 ± 0.02	3.17 ± 0.04	33.8 ± 0.5	35.6 ± 2.2	24.6 ± 2.2	56.8 ± 1.2	10.4 ± 2.2	25.0 ± 2.2	3.5
PD-28-030513-3.5	24.8 ± 0.4	7.99 ± 0.02	3.83 ± 0.04	34.2 ± 0.5	35.9 ± 2.2	24.6 ± 2.2	60.3 ± 1.1	8.9 ± 2.2	23.7 ± 2.2	4.2
PD-28-030513-4.1	25.3 ± 0.4	8.01 ± 0.02	4.48 ± 0.05	34.6 ± 0.5	36.5 ± 2.2	23.8 ± 2.2	63.3 ± 1.2	7.2 ± 2.2	22.3 ± 2.2	4.9
PD-28-030513-4.7	25.3 ± 0.4	8.00 ± 0.03	5.14 ± 0.05	34.9 ± 0.5	37.0 ± 2.2	23.8 ± 2.4	65.7 ± 1.2	6.5 ± 2.2	20.1 ± 2.2	6.4
PD-28-030513-5.3	25.5 ± 0.4	8.02 ± 0.02	5.80 ± 0.05	35.4 ± 0.5	37.8 ± 2.2	24.7 ± 2.2	67.3 ± 1.2	6.1 ± 2.2	20.4 ± 2.2	6.7
PD-28-030513-5.9	25.3 ± 0.4	8.00 ± 0.02	6.45 ± 0.06	35.8 ± 0.5	38.6 ± 2.2	24.3 ± 2.2	68.6 ± 1.1	5.8 ± 2.2	19.8 ± 2.2	7.9
PD-28-030513-6.5	25.7 ± 0.4	8.03 ± 0.02	7.11 ± 0.06	37.2 ± 0.5	40.7 ± 2.2	24.5 ± 2.2	69.0 ± 1.1	5.3 ± 2.2	19.2 ± 2.2	8.6
PD-28-030513-7.1	25.6 ± 0.4	8.02 ± 0.02	7.76 ± 0.06	38.4 ± 0.5	42.6 ± 2.2	24.5 ± 2.2	69.4 ± 1.1	5.2 ± 2.2	19.0 ± 2.2	9.4
PD-28-030513-7.8	25.4 ± 0.4	8.03 ± 0.02	8.53 ± 0.06	40.8 ± 0.5	45.8 ± 2.2	24.7 ± 2.2	70.0 ± 1.2	4.9 ± 2.2	18.4 ± 2.2	10.5
PD-28-030513-8.4	25.0 ± 0.4	8.02 ± 0.02	9.19 ± 0.07	42.8 ± 0.5	49.0 ± 2.2	24.8 ± 2.2	70.2 ± 1.9	4.6 ± 2.2	17.4 ± 2.2	12.1
PD-28-030513-9	25.1 ± 0.4	8.02 ± 0.03	9.84 ± 0.07	47.1 ± 0.5	53.4 ± 2.2	24.9 ± 2.2	69.5 ± 1.1	4.5 ± 2.2	17.3 ± 2.2	12.8
PD-28-030513-9.6	25.4 ± 0.4	8.03 ± 0.03	10.50 ± 0.07	51.5 ± 0.6	58.7 ± 2.2	25.3 ± 2.2	69.2 ± 1.2	4.5 ± 2.2	17.2 ± 2.2	13.6
PD-28-030513-10.2	25.7 ± 0.4	8.03 ± 0.02	11.15 ± 0.07	55.7 ± 0.6	64.8 ± 2.2	25.1 ± 2.2	69.2 ± 1.4	4.5 ± 2.2	16.9 ± 2.2	14.9
PD-28-030513-10.8	25.8 ± 0.4	8.02 ± 0.02	11.81 ± 0.08	62.6 ± 0.6	72.4 ± 2.3	25.1 ± 2.2	68.6 ± 1.2	4.5 ± 2.2	16.7 ± 2.2	16

Table C.125: Averaged values of measured wall surface temperature during experiment for each data point (PD-28-030513)

Test ID	TS21T (C)	TS21B (C)	TS22T (C)	TS22B (C)	TS23T (C)	TS23B (C)	TS24T (C)	TS24B (C)	TS25T (C)	TS25B (C)	TS26T (C)	TS26B (C)
PD-28-030513-1.1	34.9	33.5	39.6	34.7	38.3	35.5	39.9	35.6	42.8	37.0	43.7	37.7
PD-28-030513-1.7	38.3	36.8	45.2	37.8	42.6	38.6	44.4	38.1	47.5	39.6	49.2	40.6
PD-28-030513-2.3	41.5	39.1	50.6	40.3	47.0	41.2	48.7	40.4	53.6	42.3	56.1	43.8
PD-28-030513-2.9	44.9	41.2	56.1	42.8	51.2	43.7	53.5	42.7	60.0	44.7	63.3	46.6
PD-28-030513-3.5	49.4	44.0	62.1	46.0	56.7	46.5	59.8	45.2	67.1	47.8	71.4	50.3
PD-28-030513-4.1	55.3	47.4	68.6	49.6	63.2	49.7	66.7	48.1	75.0	51.2	80.9	54.8
PD-28-030513-4.7	61.5	51.0	74.7	53.3	69.6	52.8	73.7	50.9	83.1	54.7	90.9	59.8
PD-28-030513-5.3	69.1	55.6	82.1	57.6	76.9	56.4	81.6	54.0	92.6	59.0	102.4	66.4
PD-28-030513-5.9	76.5	60.1	89.5	61.8	83.8	59.6	89.3	57.0	101.6	63.3	113.7	72.9
PD-28-030513-6.5	85.8	66.3	97.8	66.7	89.4	63.7	98.6	61.0	113.4	69.7	128.5	83.0
PD-28-030513-7.1	93.8	72.6	106.0	71.1	96.7	67.5	107.6	65.0	124.6	76.0	142.0	92.6
PD-28-030513-7.8	100.4	79.8	112.2	75.1	103.8	72.1	117.6	70.6	138.7	84.8	159.1	104.9
PD-28-030513-8.4	105.2	85.0	118.4	78.5	110.4	76.0	126.1	75.3	150.6	92.1	173.2	115.8
PD-28-030513-9	105.2	88.1	125.3	83.1	120.3	80.9	138.8	82.2	165.5	102.7	190.4	130.8
PD-28-030513-9.6	111.2	93.7	141.4	90.6	134.2	86.4	152.8	89.4	180.6	114.2	207.3	146.6
PD-28-030513-10.2	140.3	109.2	166.3	100.7	149.8	91.6	164.9	97.3	195.1	126.1	223.7	162.1
PD-28-030513-10.8	150.4	116.9	179.8	107.9	161.2	97.7	178.7	107.4	212.2	140.5	242.6	180.4

Table C.126: Steady-state parameters of the loop (processed data) (PD-28-030513)

Test ID	Power (kW)	Flow rate (kg/s)	Inlet K	Outlet K	Outlet Temp. Calculated (C)	T11(C)
PD-28-030513-1.1	1.21 ± 0.02	0.030 ± 0.001	0	0	32.7 ± 0.2	33.2 ± 2.2
PD-28-030513-1.7	1.86 ± 0.03	0.032 ± 0.006	0	0	34.1 ± 0.6	34.6 ± 2.2
PD-28-030513-2.3	2.52 ± 0.03	0.037 ± 0.003	0	0	34.5 ± 0.2	35.2 ± 2.2
PD-28-030513-2.9	3.17 ± 0.04	0.044 ± 0.001	0	0	34.5 ± 0.1	35.6 ± 2.2
PD-28-030513-3.5	3.83 ± 0.04	0.047 ± 0.001	0	0	34.7 ± 0.1	35.9 ± 2.2
PD-28-030513-4.1	4.48 ± 0.05	0.049 ± 0.001	0	0	35.2 ± 0.2	36.5 ± 2.2
PD-28-030513-4.7	5.14 ± 0.05	0.051 ± 0.001	0	0	35.6 ± 0.3	37.0 ± 2.2
PD-28-030513-5.3	5.80 ± 0.05	0.052 ± 0.001	0	0	36.5 ± 0.3	37.8 ± 2.2
PD-28-030513-5.9	6.45 ± 0.06	0.053 ± 0.001	0	0	37.4 ± 0.4	38.6 ± 2.2
PD-28-030513-6.5	7.11 ± 0.06	0.053 ± 0.001	0	0	39.8 ± 0.6	40.7 ± 2.2
PD-28-030513-7.1	7.76 ± 0.06	0.053 ± 0.001	0	0	42.2 ± 0.8	42.6 ± 2.2
PD-28-030513-7.8	8.53 ± 0.06	0.054 ± 0.001	0	0	45.6 ± 1.1	45.8 ± 2.2
PD-28-030513-8.4	9.19 ± 0.07	0.054 ± 0.002	0	0	48.6 ± 1.9	49.0 ± 2.2
PD-28-030513-9	9.84 ± 0.07	0.054 ± 0.001	0	0	54.7 ± 1.7	53.4 ± 2.2
PD-28-030513-9.6	10.50 ± 0.07	0.053 ± 0.001	0	0	62.2 ± 2.3	58.7 ± 2.2
PD-28-030513-10.2	11.15 ± 0.07	0.053 ± 0.001	0	0	70.3 ± 3.0	64.8 ± 2.2
PD-28-030513-10.8	11.81 ± 0.08	0.053 ± 0.001	0	0	80.0 ± 3.2	72.4 ± 2.3

March 6th, 2013 - System Pressure: 8 MPa, Inlet Temperature: 25-26 ℃, Inlet valve: wide open, Outlet valve: 35° closed

Table C.127: Averaged values of measured signals during experiment for each data point (PD-29-030613)

Test ID	Inlet Temperature (RTD1) (C)	Pressure (MPa)	Power (kW)	Outlet Temp (RTD2)(C)	T11 (C)	T12(C)	CO$_2$ volumetric Flow rate (m^3/s)×10^6	HE-Inlet water Temp.(C)	HE-Outlet water Temp.(C)	Water Flow rate (lpm)
PD-29-030613-1.1	25.1 ± 0.4	8.00 ± 0.02	1.21 ± 0.02	32.0 ± 0.5	33.6 ± 2.2	25.5 ± 2.2	35.4 ± 1.7	11.3 ± 2.2	30.0 ± 2.2	0.8
PD-29-030613-1.7	25.3 ± 0.4	8.00 ± 0.02	1.86 ± 0.03	33.1 ± 0.5	34.8 ± 2.2	25.1 ± 2.2	43.7 ± 1.1	11.2 ± 2.2	28.8 ± 2.2	1.5
PD-29-030613-2.3	25.6 ± 0.4	8.01 ± 0.02	2.52 ± 0.03	33.8 ± 0.5	35.5 ± 2.2	25.1 ± 2.2	49.0 ± 1.2	10.7 ± 2.2	27.7 ± 2.2	2.1
PD-29-030613-2.9	25.7 ± 0.4	8.00 ± 0.02	3.17 ± 0.04	34.1 ± 0.5	35.9 ± 2.2	24.8 ± 2.2	53.2 ± 1.1	10.0 ± 2.2	25.3 ± 2.2	3.3
PD-29-030613-3.5	25.7 ± 0.4	8.00 ± 0.02	3.83 ± 0.04	34.5 ± 0.5	36.2 ± 2.2	25.2 ± 2.2	56.1 ± 1.1	8.1 ± 2.2	23.5 ± 2.2	4
PD-29-030613-4.1	26.2 ± 0.4	8.01 ± 0.02	4.48 ± 0.05	35.0 ± 0.5	37.0 ± 2.2	25.9 ± 2.2	58.3 ± 1.1	7.0 ± 2.2	21.3 ± 2.2	5.1
PD-29-030613-4.7	26.0 ± 0.4	8.00 ± 0.02	5.14 ± 0.05	35.5 ± 0.5	37.9 ± 2.2	25.6 ± 2.2	59.3 ± 1.1	6.2 ± 2.2	20.1 ± 2.2	6.1
PD-29-030613-5.3	25.8 ± 0.4	8.00 ± 0.02	5.80 ± 0.05	36.2 ± 0.5	39.3 ± 2.2	25.6 ± 2.2	59.5 ± 1.1	5.7 ± 2.2	19.8 ± 2.2	7.2
PD-29-030613-5.9	26.2 ± 0.4	7.99 ± 0.02	6.45 ± 0.06	37.8 ± 0.5	42.0 ± 2.2	25.0 ± 2.2	59.4 ± 1.1	5.3 ± 2.2	18.6 ± 2.2	8.3
PD-29-030613-6.5	26.5 ± 0.4	8.02 ± 0.03	7.11 ± 0.06	40.9 ± 0.5	46.0 ± 2.2	25.0 ± 2.2	59.0 ± 1.1	5.1 ± 2.2	18.7 ± 2.2	8.7
PD-29-030613-7.1	26.5 ± 0.4	8.02 ± 0.02	7.76 ± 0.06	44.5 ± 0.5	50.9 ± 2.2	25.1 ± 2.2	58.7 ± 1.1	5.1 ± 2.2	18.9 ± 2.2	9.2
PD-29-030613-7.7	26.6 ± 0.4	8.00 ± 0.02	8.42 ± 0.06	50.0 ± 0.5	57.9 ± 2.2	25.0 ± 2.2	57.8 ± 1.1	4.8 ± 2.2	18.1 ± 2.2	10.4
PD-29-030613-8.4	27.0 ± 0.4	8.02 ± 0.02	9.18 ± 0.07	59.7 ± 0.6	68.1 ± 2.2	25.3 ± 2.2	56.5 ± 1.1	4.9 ± 2.2	18.3 ± 2.2	11
PD-29-030613-9	27.1 ± 0.4	8.03 ± 0.02	9.84 ± 0.07	73.7 ± 0.6	77.6 ± 2.3	25.8 ± 2.2	56.0 ± 1.3	4.9 ± 2.2	18.2 ± 2.2	11.7
PD-29-030613-9.5	26.6 ± 0.4	8.02 ± 0.02	10.39 ± 0.07	80.8 ± 0.7	84.7 ± 2.3	25.2 ± 2.2	55.7 ± 1.1	4.7 ± 2.2	17.3 ± 2.2	13.1

Table C.128: Averaged values of measured wall surface temperature during experiment for each data point (PD-29-030613)

Test ID	TS21T (C)	TS21B (C)	TS22T (C)	TS22B (C)	TS23T (C)	TS23B (C)	TS24T (C)	TS24B (C)	TS25T (C)	TS25B (C)	TS26T (C)	TS26B (C)
PD-29-030613-1.1	36.0	34.1	40.8	35.0	39.4	36.0	41.2	36.0	43.3	37.2	44.8	38.0
PD-29-030613-1.7	39.5	37.1	46.7	37.9	44.6	38.9	46.3	38.4	48.8	39.9	51.4	41.2
PD-29-030613-2.3	43.6	39.6	53.3	40.7	50.0	41.7	51.7	41.0	55.9	43.0	59.2	44.5
PD-29-030613-2.9	48.3	42.4	60.0	43.7	55.4	44.6	57.7	43.7	63.5	46.0	67.6	48.1
PD-29-030613-3.5	54.0	45.6	67.3	47.1	61.9	47.7	64.9	46.5	71.8	49.4	77.2	52.5
PD-29-030613-4.1	61.7	50.0	76.1	51.3	69.6	51.4	73.1	49.9	81.6	53.6	88.8	58.7
PD-29-030613-4.7	69.8	54.8	85.2	55.8	77.5	55.1	81.9	53.2	91.7	58.2	101.2	65.7
PD-29-030613-5.3	78.6	60.3	94.8	60.7	86.1	59.1	91.4	57.0	102.9	63.6	115.1	74.3
PD-29-030613-5.9	88.7	67.7	106.1	66.7	95.7	63.6	102.2	61.7	116.0	71.3	132.0	86.2
PD-29-030613-6.5	99.3	75.6	119.2	73.3	106.7	68.9	114.8	68.0	131.6	81.4	151.2	100.8
PD-29-030613-7.1	109.4	82.9	132.3	79.8	117.8	74.2	127.4	74.7	147.4	91.9	170.2	116.7
PD-29-030613-7.7	120.1	91.2	146.6	87.7	130.1	80.2	141.8	83.4	165.8	106.1	192.3	136.5
PD-29-030613-8.4	133.6	101.5	164.8	97.7	146.0	88.8	161.0	96.8	190.5	126.9	221.4	163.4
PD-29-030613-9	139.2	107.6	171.8	102.6	156.7	97.1	178.2	110.2	212.3	145.7	246.4	187.2
PD-29-030613-9.5	143.0	111.9	177.3	106.2	165.6	102.8	189.9	119.3	227.0	157.6	262.5	202.4

Table C.129: Steady-state parameters of the loop (processed data) (PD-29-030613)

Test ID	Power (kW)	Flow rate (kg/s)	Inlet K	Outlet K*	Outlet Temp. Calculated (C)	T11(C)
PD-29-030613-1.1	1.21 ± 0.02	0.027 ± 0.001	0	9.1	33.2 ± 0.2	33.6 ± 2.2
PD-29-030613-1.7	1.86 ± 0.03	0.034 ± 0.001	0	9.1	34.0 ± 0.1	34.8 ± 2.2
PD-29-030613-2.3	2.52 ± 0.03	0.038 ± 0.001	0	9.1	34.5 ± 0.1	35.5 ± 2.2
PD-29-030613-2.9	3.17 ± 0.04	0.041 ± 0.001	0	9.1	34.8 ± 0.1	35.9 ± 2.2
PD-29-030613-3.5	3.83 ± 0.04	0.043 ± 0.001	0	9.1	35.1 ± 0.2	36.2 ± 2.2
PD-29-030613-4.1	4.48 ± 0.05	0.044 ± 0.001	0	9.1	35.8 ± 0.2	37.0 ± 2.2
PD-29-030613-4.7	5.14 ± 0.05	0.045 ± 0.001	0	9.1	36.8 ± 0.3	37.9 ± 2.2
PD-29-030613-5.3	5.80 ± 0.05	0.045 ± 0.001	0	9.1	38.4 ± 0.5	39.3 ± 2.2
PD-29-030613-5.9	6.45 ± 0.06	0.045 ± 0.001	0	9.1	41.8 ± 0.9	42.0 ± 2.2
PD-29-030613-6.5	7.11 ± 0.06	0.045 ± 0.001	0	9.1	47.4 ± 1.4	46.0 ± 2.2
PD-29-030613-7.1	7.76 ± 0.06	0.044 ± 0.001	0	9.1	53.6 ± 1.9	50.9 ± 2.2
PD-29-030613-7.7	8.42 ± 0.06	0.044 ± 0.001	0	9.1	62.7 ± 2.5	57.9 ± 2.2
PD-29-030613-8.4	9.18 ± 0.07	0.042 ± 0.001	0	9.1	77.7 ± 3.3	68.1 ± 2.2
PD-29-030613-9	9.84 ± 0.07	0.042 ± 0.001	0	9.1	90.3 ± 4.4	77.6 ± 2.3
PD-29-030613-9.5	10.39 ± 0.07	0.042 ± 0.001	0	9.1	97.7 ± 4.3	84.7 ± 2.3

*Equivalent K_{out}=9.1 (based on PD-2-041213)

March 7th, 2013 - System Pressure: 8 MPa, Inlet Temperature: 25-26 ℃, Inlet valve: wide open, Outlet valve: 40° closed

Table C.130: Averaged values of measured signals during experiment for each data point (PD-30-030713)

Test ID	Inlet Temperature (RTD1) (C)	Pressure (MPa)	Power (kW)	Outlet Temp (RTD2)(C)	T11 (C)	T12(C)	CO$_2$ volumetric Flow rate (m^3/s)×10^6	HE-Inlet water Temp.(C)	HE-Outlet water Temp.(C)	Water Flow rate (lpm)
PD-30-030713-1	25.3 ± 0.4	8.00 ± 0.02	1.10 ± 0.02	31.6 ± 0.5	34.2 ± 2.2	25.3 ± 2.2	34.0 ± 1.2	10.3 ± 2.2	30.1 ± 2.2	0.8
PD-30-030713-1.7	25.3 ± 0.4	8.00 ± 0.02	1.86 ± 0.03	33.1 ± 0.5	34.8 ± 2.2	25.4 ± 2.2	41.8 ± 1.0	11.0 ± 2.2	28.5 ± 2.2	1.5
PD-30-030713-2.3	25.5 ± 0.4	8.02 ± 0.02	2.52 ± 0.04	33.8 ± 0.5	35.5 ± 2.2	25.4 ± 2.2	46.4 ± 1.1	10.8 ± 2.2	27.2 ± 2.2	2.3
PD-30-030713-2.95	25.8 ± 0.4	8.00 ± 0.02	3.23 ± 0.04	34.2 ± 0.5	35.9 ± 2.2	25.7 ± 2.2	50.3 ± 1.2	9.2 ± 2.2	25.4 ± 2.2	3.1
PD-30-030713-3.5	25.7 ± 0.4	7.99 ± 0.02	3.83 ± 0.04	34.5 ± 0.5	36.4 ± 2.2	25.5 ± 2.2	52.5 ± 1.1	8.3 ± 2.2	23.6 ± 2.2	4
PD-30-030713-4.1	25.9 ± 0.4	8.01 ± 0.02	4.49 ± 0.05	35.1 ± 0.5	37.4 ± 2.2	24.8 ± 2.2	53.9 ± 1.1	7.1 ± 2.2	20.8 ± 2.2	5.4
PD-30-030713-4.7	26.0 ± 0.4	8.00 ± 0.02	5.14 ± 0.05	35.9 ± 0.5	38.7 ± 2.2	25.4 ± 2.2	54.8 ± 1.1	6.4 ± 2.2	19.8 ± 2.2	6.4
PD-30-030713-5.3	26.1 ± 0.4	8.00 ± 0.02	5.80 ± 0.05	37.3 ± 0.5	41.0 ± 2.2	25.0 ± 2.2	54.9 ± 1.1	5.8 ± 2.2	19.7 ± 2.2	7.2
PD-30-030713-5.9	26.4 ± 0.4	8.02 ± 0.02	6.45 ± 0.06	40.3 ± 0.5	45.1 ± 2.2	25.4 ± 2.2	54.2 ± 1.1	5.6 ± 2.2	18.9 ± 2.2	8.1
PD-30-030713-6.5	26.6 ± 0.4	8.01 ± 0.02	7.11 ± 0.06	44.5 ± 0.5	50.6 ± 2.2	25.7 ± 2.2	53.0 ± 1.2	5.1 ± 2.2	17.9 ± 2.2	9.1
PD-30-030713-7.4	26.7 ± 0.4	8.02 ± 0.02	8.10 ± 0.06	54.7 ± 0.6	61.1 ± 2.3	25.9 ± 2.2	51.1 ± 1.1	5.1 ± 2.2	18.1 ± 2.2	9.9
PD-30-030713-8.2	26.3 ± 0.4	8.00 ± 0.02	8.97 ± 0.07	65.6 ± 0.6	73.0 ± 2.3	25.0 ± 2.2	50.0 ± 1.1	4.9 ± 2.2	17.1 ± 2.2	11.7

Table C.131: Averaged values of measured wall surface temperature during experiment for each data point (PD-30-030713)

Test ID	TS21T (C)	TS21B (C)	TS22T (C)	TS22B (C)	TS23T (C)	TS23B (C)	TS24T (C)	TS24B (C)	TS25T (C)	TS25B (C)	TS26T (C)	TS26B (C)
PD-30-030713-1	35.4	33.6	39.6	34.5	38.4	35.4	40.2	35.5	42.5	36.7	43.5	37.3
PD-30-030713-1.7	39.9	37.2	47.8	38.0	45.8	39.0	47.6	38.5	50.9	40.2	52.8	41.4
PD-30-030713-2.3	44.3	39.8	54.8	40.8	51.6	41.9	53.6	41.2	58.4	43.3	60.9	44.8
PD-30-030713-2.95	50.5	43.1	63.3	44.4	58.7	45.3	61.1	44.3	67.4	46.9	70.9	49.4
PD-30-030713-3.5	56.6	46.4	71.0	47.8	65.4	48.4	68.3	47.2	75.3	50.3	80.8	54.1
PD-30-030713-4.1	64.8	51.2	80.8	52.4	73.7	52.4	77.3	50.8	85.7	55.0	93.3	61.0
PD-30-030713-4.7	74.2	56.8	91.6	57.6	82.5	56.5	87.1	54.7	97.2	60.7	107.6	69.9
PD-30-030713-5.3	84.4	63.8	103.9	63.7	92.4	61.2	98.2	59.2	110.5	68.0	124.5	81.4
PD-30-030713-5.9	95.5	71.8	117.6	70.9	103.7	66.7	111.1	65.5	126.4	78.2	144.5	96.5
PD-30-030713-6.5	106.5	80.1	131.8	78.4	115.9	72.5	125.1	73.1	144.0	90.5	166.5	114.9
PD-30-030713-7.4	123.4	93.0	154.4	90.7	135.7	82.8	148.7	88.2	174.4	114.5	203.2	147.9
PD-30-030713-8.2	137.9	104.1	173.4	101.8	153.0	92.3	169.5	102.9	201.0	136.9	234.6	176.5

Table C.132: Steady-state parameters of the loop (processed data) (PD-30-030713)

Test ID	Power (kW)	Flow rate (kg/s)	Inlet K	Outlet K*	Outlet Temp. Calculated (C)	T11(C)
PD-30-030713-1	1.10 ± 0.02	0.026 ± 0.001	0	20	33.1 ± 0.2	34.2 ± 2.2
PD-30-030713-1.7	1.86 ± 0.03	0.032 ± 0.001	0	20	34.1 ± 0.1	34.8 ± 2.2
PD-30-030713-2.3	2.52 ± 0.04	0.036 ± 0.001	0	20	34.6 ± 0.1	35.5 ± 2.2
PD-30-030713-2.95	3.23 ± 0.04	0.038 ± 0.001	0	20	34.9 ± 0.2	35.9 ± 2.2
PD-30-030713-3.5	3.83 ± 0.04	0.040 ± 0.001	0	20	35.3 ± 0.2	36.4 ± 2.2
PD-30-030713-4.1	4.49 ± 0.05	0.041 ± 0.001	0	20	36.4 ± 0.3	37.4 ± 2.2
PD-30-030713-4.7	5.14 ± 0.05	0.042 ± 0.001	0	20	37.9 ± 0.5	38.7 ± 2.2
PD-30-030713-5.3	5.80 ± 0.05	0.042 ± 0.001	0	20	40.8 ± 0.8	41.0 ± 2.2
PD-30-030713-5.9	6.45 ± 0.06	0.041 ± 0.001	0	20	46.5 ± 1.4	45.1 ± 2.2
PD-30-030713-6.5	7.11 ± 0.06	0.040 ± 0.001	0	20	54.8 ± 2.3	50.6 ± 2.2
PD-30-030713-7.4	8.10 ± 0.06	0.039 ± 0.001	0	20	72.6 ± 3.3	61.1 ± 2.3
PD-30-030713-8.2	8.97 ± 0.07	0.038 ± 0.001	0	20	89.4 ± 4.2	73.0 ± 2.3

*Equivalent outlet K factor: (average of mean K factors for 40º closed valve)

March 8th, 2013 - System Pressure: 8 MPa, Inlet Temperature: 25-26 ºC, Inlet valve: wide open, Outlet valve: 46º closed

Table C.133: Averaged values of measured signals during experiment for each data point (PD-31-030813)

Test ID	Inlet Temperature (RTD1) (C)	Pressure (MPa)	Power (kW)	Outlet Temp (RTD2)(C)	T11 (C)	T12(C)	CO_2 volumetric Flow rate $(m^3/s) \times 10^6$	HE-Inlet water Temp.(C)	HE-Outlet water Temp.(C)	Water Flow rate (lpm)
PD-31-030813-1.7	25.3 ± 0.4	7.99 ± 0.02	1.87 ± 0.03	33.1 ± 0.5	34.9 ± 2.2	24.9 ± 2.2	36.3 ± 1.4	10.7 ± 2.2	27.9 ± 2.2	1.5
PD-31-030813-2.3	25.6 ± 0.4	8.00 ± 0.02	2.52 ± 0.04	33.8 ± 0.5	35.5 ± 2.2	25.1 ± 2.2	40.9 ± 1.1	10.7 ± 2.2	26.2 ± 2.2	2.4
PD-31-030813-2.9	25.9 ± 0.4	8.01 ± 0.02	3.18 ± 0.04	34.4 ± 0.5	36.2 ± 2.2	25.1 ± 2.2	43.2 ± 1.1	10.3 ± 2.2	23.7 ± 2.2	3.8
PD-31-030813-3.5	25.9 ± 0.4	8.00 ± 0.02	3.84 ± 0.04	35.0 ± 0.5	37.2 ± 2.2	25.0 ± 2.2	44.2 ± 1.1	8.0 ± 2.2	21.1 ± 2.2	4.7
PD-31-030813-4.1	26.1 ± 0.4	8.00 ± 0.02	4.49 ± 0.05	36.4 ± 0.5	39.5 ± 2.2	25.2 ± 2.2	43.8 ± 1.0	6.7 ± 2.2	19.0 ± 2.2	5.9
PD-31-030813-4.7	26.1 ± 0.4	8.01 ± 0.02	5.15 ± 0.05	39.1 ± 0.5	43.2 ± 2.2	25.1 ± 2.2	42.8 ± 1.1	6.2 ± 2.2	18.1 ± 2.2	6.9
PD-31-030813-5.3	26.2 ± 0.4	8.01 ± 0.02	5.81 ± 0.05	44.5 ± 0.5	49.4 ± 2.3	25.3 ± 2.2	41.1 ± 1.1	5.8 ± 2.2	18.2 ± 2.2	7.7
PD-31-030813-5.9	26.3 ± 0.4	8.00 ± 0.02	6.46 ± 0.06	53.1 ± 0.6	59.3 ± 2.2	25.2 ± 2.2	39.4 ± 1.1	5.4 ± 2.2	16.8 ± 2.2	9
PD-31-030813-6.5	26.3 ± 0.4	8.02 ± 0.02	7.12 ± 0.06	66.0 ± 0.6	70.2 ± 2.4	25.2 ± 2.2	37.1 ± 2.0	5.2 ± 2.2	16.5 ± 2.2	9.7

Table C.134: Averaged values of measured wall surface temperature during experiment for each data point (PD-31-030813)

Test ID	TS21T (C)	TS21B (C)	TS22T (C)	TS22B (C)	TS23T (C)	TS23B (C)	TS24T (C)	TS24B (C)	TS25T (C)	TS25B (C)	TS26T (C)	TS26B (C)
PD-31-030813-1.7	41.3	37.4	50.7	38.1	49.2	39.2	51.3	38.7	54.3	40.6	56.1	42.0
PD-31-030813-2.3	47.4	40.6	60.1	41.6	57.3	42.6	59.4	42.0	63.7	44.4	66.0	46.2
PD-31-030813-2.9	55.1	44.6	70.6	45.9	66.4	46.6	68.3	45.7	74.1	48.8	78.2	52.2
PD-31-030813-3.5	64.3	49.5	82.3	51.1	76.1	51.1	78.5	49.7	85.7	54.1	92.5	60.2
PD-31-030813-4.1	75.2	56.3	96.0	57.8	87.2	56.4	90.8	55.0	100.3	61.9	110.7	72.6
PD-31-030813-4.7	86.5	63.8	110.4	65.3	99.4	62.3	104.5	61.3	117.2	72.3	132.1	88.8
PD-31-030813-5.3	98.7	72.8	126.6	74.0	113.7	69.5	121.1	70.4	138.1	87.4	159.1	110.7
PD-31-030813-5.9	110.8	82.2	142.8	82.9	128.7	77.3	139.2	81.7	161.4	106.4	188.8	137.8
PD-31-030813-6.5	123.3	91.9	159.7	92.4	145.1	86.8	159.5	97.1	188.6	130.5	222.2	168.9

Table C.135: Steady-state parameters of the loop (processed data) (PD-31-030813)

Test ID	Power (kW)	Flow rate (kg/s)	Inlet K	Outlet K	Outlet Temp. Calculated (C)	T11(C)
PD-31-030813-1.7	1.87 ± 0.03	0.028 ± 0.001	0	62	34.3 ± 0.1	34.9 ± 2.2
PD-31-030813-2.3	2.52 ± 0.04	0.031 ± 0.001	0	62	34.8 ± 0.1	35.5 ± 2.2
PD-31-030813-2.9	3.18 ± 0.04	0.033 ± 0.001	0	62	35.5 ± 0.2	36.2 ± 2.2
PD-31-030813-3.5	3.84 ± 0.04	0.034 ± 0.001	0	62	36.7 ± 0.4	37.2 ± 2.2
PD-31-030813-4.1	4.49 ± 0.05	0.033 ± 0.001	0	62	39.9 ± 0.8	39.5 ± 2.2
PD-31-030813-4.7	5.15 ± 0.05	0.033 ± 0.001	0	62	46.3 ± 1.6	43.2 ± 2.2
PD-31-030813-5.3	5.81 ± 0.05	0.031 ± 0.001	0	62	58.2 ± 2.8	49.4 ± 2.3
PD-31-030813-5.9	6.46 ± 0.06	0.030 ± 0.001	0	62	75.7 ± 4.4	59.3 ± 2.2
PD-31-030813-6.5	7.12 ± 0.06	0.028 ± 0.002	0	62	101.4 ± 10.6	70.2 ± 2.4

*Equivalent outlet K factor: 62 (based on PD-19-053013) for 46º closed valve.

March 15th, 2013 - System Pressure: 8 MPa, Inlet Temperature: 25-26 ℃, Inlet valve: wide open, Outlet valve: wide open

Table C.136: Averaged values of measured signals during experiment for each data point (PD-32-031513)

Test ID	Inlet Temperature (RTD1) (C)	Pressure (MPa)	Power (kW)	Outlet Temp (RTD2)(C)	T11 (C)	T12(C)	CO_2 volumetric Flow rate $(m^3/s) \times 10^6$	HE-Inlet water Temp.(C)	HE-Outlet water Temp.(C)	Water Flow rate (lpm)
PD-32-031513-1.1	25.0 ± 0.4	8.02 ± 0.02	1.21 ± 0.02	31.7 ± 0.5	33.4 ± 2.2	25.2 ± 2.2	38.4 ± 1.2	11.8 ± 2.2	29.9 ± 2.2	0.7
PD-32-031513-1.7	25.1 ± 0.4	8.00 ± 0.02	1.86 ± 0.03	32.8 ± 0.5	34.5 ± 2.2	24.9 ± 2.2	46.9 ± 1.1	11.5 ± 2.2	28.7 ± 2.2	1.5
PD-32-031513-2.35	25.3 ± 0.4	8.01 ± 0.02	2.57 ± 0.04	33.5 ± 0.5	35.2 ± 2.2	25.5 ± 2.2	53.3 ± 1.1	11.2 ± 2.2	27.6 ± 2.2	2.3
PD-32-031513-2.9	25.3 ± 0.4	8.00 ± 0.02	3.18 ± 0.04	33.9 ± 0.5	35.6 ± 2.2	25.3 ± 2.2	57.3 ± 1.1	10.7 ± 2.2	25.6 ± 2.2	3.4
PD-32-031513-3.55	26.0 ± 0.4	8.01 ± 0.02	3.89 ± 0.04	34.4 ± 0.5	36.2 ± 2.2	24.8 ± 2.2	61.5 ± 1.1	7.6 ± 2.2	24.2 ± 2.2	3.7
PD-32-031513-4.15	26.4 ± 0.5	8.02 ± 0.03	4.54 ± 0.05	34.8 ± 0.5	36.7 ± 2.2	25.6 ± 2.3	64.1 ± 1.1	7.0 ± 2.2	22.4 ± 2.2	4.7
PD-32-031513-4.6	26.6 ± 0.4	8.01 ± 0.02	5.03 ± 0.05	35.1 ± 0.5	37.2 ± 2.2	26.0 ± 2.2	65.8 ± 1.1	6.8 ± 2.2	21.8 ± 2.2	5.4
PD-32-031513-5.1	26.2 ± 0.4	8.03 ± 0.02	5.58 ± 0.05	35.5 ± 0.5	37.8 ± 2.2	25.1 ± 2.2	67.4 ± 1.2	6.0 ± 2.2	21.3 ± 2.2	6.1
PD-32-031513-5.7	26.2 ± 0.4	8.00 ± 0.02	6.29 ± 0.06	36.0 ± 0.5	38.7 ± 2.2	25.3 ± 2.2	68.8 ± 1.1	5.7 ± 2.2	21.3 ± 2.2	6.8
PD-32-031513-6.3	26.5 ± 0.4	8.01 ± 0.02	6.90 ± 0.06	37.0 ± 0.5	40.6 ± 2.2	25.3 ± 2.2	69.7 ± 1.2	5.6 ± 2.2	20.9 ± 2.2	7.6
PD-32-031513-6.9	26.1 ± 0.4	8.00 ± 0.02	7.55 ± 0.06	38.1 ± 0.5	42.4 ± 2.2	25.5 ± 2.2	70.0 ± 1.1	5.4 ± 2.2	19.3 ± 2.2	9.1
PD-32-031513-7.5	25.9 ± 0.4	7.99 ± 0.02	8.21 ± 0.06	40.1 ± 0.5	44.9 ± 2.2	25.2 ± 2.2	70.2 ± 1.1	5.1 ± 2.2	18.6 ± 2.2	10.1
PD-32-031513-8.1	25.9 ± 0.4	8.01 ± 0.02	8.86 ± 0.07	43.3 ± 0.5	48.4 ± 2.2	25.1 ± 2.2	70.0 ± 1.1	4.9 ± 2.2	18.5 ± 2.2	10.8
PD-32-031513-8.7	26.0 ± 0.4	8.01 ± 0.03	9.52 ± 0.07	46.8 ± 0.5	52.3 ± 2.3	25.5 ± 2.2	69.7 ± 1.1	4.6 ± 2.2	18.3 ± 2.2	11.4
PD-32-031513-9.3	26.2 ± 0.4	8.02 ± 0.02	10.18 ± 0.07	50.1 ± 0.5	57.0 ± 2.3	25.2 ± 2.2	69.6 ± 1.1	4.6 ± 2.2	18.3 ± 2.2	12.1
PD-32-031513-10	26.7 ± 0.4	8.03 ± 0.02	10.94 ± 0.07	57.7 ± 0.6	63.9 ± 2.4	25.5 ± 2.2	69.0 ± 1.1	4.7 ± 2.2	18.5 ± 2.2	12.5
PD-32-031513-10.7	26.3 ± 0.5	7.98 ± 0.02	11.71 ± 0.08	64.0 ± 0.7	73.8 ± 2.2	25.2 ± 2.2	68.8 ± 1.1	4.5 ± 2.2	17.0 ± 2.2	15.3

Table C.137: Averaged values of measured wall surface temperature during experiment for each data point (PD-32-031513)

Test ID	TS21T (C)	TS21B (C)	TS22T (C)	TS22B (C)	TS23T (C)	TS23B (C)	TS24T (C)	TS24B (C)	TS25T (C)	TS25B (C)	TS26T (C)	TS26B (C)
PD-32-031513-1.1	35.8	33.8	39.7	34.9	38.5	35.5	40.0	35.7	42.8	37.0	43.4	37.7
PD-32-031513-1.7	39.2	36.7	45.0	37.7	42.8	38.2	44.4	38.0	47.5	39.5	49.4	40.7
PD-32-031513-2.35	43.1	39.2	51.1	40.5	47.8	40.9	49.1	40.5	53.8	42.4	56.6	44.0
PD-32-031513-2.9	46.8	41.4	56.3	43.1	52.2	43.2	53.8	42.7	59.6	45.0	63.3	47.1
PD-32-031513-3.55	52.7	44.9	63.3	46.8	58.6	46.5	60.7	45.7	67.9	48.5	73.0	51.6
PD-32-031513-4.15	59.0	48.6	69.5	50.4	65.1	49.6	67.8	48.6	76.4	52.2	83.0	56.6
PD-32-031513-4.6	64.2	51.8	74.6	53.3	70.3	52.1	73.4	50.9	83.2	55.2	91.4	61.1
PD-32-031513-5.1	69.4	54.8	80.2	56.3	75.7	54.7	79.4	53.0	90.2	58.3	99.9	65.5
PD-32-031513-5.7	77.7	60.2	88.7	60.9	83.5	58.2	88.1	56.3	100.7	63.3	113.0	73.4
PD-32-031513-6.3	85.5	65.6	96.9	65.3	91.0	61.8	96.5	60.0	111.2	68.9	126.0	82.3
PD-32-031513-6.9	92.5	70.9	103.9	69.4	95.7	65.4	105.6	63.7	122.2	74.9	139.1	91.2
PD-32-031513-7.5	96.7	75.9	108.4	72.9	101.7	69.3	114.2	68.4	134.2	82.0	153.4	101.2
PD-32-031513-8.1	99.2	80.0	115.6	77.4	110.7	73.8	125.4	74.1	148.0	90.8	169.4	114.2
PD-32-031513-8.7	104.4	85.0	127.9	83.2	121.7	78.7	137.5	80.1	162.1	100.6	185.5	128.3
PD-32-031513-9.3	123.0	95.8	148.5	92.0	135.9	83.8	149.4	87.2	176.5	111.7	202.1	143.4
PD-32-031513-10	140.4	107.2	166.2	100.7	150.2	91.1	165.7	98.6	197.1	128.9	225.1	165.4
PD-32-031513-10.7	150.6	115.1	180.0	109.7	161.9	97.6	180.0	108.5	214.3	142.9	244.1	183.1

Table C.138: Steady-state parameters of the loop (processed data) (PD-32-031513)

Test ID	Power (kW)	Flow rate (kg/s)	Inlet K	Outlet K	Outlet Temp. Calculated (C)	T11(C)
PD-32-031513-1.1	1.21 ± 0.02	0.030 ± 0.001	0	0	33.0 ± 0.2	33.4 ± 2.2
PD-32-031513-1.7	1.86 ± 0.03	0.036 ± 0.001	0	0	33.7 ± 0.1	34.5 ± 2.2
PD-32-031513-2.35	2.57 ± 0.04	0.041 ± 0.001	0	0	34.3 ± 0.1	35.2 ± 2.2
PD-32-031513-2.9	3.18 ± 0.04	0.044 ± 0.001	0	0	34.5 ± 0.1	35.6 ± 2.2
PD-32-031513-3.55	3.89 ± 0.04	0.047 ± 0.001	0	0	35.0 ± 0.1	36.2 ± 2.2
PD-32-031513-4.15	4.54 ± 0.05	0.049 ± 0.001	0	0	35.5 ± 0.2	36.7 ± 2.2
PD-32-031513-4.6	5.03 ± 0.05	0.050 ± 0.001	0	0	36.0 ± 0.2	37.2 ± 2.2
PD-32-031513-5.1	5.58 ± 0.05	0.051 ± 0.001	0	0	36.6 ± 0.3	37.8 ± 2.2
PD-32-031513-5.7	6.29 ± 0.06	0.052 ± 0.001	0	0	37.7 ± 0.4	38.7 ± 2.2
PD-32-031513-6.3	6.90 ± 0.06	0.053 ± 0.001	0	0	39.6 ± 0.6	40.6 ± 2.2
PD-32-031513-6.9	7.55 ± 0.06	0.053 ± 0.001	0	0	41.5 ± 0.8	42.4 ± 2.2
PD-32-031513-7.5	8.21 ± 0.06	0.054 ± 0.001	0	0	44.3 ± 1.0	44.9 ± 2.2
PD-32-031513-8.1	8.86 ± 0.07	0.053 ± 0.001	0	0	48.7 ± 1.4	48.4 ± 2.2
PD-32-031513-8.7	9.52 ± 0.07	0.053 ± 0.001	0	0	54.4 ± 1.7	52.3 ± 2.3
PD-32-031513-9.3	10.18 ± 0.07	0.053 ± 0.001	0	0	61.4 ± 2.1	57.0 ± 2.3
PD-32-031513-10	10.94 ± 0.07	0.052 ± 0.001	0	0	72.8 ± 2.7	63.9 ± 2.4
PD-32-031513-10.7	11.71 ± 0.08	0.052 ± 0.001	0	0	81.2 ± 3.3	73.8 ± 2.2

APPENDIX D

FIGURES OF THE SUPERCRITICAL FLOW FACILITY

Figures D1 to D4 show the pictures of different parts of the loop used for current experimental study.

Figure D.1: Supercritical Flow Facilities

Figure D.2: Cold side of natural circulation loop

Figure D.3:Heated section (middle channel) and the heat exchanger

Figure D.4: Hot side of natural circulation loop